

Spectrum and Transport Properties of interacting Carbon Nanotubes



DISSERTATION ZUR ERLANGUNG DES DOKTORGRADES DER
NATURWISSENSCHAFTEN (DR. RER. NAT.) DER FAKULTÄT PHYSIK DER
UNIVERSITÄT REGENSBURG

vorgelegt von
LEONHARD MAYRHOFER AUS WALLERDORF
2007

Promotionsgesuch eingereicht am 21.11.2007

Die Arbeit wurde angeleitet von Prof. Dr. Milena Grifoni

Prüfungskommission:

Prof. Dr. Gunnar Bali

Prof. Dr. Milena Grifoni

Prof. Dr. Christoph Strunk

Prof. Dr. Klaus Richter

Lebenslauf

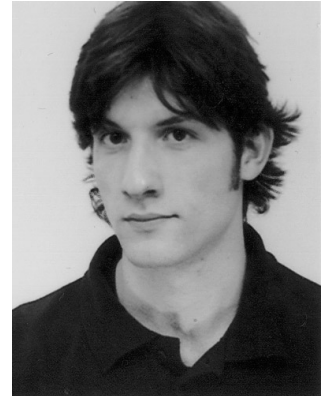
Leonhard Mayrhofer

Diplom-Physiker

* 26.07.1977 in Augsburg

Zur schönen Gelegenheit 6
93047 Regensburg

Familienstand: ledig



Hochschulbildung

11/1998 – 10/2003

Studium der Physik an der Universität Regensburg

11/2003 – 11/2004

Diplomarbeit in theoretischer Festkörperphysik bei Milena Grifoni
Thema: "Correlated Transport in Carbon Nanotubes"

Abschluss als Diplom-Physiker

seit 12/2004

Promotionsstudium im Graduiertenkolleg 638 "Nichtlinearität und
Nichtgleichgewicht in kondensierter Materie" an der Uni Regensburg
Thema der Dissertation:
"Spectrum and transport properties of interacting carbon nanotubes"

Auslandsstudium

10/2001 – 07/2002

an der ETH in Zürich mit den Schwerpunkten Glaziologie und Rechnergestützte
Physik, DAAD Stipendium

Wehrdienst

09/1997 – 06/1998

Grundwehrdienst

Schulbildung

09/1984 – 07/1988

Grundschule Rain am Lech

09/1988 – 06/1997

Gymnasium Donauwörth

Regensburg, 21.11.2007

List of publications:

L. Mayrhofer and M. Grifoni, “Non-Fermi-liquid behavior in transport across carbon nanotube quantum dots”, Phys. Rev. B **74**, 121403(R) (2006).

L. Mayrhofer and M. Grifoni, “Linear and nonlinear transport across carbon nanotube quantum dots”, Eur. Phys. J. B **56**, 107 (2007).

S. Koller, L. Mayrhofer and M. Grifoni, “Spin transport across carbon nanotube quantum dots”, New J. Phys. **9**, **348** (2007).

L. Mayrhofer and M. Grifoni, “The low energy spectrum of finite size metallic SWNTs”, arXiv:0708.1486, submitted to the Phys. Rev. Lett. (2007).

Conferences and talks:

54. Tagung der Nobelpreisträger in Lindau, June 2004.

28. Conference of Theoretical Physics, Electron Correlations in Nano and Macro systems, Ustron, Poland, September 2004.

Capri Spring School on Transport in Nanostructures, Capri, Italy, April 2005.

Nonlinear Dynamics of Nanosystems, Chemnitz, August 2006, Poster.

International Winterschool (IWEPNM 07), Kirchberg, Austria, March 2007, Talk.

71. Jahrestagung der DPG, Regensburg, March 2007, Talk.

Organisation of the annual meeting of the Graduiertenkolleg 638, Frauenchiemsee, Oktober 2007.

Seminar Institut für theoretische Physik IV, Universität Düsseldorf, November 2007, Talk.

Contents

Introduction	1
Part I	
Electronic properties of interacting single wall carbon nanotubes	7
Chapter 1. Electronic properties of noninteracting SWNTs	9
1.1. Band structure of graphene	9
1.2. Morphology of SWNTs	14
1.3. Zone folding	15
1.4. Low energy description of noninteracting armchair SWNTs	17
Chapter 2. Interacting electrons in metallic SWNTs	25
2.1. What is special about interacting SWNTs	27
2.2. Coulomb interaction in metallic SWNTs	30
2.3. The relevant scattering processes	32
2.4. Interlude: The bosonization formalism	37
2.5. Bosonization and diagonalization of the interacting SWNT Hamiltonian	40
2.6. The spectrum of metallic SWNTs	50
2.7. Conclusions	57
Part II	
Transport properties of single wall carbon nanotubes	59
Introduction	60
Chapter 3. Quantum Dots	63
3.1. Charge quantization and Coulomb blockade	64
Transport theory for weakly coupled quantum dots	67
3.2. Model Hamiltonian	67
3.3. Dynamics of the reduced density matrix	69
3.4. Current	75
Chapter 4. Metallic SWNT quantum dots with unpolarized leads	77
4.1. Electronic properties of metallic large size SWNTs	77
4.2. Generalized master equation for unpolarized SWNT quantum dots	78
4.3. Excitation lines	86
4.4. Low Bias Regime	88
4.5. High bias regime	92
Chapter 5. Metallic SWNT quantum dots with polarized leads	99

5.1. Experimental realization of SWNT spin valves	100
5.2. The model Hamiltonian	100
5.3. Generalized master equation for the SWNT spin valve	102
5.4. Coordinate transformations in spinor space	106
5.5. Linear regime	108
5.6. Nonlinear regime	114
5.7. Conclusions	117
Summary and outlook	119
Acknowledgements	123
Appendix A. Derivation of the bosonization identity	125
Appendix B. Bosonized form of the kinetic part of the Hamiltonian	129
Appendix C. Bogoliubov transformation	133
Appendix D. Modeling the interaction potential	137
Appendix E. Calculation of the matrix elements $M_{[r][F][\sigma]}(\vec{N}, \vec{m}, \vec{N}', \vec{m}', x)$	139
Appendix F. Regularization of $\langle \vec{N} \vec{m} V_{f+ b f-} \vec{N} \vec{m} \rangle$	145
Appendix G. Invariance of the transport calculation under unitary transformations U_{E_N}	149
Appendix H. The matrix elements of the electron operators	151
Bibliography	155

Introduction

“Here we have what is almost certainly the strongest, stiffest, toughest molecule that can ever be produced, the best possible molecular conductor of both heat and electricity.” R.E. Smalley

The “supermolecules” that are portrayed here by the discoverer of the C_{60} fullerenes in the foreword to [1] are the famous carbon nanotubes, seamless tubular structures of atomic carbon layers with diameters in the nanometer range and up to several microns in length. Usually the discovery of carbon nanotubes is attributed to Iijima [2] who, using transmission electron microscopy (TEM), found in the carbon soot of arc discharge experiments for the production of fullerenes clear evidence for the existence of the so called multi wall carbon nanotubes (MWNTs), nested structures of several tubes. In Fig. 0.0.1 images of MWNTs from Iijima’s original publication are shown. However, as recently pointed out in the article [3], already in the 1950’s, russian scientists reported about hollow carbon filaments with diameters of around 50nm [4]. Since the resolution of TEM at that time was not high enough in order to determine the detailed structure of the carbon filaments it is unclear if indeed carbon nanotubes were observed. Anyway, only after Iijima’s work carbon nanotubes became a rapidly expanding research field with promising perspectives for applications and fundamental science. Finally, single walled carbon nanotubes (SWNTs), the objects of interest in this thesis, were discovered independently by Iijima and Ichihashi [5] on the one side and Bethune et al. [6] on the other side. In order to understand where the spectacular properties of carbon nanotubes come from one has to take a closer look at the chemical properties of carbon atoms themselves.

Carbon is an outstanding element with respect to its ability to form a great variety of different materials. Being in the fourth main group of the periodic table of elements, carbon possesses four valence electrons that are responsible for chemical bonding. These are one electron in the $2s$ orbital and three $2p$ electrons. The inner two $1s$ electrons can be considered as chemically inert. Covalent bonding between different carbon atoms is possible due to the so called electronic hybridization. In the case of carbon materials this means that new orbitals are formed by a linear combination of the $2s$ orbital with one, two or all three of the $2p$ wave functions in order to minimize the bonding energy. According to the number of involved p electrons one is talking about $2p^n$, $n = 1, 2, 3$ hybridization. The integer n denotes at the same time the coordination number of a certain carbon atom. In diamond the sp^3 hybridization is realized, all four electrons take part in the chemical bonding, no free charge carriers remain and hence diamond is an insulator. A different situation arises for graphene, a hexagonal two-dimensional layer of carbon atoms held together by three sp^2 bonds per atom whose strength even exceeds the one of diamond. In contrast to the latter, in graphene there is still one electron per atom left in the $2p_z$ orbital which has a node in the graphene plane. Due to the crystal structure the p_z wavefunctions form two bands which touch at the corner points of the first Brillouin zone. In isolated graphene only the lower band is filled and hence graphene can be termed as zero-gap semiconductor or as a semi-metal. A detailed derivation of the graphene band structure will be provided in Chapter 1. It should be noted that in 2004 it has been possible to indeed create single graphene layers [7, 8] and graphene research itself has become an important field in

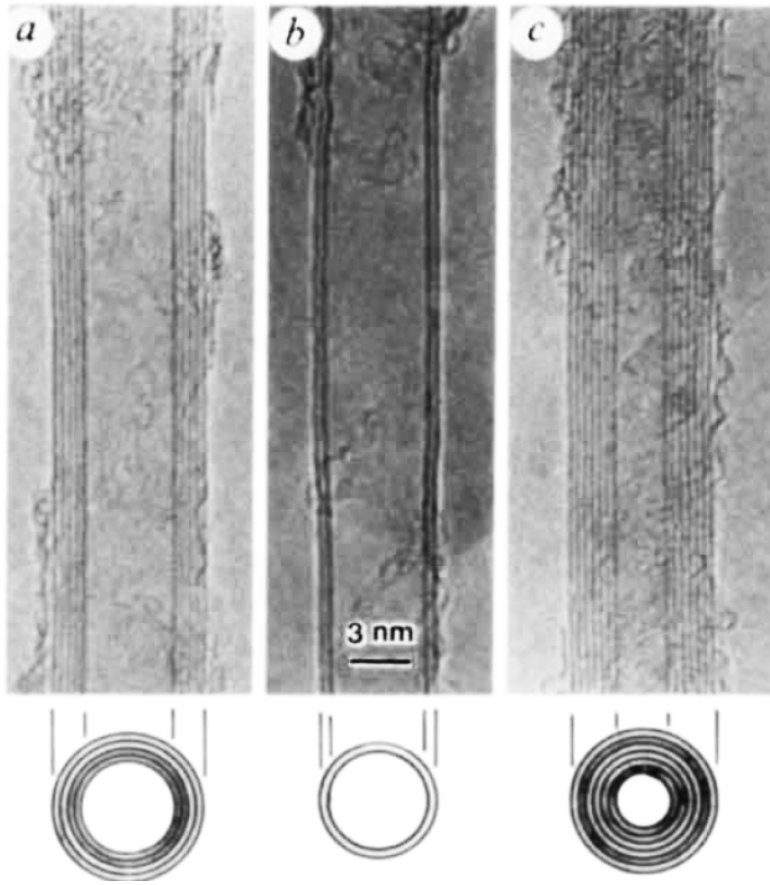


FIGURE 0.0.1. TEM images of MWNTs from Iijima's article on the discovery of carbon nanotubes [2]. The different shells of the MWNTs are clearly distinguishable.

condensed matter physics. For a review about the field we refer to [9]. But now back to SWNTs.

SWNTs are monoatomic layers of graphene wrapped up to seamless cylinders. See Fig. 0.0.2 for a schematic view. Hence it is clear that SWNTs inherit their mechanical robustness from the strong sp^2 bonds in graphene. Concerning the electronic properties of SWNTs, it crucially depends on the geometry of the nanotube whether the metallic behaviour of graphene is found or if the SWNTs behave as semiconductors. The geometry of SWNTs is determined by the way the graphene layer is rolled up, as we will see in Chapter 1. Due to the small diameter of SWNTs of the order of 1nm, quantization around the tube waist “freezes” any motion around the circumference at low enough energies (exceeding well the thermal energy at room temperature). Therefore SWNTs can be considered as almost perfect realizations of one-dimensional (1D) electronic systems. This feature of SWNTs and its interplay with electron-electron interactions are one of the main aspects of this work.

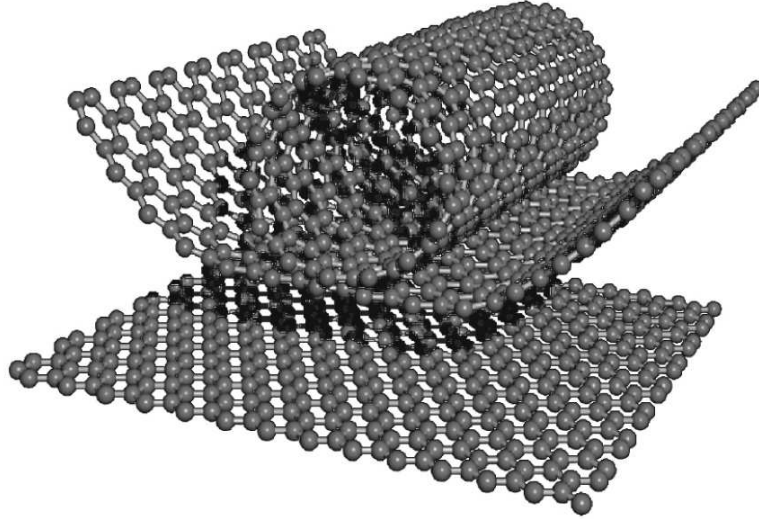


FIGURE 0.0.2. Scheme of wrapping a single layer of graphene to a SWNT [10].

This thesis

It is well known that interactions in fermionic 1D systems play a crucial role. They completely change the properties of the underlying noninteracting 1D system. A description of the 1D interacting systems in terms of fermionic quasiparticles that behave qualitatively in the same way as the corresponding noninteracting fermions, like it is provided by the Fermi liquid theory for three-dimensional (3D) systems, is not possible. This peculiar behaviour of 1D systems has attracted considerable theoretical interest since in 1950 Tomonaga showed with a pathbreaking paper [11] that the problem of interacting fermions can be mapped onto a theory of collective bosonic excitations, which are superpositions of the particle hole excitations of the original fermionic description. Great progress was achieved in the 1980's when in analogy to the Fermi liquid theory the so called Luttinger liquid (LL) theory was established [12] to describe the low energy physics of 1D interacting systems. In contrast to the Fermi liquid theory the elementary excitations in the LL theory are the collective bosonic excitations already discussed by Tomonaga. A more detailed comparison between 1D and 3D systems will be given in the introduction to Chapter 2. For a long time the discussion of interactions in 1D systems was considered as a highly interesting but rather academic issue due to a lack of experimentally accessible 1D systems. The discovery of SWNTs has changed this situation and soon theories based on the bosonization formalism establishing LL behaviour in the low energy regime for metallic SWNTs came on the market [13, 14]. For SWNTs of “infinite” length typical LL properties like a power law suppression of the tunneling density of states could indeed be confirmed

in transport experiments [15, 16]. Moreover the bosonization approach [17] made predictions about the eigenstates and the corresponding quantized energy spectrum of interacting finite size SWNTs. However, recent transport experiments by Moriyama et al. [18] revealed that the nature of low energy eigenstates deviates from the LL predictions. They found the formation of exchange split singlet and triplet states where fourfold degenerate states were expected to be observed. So far the occurrence of an exchange splitting in the energy spectrum had only been found within a mean field theory [19]. Though the mean field approach cannot explain the occurrence of a triplet state nor does it predict the collective excitations of the LL theory as they are expected to be found for an interacting 1D system. This discrepancy between theory and experiment has brought us to rederive the low energy Hamiltonian for metallic SWNTs from a microscopic description of the interacting p_z electrons. Thereby essentially no approximations have been made. Our aim was to examine whether the results in [18] can be reconciled with the bosonization approach for SWNTs and where the deviations from the LL theory come from. Using bosonization we have indeed been able to diagonalize the obtained Hamiltonian away from half-filling and to explain the exchange effects found by Moriyama et al. qualitatively and quantitatively. Moreover, we have made further predictions about the electronic structure of metallic SWNTs going beyond the LL theory which still are waiting for experimental verification. Interestingly the interaction effects not contained in the LL theory can be traced back to the 3D extension of SWNTs in position space. Only in momentum space they can be considered as strictly 1D systems!

As the previous paragraph has already demonstrated, the transport properties and the internal structure of SWNTs are closely related. All of the afore mentioned experiments investigating transport through SWNTs are based on so called quantum dot devices. Such setups consist of a SWNT weakly coupled via tunneling junctions to lead electrodes and capacitively coupled to a gate electrode that allows to control the electrochemical potential in the dot. By applying a bias voltage between the lead electrodes a current can be driven through the system. The second part of this thesis is devoted to the development of a transport theory that yields the current characteristics, i.e., the current as a function of the applied bias and gate voltages, of a SWNT quantum dot. A comparison of the results to the experiments [20] will be provided.

Our approach is general enough to also allow the investigation of spin-dependent transport through SWNT quantum dots with ferromagnetic leads, also denoted as spin-valve transistors. Over the last two decades the possibility of influencing the properties of an electronic device via the spin degree of freedom has strongly increased. SWNTs are expected to be good candidates for building up spin sensitive devices since due to a weak spin-orbit coupling (resulting in g-factors very close to 2 [21]), spin relaxation is expected to be strongly suppressed. We will show that interaction effects again play a decisive role for understanding the properties of spin-valves if arbitrary spin polarizations in the leads are allowed.

Outline

In the first part of the thesis we derive the properties of interacting electrons in metallic SWNTs. We start by giving a review in Chapter 1 on the electronic properties

of noninteracting p_z electrons in SWNTs, which can be derived from the graphene band structure using the so called zone-folding technique. The condition under which SWNTs are metallic or semiconducting is discussed. The central part of the thesis is Chapter 2 where we examine the interaction effects in finite size metallic SWNTs by using the bosonization formalism.

In the second part of this work we derive the transport properties of SWNT quantum dots. A general introduction to the physics of quantum dots will be given in Chapter 3. There we also develop a non-equilibrium transport theory for generic weakly coupled quantum dots using a density matrix approach. The properties of unpolarized metallic SWNT quantum dots in the linear and non-linear regime are calculated in Chapter 4. The corresponding generalization to SWNT spin-valve transistors is presented in Chapter 5.

Part I
**Electronic properties of interacting single
wall carbon nanotubes**

CHAPTER 1

Electronic properties of noninteracting SWNTs

In this chapter we give an introduction to the physics of noninteracting electrons in SWNTs [1, 22, 23]. The results will serve us in Chapter 2 as the basis for the inclusion of electron-electron interactions. A detailed knowledge of the energy spectrum and the structure of the eigenstates of the noninteracting system will be crucial in order to work out the interaction phenomena discussed in Chapter 2 and for the proper calculation of the transport properties in Chapters 4 and 5. For this reason we present the calculation in this chapter at some length. Before addressing noninteracting electrons in carbon nanotubes we first discuss the band structure of graphene. Due to the close relation between SWNTs and graphene it is not surprising that the SWNT band structure can be easily derived from the one of graphene by using zone folding as we show in Section 1.3. It turns out that depending on the way the graphene sheet is wrapped, either metallic or semiconducting SWNTs are obtained. It is interesting to note that the concept of zone folding has been applied to SWNTs even briefly before the discovery of carbon nanotubes by Iijima [1]. Typically not found in textbooks is the use of open boundary conditions which are necessary in order to properly take account of the finite length of a SWNT.

1.1. Band structure of graphene

As explained in the introduction, SWNTs can be regarded as graphene layers, rolled up to a seamless tube. Three out of the four valence electrons per carbon atom in the graphene sheet form sp^2 -bonds with neighbouring atoms leading to the 2D hexagonal honeycomb structure of the graphene lattice as it is depicted in Fig.1.1.1. The remaining $2p_z$ electrons determine the electronic properties of graphene. The crystal structure of graphene leads to the formation of delocalized Bloch waves. We determine the corresponding band structure, using a tight-binding approach.

Choosing the x and y directions as shown in Fig. 1.1.1 the basis vectors of the graphene lattice are given by

$$\vec{a}_{1/2} = a_0 \sqrt{3} \begin{pmatrix} \pm \frac{1}{2} \\ \frac{\sqrt{3}}{2} \end{pmatrix}. \quad (1.1.1)$$

Here a_0 denotes the distance between nearest neighbours. Its value for graphene is 0.142nm. Ignoring finite size effects for the moment, we assume in the following periodic boundary conditions for the graphene honeycomb lattice L_G . Then, according to Bloch's theorem, the single particle Schrödinger equation for the p_z electrons on L_G will be solved by wave functions $\varphi_{\alpha\vec{k}}(\vec{r})$ with a crystal momentum index \vec{k} . Because there are two atoms per unit cell an additional band index $\alpha = \pm$ is required to

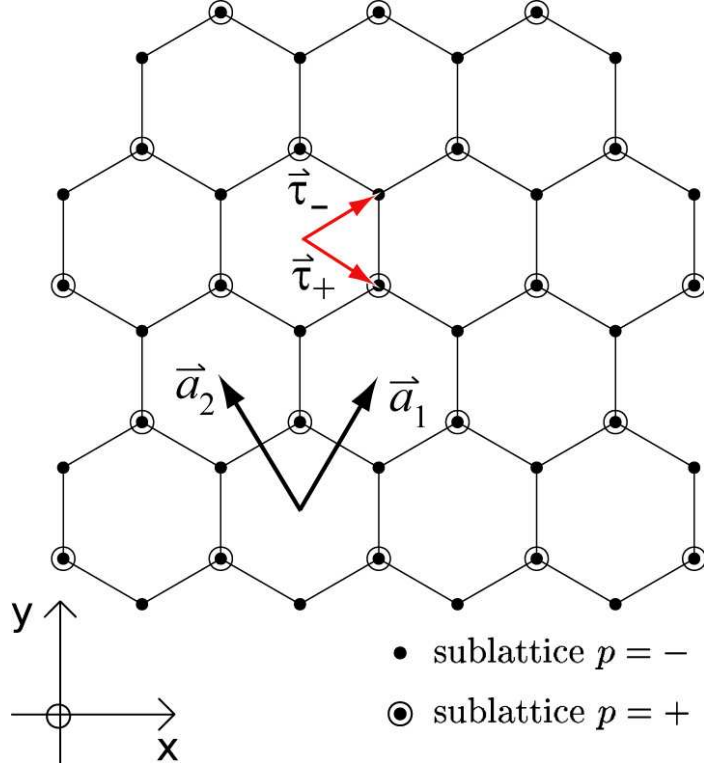


FIGURE 1.1.1. The graphene lattice with its sublattice structure.

characterize the Bloch waves. Hence we start with the ansatz

$$\varphi_{\alpha\vec{k}}(\vec{r}) = \sum_{\vec{R} \in L_G} e^{i\vec{k} \cdot \vec{R}} \sum_{p=\pm} f_{p\alpha\vec{k}} \chi(\vec{r} - \vec{R} - \vec{\tau}_p), \quad (1.1.2)$$

where $\chi(\vec{r})$ denotes a p_z orbitals centered at the origin of the coordinate system. The two carbon atoms in the unit cell are indicated by the sublattice index $p = \pm$. Their positions are given by

$$n_1 \vec{a}_1 + n_2 \vec{a}_2 + \vec{\tau}_p =: \vec{R} + \vec{\tau}_p, \quad n_1, n_2 \in \mathbb{Z}$$

(see Fig. 1.1.1). Explicitly the vectors $\vec{\tau}_p$ are

$$\vec{\tau}_{\pm} = a_0 \begin{pmatrix} \frac{\sqrt{3}}{2} \\ \pm \frac{1}{2} \end{pmatrix}.$$

Note that the Bloch waves in (1.1.2) are linear combinations of functions living on the two separate sublattices. This fact will play a decisive role later on when discussing exchange effects in SWNTs. In order to calculate the eigenenergy $\epsilon_{\alpha\vec{k}}$ of $|\varphi_{\alpha\vec{k}}\rangle$, as well as the coefficients $f_{p\alpha\vec{k}}$, we insert the ansatz (1.1.2) into the single electron Schrödinger

equation

$$h |\varphi_{\alpha\vec{k}}\rangle = \epsilon_{\alpha\vec{k}} |\varphi_{\alpha\vec{k}}\rangle. \quad (1.1.3)$$

In position representation the Hamiltonian reads

$$h(\vec{r}) = \frac{\vec{p}^2}{2m} + \sum_{\vec{R} \in L_G} \sum_p v_{atom}(\vec{r} - \vec{R} - \vec{\tau}_p), \quad (1.1.4)$$

where $v_{atom}(\vec{r} - \vec{R} - \vec{\tau}_p)$ is the potential, describing the interaction of the p_z electron with the ionized carbon atom at position $\vec{R} - \vec{\tau}_p$. So far we have not taken into account the Coulomb interactions between the electrons. It is clear that the p_z orbitals solve the Schrödinger equation of an isolated carbon atom. Thus

$$h_{atom}(\vec{r}) \chi(\vec{r}) = \epsilon_\chi \chi(\vec{r}), \quad h_{atom}(\vec{r}) = \frac{\vec{p}^2}{2m} + v_{atom}(\vec{r}).$$

Separating h into a Hamiltonian for an atom at position $\vec{\tau}_p$ and a “rest” Hamiltonian we get from (1.1.4),

$$h(\vec{r}) = \underbrace{\frac{\vec{p}^2}{2m} + v_{atom}(\vec{r} - \vec{\tau}_\pm)}_{=h_{atom}(\vec{r} - \vec{\tau}_\pm)} + \underbrace{\sum_{\vec{R} \in L_G \setminus \{0\}} \sum_p v_{atom}(\vec{r} - \vec{R} - \vec{\tau}_p)}_{=: \Delta v_\pm(\vec{r})} \quad (1.1.5)$$

Around the position $\vec{\tau}_\pm$ the rest Hamiltonian $\Delta v_\pm(\vec{r})$ is negligible. We are free to set $\epsilon_\chi = 0$. Subsequently we denote a p_z orbital centered around $\vec{R} + \vec{\tau}_p$ by $|\chi_{\vec{R},p}\rangle$. Using (1.1.5) and applying the bra $\langle \chi_{\vec{0},p} |$ from the left we obtain

$$\langle \chi_{\vec{0},p} | \Delta v_p | \varphi_{\alpha\vec{k}} \rangle = \epsilon_{\alpha\vec{k}} \langle \chi_{\vec{0},p} | \varphi_{\alpha\vec{k}} \rangle. \quad (1.1.6)$$

or with the tight-binding ansatz (1.1.2)

$$0 = \sum_{\vec{R} \in L_G} e^{i\vec{k} \cdot \vec{R}} \sum_{p'=\pm} f_{p'\alpha\vec{k}} \langle \chi_{\vec{0},p} | \Delta v_p - \epsilon_{\alpha\vec{k}} | \chi_{\vec{R},p'} \rangle, \quad p = \pm.$$

In matrix form this yields the following equation determining the energies $\epsilon_{\alpha\vec{k}}$ and the coefficients $f_{p\alpha\vec{k}}$,

$$\begin{pmatrix} A_{+,+\vec{k}} - \epsilon_{\alpha\vec{k}} S_{+,+\vec{k}} & A_{+,-\vec{k}} - \epsilon_{\alpha\vec{k}} S_{+,-\vec{k}} \\ A_{- ,+\vec{k}} - \epsilon_{\alpha\vec{k}} S_{- ,+\vec{k}} & A_{- ,-\vec{k}} - \epsilon_{\alpha\vec{k}} S_{- ,-\vec{k}} \end{pmatrix} \begin{pmatrix} f_{+\alpha\vec{k}} \\ f_{-\alpha\vec{k}} \end{pmatrix} = 0, \quad (1.1.7)$$

where we have introduced the abbreviations

$$A_{p,p',\vec{k}} := \sum_{\vec{R} \in L_G} e^{i\vec{k} \cdot \vec{R}} \langle \chi_{\vec{0},p} | \Delta v_p | \chi_{\vec{R},p'} \rangle$$

and

$$S_{p,p',\vec{k}} := \sum_{\vec{R} \in L_G} e^{i\vec{k} \cdot \vec{R}} e^{i\vec{k} \cdot \vec{R}} \langle \chi_{\vec{0},p} | \chi_{\vec{R},p'} \rangle.$$

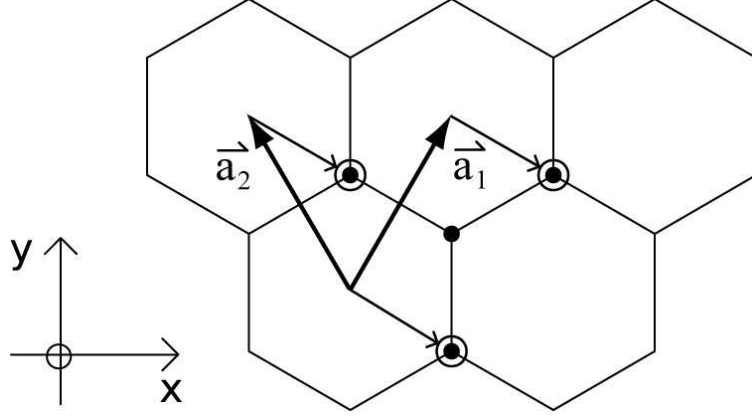


FIGURE 1.1.2. The three next neighbours of a certain carbon atom on the graphene lattice. If a carbon atom is located on sublattice p at the site \vec{R} its three nearest neighbours are situated on the other sublattice $-p$. Their lattice sites are given by $\vec{R}_{n.n.} = \vec{R} + \vec{t}$, with $\vec{t} = 0, \vec{a}_1$ and \vec{a}_2 .

Now we exploit the fact that the p_z orbitals are, with respect to the $x - y$ plane, strongly localized around their atoms. This means that we can neglect all overlap matrix elements except $\langle \chi_{\vec{0},p} | \chi_{\vec{0},p} \rangle = 1$. Thus we find

$$S_{+,+,\vec{k}} = S_{-,-,\vec{k}} \approx 1, \quad S_{+,-,\vec{k}} = S_{-,+,\vec{k}}^* \approx 0. \quad (1.1.8)$$

Additionally we conclude that $\langle \chi_{\vec{0},p} | \Delta v_p | \chi_{\vec{R},p'} \rangle$ is only of importance for the next nearest neighbours of the atom at position \vec{r}_p since $\Delta v_p(\vec{r})$ is, by definition, rather small at the atom position \vec{r}_p , and for atoms farther away than the next neighbours we expect the overlap of the p_z orbitals to vanish. Furthermore we exploit the radial symmetry of the p_z orbitals within the lattice plane, which means that the matrix elements

$$V_{\vec{R}_{n.n.},p,p'} := \langle \chi_{\vec{0},p} | \Delta v_p | \chi_{\vec{R}_{n.n.},p'} \rangle$$

must be equal for all next neighbour sites $\vec{R}_{n.n.} + \vec{r}_{p'}$. With the help of Fig. 1.1.2 we can determine $\vec{R}_{n.n.} + \vec{r}_{p'}$ and obtain the following expressions,

$$\begin{aligned} A_{+,+,\vec{k}} &= A_{-,-,\vec{k}} \approx 0, \\ A_{+,-,\vec{k}} &= A_{-,+,\vec{k}}^* \approx (1 + e^{i\vec{k} \cdot \vec{a}_1} + e^{i\vec{k} \cdot \vec{a}_2}) \langle \chi_{\vec{0},+} | \Delta v_+ | \chi_{\vec{R}_{n.n.},-} \rangle. \end{aligned} \quad (1.1.9)$$

Let us introduce the quantities $\beta_{\vec{k}} := 1 + e^{i\vec{k} \cdot \vec{a}_1} + e^{i\vec{k} \cdot \vec{a}_2}$ and $\gamma := \langle \chi_{\vec{0},+} | \Delta v_+ | \chi_{\vec{R}_{n.n.},-} \rangle$. Then, using the simplifications (1.1.8) to (1.1.9), the eigenvalue problem (1.1.7) takes the form

$$\begin{pmatrix} -\epsilon_{\alpha\vec{k}} & \beta_{\vec{k}}\gamma \\ \beta_{\vec{k}}^*\gamma^* & -\epsilon_{\alpha\vec{k}} \end{pmatrix} \begin{pmatrix} f_{+\alpha\vec{k}} \\ f_{-\alpha\vec{k}} \end{pmatrix} = 0. \quad (1.1.10)$$

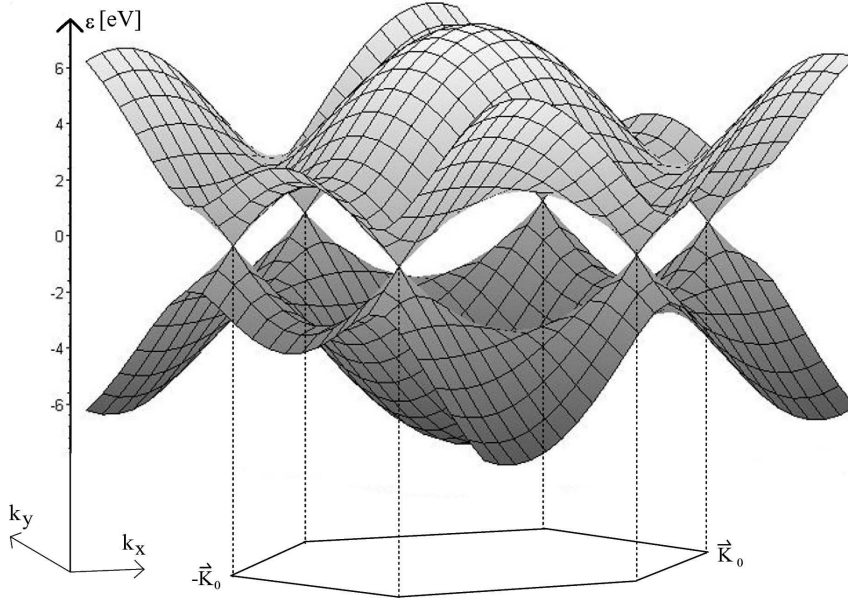


FIGURE 1.1.3. Band structure of graphene. The valence and the conduction band touch at the corner points of the 1. Brillouin zone.

Setting the determinant of the matrix above to zero reveals the dispersion relation for the valence and the conduction band:

$$\epsilon_{\alpha=\pm\vec{k}} = \pm |\gamma\beta_{\vec{k}}| = \pm |\gamma| \sqrt{1 + 4 \cos\left(\frac{3a_0k_y}{2}\right) \cos\left(\frac{\sqrt{3}a_0k_x}{2}\right) + 4 \cos^2\left(\frac{\sqrt{3}a_0k_x}{2}\right)}. \quad (1.1.11)$$

As it can be seen from Fig. 1.1.3, the two bands touch at certain values of \vec{k} , which will turn out to be just the corner points of the first Brillouin zone (BZ) of graphene, and which we are going to call \vec{K} -points.

The basis $\{\vec{b}_1, \vec{b}_2\}$ of the reciprocal lattice, denoted by L_G^{-1} , is given by the condition $\vec{b}_i \cdot \vec{a}_j = 2\pi\delta_{ij}$, i.e.,

$$\begin{aligned} \vec{b}_1 &= \frac{2\pi}{3a_0} \begin{pmatrix} \sqrt{3} \\ 1 \end{pmatrix}, \\ \vec{b}_2 &= \frac{2\pi}{3a_0} \begin{pmatrix} -\sqrt{3} \\ 1 \end{pmatrix}. \end{aligned}$$

L_G^{-1} together with the first BZ is sketched in Fig. 1.1.4. We can see that the corner points of the first BZ can be divided into two sets à three points, indicated by the black circles and the black/white circles in Fig. 1.1.4. Each point of a certain set is equivalent to the other points within the same set, since they differ only by a reciprocal lattice vector, whereas points from different sets are independent points in the 1. BZ.

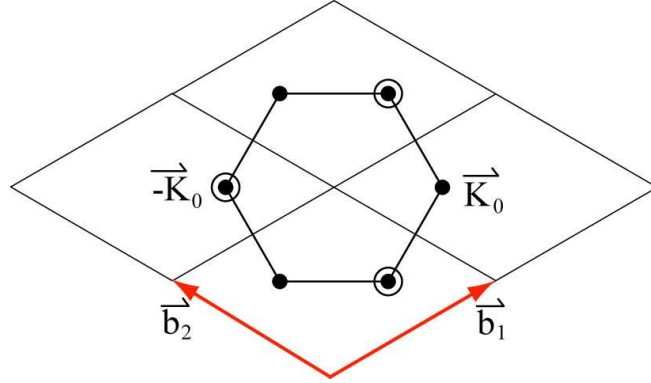


FIGURE 1.1.4. The reciprocal lattice of graphene with its hexagonal Brillouin zone.

As representatives of the two sets we choose

$$\pm \vec{K}_0 = \pm \frac{4\pi}{3\sqrt{3}a_0} \vec{e}_x.$$

Inserting $\pm \vec{K}_0$ into the dispersion relation (1.1.11) yields $\varepsilon_{\alpha, \pm \vec{K}_0} = 0$ which means that the two bands touch at the corner points of the 1. BZ. Since the number of allowed \vec{k} -values within the 1. BZ is equal to the number of lattice sites and taking into account the two spin degrees of freedom, the p_z valence electrons (two per lattice site) just fill up the low lying band whereas the higher band is unoccupied, if isolated graphene is regarded. Consequently rather than a Fermi surface or line graphene has two independent Fermi points that connect the valence and the conductance band. That is why graphene is often called a semi-metal. Another consequence of the very special band structure of graphene is that the low energy physics takes place in a small region around $\pm \vec{K}_0$. In this respect it is of great relevance for the discussion of the low energy regime of metallic SWNTs later on that near the Fermi points ab initio calculations of the graphene band structure qualitatively do not differ from our simple tight-binding result (1.1.11), but only lead to slight quantitative corrections [23].

The band structure of SWNTs can easily be determined from the one of graphene once we will have analyzed the different ways of wrapping up a graphene sheet to form a SWNT. Thus let us now discuss the morphology of SWNTs.

1.2. Morphology of SWNTs

Having a graphene sheet like the one shown in Fig. 1.2.1 how can we construct a SWNT? For this purpose we choose two different lattice sites A and B on the honeycomb lattice and connect them by the so called wrapping or chiral vector which reads in terms of the graphene lattice basis vectors,

$$\vec{w}_{n,m} = n\vec{a}_1 + m\vec{a}_2, \quad n, m \in \mathbb{N}_0.$$

Now we roll the graphene layer onto a tube in such a way that A and B coincide. Then automatically the tube axis is perpendicular to $\vec{w}_{n,m}$. Due to the sixfold symmetry

of the graphene lattice already the set of wrapping vectors $\{\vec{w}_{n,m}\}$ with $0 \leq |m| \leq n$ covers all possible geometries of SWNTs. It is distinguished between chiral and achiral tubes. In achiral tubes one side of the hexagons is parallel or perpendicular to the cylinder axis. The other tubes are called chiral tubes, since they exhibit a spiral symmetry, i.e., their mirror image is not congruent to the original one. The achiral tubes are furthermore divided into armchair tubes and zigzag tubes. Armchair tubes are described by wrapping vectors $\vec{w}_{n,n}$, whereas wrapping vectors $\vec{w}_{n,0}$ characterize the so called zigzag tubes (see Fig. 1.2.1).

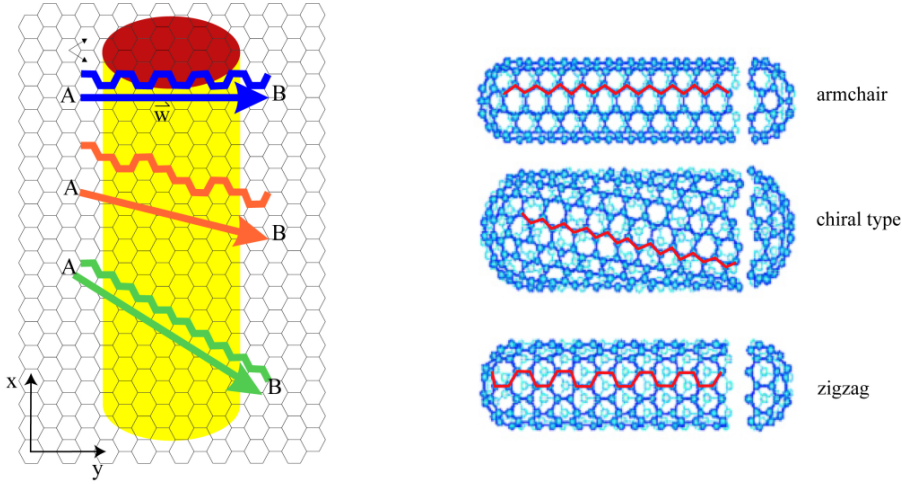


FIGURE 1.2.1. Different wrapping vectors lead to different geometries of the SWNTs.

The unit cell of the nanotube lattice is defined by the chiral vector and the translational vector $\vec{T} = t_1 \vec{a}_1 + t_2 \vec{a}_2$ which is the shortest vector pointing along the tube axis and connecting two carbon atoms. For a given wrapping vector the integers t_1 and t_2 are determined via the condition $\vec{w}_{n,m} \cdot \vec{T} = 0$ leading to

$$t_1 = \pm \frac{2m + n}{\text{GCD}(m, n)}, \quad t_2 = \mp \frac{2n + m}{\text{GCD}(m, n)}.$$

The division by the greatest common divisor GCD of the wrapping indices in the previous equation ensures that we find indeed the shortest translational vector. Another important quantity is the tube diameter d which depends on the wrapping vector according to

$$d = \frac{|\vec{w}_{n,m}|}{\pi} = \frac{a_0}{\pi} \sqrt{3(n^2 + m^2 + nm)}.$$

1.3. Zone folding

As explained in 1.2 the lattice structure of SWNTs is, except for the tubular shape, identical with the graphene structure. Neglecting curvature effects, also the chemical sp^2 bondings of a SWNT and a graphene sheet are identical, and so the question arises if SWNTs inherit the metallic behaviour of graphene. The answer is, as we will see,

that this depends on the chirality of the tube. The key to the answer can be found in the boundary conditions that must be fulfilled by the nanotube Bloch waves. Whereas for the graphene calculations periodic boundary conditions (PBCs) were merely used as a mathematical trick in order to get a proper quantization condition for the \vec{k} -values, in the case of SWNTs the Bloch waves indeed have to fulfill the PBCs around the tube waist. Because of the high aspect ratio of the tubes this means rather big quantization steps for the \vec{k} -components perpendicular to the tube axis, whereas parallel to the tube axis the \vec{k} -value separation is much smaller. To calculate the SWNT band structure, we apply the so called zone folding technique, which assumes that the electronic properties of a SWNT associated with one of the allowed \vec{k} -values are identical to those of graphene.

In more detail: First we separate \vec{k} into a part parallel to the tube axis and a part perpendicular to it

$$\vec{k} = k_{\parallel} \vec{e}_{\parallel} + k_{\perp} \vec{e}_{\perp}.$$

The quantization condition for \vec{k} is determined by the wrapping vector $\vec{w} = n\vec{a}_1 + m\vec{a}_2$ and the length of the tube. Bloch's theorem together with the PBC around the waist of the tube, and the usual Born- von Karmann PBC along the tube axis require

$$\begin{aligned} \varphi_{\vec{k}}(\vec{r} + \vec{w}) &= e^{ik_{\perp}|\vec{w}|} \varphi_{\vec{k}}(\vec{r}) = \varphi_{\vec{k}}(\vec{r}), \\ \varphi_{\vec{k}}(\vec{r} + \vec{e}_{\parallel}L) &= e^{ik_{\parallel}L} \varphi_{\vec{k}}(\vec{r}) = \varphi_{\vec{k}}(\vec{r}), \end{aligned}$$

where L is the length of the nanotube. We arrive at the quantization conditions

$$k_{\perp} = \frac{2\pi}{|\vec{w}|}p, \quad k_{\parallel} = \frac{2\pi}{L}q, \quad p, q \in \mathbb{Z}. \quad (1.3.1)$$

Note that in general $\frac{2\pi}{|\vec{w}|} \gg \frac{2\pi}{L}$, which affirms that k_{\parallel} is a quasi-continuous variable if compared to k_{\perp} . The allowed \vec{k} -values for different types of SWNTs are shown in Fig. 1.3.1. Now we can tackle the question, under which condition a SWNT is semiconducting or metallic. If the quantization condition (1.3.1) allows \vec{k} values that

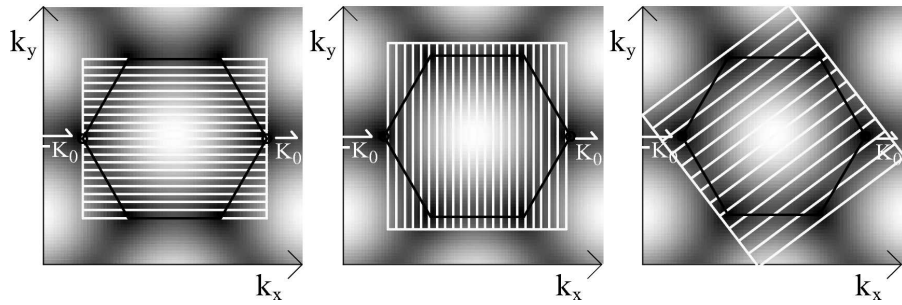


FIGURE 1.3.1. Examples for the allowed \vec{k} -values in an armchair-, zigzag- and chiral- SWNT (from left to right). The dark spots indicate a small distance between valence and conduction band, whereas the bright areas represent large gaps between the two bands.

coincide with $\pm \vec{K}_0$ we have metallic nanotubes otherwise there is a energy gap between occupied and unoccupied states and we have semiconducting ones. Since the set of allowed \vec{k} values is given by the chirality of the tube, the wrapping vector \vec{w} determines whether the SWNT exhibits metallic behaviour or not. Regarding k_{\parallel} as continuous variable condition (1.3.1) is satisfied for the Fermi points if

$$\vec{K}_0 \cdot \vec{w} = \frac{4\pi}{3\sqrt{3}a_0} \vec{e}_x \cdot (n\vec{a}_1 + m\vec{a}_2) \stackrel{!}{=} 2\pi p, \quad p \in \mathbb{Z}. \quad (1.3.2)$$

With (1.1.1) we obtain

$$\frac{2\pi}{3}(n - m) = 2\pi p, \quad p \in \mathbb{Z}.$$

Hence it is obvious that according to the zone folding procedure a SWNT is metallic, if

$$\frac{n - m}{3} \in \mathbb{Z}. \quad (1.3.3)$$

For the sake of simplicity we concentrate on armchair tubes ($n - m = 0$) from now on. This can be done without loss of generality for our purpose of examining interacting electrons in metallic SWNTs since correlation effects are universal at low energies, i.e., they do not depend on the chirality, as shown in [24]. Whenever deviations from the armchair behaviour occur for the other types of SWNTs we will explicitly mention it. Additionally we notice that if curvature effects are included only armchair SWNTs remain to be truly metallic whereas for the other SWNT geometries fulfilling condition (1.3.3) a small gap opens at the Fermi points. In Fig. 1.3.2, the full band structure of a ($n = 10, m = 10$) armchair tube is shown. As expected there is no gap in the band structure since two of the subbands touch at the Fermi points.

1.4. Low energy description of noninteracting armchair SWNTs

From Fig. 1.3.2 it can be seen that for a typical SWNT like the (10,10) tube there is a gap of around 1eV between the Fermi level and those subbands which do not touch it. For comparison, 1eV corresponds to a temperature of about 10^4 K, if we consider the thermal energy $k_B T$. Thus even at very high temperatures the low energy physics merely takes place in the “gapless” subbands touching at the Fermi points. Until now we have neglected the Coulomb interaction between the p_z electrons, but, as we know from the introduction, interactions in 1D systems change the properties of the corresponding noninteracting system tremendously. Before we derive the low energy many body Hamiltonian for armchair tubes, including the electron- electron correlations, we construct a suitable basis set of single electron states. For this purpose we start from the graphene Bloch waves 1.1.2, and using the zone folding again, we obtain the proper SWNT wave functions for PBCs along the tube axis. However, in order to adapt this procedure to a finite size system we will finally change from PBCs to open boundary conditions (OBCs) and obtain standing rather than travelling waves.

1.4.1. Noninteracting electrons in finite size armchair SWNTs (PBCs) . For armchair SWNTs, the set of allowed wave vectors that correspond to the two touching

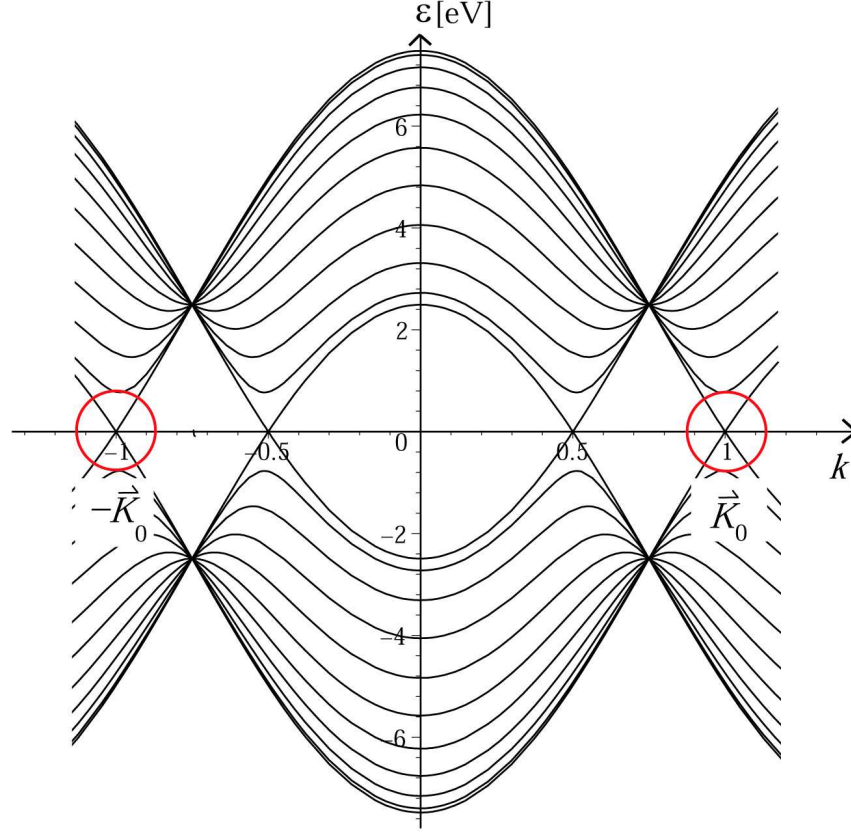


FIGURE 1.3.2. The subbands of a (10,10) armchair nanotube. Note that there seem to exist four k -values, where subbands touch the Fermi level, but only two of them are independent. The k -values corresponding to $\pm \vec{K}_0$ are encircled.

subbands in Fig. 1.3.2 are given by

$$\vec{k} := k\vec{e}_x = \frac{2\pi}{L}q_k\vec{e}_x, \quad q_k \in \mathbb{Z}, \quad (1.4.1)$$

where \vec{e}_x points along the tube axis and L is the tube length. Only \vec{k} vectors in the vicinity of the Fermi points, i.e., $\vec{k} \approx \pm \vec{K}_0$, are relevant for low energy processes. Let us therefore write k in the following way:

$$k = \kappa + F, \quad (1.4.2)$$

where κ measures the distance between k and $F = \pm K_0$ in the reciprocal space. If we restrict ourselves to low energy excitations, we can directly deduce from (1.4.1), that armchair nanotubes are indeed realizations of ideal 1D quantum wires.

Let us turn to the evaluation of the armchair Bloch functions and energy dispersion relation. Since we are only interested in the region near $\pm \vec{K}_0$ in \vec{k} -space, it is sufficient to expand β_k in (1.1.10) up to first order in κ around $F = \pm K_0 = \pm \frac{4\pi}{3\sqrt{3}a_0}$. We start

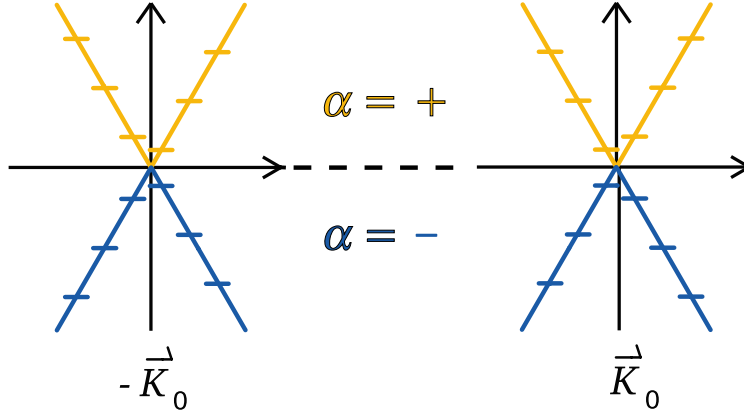


FIGURE 1.4.1. Energy dispersion relation near the $\pm\vec{K}_0$ points. For metallic SWNTs the valence band (dark blue) and the conduction band (orange) touch at the Fermi points. The energy dispersion is linear near $\pm\vec{K}_0$. Note that the PBC quantization condition (1.4.1) leads to an energy level separation of $\frac{\hbar v_F 2\pi}{L} \approx 3\text{meV} \frac{\mu\text{m}}{L}$.

with

$$\beta_{\vec{k}} = 1 + e^{i\vec{k} \cdot \vec{a}_1} + e^{i\vec{k} \cdot \vec{a}_2}.$$

Using (1.4.2) and the definitions of the lattice basis vectors from (1.1.1) we get after the expansion around F ,

$$\beta_{\kappa F} \approx -\text{sgn}(F) \sqrt{3} a_0 \kappa \sin(2\pi/3) = -\text{sgn}(F) \frac{3a_0}{2} \kappa. \quad (1.4.3)$$

Note that we have replaced \vec{k} in $\beta_{\vec{k}}$ by the two indices κ and F . With (1.4.3) equation (1.1.10) which determines the tight binding parameters becomes

$$\begin{bmatrix} -\epsilon_{\alpha\kappa} & -\text{sgn}(F) \frac{3a_0}{2} \kappa \gamma \\ -\text{sgn}(F) \frac{3a_0}{2} \kappa \gamma^* & -\epsilon_{\alpha\kappa} \end{bmatrix} \begin{bmatrix} f_{+\alpha\kappa F} \\ f_{-\alpha\kappa F} \end{bmatrix} = 0. \quad (1.4.4)$$

Therefore the energy relation around both Fermi points is linear,

$$\epsilon_{\alpha\kappa} = \alpha \frac{3a_0}{2} |\gamma| |\kappa| = \pm \hbar v_F |\kappa|, \quad (1.4.5)$$

as also depicted in Fig. 1.4.1. Here $v_F = \frac{3a_0|\gamma|}{2\hbar} \approx 8.1 \cdot 10^5 \frac{\text{m}}{\text{s}}$ is the group velocity at the Fermi points. Solving equation (1.4.4) we get the following relation between the wave function coefficients $f_{p\alpha\kappa F}$ on the different sublattices,

$$f_{p=-\alpha\kappa F} = -\alpha \text{sgn}(F) \frac{|\kappa_{qF}|}{\kappa_{qF}} f_{p=+\alpha\kappa F}. \quad (1.4.6)$$

We can satisfy (1.4.6) by choosing

$$f_{+\alpha\kappa F} = \frac{1}{\sqrt{2}}, \quad f_{-\alpha\kappa F} = -\frac{\alpha}{\sqrt{2}} \text{sgn}(\kappa F). \quad (1.4.7)$$

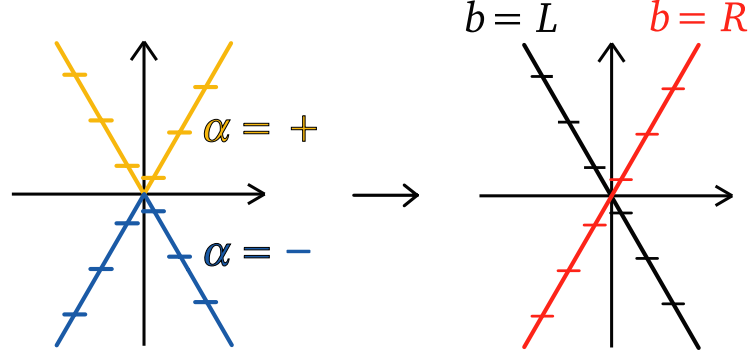


FIGURE 1.4.2. Introduction of right and left moving states. Instead of characterizing using the different low energy subbands in a metallic SWNT by the band index α for valence and conduction band, we introduce the branch index $b = R/L$ for right and left moving electrons.

In order to normalize our Bloch functions to unity, we still have to introduce a prefactor $\frac{1}{\sqrt{N_L}}$, where N_L is the total number of sites in the nanotube lattice. Inserting (1.4.7) into the tight binding ansatz (1.1.2) we finally obtain for the armchair nanotube Bloch waves near the Fermi points $F = \pm K_0$ the following expression

$$\varphi_{\alpha\kappa F}(\vec{r}) = \frac{1}{\sqrt{N_L}} \sum_{\vec{R} \in L_G} e^{i(\kappa+F)R_x} \sum_{p=\pm} f_{p\alpha\kappa F} \chi(\vec{r} - \vec{R} - \vec{\tau}_p). \quad (1.4.8)$$

For our further discussion it will be convenient to introduce the notion of right and left moving states: Bloch waves on branches with positive (negative) group velocity are called right (left) movers. As it can be seen from Fig. 1.4.2 this allows us to switch from the band index α and wave number κ_q to a new index $b = R/L$, where R corresponds to right and L to left movers. In detail the relation between α and b is given by

$$b = R \longleftrightarrow \begin{cases} \alpha = +, \kappa > 0 \\ \alpha = -, \kappa < 0 \end{cases}, \quad b = L \longleftrightarrow \begin{cases} \alpha = +, \kappa < 0 \\ \alpha = -, \kappa > 0 \end{cases}. \quad (1.4.9)$$

Introducing the label b leads to the following expression for the Bloch wave functions of an armchair SWNT near the Fermi points:

$$\varphi_{bF\kappa}(\vec{r}) = \frac{1}{\sqrt{N_L}} \sum_p \sum_{\vec{R} \in L_G} f_{pbF} e^{i(\kappa+F)R_x} \chi(\vec{r} - \vec{R} - \vec{\tau}_p) =: \sum_p f_{pbF} \varphi_{pF\kappa}(\vec{r}). \quad (1.4.10)$$

The factors f_{pbF} can be derived from the coefficients $f_{p\alpha F, \kappa}$ with the help of (1.4.9), obtaining

$$f_{+bF} = \frac{1}{\sqrt{2}}, \quad f_{-bF} = -\frac{1}{\sqrt{2}} \text{sgn}(b) \text{sgn}(F), \quad \text{sgn}(b) := \begin{cases} 1 & , b = R \\ -1 & , b = L \end{cases}. \quad (1.4.11)$$

Another simplification can be achieved by expanding $\varphi_{pF\kappa}(\vec{r})$ around the Fermi point F which gives

$$\varphi_{pF\kappa}(\vec{r}) = e^{i\kappa x} \varphi_{pF}(\vec{r}), \quad \text{with } \varphi_{pF}(\vec{r}) := \frac{1}{\sqrt{N_L}} \sum_{\vec{R} \in L_G} e^{iF R_x} \chi(\vec{r} - \vec{R} - \vec{\tau}_p). \quad (1.4.12)$$

Hence the final result for the armchair single electron wave functions at low energies is given by

$$\varphi_{bF\kappa}(\vec{r}) = e^{i\kappa x} \sum_p f_{pbF} \varphi_{pF}(\vec{r}) =: e^{i\kappa x} \varphi_{bF}(\vec{r}). \quad (1.4.13)$$

1.4.2. Noninteracting electrons in finite size armchair SWNTs (OBCs). So far we have assumed PBCs along the tube axis, i.e., $\varphi_{bF\kappa}(\vec{r} + L\vec{e}_{||}) = \varphi_{bF\kappa}(\vec{r})$. This choice of boundary conditions is appropriate if one is interested in bulk properties of long enough SWNTs. But since we want to take into account finite size effects, OBCs are the natural choice for our purposes. That means that we have to look for solutions $\varphi_{r\kappa}(\vec{r})$ of the single electron Schrödinger equation (1.1.3) fulfilling the condition

$$\varphi_{r\kappa}(x = 0, y, z) = \varphi_{r\kappa}(x = L, y, z) = 0, \quad (1.4.14)$$

where the index r still has to be specified. To find the functions $\varphi_{r\kappa}(\vec{r})$ we let us lead by [25], where a generic spinless 1D system with OBCs is treated, and build up the OBC waves as linear combinations of the Bloch waves $\varphi_{bF\kappa}(\vec{r})$ in analogy to standing waves in 1D quantum boxes. Since we have right and left moving states at *each* Fermi point there are two different solutions of (1.1.3) fulfilling OBCs for an appropriate choice of κ :

$$\varphi_{r=+\kappa}(\vec{r}) := \frac{1}{\sqrt{2}} \varphi_{RK_0\kappa}(\vec{r}) - \frac{1}{\sqrt{2}} \varphi_{L-K_0-\kappa}(\vec{r}), \quad (1.4.15)$$

$$\varphi_{r=-\kappa}(\vec{r}) := \frac{1}{\sqrt{2}} \varphi_{LK_0\kappa}(\vec{r}) - \frac{1}{\sqrt{2}} \varphi_{R-K_0-\kappa}(\vec{r}). \quad (1.4.16)$$

Using equations (1.4.11) and (1.4.10) we can also rewrite $\varphi_{r\kappa}(\vec{r})$ in terms of the sublattice wave functions $\varphi_{pF}(\vec{r})$:

$$\varphi_{r\kappa}(\vec{r}) = \frac{1}{\sqrt{2}} \sum_F \text{sgn}(F) e^{i\text{sgn}(F)\kappa x} \sum_p f_{pr} \varphi_{pF}(\vec{r}), \quad (1.4.17)$$

with

$$f_{pr} := \frac{1}{\sqrt{2}} \begin{cases} 1 & , p = + \\ -\text{sgn}(r) & , p = - \end{cases}. \quad (1.4.18)$$

In the course of this thesis we will see that the index r has properties very similar to the electron spin. Therefore we also refer to r as pseudo spin in the following. As sketched in Fig. 1.4.3, the energy eigenvalues ε_κ belonging to $\varphi_{r\kappa}(\vec{r})$ by definition show the energy dispersion relation of right and left movers, respectively. Putting together equations (1.4.10), (1.4.15) and (1.4.16) we obtain the following expressions

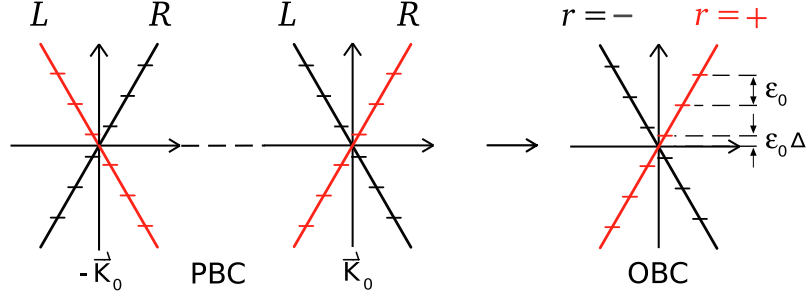


FIGURE 1.4.3. The PBC band structure of armchair SWCNTs (left) can be mapped onto the OBC band structure (right) by constructing suitable linear combinations of Bloch waves from the R/L - band at \vec{K}_0 and the L/R - band at $-\vec{K}_0$.

for the standing waves $\varphi_{r\kappa}(\vec{r})$:

$$\varphi_{+\kappa}(\vec{r}) = \frac{i}{\sqrt{N_L}} \sum_{\vec{R} \in L_G} \sin((K_0 + \kappa) R_x) \sum_p p \chi(\vec{r} - \vec{R} - \vec{\tau}_p), \quad (1.4.19)$$

$$\varphi_{-\kappa}(\vec{r}) = \frac{i}{\sqrt{N_L}} \sum_{\vec{R} \in L_G} \sin((K_0 + \kappa) R_x) \sum_p \chi(\vec{r} - \vec{R} - \vec{\tau}_p). \quad (1.4.20)$$

We know that the p_z orbitals are strongly localized around $\vec{R} + \vec{\tau}_p$. This is why we can reduce the sum over all lattice sites \vec{R} to a sum over all lattice sites whose x -component is approximately equal to a given x_0 :

$$\begin{aligned} \varphi_{\pm\kappa}(\vec{r}_0) &= \\ &= \frac{i}{\sqrt{N_L}} \sum_{\{\vec{R} \in L_G | R_x \approx x_0\}} \sin((K_0 + \kappa) R_x) \left[\chi(\vec{r}_0 - \vec{R} - \vec{\tau}_1) \pm \chi(\vec{r}_0 - \vec{R} - \vec{\tau}_2) \right]. \end{aligned} \quad (1.4.21)$$

Let us choose explicitly $x_0 = 0$ and $x_0 = L$. Then according to (1.4.21) and (1.4.14), the OBCs are formally fulfilled if $(K_0 + \kappa)L = \pi m$, $m \in \mathbb{Z}$ or if

$$\kappa = \frac{\pi}{L} (n_\kappa + \Delta), \quad n_\kappa \in \mathbb{Z}. \quad (1.4.22)$$

Here Δ is a small off-set that is necessary if $K_0 \neq \frac{\pi}{L}m$, $m \in \mathbb{Z}$. It is worth to mention that a value of Δ different from 0 or $\pm 1/2$ causes a mismatch ε_Δ between the energy levels of the $r = +$ and $r = -$ branch, as can be deduced from Fig. 1.4.3. The physical meaning of this mismatch is, that one of the bands will be energetically favoured, if a new electron is added to the nanotube.

Note that we are discussing the low-energy-regime where only small values of κ are of physical importance. By comparing (1.4.22) and (1.3.1) we recognize that the spacing between two neighboring κ values in the OBCs is half as large as in the case of PBCs (consequently the same is true for the energy level spacing). Fig. 1.4.4 shows an

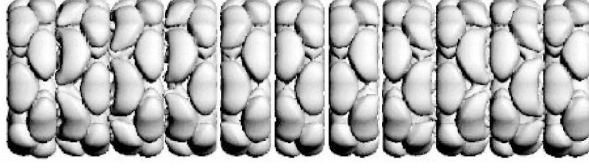


FIGURE 1.4.4. Squared amplitude of the standing wave function $\varphi_{+\kappa}(\vec{r})$ for $\kappa = 0$ and $\Delta = 0$ as they were obtained by DFT calculations [26].

image of $|\varphi_{+\kappa}(\vec{r})|^2$ for $\kappa = 0$ and $\delta = 0$ from [26]. Instead of using the tight-binding method, the standing wave pattern was calculated by an ab initio density functional theory calculation (DFT), yielding qualitatively the same result.

1.4.3. The Hamiltonian of noninteracting metallic SWNTs. From the dispersion relation of the standing waves $\varphi_{r\kappa}(\vec{r})$ shown in Fig. 1.4.3 it is easy to derive the kinetic part of the Hamiltonian describing p_z electrons at low energies. As we know from our discussion in Section 1.4.1, the two branches in the dispersion relation have slopes given by $r\hbar v_F$. Hence, including the spin degree of freedom, the Hamiltonian of the noninteracting electrons is given by

$$H_0 = \hbar v_F \sum_{r\sigma} r \sum_{\kappa} \kappa c_{r\sigma\kappa}^\dagger c_{r\sigma\kappa}, \quad \kappa = \frac{\pi}{L} (n + \Delta), \quad n \in \mathbb{Z},$$

with $c_{r\sigma\kappa}$ being the operator which annihilates $|\varphi_{r\kappa}\rangle|\sigma\rangle$. Note that the summation over κ corresponds to states in the vicinity of the Fermi points. Using relation (1.4.22) for the quantized values of κ the Hamiltonian reads

$$H_0 = \varepsilon_0 \sum_{r\sigma} r \sum_{n_\kappa} n_\kappa c_{r\sigma\kappa}^\dagger c_{r\sigma\kappa} + \varepsilon_0 \Delta \sum_{r\sigma} r \mathcal{N}_{r\sigma}, \quad (1.4.23)$$

where we have defined the operator $\mathcal{N}_{r\sigma}$ counting the number of electrons characterized by a certain index pair $r\sigma$. The level spacing of noninteracting SWNTs is given by

$$\varepsilon_0 := \hbar v_F \frac{\pi}{L}. \quad (1.4.24)$$

In total we have to distinguish between the four different electron species $r\sigma = +\uparrow, +\downarrow, -\uparrow, -\downarrow$. The possible energy mismatch between the $r = +$ and $r = -$ electrons is taken into account by the second term on the right hand side of (1.4.23).

1.4.4. The electron operator. Before including the Coulomb interaction between the electrons we introduce the electron operator of the low energy system thus being enabled to write down the interaction part of the Hamiltonian in position representation. Including the spin degree of freedom and restricting ourselves to the subspace of states spanned by $\{|\varphi_{r\kappa}\rangle\}$ (low energy regime) we can write the 3D electron operator as

$$\Psi(\vec{r}) = \sum_{r\sigma\kappa} \varphi_{r\kappa}(\vec{r}) c_{r\sigma\kappa} =: \sum_{\sigma} \Psi_{\sigma}(\vec{r}). \quad (1.4.25)$$

With the help of the decomposition of $\varphi_{r\kappa}(\vec{r})$ into its sublattice contributions, equation (1.4.17), we obtain from (1.4.25),

$$\Psi_{\sigma}(\vec{r}) = \frac{1}{\sqrt{2}} \sum_{rF\kappa} \text{sgn}(F) e^{i\text{sgn}(F)\kappa x} c_{r\sigma\kappa} \sum_p f_{pr} \varphi_{pF}(\vec{r}).$$

In regard to the application of bosonization techniques later on it is crucial to introduce the slowly varying 1D electron operators

$$\psi_{rF\sigma}(x) := \frac{1}{\sqrt{2L}} \sum_{\kappa} e^{i\text{sgn}(F)\kappa x} c_{r\sigma\kappa}, \quad (1.4.26)$$

which can be rewritten in terms of bosonic creation and annihilation operators as we will demonstrate in Section 2.4.3. Using the definition of the 1D electron operators, (1.4.26), we arrive at

$$\Psi_{\sigma}(\vec{r}) = \sqrt{L} \sum_{rF} \text{sgn}(F) \psi_{rF\sigma}(x) \sum_p f_{pr} \varphi_{pF}(\vec{r}). \quad (1.4.27)$$

Notice that the operators $\psi_{rF\sigma}$ and $\psi_{r-F\sigma}$ are not independent. According to (1.4.26) the relation

$$\psi_{rF\sigma}(x) = \psi_{r-F\sigma}(-x)$$

holds. This is not surprising since after changing from PBCs to OBCs, the Fermi point index F distinguishes not between different electron species any more.

CHAPTER 2

Interacting electrons in metallic SWNTs

This chapter has been worked out in collaboration with Milena Grifoni. A manuscript containing the major achievements discussed in this chapter has been submitted to the Physical Review Letters, preprint arXiv:0708.1486.

As described in the introduction of this thesis, SWNTs have remarkable mechanical and electronic properties. The main focus of the present work is on the interplay between the 1D nature of SWNTs and electron-electron correlations.

For 3D systems of repulsively interacting spin 1/2 particles, Landau established the validity of the so called Fermi liquid theory in the limit of low excitation energies, for a review see [27]. Landau's theory is based on the assumption that the excitation spectrum of interacting fermions is qualitatively equivalent to the one of the corresponding noninteracting system. In other words, it is expected that the elementary excitations in the interacting system, the so called quasiparticles, have the same quantum numbers as the particles in the noninteracting system. Only parameters as the mass are renormalized. Hence in 3D, interacting fermions can be mapped onto a noninteracting Fermi gas. Especially also the existence of a well defined Fermi surface at energy E_F should be unaffected by particle-particle correlations. The stability of the Fermi surface in the presence of interactions is reflected in a discontinuity in the single particle momentum distribution $n(k)$ at $T = 0$ (for a noninteracting Fermi gas the momentum distribution at zero temperature is of course given by the step function $\Theta(k_F - |\vec{k}|)$, with the Fermi wave number k_F). Indeed the jump in the function $n(k)$ at the Fermi energy can be derived for 3D systems [27]. In this respect the applicability of Fermi liquid theory in 1D becomes questionable as already a perturbative calculation of $n(k)$ up to second order for interacting spinless fermions on a ring leads to a continuous expression [28, 29, 30]. This finding indicates that the Fermi liquid quasiparticles are no stable excitations in 1D.

But what are the low energy excitations of interacting fermions in 1D? To answer this question it is important to notice that around the Fermi points of a 1D system we can always linearize the dispersion relation. This means that all particle-hole excitations with a certain momentum q have the same energy ε_q and hence the same propagation velocity, see Fig. 2.0.1. Thus it is tempting to consider all particle-hole excitations associated with a fixed q as *one* collective excitation. It was already realized by Tomonaga in 1950 [11] that this new quasiparticles are bosonic in nature. Of course this kind of excitations also exists in 3D. But, as realized by Tomonaga and as we are going to proof in Appendix B for metallic SWNTs, in 1D they represent a complete basis of the Hilbert space containing all possible particle hole excitations!

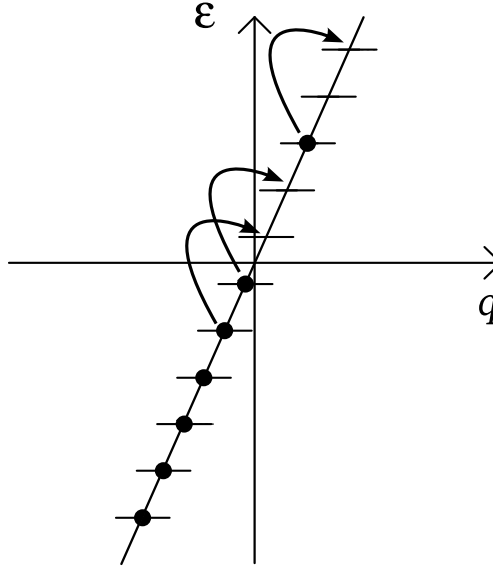


FIGURE 2.0.1. Excitations in a fermionic 1D system. All particle-hole excitations with a certain momentum q have the same energy ε_q .

For this very reason it is possible to rewrite the Hamiltonian for a system of interacting fermions in terms of bosonic operators. It is interesting to note here that at the time of the publication, Tomonaga himself considered his discussion of 1D systems as [11] “of rather mathematical nature without entering into real physical problems.”

Restricting the discussion to density-density interactions, the form of the resulting Hamiltonian is quadratic in bosonic operators, the so called Tomonaga-Luttinger model. Hence in this case the seemingly complex many body problem of interacting electrons can be easily solved once the theory has been bosonized. In analogy to the Fermi liquid theory it has been established that at low excitation energies the physics of interacting fermions in 1D is captured by the Luttinger liquid (LL) theory [31], a simplified version of the Tomonaga-Luttinger model: The interactions result merely in the energy renormalization of certain collective excitations, described by a single parameter g .

Deviations from the LL theory are found in systems with low densities where the interaction energy exceeds the kinetic energy by far [32], as well as in the vicinity of half-filling where, as we will show in Section 2.5.4, umklapp processes of non-density-density form of considerable strength become relevant. In one-dimensional metallic systems of infinite length the effect of umklapp scattering is the opening of a gap in the bosonic excitation spectrum, the so called Mott metal-insulator transition, see e.g. [14, 33, 34]. As we are going to demonstrate in this chapter, interaction effects not contained in the LL theory can also result from the fact that real condensed matter systems that can be considered as strictly 1D in momentum space actually do have a 3D extension in position space.

It should be emphasized that only the possibility of reexpressing also the electron operators in terms of the bosonic operators, discovered by Haldane [12], leads to the great predictive power of bosonization, as it is necessary in order to determine measurable physical properties of the system via the calculation of correlation functions or general matrix elements between eigenstates of the 1D system. In the course of this thesis we will make extensive use of this so called bosonization identity.

For detailed reviews about correlated fermions in 1D and bosonization we refer to [33, 34, 35].

2.1. What is special about interacting SWNTs

With respect to metallic SWNTs it was realized in the seminal theoretical works [13, 14] that due to the 1D nature of the electrons, correlations have to be described within the LL picture. The accompanying occurrence of power-laws for various transport properties could indeed be observed experimentally [15, 16]. Electron-electron interactions in finite-size SWNTs were treated by Kane et al. [17], where the discrete energy spectrum was derived within the Tomonaga-Luttinger model. Since the electrons in SWNTs exhibit additionally to the spin also an orbital degree of freedom, the pseudo spin r from Chapter 1, it has been found that the excitations which are of bosonic nature can be divided into four instead of two different types, related to total and relative (with respect to the pseudo spin) spin and charge excitations. The most striking effect of the repulsive Coulomb interaction is that the total charge mode has strongly enhanced excitation energies and an accordingly enlarged propagation velocity compared to the remaining three excitations. This very specific feature of interacting 1D systems has become famous as spin-charge separation. A direct experimental verification of this phenomenon has been achieved for SWNTs [37] and also for 1D wires in a GaAs/AlGaAs heterostructure [36].

As already mentioned, at low energies the electrons in SWNTs are strictly confined in a 1D momentum space due to quantization around the circumference of the tube, however their wave functions live in a 3D position space. As a consequence of the special structure of the honeycomb lattice of SWNTs this leads to short ranged interaction processes which are *not* accounted for in the LL theory. The role of those so called non-forward scattering parts of the Coulomb interaction has only been discussed for SWNTs of infinite length by renormalization group techniques [13, 14]. In [13] deviations from conventional LL behaviour have been found only for very small temperatures $T \lesssim 0.1$ mK provided that the interaction is long ranged. The work of Yoshioka and Odintsov [14] additionally took into account the situation at half filling where, as already mentioned, the formation of a Mott insulating state was predicted. In the works treating electron-electron interactions in finite size SWNTs within the bosonization formalism, the effect of non-forward scattering and hence of non-density-density processes has been neglected completely so far. This approximation leading to a Tomonaga-Luttinger model for SWNTs we will call the “standard” theory in the following. In the case of SWNTs it is valid if moderate to large diameter tubes ($\varnothing \gtrsim 1.5$ nm) are considered [17], or if finite size effects can be neglected since the relevant energies exceed the level spacing of the SWNT as in the experiments [15, 16]. Recent experiments [18, 38, 20] however, have found exchange effects in the

ground state spectra of small diameter tubes which can not be explained using the “standard” bosonization theory for interacting SWNTs, see Fig. 2.1.1. Oreg et al. [19] have presented a mean-field Hamiltonian for the low energy spectrum of SWNTs including an exchange term favouring the spin alignment of electrons in different bands. The values for the exchange splitting observed in the experiments agree well with the mean-field predictions. However, the mean field approach does not allow for the mixing of states with a different shell filling, i.e., of states with a different number of electrons with certain spin and pseudo spin quantum numbers, and therefore fails to describe important interaction processes. Moreover, in contrast to the bosonization procedure it can not predict the correct excitations spectrum because it completely misses the effect of the long ranged part of the Coulomb interaction responsible for the LL behaviour.

In this thesis we go beyond the mean field approach, deriving a low-energy¹ many-body Hamiltonian for finite size metallic SWNTs, thereby including for the first time *all* relevant interaction processes. This allows us to identify the microscopic mechanisms that lead to the various exchange effects seen in experiments and to predict new features not observed so far. Moreover the occurrence of further finite size effects like the quantization of charge and energy levels arises naturally from our approach. An interesting situation occurs near half-filling since there additional processes become relevant which can not be considered as small compared to the dominating forward scattering terms. Unfortunately, we have not found a reliable way of diagonalizing the Hamiltonian in that situation so far.

Using bosonization we determine the spectrum and eigenstates of the SWNT Hamiltonian. For this purpose we collect all the parts of the Hamiltonian which can be described by a Tomonaga-Luttinger type of Hamiltonian and we diagonalize the resulting Hamiltonian using standard techniques from the bosonization formalism. Of the remaining terms we will calculate the matrix elements in the eigenbasis of the Tomonaga-Luttinger Hamiltonian and diagonalize the total Hamiltonian in a truncated basis.

Concerning the ground state properties, we find under the condition of degenerate bands, a spin 1 triplet as ground state if $4m + 2$ electrons occupy the nanotube. This is insofar remarkable as a fundamental theorem worked out by Lieb and Mattis [39] states for any single-band Hubbard model in 1D with nearest-neighbour hopping that the ground state can only have spin 0 or $1/2$. However, at the end of their article they explicitly pose the question whether ground states with higher spin could be realized in 1D systems with orbital degeneracy, which in the case of SWNTs is present due to the substructure of the underlying honeycomb lattice. Our findings answer this question with yes, hence proving that the theorem by Lieb and Mattis can not be generalized to multi-band systems. Moreover, it is interesting to note that all of the processes favouring higher spin states in SWNTs involve non-forward scattering with respect to the *orbital* degree of freedom. On the experimental side an exchange splitting in the low

¹Low energy here means that we consider only electrons residing in the subbands touching at the Fermi level of a uncharged SWNT. For typical SWNTs this corresponds to an energy range of about 1eV around the charge neutrality point where the energy dispersion of the noninteracting system is linear. Concerning the thermal energy $k_B T$, 1eV corresponds to a temperature of approximately $10^4 K$.

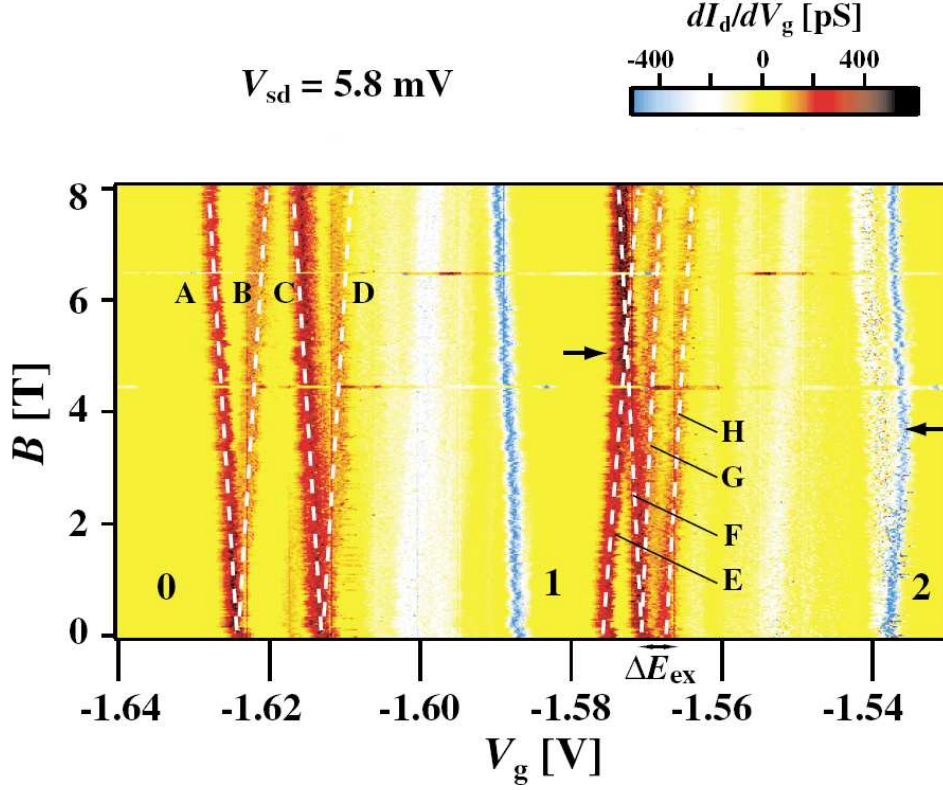


FIGURE 2.1.1. Transport measurement on a SWNT in a magnetic field B , from [18]. Shown is the differential conductance dI/dV_g as a function of the gate voltage V_g at fixed bias voltage V_b . Lines indicate changes in the current which are either due to new states becoming available for transport ($dI/dV_g > 0$) as V_g is increased or states dropping out of the transport window ($dI/dV_g < 0$). Of special interest here are the lines E to H related to states of a SWNT occupied by $4m + 2$ electrons. E corresponds to the singlet ground state, F and G to a triplet state that is Zeeman split for finite B (one might expect three lines for the triplet but one transition is not allowed) and H to a singlet state again. According to the standard theory, the lines F to H should meet at $B = 0$.

energy spectrum of the $4m + 2$ charge state has indeed been observed [18, 38, 20]. However, all the experiments demonstrating exchange splitting were carried out for SWNTs with a large band mismatch such that the ground states are supposed to be spin 0 singlets. Especially Moriyama et al. have proven that this is the case in their experiments [18] by carrying out magnetic field measurements, cf. Fig. 2.1.1. Thus, the threefold degenerate spin 1 ground state has not been observed yet, since its occurrence requires a band mismatch that is small compared to the exchange energy. Additionally to the ground state properties of metallic SWNTs we have also determined the

excitation spectra. We find that the huge degeneracies as obtained by only retaining the forward scattering processes are partly lifted and the spectrum becomes more and more continuous when going to higher energies. Finally this leads to a lifting of the spin-charge separation predicted by the “standard” theory.

The outline of the remaining of this chapter is the following. Based on our examination of the low energy physics of noninteracting electrons in finite size metallic SWNTs in Chapter 1 we include the Coulomb interaction and derive the effectively one-dimensional Hamiltonian for the low energy regime in Section 2.2. The analysis of the effective 1D interaction potential in Section 2.3 allows us to sort out the irrelevant interaction processes. The remaining interaction terms are either of density-density or non-density-density form. Before diagonalizing the obtained Hamiltonian we introduce the powerful bosonization formalism in Section 2.4.

The density-density part of the interaction we diagonalize together with the kinetic part of the Hamiltonian by bosonization and by applying the Bogoliubov transformation in Section 2.5.3. Using the obtained eigenstates as basis we calculate the corresponding matrix elements for the non-density-density part of the interaction with the help of the bosonization identity of the electron operators, Section 2.5.4. In Section 2.5.5 we calculate the ground state and excitation spectra by diagonalizing the Hamiltonian including the non-density-density processes in a truncated basis and discuss the results.

2.2. Coulomb interaction in metallic SWNTs

In this section we derive the exact form of the electron-electron interaction in metallic SWNTs. As announced in Chapter 1 we focus on armchair tubes. This we can do without loss of generality, since, as shown in [24], electron-electron interactions are universal for all types of metallic SWNTs. According to the 1D nature of SWNTs we will show how to express the Coulomb potential in terms of an effective 1D interaction potential. Though, the actual 3D structure of a nanotube lattice will still be reminiscent. A detailed discussion of this point will clarify in Section 2.3 which of the possible interaction scattering processes are indeed non-vanishing. We start with the general expression for the Coulomb interaction in second quantization,

$$V = \frac{1}{2} \sum_{\sigma\sigma'} \int d^3r \int d^3r' \Psi_{\sigma}^{\dagger}(\vec{r}) \Psi_{\sigma'}^{\dagger}(\vec{r}') U(\vec{r} - \vec{r}') \Psi_{\sigma'}(\vec{r}') \Psi_{\sigma}(\vec{r}), \quad (2.2.1)$$

where $U(\vec{r} - \vec{r}')$ is the possibly screened Coulomb potential. For the actual calculations we model $U(\vec{r} - \vec{r}')$ by the so called Ohno potential which takes into account the localized character of the p_z orbitals; it interpolates between U_0 , the interaction energy between two p_z electrons in the same orbital for $\vec{r} = \vec{r}'$ and $\frac{e^2}{4\pi\epsilon_0\epsilon|\vec{r} - \vec{r}'|}$ for large values of $|\vec{r} - \vec{r}'|$. Measuring distances in units of Å and energy in eV, it is given by [40]

$$U(\vec{r} - \vec{r}') = U_0 / \sqrt{1 + (U_0\epsilon|\vec{r} - \vec{r}'|/14,397)^2} \text{ eV}. \quad (2.2.2)$$

In our case a reasonable choice is $U_0 = 15 \text{ eV}$ [41]. The dielectric constant for SWNTs is expected to be in the range $\epsilon \approx 1.4 - 2.4$ [13].

In order to reduce the dimensions of the problem from three to one, we reexpress the 3D electron operators $\Psi_{\sigma}(\vec{r})$ from (2.2.1) in terms of the 1D operators $\psi_{rF\sigma}(x)$,

cf. equation (1.4.27). After integrating over the coordinates perpendicular to the tube axis, we obtain a truly 1D description of the interaction,

$$V = \frac{1}{2} \sum_{\sigma\sigma'} \sum_{\{[r],[F]\}} \text{sgn}(F_1 F_2 F_3 F_4) \int dx \int dx' U_{[r][F]}(x, x') \times \psi_{r_1 F_1 \sigma}^\dagger(x) \psi_{r_2 F_2 \sigma'}^\dagger(x') \psi_{r_3 F_3 \sigma'}(x') \psi_{r_4 F_4 \sigma}(x), \quad (2.2.3)$$

where $\sum_{\{[r],[F]\}}$ denotes the sum over all quadruples $[r] = (r_1, r_2, r_3, r_4)$ and $[F] = (F_1, F_2, F_3, F_4)$. Under the assumption — justified by the localized character of the p_z orbitals — that the Bloch waves on the different sublattices $\varphi_{pF}(\vec{r})$ and $\varphi_{-pF}(\vec{r})$ do not overlap, i.e., $\varphi_{pF}(\vec{r})\varphi_{-pF}(\vec{r}) \equiv 0$, our procedure leads to the following effective 1D interaction potential $U_{[r][F]}(x, x')$ in (2.2.3),

$$U_{[r][F]}(x, x') = L^2 \int d^2 r_\perp \int d^2 r'_\perp \sum_{p,p'} f_{pr_1} f_{p'r_2} f_{p'r_3} f_{pr_4} \times \varphi_{pF_1}^*(\vec{r}) \varphi_{p'F_2}^*(\vec{r}') \varphi_{p'F_3}(\vec{r}') \varphi_{pF_4}(\vec{r}) U(\vec{r} - \vec{r}'). \quad (2.2.4)$$

Using relation (1.4.18) for the coefficients f_{pr} and performing the sum over p, p' , we can separate $U_{[r][F]}$ into a part describing the interaction between electrons living on the same (intra) and on different (inter) sublattices,

$$U_{[r][F]}(x, x') = \frac{1}{4} \left[U_{[F]}^{intra}(x, x')(1 + r_1 r_2 r_3 r_4) + U_{[F]}^{inter}(x, x')(r_2 r_3 + r_1 r_4) \right], \quad (2.2.5)$$

where

$$U_{[F]}^{intra/inter}(x, x') = L^2 \int \int d^2 r_\perp d^2 r'_\perp \times \varphi_{pF_1}^*(\vec{r}) \varphi_{\pm pF_2}^*(\vec{r}') \varphi_{\pm pF_3}(\vec{r}') \varphi_{pF_4}(\vec{r}) U(\vec{r} - \vec{r}'). \quad (2.2.6)$$

Here $\int \int d^2 r_\perp d^2 r'_\perp$ denotes the integration over the coordinates perpendicular to the tube axis. Note that the 3D extension of the considered SWNT enters the effective 1D interaction potential via equation (2.2.6). The interaction potentials $U_{[F]}^{intra}$ and $U_{[F]}^{inter}$ are completely symmetric with respect to the two sublattices and thus do not depend on the actual choice of p in (2.2.6). For the subsequent discussion of the non-vanishing interaction processes it will be of importance that the intra- and inter-lattice interaction potentials only differ considerably on small length scales $|x - x'| \lesssim a_0$ [13]. The reason for this is quite simple: Consider two atoms at sites \vec{r} and \vec{r}' on a SWNT lattice with $|x - x'| \lesssim a_0$. Then the distance between the two atoms (and hence the strength of the Coulomb interaction between p_z electrons from those two atoms) will strongly depend on whether or not both atoms are from the same sublattice or not. Whereas for large $|x - x'| \gg a_0$ the distance between both atoms will be insensitive to the sublattice structure and will be approximately given by $|x - x'|$. In Appendix D we show how we actually determine the values for the potentials $U_{[F]}^{intra/inter}(x, x')$ for specific SWNTs.

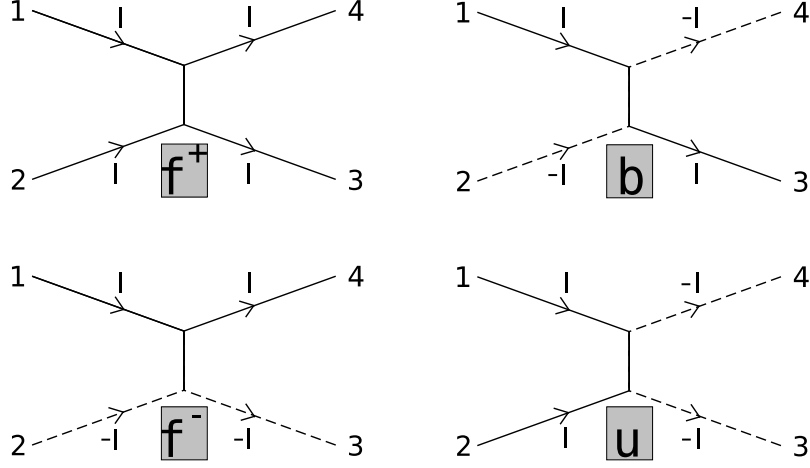


FIGURE 2.3.1. The relevant scattering processes. Forward/back/umklapp scattering are denoted by $f^\pm/b/u$. The index I represents one of the three degrees of freedom r, F, σ (branch, Fermi point and spin, respectively).

2.3. The relevant scattering processes

Not all of the terms in (2.2.3) contribute to the interaction because the corresponding potential $U_{[r][F]}$ vanishes or has a very small amplitude. In order to pick out the relevant terms, it is convenient to introduce the notion of forward (f)-, back (b)- and umklapp (u)- scattering with respect to an arbitrary index quadruple $[I] = (I_1, I_2, I_3, I_4)$ associated to the electron operators in (2.2.3). Denoting the scattering type by S_I we write $[I]_{S_I=f^\pm}$ for $[I, \pm I, \pm I, I]$. Furthermore we use $[I]_{S_I=b}$ for $[I, -I, I, -I]$ and $[I]_{S_I=u}$ is equivalent to $[I, I, -I, -I]$, cf. Fig. 2.3.1. Keeping only the relevant terms, the interaction part of the Hamiltonian acquires the form,

$$V = \sum_{S_r=f,b,u} \sum_{S_F=r,b} \sum_{S_\sigma=f} V_{S_r S_F S_\sigma}, \quad (2.3.1)$$

where

$$V_{S_r S_F S_\sigma} := \frac{1}{2} \sum_{\{[r]_{S_r}, [F]_{S_F}, [\sigma]_{S_\sigma}\}} \int \int dx dx' U_{[r][F]}(x, x') \times \psi_{r_1 F_1 \sigma}^\dagger(x) \psi_{r_2 F_2 \sigma'}^\dagger(x') \psi_{r_3 F_3 \sigma'}(x') \psi_{r_4 F_4 \sigma}(x), \quad (2.3.2)$$

as we are going to demonstrate in the following. Similarly to before the summation $\sum_{\{[r]_{S_r}, [F]_{S_F}, [\sigma]_{S_\sigma}\}}$ extends over all quadruples $[r], [F]$ and $[\sigma]$ corresponding to the scattering types S_r, S_F and S_σ respectively.

Relevant scattering processes of r . We start with an examination of the possible scattering events related to the pseudo spin r . From (2.2.5) we can immediately read off that the interaction potential $U_{[r][F]}$ does not vanish only if $r_2 r_3 = r_1 r_4$. Thus we find the following cases determining the relevant scattering types,

$$i) \ r_1 = r_4, \ r_2 = r_3, \quad ii) \ r_1 = -r_4, \ r_2 = -r_3.$$

Relation $i)$ summarizes all the forward scattering processes with respect to r and the associated interaction potential is proportional to the sum of intra- and inter- lattice interaction,

$$U_{[r]f[F]}(x, x') = \frac{1}{2} \left[U_{[F]}^{intra}(x, x') + U_{[F]}^{inter}(x, x') \right] =: U_{[F]}^+(x, x'). \quad (2.3.3)$$

Case $ii)$ includes all $S_r = b$ and $S_r = u$ processes and the interaction potential is proportional to the difference between $U_{[F]}^{intra}$ and $U_{[F]}^{inter}$,

$$U_{[r]b/u[F]}(x, x') = \frac{1}{2} \left[U_{[F]}^{intra}(x, x') - U_{[F]}^{inter}(x, x') \right] =: U_{[F]}^\Delta(x, x'). \quad (2.3.4)$$

As we already know, $U_{[F]}^{intra}$ and $U_{[F]}^{inter}$ only differ on small length scales $|x - x'| \lesssim a_0$. This means that in general $U_{[F]}^\Delta(x, x')$ is a short ranged interaction.

Scattering of F . The determination of the essential scattering processes with respect to F can be achieved by exploiting the approximate conservation of quasi momentum. Looking at expression (1.4.12) for the wave functions $\varphi_{pF}(\vec{r})$, we find from equation (2.2.6) that the interaction potentials $U_{[F]}^{intra}$ and $U_{[F]}^{inter}$ contain phase factors of the form $e^{-i(F_1 - F_4)R_x} e^{-i(F_2 - F_3)R'_x}$. Although we are considering a finite system, therefore not having perfect translational symmetry, after the integration along the tube axis in (2.2.3), only terms without fast oscillations survive². The corresponding condition is given by

$$F_1 - F_4 + F_2 - F_3 = 0, \quad (2.3.5)$$

that means only the $S_F = f$ and $S_F = b$ terms remain. We have explicitly checked that due to the discrete nature of the SWNT lattice also the $S_F = u$ processes have very small amplitudes and can be neglected. Note that condition (2.3.5) leads to $\text{sgn}(F_1 F_2 F_3 F_4) = 1$ in (2.2.3).

Scattering of σ . It is clear that with respect to the spin only forward scattering, i.e., $S_\sigma = f$, is allowed, since the Coulomb interaction is spin independent.

Altogether, the previous considerations proof equation (2.3.1).

²For a perfectly translational invariant 1D system it holds

$$\int_0^L dx' \int_0^L dx U(x-x') e^{ikx} e^{ik'x'} = \int_0^L dx' \int_{-x'}^{L-x'} dy U(y) e^{iky} e^{i(k+k')x'} = \tilde{U}_k \int_0^L dx' e^{i(k+k')x'},$$

where $\tilde{U}_k = \int_{-x'}^{L-x'} dy U(y) e^{iky}$ does not depend on x' because of the translational invariance. So it is clear that the double integral vanishes unless $k + k' \approx 0$.

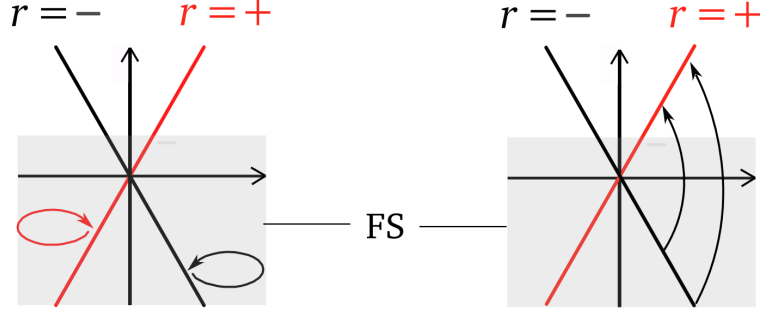


FIGURE 2.3.2. Examples of \vec{N} conserving and \vec{N} non-conserving processes deep inside the Fermi sea (FS). In the former case (left side) processes with vanishing excitation energy are possible, whereas in the latter case (left side) such processes are inevitably connected with a huge excitation energy.

2.3.1. Processes conserving or not conserving the fermionic configuration.

From the discussion in Chapter 1 we already know that we have to distinguish between electrons with different spin σ and pseudo spin r . In the following we will denote the number of electrons of a certain species by $N_{r\sigma}$ and we will refer to the quantity $\vec{N} = (N_{+\uparrow}, N_{+\downarrow}, N_{-\uparrow}, N_{-\downarrow})$ as *fermionic configuration*. Not all of the scattering processes in (2.3.1) conserve \vec{N} . In more detail, for terms with $(S_r, S_\sigma) = (u, f^+)$, $(S_r, S_\sigma) = (b, f^-)$ and $(S_r, S_\sigma) = (u, f^-)$ \vec{N} is not a good quantum number as it can be easily verified by using equation (2.3.2). In general, only processes described by the \vec{N} conserving terms are sensitive to the total number of electrons in the dot. As example we mention the charging energy contribution proportional to N_c^2 , $N_c := \sum_{r\sigma} N_{r\sigma}$ arising from the $(S_r, S_F, S_\sigma) = (f, f, f)$ processes explicitly appearing later on in the interaction Hamiltonian. On the other hand for the \vec{N} non-conserving terms, only the vicinity of the Fermi surface is of relevance. The physical reason is that due to the Pauli principle and the large number of states below the Fermi surface, \vec{N} non-conserving processes depending on all the occupied states of a certain branch $r\sigma$ would correspond to an extremely huge *excitation* energy by far exceeding the low energy regime we are considering, cf. Fig. 2.3.2.

2.3.2. Processes only relevant near half-filling. Away from half-filling we find that terms with

$$r_1 F_1 + r_2 F_2 - r_3 F_3 - r_4 F_4 \neq 0, \quad (2.3.6)$$

i.e., the umklapp scattering terms with respect to the product rF ³ can be neglected in (2.2.3). For the \vec{N} non-conserving terms fulfilling (2.3.6) this is a consequence of the approximate conservation of quasi momentum, arising from the slow oscillations of the 1D electron operators in (2.3.2) which near the Fermi surface are given by the

³There are simple rules for determining the scattering type S_{rF} if S_r and S_F are known. Defining a product by $S_{rF} = S_r S_F = S_F S_r$ it holds, $S f^+ = S$; $S^2 = f^+$; $f^- u = b$; $f^- b = u$ and $ub = f^-$.

exponential

$$e^{-i[(r_1 F_1 N_{r_1 \sigma_1} - r_4 F_4 N_{r_4 \sigma_4})x + (r_2 F_2 N_{r_2 \sigma_2} - r_3 F_3 N_{r_3 \sigma_3})x']},$$

After performing the integrations in (2.3.2) this leads approximately to (2.3.6). The \vec{N} conserving terms obeying (2.3.6), V_{f-bf} and V_{bf-f+} , which describe not only processes near the Fermi level, add a term proportional to the number of electrons above half-filling to the Hamiltonian, therefore just giving rise to a shift of the chemical potential.

2.3.3. Long ranged vs. short ranged interactions. Another property which can be used to classify the various scattering processes is their interaction range. Except of $U_{[r]_f[F]_f} = U_{[F]_f}^+$, all relevant interaction potentials $U_{[r][F]}$ can effectively be treated as local interactions: In the case of $U_{[F]_b}^+$ this is due to the appearance of phase factors $e^{i2F(R_x - R'_x)}$ in (2.2.6), arising from the Bloch waves $\varphi_{pF}(\vec{r})$, cf. equation (1.4.12), oscillating much faster than the electron operators $\psi_{r\sigma F}(x)$. The potentials $U_{[F]}^\Delta$, being proportional to the difference of the inter- and intra-lattice interaction potentials, are in general short ranged, since as we have already discussed subsequently to equation (2.2.6), $U_{[F]}^{intra}(x, x')$ and $U_{[F]}^{inter}(x, x')$ only have considerably differing values for $|x - x'| \lesssim a_0$. Summarizing, *only the processes with $(S_r, S_F) = (f, f)$ are long ranged*. All other terms can effectively be written as local interactions. That is, for $(S_r, S_F) \neq (f, f)$ we can replace equation (2.2.4) by the approximation

$$\frac{1}{2}U_{[r]_{S_r}[F]_{S_F}}(x, x') \approx Lu_{S_r S_F} \delta(x - x'), \quad (2.3.7)$$

where we have introduced the coupling parameters

$$u_{S_r S_F} := 1/(2L^2) \int \int dx dx' U_{[r]_{S_r}[F]_{S_F}}(x, x'). \quad (2.3.8)$$

Using the approximation (2.3.7) we obtain from (2.3.2) in the case $(S_r, S_F) \neq (f, f)$ the following expression for the non-forward scattering interaction terms,

$$V_{S_r S_F S_\sigma} \approx Lu_{S_r S_F} \sum_{\{[r]_{S_r}, [F]_{S_F}, [\sigma]_f\}} \times \int_0^L dx \psi_{r_1 F_1 \sigma}^\dagger(x) \psi_{r_2 F_2 \sigma'}^\dagger(x) \psi_{r_3 F_3 \sigma'}(x) \psi_{r_4 F_4 \sigma}(x). \quad (2.3.9)$$

Let us introduce the abbreviations $u^+ := u_{fb}$ and $u_{S_F}^\Delta := u_{bS_F} = u_{uS_F}$. For details about calculating the values of those coupling constants for a specific SWNT, see Appendix D. We find that in general the coupling constants u^+ and $u_{S_F}^\Delta$ scale inversely with the total number of lattice sites, i.e., like $1/Ld$, where d is the tube diameter. From a physical point of view this is due to an increasing attenuation of the wave functions for a growing system size such that short ranged interaction become less effective⁴. Because the level spacing of the noninteracting system ε_0 scales like $1/L$, cf. (1.4.24),

⁴Consider e.g. the classical Hartree energy E_H of a homogeneous density on a tube, $n(\vec{x}) = N_c/Ld$, $\vec{x} = (x, y)$ for a δ -function like interaction potential $U_\delta(\vec{x}) = u\delta(\vec{x})$. Then it holds $E_H = \int d^2x \int d^2x' n(\vec{x})U_\delta(\vec{x} - \vec{x}')n(\vec{x}') = uN_c^2/Ld$, i.e., E_H scales like the system size.

	$\frac{u^+ d}{\epsilon_0}$	$\frac{u_f^\Delta d}{\epsilon_0}$	$\frac{u_b^\Delta d}{\epsilon_0}$
$\epsilon = 1.4$	0.22 Å	0.14 Å	0.22 Å
$\epsilon = 2.4$	0.28 Å	0.22 Å	0.28 Å

TABLE 1. The dependence of the coupling constants u^+ , u_f^Δ and u_b^Δ on the tube diameter d and on the dielectric constant ϵ .

the products $u^+ d/\epsilon_0$ and $u_{S_F}^\Delta d/\epsilon_0$ are constants. The corresponding numerical values for different dielectric constants ϵ , cf. equation (2.2.2), are given in table 1.

2.3.4. Density-density vs. non-density-density processes . The interaction processes can furthermore be divided into density-density terms — easily diagonalizable by bosonization as we will see — and non-density-density terms, respectively. It is clear that the forward scattering interaction

$$V_{f f f} = \frac{1}{2} \sum_{r r'} \sum_{F F'} \sum_{\sigma \sigma'} \int \int dx dx' U_{[F]f}^+(x, x') \psi_{r F \sigma}^\dagger(x) \psi_{r' F' \sigma'}^\dagger(x') \psi_{r' F' \sigma'}(x') \psi_{r F \sigma}(x)$$

is of density-density form, since with the densities

$$\rho_{r F \sigma}(x) = \psi_{r F \sigma}^\dagger(x) \psi_{r F \sigma}(x)$$

we obtain

$$V_{f f f} = \frac{1}{2} \sum_{r r'} \sum_{F F'} \sum_{\sigma \sigma'} \int \int dx dx' U_{[F]f}^+(x, x') \rho_{r F \sigma}(x) \rho_{r' F' \sigma'}(x'). \quad (2.3.10)$$

But since we treat the short ranged interactions as local, also $V_{f^+ b f^+}$,

$$\begin{aligned} V_{f^+ b f^+} &= L u^+ \sum_{r \sigma F} \int_0^L dx \psi_{r F \sigma}^\dagger(x) \psi_{r-F \sigma}^\dagger(x) \psi_{r F \sigma}(x) \psi_{r-F \sigma}(x) \\ &= -L u^+ \sum_{r \sigma F} \int_0^L dx \rho_{r F \sigma}(x) \rho_{r-F \sigma}(x), \end{aligned} \quad (2.3.11)$$

and similarly $V_{b f^+ / b f^+}$,

$$V_{b f^+ / b f^+} = -L u_{f/b}^\Delta \sum_{r \sigma F} \int_0^L dx \rho_{r F \sigma}(x) \rho_{-r \pm F \sigma}(x), \quad (2.3.12)$$

are density-density interactions. In total the density-density part of the interaction therefore is given by

$$V_{\rho\rho} = V_{f f f} + V_{f^+ b f^+} + V_{b f^+ f^+} + V_{b b f^+}. \quad (2.3.13)$$

The remaining terms are not of density-density form and are collected in the operator $V_{n\rho\rho}$. Including only the contributions relevant away from half-filling, we obtain,

$$V_{n\rho\rho} = V_{f^+ b f^-} + V_{b f^+ f^-} + V_{b b f^-} + V_{u f^- f} + V_{u b f}. \quad (2.3.14)$$

Near half-filling additionally the processes

$$V_{f-bf}, V_{bf-f} \text{ and } V_{uf+f-}, \quad (2.3.15)$$

satisfying condition (2.3.6), contribute to $V_{n\rho\rho}$. Overall, the SWNT Hamiltonian acquires the form

$$H = H_0 + V_{\rho\rho} + V_{n\rho\rho}. \quad (2.3.16)$$

2.4. Interlude: The bosonization formalism

Before we continue our examination of the low energy physics of SWNTs we have to introduce *the* method of choice for the treatment of interacting electrons in 1D: bosonization. It will be the key tool that will enable us to perform main parts of the remaining calculations in this thesis. In general bosonization means rewriting a fermionic theory i.e., a theory in terms of fermionic creation and annihilation operators, as a theory whose excitations are described by bosonic operators. Since Fermi liquid theory is not applicable to correlated 1D systems of fermions as we have explained in the introduction to this chapter, bosonization has become the key technique for the low-energy treatment of those systems.

In this section we will give a short summary about the most important aspects and relations of the so called constructive bosonization approach, introduced by Haldane [12] and reviewed in great detail by von Delft and Schoeller [35, 29, 30]. This theory provides an exact bosonization identity for the 1D electron operators $\psi_{rF\sigma}(x)$ in Fock space, since it assures that $\psi_{rF\sigma}^\dagger$ and $\psi_{rF\sigma}$ have the correct creation/annihilation properties of fermionic operators. This is crucial for the discussion of systems with a finite number of particles.

2.4.1. Extension of the Fock space. In the discussion of the low energy physics of a noninteracting SWNT we have pointed out that we restrict ourselves to states in the vicinity of the Fermi points, i.e. to standing waves $\varphi_{r\kappa}$ with wave numbers $|\kappa| \ll K_0$. However, the bosonization approach requires a dispersion relation that is unbound from below. Therefore we artificially extend the $r = \pm$ branches to κ values ranging from $-\infty$ to ∞ thereby keeping the linearity of the dispersion relation over the whole range. To avoid unphysical contributions from the artificially added states, we have to make sure that states far below the Fermi level of the unbiased noninteracting system are always occupied, whereas states far above the Fermi level are strictly empty, i.e., we have to require

$$c_{r\sigma-\kappa_r}^\dagger = 0, \quad c_{r\sigma\kappa_r} = 0, \quad \kappa_r = r \cdot \kappa, \quad \kappa \gg 0.$$

As was already pointed out by Tomonaga, the extension of the dispersion relation is justified, if we assume the interaction to be long ranged enough. In this case the Fourier transform of the interaction potential has a cut-off κ_c , that lies within the interval of κ values of our original system. Thus, no excitations involving the new artificially added states occur. Since for SWNTs the main contribution to the electron-electron interaction is from long ranged forward scattering processes, Tomonaga's argument indeed holds in our case. In order to retain finite expressions for the energies of the system we use the groundstate $|FS\rangle$ of the undoped system as reference and measure energies henceforth relative to this state we are denoting as Fermi sea in the following.

More precisely we define $|FS\rangle$ via its properties

$$\begin{aligned} c_{r\sigma\kappa} |FS\rangle &= 0, & r\kappa > 0, \\ c_{r\sigma\kappa}^\dagger |FS\rangle &= 0, & r\kappa \leq 0. \end{aligned}$$

It will be useful to introduce normal ordering of the fermionic operators $c_{r\sigma\kappa}$ and $c_{r\sigma\kappa}^\dagger$ with respect to $|FS\rangle$,

$$:ABC...: := ABC... - \langle FS|ABC...|FS\rangle,$$

where $:ABC...:$ is an arbitrary product of fermionic operators.

2.4.2. The elementary bosonic operators. The starting point for the derivation of the bosonization formalism are the commutation relations for the Fourier components of the electron density operators $\rho_{rF\sigma}(x) = \psi_{rF\sigma}^\dagger(x)\psi_{rF\sigma}(x)$. Using the representation of the 1D electron operators in terms of the fermionic annihilation operators $c_{r\sigma\kappa}$, cf. equation (1.4.26), the electron densities can be written as

$$\begin{aligned} \rho_{rF\sigma}(x) &= \frac{1}{2L} \sum_{\kappa, q=-\infty}^{\infty} e^{i \operatorname{sgn}(F) qx} c_{r\sigma\kappa}^\dagger c_{r\sigma\kappa+q} \\ &=: \frac{1}{2L} \sum_{q=-\infty}^{\infty} e^{i \operatorname{sgn}(F) qx} \rho_{r\sigma q}, \end{aligned} \quad (2.4.1)$$

where we have defined

$$\rho_{r\sigma q} = \rho_{r\sigma-q}^\dagger = \sum_{\kappa=-\infty}^{\infty} c_{r\sigma\kappa}^\dagger c_{r\sigma\kappa+q}.$$

As shown explicitly in [35, 29] the commutation relations of the $\rho_{r\sigma q}$ operators resemble very much those of bosonic operators:

$$[\rho_{r\sigma q}, \rho_{r'\sigma'-q'}] = [\rho_{r\sigma q}, \rho_{r'\sigma'q'}^\dagger] = r n_q \delta_{rr'} \delta_{\sigma\sigma'} \delta_{q,q'}, \quad q = \frac{\pi}{L} n_q, \quad n_q \in \mathbb{Z}. \quad (2.4.2)$$

An explicit derivation of (2.4.2) can be found for example in [29, 35]. Equation (2.4.2) motivates us to define genuine bosonic operators $b_{r\sigma q}$ and $b_{r\sigma q}^\dagger$ by

$$b_{r\sigma q} := \frac{1}{\sqrt{n_q}} \rho_{r\sigma q_r} \quad (2.4.3)$$

$$= \frac{1}{\sqrt{n_q}} \sum_{\kappa} c_{r\sigma\kappa}^\dagger c_{r\sigma\kappa+q_r}, \quad q_r := r \cdot q, \quad q > 0. \quad (2.4.4)$$

Due to $\rho_{r\sigma q} = \rho_{r\sigma-q}^\dagger$ we obtain for the corresponding creation operators

$$b_{r\sigma q}^\dagger = \frac{1}{\sqrt{n_q}} \rho_{r\sigma-q_r}, \quad q > 0. \quad (2.4.5)$$

With (2.4.2), it is easily shown that the canonical bosonic commutation relations are valid for $b_{\sigma q}$ and $b_{\sigma q}^\dagger$:

$$[b_{r\sigma q}, b_{r'\sigma'q'}^\dagger] = \delta_{rr'} \delta_{\sigma\sigma'} \delta_{q,q'}. \quad (2.4.6)$$

Besides it is significant to notice, that $b_{r\sigma q}$ and $b_{r\sigma q}^\dagger$ commute with the zero modes of the density operators $\rho_{rF\sigma}$, namely the number counting operators $\mathcal{N}_{r\sigma}$,

$$[b_{r\sigma q}, \mathcal{N}_{r'\sigma'}] = 0. \quad (2.4.7)$$

NOTE. As pointed out in [35] the “deep reason” why bosonization works is the somewhat astonishing fact that the set of bosonic excitations

$$\left\{ \prod_{r\sigma q > 0} \frac{(b_{r\sigma q}^\dagger)^{m_{r\sigma q}}}{\sqrt{m_{r\sigma q}!}} \left| \vec{N}, 0 \right\rangle \right\} =: \left\{ \left| \vec{N}, \vec{m} \right\rangle \right\}, \quad (2.4.8)$$

forms a complete basis of the Hilbert space $\mathcal{H}_{\vec{N}}$ of states with a fixed fermionic configuration \vec{N} . For a noninteracting system the state $|\vec{N}, 0\rangle$ is the energetically lowest lying state in $\mathcal{H}_{\vec{N}}$ and has no particle-hole excitations, thus

$$b_{r\sigma q} |\vec{N}, 0\rangle = 0. \quad (2.4.9)$$

We will proof the completeness of the states $|\vec{N}, \vec{m}\rangle$ along the way when deriving the bosonization representation of the noninteracting Hamiltonian H_0 in Appendix B.

2.4.3. Bosonization identity of the 1D electron operators. In order to perform actual calculations within the bosonization formalism, especially determining matrix elements of the electron operators between states of the form $|\vec{N}, \vec{m}\rangle$, we will have to pass from a description of the 1D electron operators $\psi_{rF\sigma}(x)$ in terms of the fermionic operators $c_{r\sigma\kappa}$, cf. equation (1.4.26), to a representation in terms of the bosonic operators $b_{r\sigma q}$ and $b_{r\sigma q}^\dagger$. As we will derive explicitly for the interested reader in Appendix A, the so called bosonization identity reads

$$\psi_{rF\sigma}(x) = \eta_{r\sigma} K_{rF\sigma}(x) e^{i\phi_{rF\sigma}^\dagger(x)} e^{i\phi_{rF\sigma}(x)}. \quad (2.4.10)$$

The first operator $\eta_{r\sigma}$ on the right hand side (rhs) of (A.0.15) is the so called Klein factor. It takes care of the correct anticommutation relation for $\psi_{rF\sigma}(x)$. Acting on a state $|\vec{N}, \vec{m}\rangle$ it decreases the number of electrons in the $r\sigma$ branch by one and yields a sign factor expressing the fermionic nature of $\psi_{rF\sigma}(x)$:

$$\eta_{r\sigma} |\vec{N}, \vec{m}\rangle = T_{r\sigma\vec{N}} |\vec{N} - \vec{e}_{r\sigma}, \vec{m}\rangle, \quad (2.4.11)$$

where

$$T_{r\sigma\vec{N}} = \prod_{j=1}^{r\sigma-1} (-1)^{N_j}.$$

Here we use the convention $r\sigma = +\uparrow, +\downarrow, -\uparrow, -\downarrow = 1, 2, 3, 4$. Important relations for the Klein factors are

$$[\mathcal{N}_{r\sigma}, \eta_{r'\sigma'}] = -\delta_{rr'} \delta_{\sigma\sigma'} \eta_{r\sigma}, \quad (2.4.12)$$

$$[\mathcal{N}_{r\sigma}, \eta_{r'\sigma'}^\dagger] = \delta_{rr'} \delta_{\sigma\sigma'} \eta_{r\sigma}^\dagger, \quad (2.4.13)$$

$$\eta_{r\sigma} \eta_{r\sigma}^\dagger = \eta_{r\sigma}^\dagger \eta_{r\sigma} = 1. \quad (2.4.14)$$

The second operator on the rhs yields phase factor depending on \vec{N} , in more detail

$$K_{rF\sigma}(x) = \frac{1}{\sqrt{2L}} e^{i \frac{\pi}{L} \text{sgn}(F)(r\mathcal{N}_{r\sigma} + \Delta)x}. \quad (2.4.15)$$

Finally the operators $i\phi_{rF\sigma}(x)$ and $i\phi_{rF\sigma}^\dagger(x)$ contain the dependence of $\psi_{rF\sigma}(x)$ on the bosonic operators $b_{r\sigma q}$ and $b_{r\sigma q}^\dagger$:

$$i\phi_{rF\sigma}(x) = \sum_{q>0} \frac{e^{i\text{sgn}(F)qx}}{\sqrt{n_q}} b_{r\sigma q}. \quad (2.4.16)$$

The commutation relations of the bosonic fields $i\phi_{rF\sigma}(x)$ are given by

$$\begin{aligned} [i\phi_{rF\sigma}(x), i\phi_{r'\pm F\sigma'}(x')] &= 0, \\ [i\phi_{rF\sigma}^\dagger(x), i\phi_{r'\pm F\sigma'}(x')] &= \delta_{rr'} \delta_{\sigma\sigma'} \sum_{q>0} \frac{1}{n_q} e^{-i\text{sgn}(rF)q(x\mp x')} \\ &= -\delta_{rr'} \delta_{\sigma\sigma'} \ln(1 - e^{-i\text{sgn}(rF)\frac{x}{L}(x\mp x')}). \end{aligned}$$

In summary, we have introduced the bosonization formalism which enables us to reformulate a fermionic theory by passing over to a description in terms of bosonic excitations generated/annihilated by operators $b_{r\sigma q}^\dagger$ and $b_{r\sigma q}$. Additionally we also succeeded in expressing the 1D electron operators $\psi_{rF\sigma}(x)$ by means of the bosonic operators.

2.5. Bosonization and diagonalization of the interacting SWNT Hamiltonian

We resume our discussion of the low energy properties of SWNTs from Section 2.3 where we have found that the Hamiltonian of metallic SWNTs is of the form

$$H_0 + V_{\rho\rho} + V_{n\rho\rho}.$$

With help of the bosonization technique that we have presented in the previous section we are going to demonstrate that we can recast $H_0 + V_{\rho\rho}$ into a form that is bilinear in the bosonic operators $b_{r\sigma q}$ and $b_{r\sigma q}^\dagger$. Then, by introducing new bosonic operators via a Bogoliubov transformation, the Hamiltonian $H_0 + V_{\rho\rho}$ can be diagonalized.

Away from half-filling the operator $H_0 + V_{\rho\rho}$ is the dominating contribution to the total Hamiltonian H . Nevertheless $V_{n\rho\rho}$ leads to qualitatively new aspects in the low energy regime of SWNT, as discussed in the following. In order to examine the effect of $V_{n\rho\rho}$ on the electronic properties we are going to express $V_{n\rho\rho}$ in the eigenbasis of $H_0 + V_{\rho\rho}$. The subsequent diagonalization of $V_{n\rho\rho}$ in a truncated eigenbasis of $H_0 + V_{\rho\rho}$, discussed in Section 2.5.5, yields to a good approximation the correct eigenstates and the spectrum of the total Hamiltonian H .

2.5.1. Bosonization of H_0 . We start with the bosonization of H_0 . Measuring energies relative to the Fermi sea $|FS\rangle$ in order to avoid divergences due to the extension of the linear dispersion relation for the noninteracting system to infinity as discussed in Section 2.4, expression (1.4.23) for H_0 becomes

$$H_0 = \varepsilon_0 \sum_{r\sigma} r \sum_{n_\kappa=-\infty}^{\infty} n_\kappa : c_{r\sigma\kappa}^\dagger c_{r\sigma\kappa} : + \varepsilon_0 \Delta \sum_{r\sigma} r : \mathcal{N}_{r\sigma} :,$$

with the level spacing of the noninteracting system, $\varepsilon_0 = \hbar v_F \frac{\pi}{L}$. The bosonized expression for H_0 has been known for a long time [11], it reads

$$H_{0,\text{boson}} = \varepsilon_0 \sum_{r\sigma} \left(\sum_{q>0}^{\infty} n_q b_{rq\sigma}^\dagger b_{rq\sigma} + \frac{\mathcal{N}_{r\sigma}^2}{2} + r\varepsilon_\Delta \frac{\mathcal{N}_{r\sigma}}{2} \right). \quad (2.5.1)$$

Terms proportional to the total number of electrons in the SWNT have been omitted since they merely lead to a shift of the chemical potential. Additionally we have implicitly assumed normal ordering of the operators $\mathcal{N}_{r\sigma}$ and therefore have omitted the normal ordering symbol. The summand quadratic in $\mathcal{N}_{r\sigma}$ is a direct consequence of the Pauli principle: Adding new electrons to the system requires the occupation of higher and higher energy levels. Due to the linear dispersion relation the energy dependence of the shell filling is quadratic. The relation of the energy mismatch between the $r = +$ and $r = -$ band to Δ is given by

$$\varepsilon_\Delta := \begin{cases} 2\Delta\varepsilon_0, & |\Delta| \leq 1/4 \\ 2\Delta\varepsilon_0 - \text{sgn}(\Delta), & 1/4 < |\Delta| < 1/2 \end{cases}.$$

For the reader who wants to gain deeper insight into the relation between fermionic and bosonic excitations we present in Appendix B the equivalence of H_0 and $H_{0,\text{boson}}$, which by the way also demonstrates the completeness of the bosonic excitations mentioned in the introduction to bosonization, Section 2.4. More details can be found in Appendix B.

2.5.2. Bosonization of $V_{\rho\rho}$. The density-density part of the interaction,

$$V_{\rho\rho} = V_{ffff} + V_{f+bff} + V_{bf+ff} + V_{bbff},$$

can be bosonized in a straightforward way. Using (2.4.1) and (2.4.4), we find for the density operators ,

$$\rho_{rF\sigma}(x) = \frac{1}{2L} \sum_{q>0} \sqrt{n_q} \left(e^{i \text{sgn}(F) qrx} b_{rq\sigma} + e^{-i \text{sgn}(F) qrx} b_{rq\sigma}^\dagger \right) + \frac{1}{2L} \mathcal{N}_{r\sigma}. \quad (2.5.2)$$

Inserting (2.5.2) into expressions (2.3.10), (2.3.11) and (2.3.12), we obtain the bosonized versions of V_{ffff} , V_{f+bff} , V_{bf+ff} and V_{bbff} . For V_{ffff} this procedure leads to

$$\begin{aligned} V_{ffff} &= \frac{1}{2} \sum_{qq'>0} \sqrt{n_q n_{q'}} W_{qq'} \sum_{rr'} \sum_{\sigma\sigma'} \left(b_{rq\sigma} + b_{rq\sigma}^\dagger \right) \left(b_{r'\sigma'q'} + b_{r'\sigma'q'}^\dagger \right) \\ &+ \sum_{q>0} \sqrt{n_q} W_{q0} \sum_{r\sigma} \left(b_{rq\sigma} + b_{rq\sigma}^\dagger \right) \sum_{r'\sigma'} \mathcal{N}_{r'\sigma'} + \frac{1}{2} W_{00} \sum_{r\sigma} \mathcal{N}_{r\sigma} \sum_{r'\sigma'} \mathcal{N}_{r'\sigma'}, \end{aligned}$$

where the coupling constants $W_{qq'}$ are given by

$$W_{qq'} = \frac{1}{(2L)^2} \int \int dx dx' U_{[F]_f}^+(x, x') \sum_{FF'} e^{i \text{sgn}(F) qx} e^{i \text{sgn}(F') q' x'}.$$

For systems of infinite length, off-diagonal elements of $W_{qq'}$ are exactly 0. But also in the case of finite length nanotubes without translational invariance, the dominant contributions are given by W_{qq} and off-diagonal elements can be considered as irrelevant

[25]. Defining

$$W_q := W_{qq} = \frac{1}{(2L)^2} \int \int dx dx' U_{[F]_f}^+(x, x') \sum_{FF'} e^{iq(\text{sgn}(F)x + \text{sgn}(F')x')}$$

we arrive at

$$V_{f f f} = \frac{1}{2} \sum_{q>0} n_q W_q \sum_{rr'} \sum_{\sigma\sigma'} \left(b_{r\sigma q} + b_{r\sigma q}^\dagger \right) \left(b_{r'\sigma'q'} + b_{r'\sigma'q'}^\dagger \right) + \frac{1}{2} W_0 \mathcal{N}_c^2, \quad (2.5.3)$$

where $\mathcal{N}_c := \sum_{r\sigma} \mathcal{N}_{r\sigma}$ counts the total number of electrons in the SWNT. The first term on the right hand side of (2.5.3) describes bosonic excitations independent of the fermionic configuration of the system, whereas the second term denotes the so called charging energy taking into account the energy cost for adding an electron to the system as a consequence of the repulsive Coulomb interaction.

Let us now turn to the bosonization of

$$V_{f+ b f+} = -L u^+ \sum_{r\sigma F} \int_0^L dx \rho_{rF\sigma}(x) \rho_{r-F\sigma}(x).$$

In this case Fourier expansion (2.5.2) yields,

$$\begin{aligned} V_{f+ b f+} &= -\frac{u^+}{4L} \sum_{r\sigma F} \int_0^L dx \sum_{q,q'>0} \sqrt{n_q n_{q'}} \\ &\times \left(b_{r\sigma q} e^{i\text{sgn}(rF)qx} + b_{r\sigma q}^\dagger e^{-i\text{sgn}(rF)qx} \right) \\ &\times \left(b_{r\sigma q'} e^{-i\text{sgn}(rF)q'x} + b_{r\sigma q'}^\dagger e^{i\text{sgn}(rF)q'x} \right) - \frac{u^+}{2} \sum_{r\sigma} \mathcal{N}_{r\sigma}^2. \end{aligned} \quad (2.5.4)$$

Since $V_{f+ b f+}$ is a local interaction the conservation of pseudo momentum is exact, such that only the non-oscillating terms in (2.5.4) survive. For the same reason we have already omitted all products between the bosonic operators and the number counting operators. In total after the integration over x in (2.5.4) we are left with

$$V_{f+ b f+} = -\frac{u^+}{2} \left(\sum_{r\sigma q>0} n_q (b_{r\sigma q} b_{r\sigma q} + h.c.) + \sum_{r\sigma} \mathcal{N}_{r\sigma}^2 \right). \quad (2.5.5)$$

Note that the term $\sim \sum_{r\sigma} \mathcal{N}_{r\sigma}^2$ in $V_{f+ b f+}$ in total comes with a negative sign and hence is attractive in contrast to the shell filling energy in V_{fff} . Since in realistic SWNTs $\varepsilon_0 \gg u^+$, in total the cost for filling up more and more shells in a SWNT remains positive.

Analogously to V_{f+bf+} we obtain for the remaining density conserving interactions

$$V_{bf+f+} + V_{bbf+} = -\frac{J}{2} \sum_{\sigma} \mathcal{N}_{+\sigma} \mathcal{N}_{-\sigma} - \left[\frac{1}{2} \left(u_f^{\Delta} \sum_{r\sigma q > 0} n_q b_{r\sigma q} b_{-r\sigma q} + u_b^{\Delta} \sum_{r\sigma q > 0} n_q b_{r\sigma q}^{\dagger} b_{-r\sigma q} \right) + h.c. \right], \quad (2.5.6)$$

where we have defined the exchange energy

$$J := 2(u_f^{\Delta} + u_b^{\Delta}).$$

Again it is instructive to examine the term depending on the number counting operators in (2.5.6). It favours the spin alignment of electrons with different pseudo spin and therefore of ferromagnetic correlations.

2.5.3. Diagonalizing $H_0 + V_{\rho\rho}$. As we have shown in the previous section we could indeed recast the Hamiltonian $H_0 + V_{\rho\rho}$ into a form that is quadratic in the bosonic operators $b_{r\sigma q}$ and $b_{r\sigma q}^{\dagger}$. Hence we can diagonalize $H_0 + V_{\rho\rho}$ with the help of a Bogoliubov transformation. Before tackling the actual diagonalization, we simplify the problem by dividing $H_0 + V_{\rho\rho}$ into decoupled collective spin and charge excitations. The possibility of performing the spin-charge separation is one of the most prominent features of interacting one-dimensional systems. However, as we will see, in the case of SWNTs the inclusion of the non-density-density processes will partially spoil the spin-charge separation. But now let us introduce the total (+) and relative (−) charge (c) and spin (s) operators $b_{j\delta q}$, $j\delta = c+, c-, s+, s-$ which are related to the old operators $b_{r\sigma q}$ via the following transformation between $j\delta = c+, c-, s+, s-$ and $r\sigma = +\uparrow, +\downarrow, -\uparrow, -\downarrow$:

$$b_{r\sigma q} =: \Lambda_{r\sigma}^{j\delta} b_{j\delta q}, \quad q > 0, \quad (2.5.7)$$

where Einstein's summation convention is used and with

$$\Lambda_{r\sigma}^{j\delta} = \frac{1}{2} \begin{pmatrix} 1 & 1 & 1 & 1 \\ 1 & 1 & -1 & -1 \\ 1 & -1 & 1 & -1 \\ 1 & -1 & -1 & 1 \end{pmatrix}. \quad (2.5.8)$$

Inserting (2.5.7) into the bosonized contributions to $H_0 + V_{\rho\rho}$ the different $j\delta$ excitations indeed separate. A lengthy but simple calculation yields

$$H_0 = \varepsilon_0 \sum_{j\delta q > 0} n_q b_{j\delta q}^{\dagger} b_{j\delta q} + \varepsilon_0 \sum_{r\sigma} \left(\frac{\mathcal{N}_{r\sigma}^2}{2} + \Delta r \mathcal{N}_{r\sigma} \right)$$

and

$$\begin{aligned}
V_{\rho\rho} &= 2 \sum_{q>0} n_q W_q \left(b_{c+q} + b_{c+q}^\dagger \right)^2 - \frac{u^+}{2} \sum_{j\delta q>0} n_q (b_{j\delta q} b_{j\delta q} + h.c.) \\
&- \frac{1}{2} \left[\sum_{j\delta q>0} \delta \left(u_f^\Delta n_q b_{j\delta q} b_{j\delta q} + u_b^\Delta n_q b_{j\delta q}^\dagger b_{j\delta q} \right) + h.c. \right] \\
&- \frac{u^+}{2} \sum_{r\sigma} \mathcal{N}_{r\sigma}^2 - \frac{J}{2} \sum_{\sigma} \mathcal{N}_{+\sigma} \mathcal{N}_{-\sigma} + \frac{1}{2} W_0 \mathcal{N}_c^2.
\end{aligned}$$

Collecting the contributions from the single modes we can also write

$$\begin{aligned}
H_0 + V_{\rho\rho} &= \sum_{j\delta} H_{j\delta} + \\
&- \frac{u^+}{2} \sum_{r\sigma} \mathcal{N}_{r\sigma}^2 - \frac{J}{2} \sum_{\sigma} \mathcal{N}_{+\sigma} \mathcal{N}_{-\sigma} + \varepsilon_0 \sum_{r\sigma} \left(\frac{\mathcal{N}_{r\sigma}^2}{2} + \Delta r \mathcal{N}_{r\sigma} \right) + \frac{1}{2} W_0 \mathcal{N}_c^2. \quad (2.5.9)
\end{aligned}$$

with the operators

$$\begin{aligned}
H_{j\delta} &= \varepsilon_0 \sum_{q>0} n_q b_{j\delta q}^\dagger b_{j\delta q} \\
&+ \frac{1}{2} \sum_{q>0} n_q \left(4\delta_{j\delta, c+} W_q - \delta u_b^\Delta \right) \left(b_{j\delta q} + b_{j\delta q}^\dagger \right)^2 \\
&- \frac{1}{2} \sum_{q>0} n_q (b_{j\delta q} b_{j\delta q} + h.c.) \left(u^+ + \delta u_f^\Delta - \delta u_b^\Delta \right), \quad (2.5.10)
\end{aligned}$$

describing the bosonic excitations of mode $j\delta$. As we demonstrate in Appendix C we can separately diagonalize the Hamiltonians $H_{j\delta}$ by introducing new bosonic operators $a_{j\delta q}$ and $a_{j\delta q}^\dagger$ via the Bogoliubov transformation given below by equation (2.5.15). We obtain

$$\begin{aligned}
H_0 + V_{\rho\rho} &= \sum_{j\delta q>0} \varepsilon_{j\delta q} a_{j\delta q}^\dagger a_{j\delta q} + \frac{1}{2} E_c \mathcal{N}_c^2 \\
&+ \frac{1}{2} \sum_{r\sigma} \mathcal{N}_{r\sigma} \left[-\frac{J}{2} \mathcal{N}_{-r\sigma} + (\varepsilon_0 - u^+) \mathcal{N}_{r\sigma} + r \varepsilon_\Delta \right]. \quad (2.5.11)
\end{aligned}$$

The excitation energies $\varepsilon_{j\delta q}$ and the relation between the new bosonic operators $a_{j\delta q}$ and the old operators $b_{r\sigma q}$ are determined by the Bogoliubov transformation. In detail, we find with $\varepsilon_{0q} := \varepsilon_0 n_q$,

$$\varepsilon_{c+q} = \varepsilon_{0q} \sqrt{1 + 8W_q/\varepsilon_0}, \quad (2.5.12)$$

$$\varepsilon_{s-q} = \varepsilon_{c-q} = \varepsilon_{0q} (1 - u_b^\Delta/\varepsilon_0) \quad (2.5.13)$$

and

$$\varepsilon_{s+q} = \varepsilon_{0q} (1 + u_b^\Delta/\varepsilon_0). \quad (2.5.14)$$

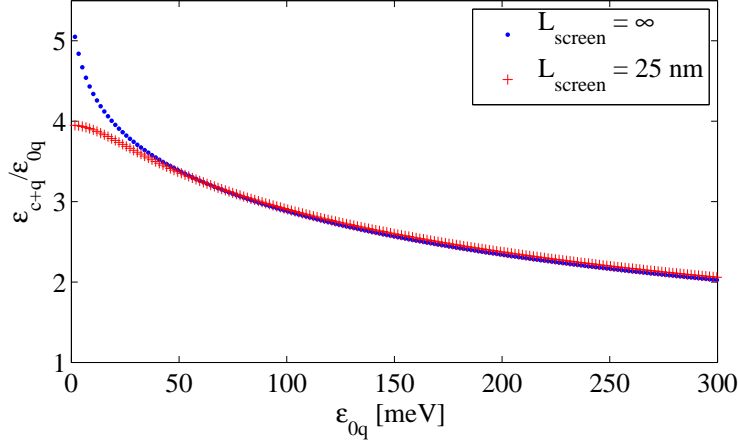


FIGURE 2.5.1. The ratio $\varepsilon_{c+q}/\varepsilon_{0q}$ as a function of ε_{0q} for a (20,20) armchair SWNT of 980 nm length. Here we show the decay of $\varepsilon_{c+q}/\varepsilon_{0q}$ for an unscreened and a screened (screening length 25 nm) Coulomb interaction. In both cases, a dielectric constant ϵ of 1.4, see Ref. [13], is assumed.

The energies of the $c+$ channel are largely enhanced compared to the other excitations because of the dominating V_{fff} contribution. For small q the ratio $g_q := \varepsilon_{0q}/\varepsilon_{c+q}$ is approximately 0.2, whereas for large q it tends to 1, since V_{fff} is not a local interaction. In Fig. 2.5.1 we show exemplarily the dispersion relation for ε_{c+q} of a (20,20) armchair SWNT. Small corrections due to the coupling constants u_f^Δ and u^+ have been neglected in the relations (2.5.12) to (2.5.14). Note that only the excitation energies of the $j\delta = c-, s-$ modes are identical. For the transformation from the old bosonic operators $b_{r\sigma q}$ to the new ones $a_{j\delta q}$ we find

$$b_{r\sigma q} = \sum_{j\delta} \Lambda_{r\sigma}^{j\delta} \left(B_{j\delta q} a_{j\delta q} + D_{j\delta q} a_{j\delta q}^\dagger \right), \quad q > 0 \quad (2.5.15)$$

where the transformation coefficients $B_{j\delta q}$ and $D_{j\delta q}$ in the case of the three modes $j\delta = c-, s+, s-$ are given by

$$B_{j\delta q} = 1 \text{ and } D_{j\delta q} = 0 \quad (2.5.16)$$

and for $j\delta = c+$ we obtain

$$B_{j\delta q} = \frac{1}{2} \left(\sqrt{g_q} + \frac{1}{\sqrt{g_q}} \right), \quad D_{j\delta q} = \frac{1}{2} \left(\sqrt{g_q} - \frac{1}{\sqrt{g_q}} \right), \quad (2.5.17)$$

with $g_q = \frac{\varepsilon_{0q}}{\varepsilon_{c+q}}$. Small corrections to (2.5.16) and (2.5.17) resulting from the terms $V_{f+b f+}$ and $V_{b f+/b f+}$ have again been neglected.

Let us also shortly recall the physical meaning of the fermionic contributions in (2.5.11). The Pauli shell filling energy $\frac{\varepsilon_0}{2} \sum_{r\sigma} \mathcal{N}_{r\sigma}^2 + r\varepsilon_\Delta$ and the charging energy $\frac{1}{2} E_c \mathcal{N}_c^2$ stem from H_0 and V_{fff} , respectively. The shortranged interaction terms

$V_{f+b f+}$ and $V_{b f+ f+} + V_{b b f+}$ lead to an energy gain for aligning the spin of electrons with different r and to an attractive contribution counteracting the shell filling energy respectively, cf. equations (2.5.5) and (2.5.6).

An eigenbasis of $H_0 + V_{\rho\rho}$ is formed by the states

$$|\vec{N}, \vec{m}\rangle := \prod_{j\delta q > 0} \frac{(a_{j\delta q}^\dagger)^{m_{j\delta q}}}{\sqrt{m_{j\delta q}!}} |\vec{N}, 0\rangle, \quad (2.5.18)$$

where $|\vec{N}, 0\rangle$ has no bosonic excitation. Remember that the fermionic configuration $\vec{N} = (N_{-\uparrow}, N_{-\downarrow}, N_{+\uparrow}, N_{+\downarrow})$ defines the number of electrons in each of the branches $(r\sigma)$. Note that the states $|\vec{N}, 0\rangle$ from (2.5.18) are not identical to the eigenstates $|\vec{N}, 0\rangle$ of the noninteracting system in equation (2.4.8), since for the former states it holds

$$b_{r\sigma q} |\vec{N}, 0\rangle = \sum_{j\delta} \Lambda_{r\sigma}^{j\delta} (B_{j\delta q} a_{j\delta q} + D_{j\delta q} a_{j\delta q}^\dagger) |\vec{N}, 0\rangle \neq 0,$$

whereas for the latter states equation (2.4.8), i.e., $b_{r\sigma q} |\vec{N}, 0\rangle = 0$ holds. In the following we will use the states from (2.5.18) as basis to examine the effect of $V_{n\rho\rho}$. For this purpose we evaluate in the next section the corresponding matrix elements using the bosonization identity for the 1D electron operators.

2.5.4. The matrix elements $\langle \vec{N} \vec{m} | V_{n\rho\rho} | \vec{N}' \vec{m}' \rangle$. Generally, due to $V_{n\rho\rho}$, the quantities \vec{N} and \vec{m} are not conserved. Especially, the terms with $S_r = b, u$ in (2.3.14) mix states with different \vec{N} . However, denoting

$$N_s := \sum_{r\sigma} \text{sgn}(\sigma) N_{r\sigma}, \quad \text{sgn}(\uparrow, \downarrow) = \pm 1,$$

$$N_c^- := \sum_{r\sigma} \text{sgn}(r) N_{r\sigma}$$

and

$$N_s^- := \sum_{r\sigma} \text{sgn}(r\sigma) N_{r\sigma}$$

we find that $(N_c, N_s, N_c^- \bmod 4, N_s^- \bmod 4)$ is conserved, i.e., states differing in those quantities do not mix, such that the corresponding matrix elements of $V_{n\rho\rho}$ are zero. Note that in contrast to the real spin $S_z = \frac{1}{2} N_s$, the pseudo spin $\tilde{S}_z := \frac{1}{2} N_c^-$ is not conserved in general.

We already know from our discussion in Sections 2.3.3 and 2.3.4 that all the processes $V_{S_r S_F S_\sigma}$ contained in $V_{n\rho\rho}$ are effectively local interactions, i.e., of the form (2.3.9). From that equation it is clear that the key ingredient for the calculation of the corresponding matrix elements $\langle \vec{N} \vec{m} | V_{S_r S_F S_\sigma} | \vec{N}' \vec{m}' \rangle$ is the derivation of a general expression for

$$M_{[r][F][\sigma]}(\vec{N}, \vec{m}, \vec{N}', \vec{m}', x) := \left\langle \vec{N} \vec{m} \left| \psi_{r_1\sigma F_1}^\dagger(x) \psi_{r_2\sigma' F_2}^\dagger(x) \psi_{r_3\sigma' F_3}(x) \psi_{r_4\sigma F_4}(x) \right| \vec{N}' \vec{m}' \right\rangle. \quad (2.5.19)$$

For this purpose we express the operators $\psi_{r\sigma F}(x)$ in terms of the bosonic operators $b_{r\sigma q}$ and $b_{r\sigma q}^\dagger$, $q > 0$, using the bosonization identity (A.0.15) from Section 2.4.3,

$$\psi_{r\sigma F}(x) = \eta_{r\sigma} K_{r\sigma F}(x) e^{i\phi_{r\sigma F}^\dagger(x)} e^{i\phi_{r\sigma F}(x)}. \quad (2.5.20)$$

In Appendix E we demonstrate that the matrix elements from equation (2.5.19) factorize into a fermionic (depending on the fermionic configurations \vec{N} and \vec{N}') and a bosonic part (depending on \vec{m} and \vec{m}'),

$$M_{[l]}(\vec{N}, \vec{N}', x) = \left\langle \vec{N} \left| K_{l_1}^\dagger(x) \eta_{l_1}^\dagger K_{l_2}^\dagger(x) \eta_{l_2}^\dagger K_{l_3}(x) \eta_{l_3} K_{l_4}(x) \eta_{l_4} \right| \vec{N}' \right\rangle,$$

where the fermionic part is given by

$$M_{[l]}(\vec{N}, \vec{N}', x) = \left\langle \vec{N} \left| K_{l_1}^\dagger(x) \eta_{l_1}^\dagger K_{l_2}^\dagger(x) \eta_{l_2}^\dagger K_{l_3}(x) \eta_{l_3} K_{l_4}(x) \eta_{l_4} \right| \vec{N}' \right\rangle$$

and the bosonic part reads

$$M_{[l]}(\vec{m}, \vec{m}', x) = \langle \vec{m} | e^{-i\phi_{l_1}^\dagger(x)} e^{-i\phi_{l_1}(x)} e^{-i\phi_{l_2}^\dagger(x)} e^{-i\phi_{l_2}(x)} \\ \times e^{i\phi_{l_3}^\dagger(x)} e^{i\phi_{l_3}(x)} e^{i\phi_{l_4}^\dagger(x)} e^{i\phi_{l_4}(x)} | \vec{m}' \rangle. \quad (2.5.21)$$

For a better readability we have replaced the indices $rF\sigma$ by a single index l . As we demonstrate in Appendix E, the explicit evaluation yields

$$M_{[r][F][\sigma]}(\vec{N}, \vec{N}', x) = \frac{1}{(2L)^2} \delta_{\vec{N}, \vec{N}' + \vec{E}_{[r][\sigma]}} T_{\vec{N} \vec{N}' [r][\sigma]} Q_{\vec{N} \vec{N}' [r][F]}(x), \quad (2.5.22)$$

where $\vec{E}_{[r][\sigma]} := \vec{e}_{r_1\sigma} + \vec{e}_{r_2\sigma'} - \vec{e}_{r_3\sigma'} - \vec{e}_{r_4\sigma}$. The Klein factors in (2.5.20) lead to the sign factor $T_{\vec{N} \vec{N}' [r][\sigma]}$ which is either $+1$ or -1 and $Q_{\vec{N} \vec{N}' [r][F]}(x)$ yields a phase depending on \vec{N} . Explicit expressions can be found in Appendix E, equations (E.1.1) to (E.1.4).

For the bosonic part of $M_{[r][F][\sigma]}(\vec{N}, \vec{m}, \vec{N}', \vec{m}', x)$ the calculation in Appendix E leads to

$$M_{[r][F][\sigma]}(\vec{m}, \vec{m}', x) = C_{[r][F][\sigma]}(x) \\ \times A_{S_{rF}}(x) \prod_{j\delta q} F(\tilde{\lambda}_{[r][F][\sigma]}^{j\delta q}(x), m_{j\delta q}, m'_{j\delta q}). \quad (2.5.23)$$

The function $F(\lambda, m, m')$, which determines the coupling between states with different bosonic excitations, stems from the evaluation of matrix elements of the form $\langle m | e^{-\lambda^* a^\dagger} e^{\lambda a} | m' \rangle$, where the bosonic excitations $|m\rangle$ are created by the operators a^\dagger , i.e., $|m\rangle = (a^\dagger)^m / \sqrt{m!} |0\rangle$. For the explicit form of $F(\lambda, m, m')$, which can be written in terms of the Laguerre polynomials L_n^m , and the coefficients $\tilde{\lambda}_{[r][F][\sigma]}^{j\delta q}(x)$, we again refer to Appendix E. The function $C_{[r][F][\sigma]}(x)$ is conveniently considered in combination with $Q_{\vec{N} \vec{N}' [r][F]}(x)$, namely the product

$$\tilde{K}_{\vec{N} \vec{N}' [r][F]}(x) := Q_{\vec{N} \vec{N}' [r][F]}(x) C_{[r][F][\sigma]}(x)$$

can be reexpressed as

$$\tilde{K}_{\tilde{N}[r][F][\sigma]}(x) = \tilde{Q}_{\tilde{N}[r][F]}(x) \tilde{C}_{S_r S_F S_\sigma}(x), \quad (2.5.24)$$

where

$$\tilde{Q}_{\tilde{N}[r][F]}(x) = \exp \left\{ -i \frac{\pi}{L} \left[\sum_{j=1}^4 \text{sgn}(r_j F_j) N_{r_j \sigma_j} + \sum_{j=3}^4 \text{sgn}(r_j F_j) \right] x \right\}.$$

Here $\sum_{l=1}^4 a_l$ denotes the sum $a_1 + a_2 - a_3 - a_4$. For $\tilde{C}_{S_r S_F S_\sigma}(x)$ we obtain

$$\tilde{C}_{f+bf-}(x) = -\tilde{C}_{f-bf}(x) = -\tilde{C}_{bf-f+}(x) = 1/4 \sin^2 \left(\frac{\pi}{L} x \right), \quad (2.5.25)$$

$$\tilde{C}_{ubf+}(x) = -\tilde{C}_{uf-f+}(x) = 4 \sin^2 \left(\frac{\pi}{L} x \right) \quad (2.5.26)$$

and $\tilde{C}_{S_r S_F S_\sigma}(x) \equiv 1$ for the remaining processes of $V_{n\rho\rho}$.

The calculation of $M_{[l]}(\vec{m}, \vec{m}', x)$ in the appendix requires normal ordering of the bosonic operators. This procedure leads to the functions $A_{S_{rF}}(x)$, which are of special interest for the interaction processes that fulfill $S_{rF} = u$ and hence are restricted to the region around half filling (cf. Section 2.3.2). Only for those processes $A_{S_{rF}}(x)$ differs from 1. The reason for this is that only for the $S_{rF} = u$ terms the coefficients $\tilde{\lambda}_{[r][F][\sigma]}^{c+q}(x)$ related to the charged $c+$ mode are not vanishing and thus $A_u(x)$ depends strongly on the energy dispersion of the $c+$ mode and therefore on the forward scattering part of the interaction, in detail

$$A_u(x) = \exp \left[2 \sum_{q>0} \frac{1}{n_q} \left(1 - \frac{\varepsilon_{0q}}{\varepsilon_{c+q}} \right) \sin^2(qx) \right],$$

as we derive in Appendix E. Since for the repulsive Coulomb interaction $\varepsilon_{0q}/\varepsilon_{c+q} < 1$ holds, we find $A_{S_{rF}=u}(x) \geq 1$. In Fig. 2.5.2 we show $A_{S_{rF}=u}(x)$ for a (6,6) SWNT. The large magnitude of $A_u(x)$ leads to a strong enhancement of the coupling between different states $|\vec{N}, \vec{m}\rangle$ and $|\vec{N}', \vec{m}'\rangle$. We therefore conclude that the eigenbasis (2.5.18) is not a well suited starting point for the examination of $V_{n\rho\rho}$ any more. As a matter of fact our truncation scheme for the diagonalization of the total Hamiltonian *fails near half-filling*: The resulting spectrum does not converge when enlarging the truncated basis. So far the question if finite size SWNTs change their behaviour completely at half-filling remains unsettled and further investigations of this point seem to be worthwhile. In fact, the situation at half-filling has only been discussed in the work [14] by Yoshioka and Odintsov for SWNTs of infinite length. Applying renormalization group techniques they find a Mott insulator state at half-filling. Altogether, we get

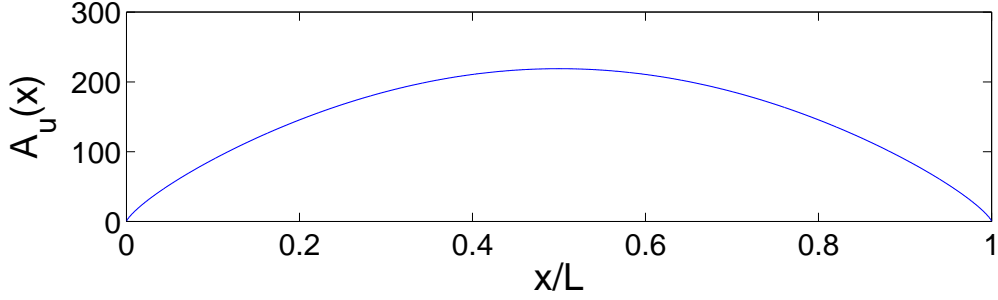


FIGURE 2.5.2. $A_{S_{rF}=u}(x)$ as a function of x for a (6,6)-SWNT. Note the large magnitude of $A_{S_{rF}=u}(x)$ compared to $A_{S_{rF}\neq u}(x) \equiv 1$ for the processes only relevant away from half-filling!

with equations (2.3.9), (2.5.22) and (2.5.23) for the single contributions to $V_{n\rho\rho}$,

$$\begin{aligned} \left\langle \vec{N}\vec{m} \left| V_{S_r S_F S_\sigma} \right| \vec{N}'\vec{m}' \right\rangle = & \\ & \times \frac{1}{4L} u_{S_r S_F} \sum_{\{[r]_{S_r}, [F]_{S_F}, [\sigma]_{S_\sigma}\}} \delta_{\vec{N}, \vec{N}' + \vec{E}_{[r]_{S_r} \sigma}} T_{\vec{N} S_r S_\sigma} \\ & \times \int dx \tilde{K}_{\vec{N}[r][F]}(x) A_{S_{rF}}(x) \prod_{j\delta q} F(\tilde{\lambda}_{[r][F][\sigma]}^{j\delta q}(x), m_{j\delta q}, m'_{j\delta q}). \quad (2.5.27) \end{aligned}$$

The evaluation of (2.5.27) causes no problems except for the \vec{N} conserving terms with $(S_r, S_F, S_\sigma) = (f^+, b, f^-), (f^-, b, f), (b, f^-, f^+)$, since then we find $\tilde{K}_{\vec{N}[r][F][\sigma]} \sim 1/4 \sin^2(\frac{\pi}{L}x)$, cf. (2.5.24) and (2.5.25), causing the integral in (2.5.27) to diverge if $\sum_{j\delta q} |m_{j\delta q} - m'_{j\delta q}| \leq 1$, such that the evaluation of the corresponding matrix elements needs special care in this case. The origin of this divergence lies in the fact that for matrix elements with $\sum_{j\delta q} |m_{j\delta q} - m'_{j\delta q}| \leq 1$, the \vec{N} conserving processes depend on the total number of electrons in the single branches (compare to the fermionic contributions to $H_0 + V_{\rho\rho}$ in (2.5.11)). Since the bosonization approach requires the assumption of an infinitely deep Fermi sea, cf. Section 2.4, this leads, without the correct regularization, necessarily to divergent expressions. In contrast, electrons deep in the Fermi sea do not contribute to the \vec{N} non-conserving processes due to associated huge excitation energies, see Fig. 2.3.2. Hence those processes can not depend on the number of electrons in the nanotube. In Appendix F we show how the proper regularizations can be performed. Here we give the regularized result for $\left\langle \vec{N}\vec{m} \left| V_{f^+ b f^-} \right| \vec{N}\vec{m} \right\rangle$, since it is of special importance for the discussion of the ground state spectra away from

half-filling,

$$\begin{aligned}
\langle \vec{N} \vec{m} | V_{f+b, f-} | \vec{N} \vec{m} \rangle &= u^+ \sum_r \min(N_{r\uparrow}, N_{r\downarrow}) \\
&+ \frac{1}{4L} u^+ \sum_{\{[r]_{f+}, [F]_b, [\sigma]_{f-}\}} \int dx \tilde{K}_{\vec{N}[r][F]}(x) \\
&\times \left(\prod_{j\delta q} F(\lambda_{[r][F][\sigma]}^{j\delta q}(x), m_{j\delta q}, m_{j\delta q}) - 1 \right) \quad (2.5.28)
\end{aligned}$$

2.5.5. Diagonalizing $H_0 + V_{\rho\rho} + V_{n\rho\rho}$. In Section 2.5.3 we have diagonalized $H_0 + V_{\rho\rho}$ and in Section 2.5.4 we have determined the matrix elements of $V_{n\rho\rho}$ in the eigenbasis of $H_0 + V_{\rho\rho}$. From the discussion of the different interaction processes we know that the corresponding coupling constants for the short ranged interactions scale like ε_0/d . For a small diameter SWNT like a (6,6) armchair tube with $d = 0.8\text{nm}$ we find with the values in table 1, $u^+, u_f^\Delta \approx 0.02 - 0.04\varepsilon_0$. Therefore the magnitude of $V_{n\rho\rho}$ is only small compared to the one of $H_0 + V_{\rho\rho}$ and we can easily analyze the effect of the non-density-density interaction $V_{n\rho\rho}$ on the SWNT spectrum by representing the total Hamiltonian $H_0 + V_{\rho\rho} + V_{n\rho\rho}$ in a truncated eigenbasis of $H_0 + V_{\rho\rho}$. However, remember that the strength of the short ranged interaction processes that are only of relevance near half-filling is enhanced by approximately two orders of magnitude as a consequence of the function $A_u(x)$. Hence near half-filling $V_{n\rho\rho}$ is even the dominating part of the Hamiltonian and the truncation procedure described above fails.

2.6. The spectrum of metallic SWNTs

With the recipe from Section 2.5.5 we are now able to determine the spectrum of metallic SWNTs away from half-filling. We start with the examination of the ground and low energy states.

2.6.1. Low energy spectrum. For the analysis of the ground states and nearby small excitations we use the lowest lying eigenstates of $H_0 + V_{\rho\rho}$ without bosonic excitations as a basis. The calculation of the spectra is split into the cases $N_c = 4m$, $N_c = 4m + 1$, $N_c = 4m + 3$ on the one side and $N_c = 4m + 2$ on the other side.

$$N_c = 4m, N_c = 4m + 1, N_c = 4m + 3$$

First we consider the charge states $N_c = 4m$, $N_c = 4m + 1$ and $N_c = 4m + 3$. In that case the lowest lying eigenstates of $H_0 + V_{\rho\rho}$, shown in Fig. 2.6.1, which are of the form $|\vec{N}, 0\rangle$ and therefore uniquely characterized by \vec{N} , do not mix via $V_{n\rho\rho}$. That means that the only correction from $V_{n\rho\rho}$ to $H_0 + V_{\rho\rho}$ stems from the \vec{N} conserving process $V_{f+b, f-}$. For states without bosonic excitations, equation (2.5.28)

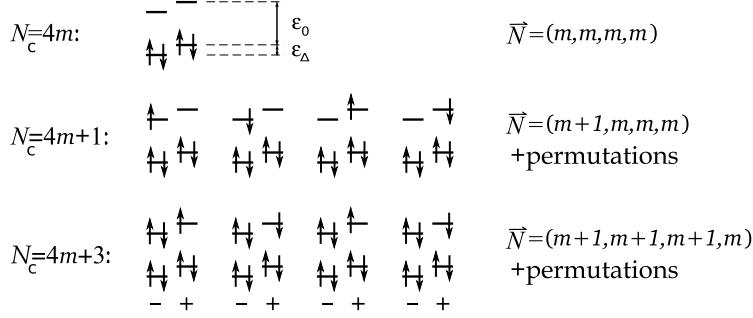


FIGURE 2.6.1. The lowest lying eigenstates of $H_0 + V_{\rho\rho}$ without bosonic excitations for the charge states $N_c = 4m$, $N_c = 4m + 1$ and $N_c = 4m + 3$. On the right side the fermionic configurations are given. We use the convention $\vec{N} = (N_{+\uparrow}, N_{+\downarrow}, N_{-\uparrow}, N_{-\downarrow})$.

yields, because of $F(\lambda, 0, 0) = 1$,

$$\langle \vec{N}, 0 | V_{n\rho\rho} | \vec{N}, 0 \rangle = \langle \vec{N}, 0 | V_{f+b f-} | \vec{N}, 0 \rangle = u^+ \sum_r \min(N_{r\uparrow}, N_{r\downarrow}). \quad (2.6.1)$$

Hence here $V_{n\rho\rho}$ yields an energy penalty for occupying the same branch r . This effect has already been found in the mean field theory of Oreg et al. [19]. The parameter δU there corresponds to our constant u^+ . The energies of the lowest lying states for $N_c = 4m$, $N_c = 4m + 1$ and $N_c = 4m + 3$ only depend on \vec{N} . In detail we find with (2.5.11) and (2.6.1),

$$E_{\vec{N}} = \frac{1}{2} E_c \mathcal{N}_c^2 + u^+ \sum_r \min(N_{r\uparrow}, N_{r\downarrow}) + \frac{1}{2} \sum_{r\sigma} \mathcal{N}_{r\sigma} \left[-\frac{J}{2} \mathcal{N}_{-r\sigma} + (\epsilon_0 - u^+) \mathcal{N}_{r\sigma} + r \epsilon_\Delta \right]. \quad (2.6.2)$$

From (2.6.2) it follows that for the states depicted in Fig. 2.6.1 the interaction dependent part of $E_{\vec{N}}$ is the same for all fermionic configurations \vec{N} corresponding to a given charge state N_c . Hence the interaction leads merely to a common shift of the lowest lying energy levels for fixed N_c .

$$N_c = 4m + 2$$

Of special interest is the ground state structure of the $N_c = 4m + 2$ charge state, since here the lowest lying six eigenstates of $H_0 + V_{\rho\rho}$ without bosonic excitations, denoted $|\vec{N}, 0\rangle$ with $\vec{N} = (n+1, n+1, n, n) + \text{permutations}$, mix via $V_{n\rho\rho}$, leading to a $S = 1$ triplet state and to three non-degenerate states with spin 0. For $\epsilon_\Delta \approx 0$ (the meaning of ≈ 0 will become clear in the following) the triplet is the ground state. In the following we denote $|(n+1, n+1, n, n), 0\rangle$ by $|\uparrow\downarrow, -\rangle$, $|(n+1, n, n, n+1), 0\rangle$ by $|\uparrow, \downarrow\rangle$ and analogously for the remaining four states. Ignoring interactions, the six

considered states are degenerate for $\varepsilon_\Delta = 0$. As we can conclude from (2.5.11) the degeneracy of the six considered states is already lifted if including only the density-density interaction $V_{\rho\rho}$, since then the energy of the spin 1 states $|\uparrow, \uparrow\rangle$ and $|\downarrow, \downarrow\rangle$ is lowered by

$$J/2 = u_f^\Delta + u_b^\Delta$$

relatively to the other ground states. Let us now consider the effects of $V_{n\rho\rho}$. The diagonal matrix elements $\langle \vec{N}, 0 | V_{n\rho\rho} | \vec{N}, 0 \rangle$ are again determined by equation (2.6.1), leading to a relative energy penalty for the states $|\uparrow\downarrow, -\rangle$ and $|- , \uparrow\downarrow\rangle$. Mixing occurs between the states $|\uparrow, \downarrow\rangle$ and $|\downarrow, \uparrow\rangle$ via V_{bf+f-} and V_{bbf-} and between $|\uparrow\downarrow, -\rangle$ and $|- , \uparrow\downarrow\rangle$ via V_{uf-f-} and V_{ubf-} . With equation (2.5.27) we find

$$\langle \uparrow, \downarrow | V_{n\rho\rho} | \downarrow, \uparrow \rangle = -\frac{J}{2} = -\langle \uparrow\downarrow, - | V_{n\rho\rho} | - , \uparrow\downarrow \rangle.$$

In total, the SWNT Hamiltonian $H = H_0 + V_{\rho\rho} + V_{n\rho\rho}$ restricted to the basis spanned by the six states $|\uparrow, \uparrow\rangle$, $|\downarrow, \downarrow\rangle$, $|\uparrow, \downarrow\rangle$, $|\downarrow, \uparrow\rangle$, $|\uparrow\downarrow, -\rangle$ and $|- , \uparrow\downarrow\rangle$ is represented by the matrix,

$$H = E_{0,4m+2} + \begin{pmatrix} -\frac{J}{2} & & & & & 0 \\ & -\frac{J}{2} & & & & \\ & & 0 & -\frac{J}{2} & & \\ & & -\frac{J}{2} & 0 & & \\ & & & & u^+ - \varepsilon_\Delta & \frac{J}{2} \\ 0 & & & & \frac{J}{2} & u^+ + \varepsilon_\Delta \end{pmatrix}, \quad (2.6.3)$$

where $E_{0,4m+2} = \frac{1}{2}E_c N_c^2 + (2n^2 + 2n + 1)(\varepsilon_0 - u^+) - J(n^2 + n) + 2u^+n$. Diagonalizing the matrix in (2.6.3), we find that its eigenstates are given by the spin 1 triplet

$$|\uparrow, \uparrow\rangle, |\uparrow, \uparrow\rangle, 1/\sqrt{2}(|\uparrow, \downarrow\rangle + |\downarrow, \uparrow\rangle),$$

the spin 0 singlet

$$1/\sqrt{2}(|\uparrow, \downarrow\rangle - |\downarrow, \uparrow\rangle),$$

and the two states

$$\frac{1}{\sqrt{c_{1/2}^2 + 1}} (c_{1/2} |\uparrow\downarrow, -\rangle \pm |- , \uparrow\downarrow\rangle),$$

where the coefficients $c_{1/2}$ are given by

$$c_{1/2} = \frac{\sqrt{\varepsilon_\Delta^2 + (J/2)^2} \mp \varepsilon_\Delta}{J/2}.$$

Relatively to $E_{0,4m+2}$, the corresponding eigenenergies are $-J/2$ for the triplet states, $J/2$ for the singlet state and $u^+ \pm \sqrt{\varepsilon_\Delta^2 + (J/2)^2}$ for the remaining two states. Thus under the condition

$$J/2 > \sqrt{\varepsilon_\Delta^2 + (J/2)^2} - u^+,$$

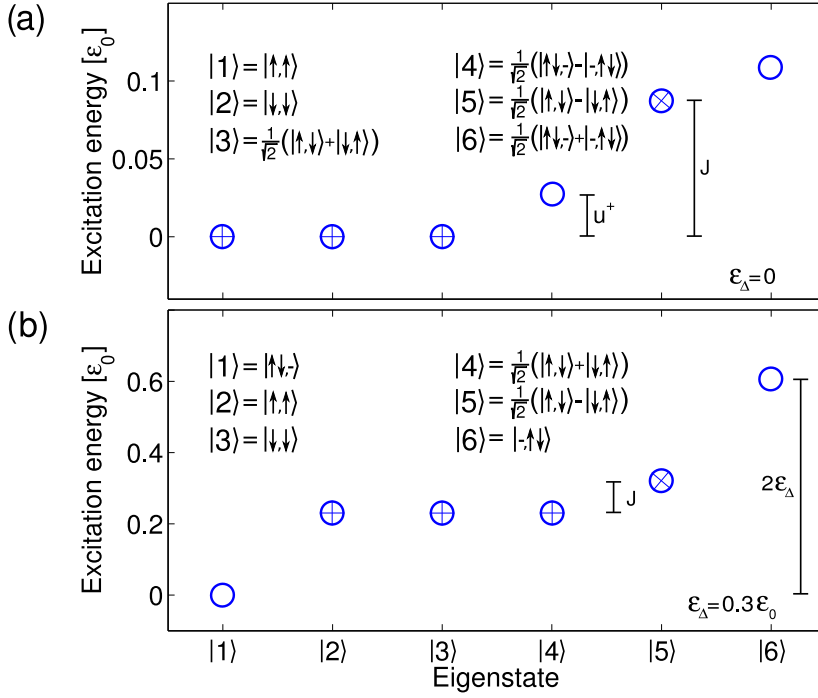


FIGURE 2.6.2. Low energy spectrum of a (6,6) SWNT for the charge state $N_c = 4m + 2$. (a) In the case $\epsilon_\Delta = 0$ the ground state is formed by the spin 1 triplet ($\rightarrow \oplus$) and the states $|\uparrow\downarrow, -\rangle$ and $|- , \uparrow\downarrow\rangle$ mix ($\rightarrow \circ$ states). (b) For $\epsilon_\Delta \gg J/2$ the ground state is given by the spin 0 state $|\uparrow\downarrow, -\rangle$. The spin 0 singlet state $(|\uparrow\downarrow\rangle - |\downarrow\uparrow\rangle)/\sqrt{2}$ is indicated by \otimes . The coupling parameters are $J = 0.09\epsilon_0$ and $u^+ \approx 0.03\epsilon_0$.

i.e., for a small band mismatch $\epsilon_\Delta \lesssim J/2$ the ground state is degenerate and formed by the spin 1 triplet, otherwise by $\frac{1}{\sqrt{c_2^2+1}}(c_2|\uparrow\downarrow, -\rangle + |- , \uparrow\downarrow\rangle)$. The ground state spectra for the two cases $\epsilon_\Delta = 0$ and $\epsilon_\Delta \gg J/2$ are shown in Fig. 2.6.2 for a (6,6) armchair SWNT (corresponding to a diameter of 0.8 nm). Assuming a dielectric constant of $\epsilon = 1.4$ [13], the calculation of the coupling parameters according to Appendix D yields values of $J = 2(u_f^\Delta + u_b^\Delta) = 0.09\epsilon_0$ and $u^+ \approx 0.03\epsilon_0$ which agree well with the experiments [18, 38, 20], where nanotubes with $\epsilon_\Delta \gg J/2$ were considered. To our knowledge, experiments in the regime $\epsilon_\Delta \lesssim J/2$ demonstrating exchange effects, have not been carried out so far, such that a validation of our predictions for this case, namely the existence of the ground state spin 1 triplet and the mixing of the states $|\uparrow\downarrow, -\rangle$ and $|- , \uparrow\downarrow\rangle$ is still missing. The latter effect could be of relevance for the understanding of the so called singlet-triplet Kondo effect [42] in SWNTs.

It should be stressed that all exchange effects, leading amongst others to the spin 1 triplet as ground state, result from $S_r \neq f$ interaction processes. In the work of Mattis and Lieb [39], however, there is no such additional pseudo spin degree of freedom.

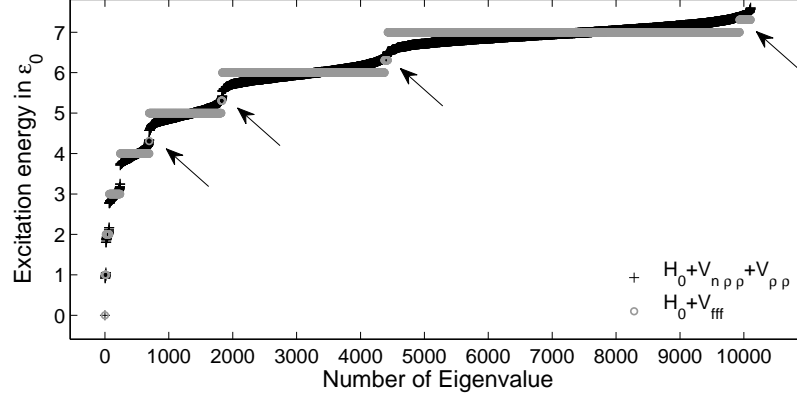


FIGURE 2.6.3. The excitation spectrum for a (6,6) SWNT occupied by $N_c = 4m$ electrons. In grey we show the spectrum as obtained by diagonalizing the Hamiltonian of the standard theory $H_{st} = H_0 + V_{ff} + V_{\rho\rho}$ and in black for the full Hamiltonian $H = H_0 + V_{\rho\rho} + V_{n\rho\rho}$. A band mismatch $\varepsilon_\Delta = 0$ is assumed. The energy of the lowest $c+$ excitation is $4.3\varepsilon_0$. All other interaction parameters are as in Fig. 2.6.2. Arrows indicate eigenenergies of the “standard” Hamiltonian $H_{st} = H_0 + V_{ff}$ involving excitations of the $c+$ mode.

Hence we suspect that this is the reason why their theorem can not be applied in our situation.

2.6.2. Excitation spectra away from half-filling. Until now our discussion of the energy spectra was based on states $|\vec{N}, 0\rangle$ without any bosonic excitations and so far the effect of $V_{n\rho\rho}$ on the spectrum even could have been treated without using bosonization. But for the determination of the excitation spectrum of H we do need the general expression for the matrix elements of $V_{n\rho\rho}$ between the eigenstates of $H_0 + V_{\rho\rho}$ as given by (2.5.27). For the actual calculation we truncate the eigenbasis of $H_0 + V_{\rho\rho}$ for a fixed charge state N_c at a certain excitation energy and represent H in this shortened basis. After the diagonalization we find to a good approximation the correct eigenstates and eigenenergies of H . For the results shown in Figs. 2.6.3 to 2.6.6 we have checked that convergence has been reached, i.e., the extension of the considered basis states does not lead to a significant change of the spectrum.

Exemplarily we present the results for the charge state $N = 4m$. Similar excitation spectra are found for the other charge states. In Fig. 2.6.3 we show for comparison and in order to demonstrate the effect of the non-forward scattering processes the findings for the “standard” theory, i.e., the spectrum of $H_{st} = H_0 + V_{ff}$ as well as the spectrum of the full Hamiltonian $H = H_0 + V_{\rho\rho} + V_{n\rho\rho}$ for a (6, 6) armchair nanotube. Thereby a non-vanishing band mismatch $\varepsilon_\Delta = 0$ is assumed. Striking is the partial breaking of the huge degeneracies of the “standard” spectrum. Note also the lifting of

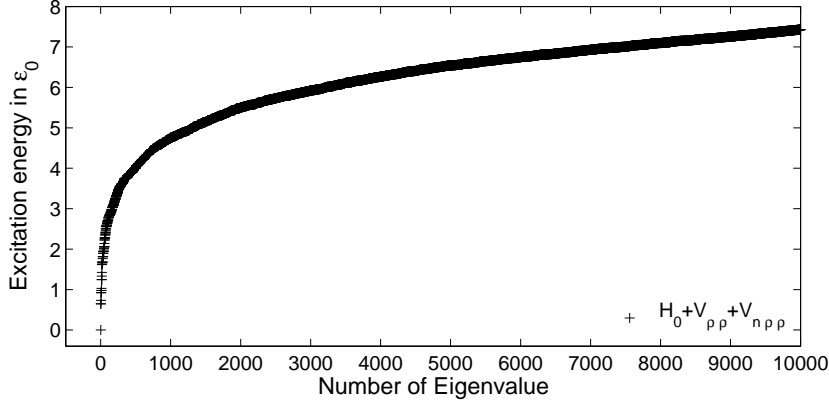


FIGURE 2.6.4. The excitation spectrum for a (6,6) SWNT obtained by diagonalizing the full Hamiltonian $H = H_0 + V_{\rho\rho} + V_{n\rho\rho}$ for $N_c = 4m$ and $\varepsilon_\Delta = 0.3\varepsilon_0$. The spectrum becomes quasicontinuous at relatively small energies. Shown are the lowest 10000 eigenenergies.

the spin-charge separation when including the non-forward scattering processes. To illustrate this point we have indicated eigenenergies of H_{st} including $c+$ excitations by arrows in Fig. 2.6.3.

At higher energies a quasi continuum forms in the case of the full Hamiltonian H , a feature becoming especially apparent for a finite band mismatch. In Fig. 2.6.4 the spectra of the full Hamiltonian H is shown for $\varepsilon_\Delta = 0.3\varepsilon_0$.

As we have already discussed, the importance of non-forward scattering terms should decrease with increasing tube diameter. And indeed the excitation spectrum of the full Hamiltonian for a (20, 20) SWNT resembles much more the result of the “standard” theory than it is the case for a (6, 6) SWNT as can be seen from Fig. 2.6.5.

It is also interesting to regard the effect of the total interaction $V_{\rho\rho} + V_{n\rho\rho}$ on the nanotube spectrum. For this purpose, in Fig. 2.6.6 the spectrum of H_0 describing the noninteracting system is compared to the spectrum of the full Hamiltonian H , again for a (6, 6) SWNT with vanishing band mismatch. Of special significance is the strong reduction of the number of eigenstates below a certain energy if the interaction is “switched on”. This can be mainly traced back to V_{fff} which leads to the formation of the bosonic $c+$ excitations with considerably enlarged energies. Concerning the transport properties of SWNTs the reduction of relevant states plays an important role for the occurrence of the power law dependence of various transport quantities in the case of infinitely long tubes but also for the appearance of negative differential conductance in highly asymmetric SWNT quantum dots as will be discussed in Chapter 4.

2.6.3. Comparison to the mean field results. We shortly want to compare the results of the mean field theory by Oreg et al. [19] and our approach. Concerning the

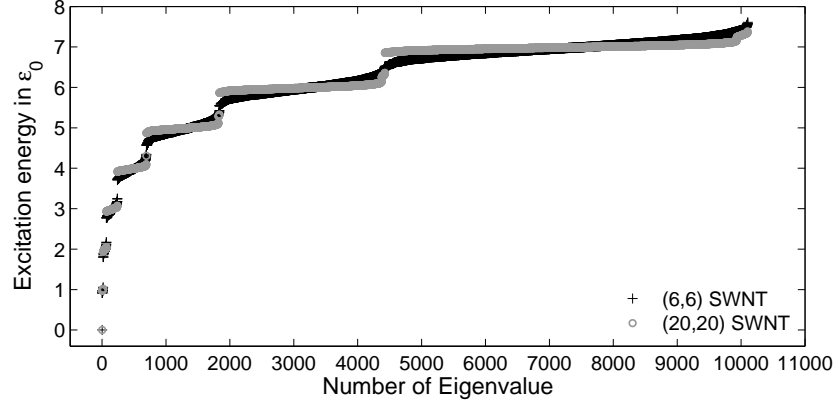


FIGURE 2.6.5. The excitation spectrum for a (6,6) SWNT (black) compared to the spectrum of a (20,20) SWNT (grey). The effects of the non-forward scattering processes are by far less pronounced in the latter case. $N_c = 4m$ and $\varepsilon_\Delta = 0$.

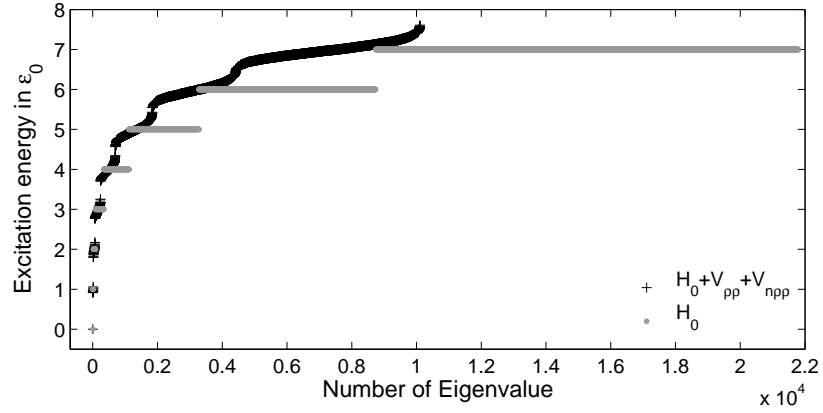


FIGURE 2.6.6. The excitation spectrum for a (6,6) SWNT obtained by diagonalizing the Hamiltonian of the noninteracting system H_0 (grey) and the full Hamiltonian $H = H_0 + V_{\rho\rho} + V_{n\rho\rho}$ (black).

groundstate structure, differences between the two works arise for the $N_c = 4m + 2$ charge state. In this situation the mean field Hamiltonian can essentially be recovered by setting all off-diagonal elements in (2.6.3) to zero. Therefore in [19] the degenerate triplet state can not be predicted but twofold degeneracies of the states $|\uparrow, \uparrow\rangle, |\downarrow, \downarrow\rangle$ and of $|\uparrow, \downarrow\rangle, |\downarrow, \uparrow\rangle$, respectively are found. Moreover contrary to our theory in [19] no

mixing of the states $|\uparrow\downarrow, -\rangle$ and $|-,\uparrow\downarrow\rangle$ can occur for $\varepsilon_\Delta \lesssim J/2$, an important point regarding the singlet-triplet Kondo effect [42].

Also the excitation spectrum shows considerable differences in both approaches, since the mean field theory misses the formation of the collective electronic excitations as the $c+$ mode, with its dispersion relation strongly renormalized by the forward scattering part of the Coulomb interaction.

2.7. Conclusions

In summary, we have derived the low energy Hamiltonian for metallic finite size SWNTs including all relevant interaction terms, especially the short ranged processes whose coupling strength scales inversely proportional to the SWNT size. We have started our examination from a tight-binding description of the p_z electrons on the honeycomb lattice of graphene. Imposing periodic boundary conditions around the circumference of the SWNT and open boundary conditions along the tube axis, we constructed standing waves $\varphi_{r\kappa}(\vec{r})$ that solve the single electron Hamiltonian of the noninteracting system. From the sublattice structure of the honeycomb lattice the pseudo spin degree of freedom r arises. The Hamiltonian of the noninteracting system, H_0 , together with the density-density part of the interaction, $V_{\rho\rho}$, could be diagonalized by bosonization and Bogoliubov transformation. In $H_0 + V_{\rho\rho}$ the different collective excitations $c+, c-, s+, s-$ do not couple. As a consequence of the forward scattering interaction V_{fff} the energies and therefore the velocity of the $c+$ excitations are strongly enhanced. The different propagation of the collective excitations, a typical feature of interacting 1D systems, has become famous under the designation of spin-charge separation. Considering only the situation away from half-filling, we obtained the spectrum of the total SWNT Hamiltonian by exploiting the small magnitude of the non-density-density contribution $V_{n\rho\rho}$ to the interaction: we have calculated the matrix elements of $V_{n\rho\rho}$ in a truncated eigenbasis of $H_0 + V_{\rho\rho}$ and diagonalized the resulting matrix to obtain the SWNT spectrum and the corresponding eigenstates. We want to point out that the applied truncation procedure is basically exact due to the large number of included eigenstates of $H_0 + V_{\rho\rho}$. We have checked that the calculated excitation spectra, shown in Figures 2.6.3 to 2.6.6, are not altered by extending the truncated eigenbasis. The calculation of the properties of the ground states and low excitations in Subsection 2.6.1 essentially corresponds to a first order perturbation treatment for degenerate systems. The results are only changed marginally if the truncated eigenbasis is enlarged.

Of special interest, concerning the ground state spectra, is the formation of a spin 1 triplet for the charge state $N_c = 4m + 2$, whose existence has clearly been proven in the experiments of Moriyama et al. [18], see Fig. 2.1.1. In the case of a band mismatch ε_Δ that is small compared to the exchange energy J , the spin 1 triplet is the ground state of the system. This finding is interesting since according to a theorem by Lieb and Mattis [39], only ground states with spin 0 or 1/2 are allowed for a 1D Hubbard model with next-neighbour hopping and no orbital degeneracies. Since our SWNT Hamiltonian includes an orbital degree of freedom we conclude that scattering processes with respect to this degree of freedom are the reason for the finding of a spin 1 ground state. Additionally we predict for $\varepsilon_\Delta \lesssim J/2$, the mixing of the states $|\uparrow\downarrow, -\rangle$

and $|-, \uparrow\downarrow\rangle$ with an accompanying energy splitting. The degree of mixing between $|\uparrow\downarrow, -\rangle$ and $|-, \uparrow\downarrow\rangle$ is of importance for the singlet-triplet Kondo effect, as discussed in [42]. An experimental confirmation of our findings in the case $\varepsilon_\Delta \lesssim J/2$ is still missing, but well within reach.

With regard to the excitation spectrum, the different bosonic modes are mixed by the non-density-density interaction processes $V_{n\rho\rho}$. Therefore the spin-charge separation is lifted. Moreover we find that the huge degeneracies which are obtained by the “standard” theory that retains only forward scattering processes are partially broken. This leads to a more and more continuous energy spectrum for higher energies.

For tubes with large diameters, the short ranged interactions become less important, and hence the “standard” Hamiltonian for strictly 1D systems, $H_0 + V_{fff}$, provides a good description of the interacting electrons, cf. Fig. 2.6.5. On a first glance that is quite counterintuitive since increasing the diameter pronounces the 3D nature of a SWNT in position space.

Because the occurrence of non-forward scattering processes with respect to the pseudo spin is strongly related with the honeycomb structure of the SWNT lattice we conjecture that exchange effects similar to the ones discussed in this chapter should also be present in other small size graphene-based structures as graphene nanoribbons or semiconducting SWNTs.

Part II
**Transport properties of single wall carbon
nanotubes**

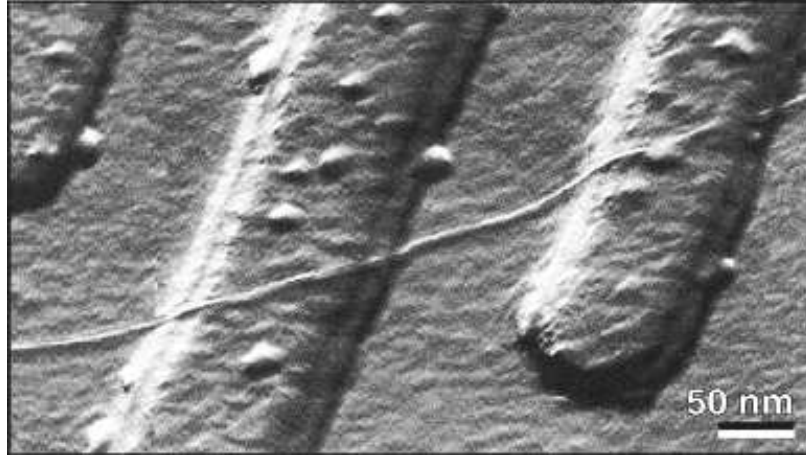


FIGURE 2.7.1. AFM picture of the first SWNT quantum dot device [43]. An individual SWNT is deposited between two Pt electrodes on a Si/SiO₂ substrate.

Introduction

As we have seen in Chapter 2 the low energy properties of interacting SWNTs differ fundamentally from the properties of higher dimensional metallic systems. Since the fabrication of electronic devices based on individual nanotubes is possible, the examination of the intriguing properties of these systems via the determination of their transport characteristics has attracted great interest of experimentalists and theoreticians. On the experimental side the investigation of transport through SWNTs started with the work [43] where for the first time current through an individual SWNT was driven. For this purpose a quantum dot setup was created. A SWNT is contacted to lead electrodes and deposited on an insulating substrate which in turn is connected to a gate electrode which allows to control the electric potential on the substrate surface and therefore the electrochemical potential in the SWNT. The device is depicted in Fig. 2.7.1. Resonant tunneling through single energy levels could be observed indicating that electrons within a SWNT propagate coherently. Moreover Coulomb blockade due to the repulsive electron-electron interactions (a detailed explanation of the Coulomb blockade will be given below) was found. As already mentioned, the verification of LL behaviour in SWNTs was achieved shortly afterwards [15, 16]. With increasing quality of the grown SWNTs also the obtained data have improved and the effect of shell filling could be observed. The discussion in the first part of the thesis has shown that four different electron species characterized by $r\sigma$ are present in SWNTs. Since electrons obey the Pauli principle, shells occupying four electrons each are formed. In transport measurements this results in a characteristic even-odd [44] or fourfold [18, 38, 20, 44] periodicity of the Coulomb blockade features with the gate voltage. Whereas the Coulomb blockade can be explained by regarding ground state properties only, the determination of the current at a higher bias voltage requires to take into account transitions of the system to excited states. Whenever new energy states enter

the bias window the current will change, leading to excitation lines in the bias- gate-voltage plane. The position of the excitation lines depends directly on the energy spectrum of the SWNT. So far excitation lines of SWNT quantum dots have only been discussed in [19, 45, 46] using a meanfield approach. In this thesis we do not only calculate the expected excitation lines but also give a quantitative calculation of the non-linear current across a SWNT quantum dot as a function of the gate and bias voltage. Prior to our work [47, 48] no quantitative analysis of the current characteristics for SWNT quantum dots had been available. In Chapter 4 we consider the case of quantum dots with non-magnetic lead electrodes. A generalization to spin dependent transport through SWNT quantum dots with ferromagnetic leads will be presented in Chapter 5. As basis we will use our almost exact results for the SWNT spectrum from Chapter 2. However, the main focus will be on medium to large diameter SWNTs where exchange effects can be neglected.

Before we actually address the physics of SWNT quantum dot, we present in the following chapter an overview of general aspects of quantum dots. Moreover a transport theory for generic quantum dots weakly coupled to the lead electrodes is derived. We are going to show in detail how the stationary current through a generic quantum dot can be determined as a function of the electrochemical potentials in the leads and in the dot. The state of the dot itself is characterized by the reduced density matrix (RDM). Its dynamics yields the current through the dot. As explained above, a net current can flow through a quantum dot if the electrochemical potentials of source and drain are adjusted to different values by the voltages V_s and V_d . Since current can only flow if one transport direction is favored, the current-carrying system will have to be treated out of equilibrium if going beyond the linear response regime. Hence, the state of the quantum dot will in general be described by a non-equilibrium density matrix. Its time evolution in the weak coupling regime is conventionally determined by Pauli rate equations [49]. However, this approach fails in general when considering degenerate systems [50]. The reason is the invariance of the Pauli rate equations under unitary transformations within the degenerate eigenstates of the dot system. In order to cure this problem we generalize the derivation of the Pauli master equation in [56] based on the Liouville equation for the RDM to degenerate systems. For this purpose we have to include coherences between degenerate states in our calculation. We have seen in our discussion of the SWNT spectrum that the latter has highly degenerate energy levels, especially if large diameter tubes are regarded for which exchange effects are absent. Thus, considerable influence of the coherences on the transport properties of SWNT quantum dots can be expected. As we shall see in Chapter 5 the inclusion of coherences is also crucial for spin degenerate energy levels of the dot in the case of arbitrarily spin polarized leads. It should be mentioned that equivalent equations of motion for the RDM can be obtained by applying the Keldysh formalism to weakly coupled quantum dots, cf. e.g. [51, 52] where transport across single level spin-valve transistors have been examined. In the derivation of the generalized master equation we will explicitly keep the dependence on the geometry of the tunneling contacts. In Chapter 4 this will reveal interesting insight into the possibility of pseudo spin polarized leads in SWNT quantum dots. It should also be mentioned that our theoretical

approach to transport via the Liouville equation can be extended to include higher order tunneling processes, thus we shall be able to go beyond weak coupling in the future **[53]**.

CHAPTER 3

Quantum Dots

In this chapter we introduce the basic concepts of quantum dots and derive a transport theory for those devices. In the subsequent chapters we are going to apply the results to examine quantum dots based on metallic finite size SWNTs.

Over the last few decades great progress has been made in creating well defined solid state devices of decreasing size. Quantum dots, objects small enough that the electron confinement leads to quantum mechanical quantization effects, have been studied extensively over the last years. A huge variety of different quantum dot setups has been examined. Examples are semiconducting dots produced by submicron fabrication techniques, metal particles, carbon nanotubes or even smaller organic molecules. Attaching leads to the quantum dots via tunneling junctions a current can be driven through the device if a bias voltage is impressed between the source and drain electrodes. In order to change the electrochemical potential, and hence the average number of electrons, the quantum dot is capacitively coupled to a gate electrode. In Fig. 3.0.1 a generic quantum dot setup is depicted.

Quantum dot setups offer excellent possibilities to study the internal electronic structure of the dots itself: The electronic transport properties, i.e., the current through the system as a function of the gate and bias voltage depends sensitively on the energy spectrum but also on the actual form of the dot eigenstates. In this chapter we make the theoretical link between the electronic properties of an interacting system like a

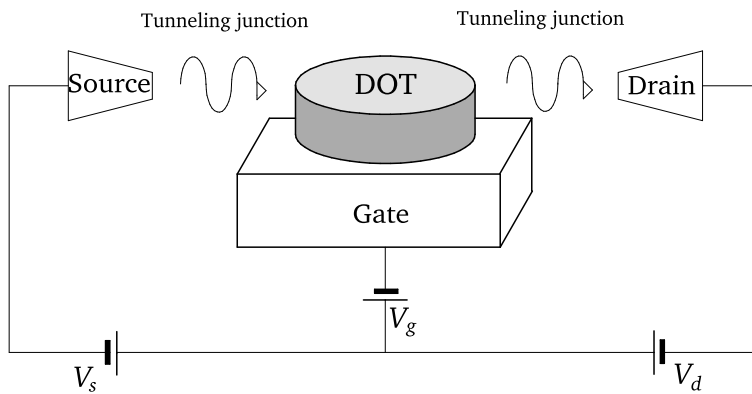


FIGURE 3.0.1. Scheme of a generic quantum dot. Source and drain electrodes are coupled to the dot via tunneling junctions. The gate allows to control the electrochemical potential in the dot.

metallic SWNT and the transport properties of the corresponding quantum dot. To start with we give a brief introduction to the general aspects of quantum dot physics.

3.1. Charge quantization and Coulomb blockade

Due to the small distances between the free charge carriers in quantum dots, the energy per electron resulting from the mutual Coulomb repulsion has a considerable value. Without caring about the details of the underlying many body processes, in the so called constant-interaction model the interaction is taken into account by assigning phenomenologically a certain capacitance C to the dot. Putting a single new electron on the dot costs the additional charging energy $E_c = \frac{e^2}{C}$. Having very small capacitances of 10^{-15} F and less, charging energies are of the order of meV and more. In carbon nanotube devices charging energies as large as 120 meV have been measured [16], exceeding the thermal energy $k_B T$ at room temperature by far.

If the coupling to the leads is weak enough such that the wavefunction of the electrons is almost entirely localized inside the dot also the number of charges in the dot is quantized. Then the number of electrons on the dot can only change by tunneling of one single electron into or out of the dot. Such a quantum dot is commonly referred to as single electron transistor or shortly as SET. In a SET setup there is always a definite integer number of electrons in the dot. Applying a bias voltage across source and drain electrodes induces transport of electrons through the dot. For temperatures with $k_B T \ll E_c$ the transport properties are strongly influenced by the charging energy. Depending on the gate voltage V_g , tunneling into the dot is forbidden if the additional charging energy cannot be compensated by the bias voltage. The absence of tunneling and hence of a current due to E_c is known under the designation Coulomb blockade. The situation can be best described in terms of the electrochemical potential in the leads and in the quantum dot (see Fig. 3.1.1). In the source and drain electrode the electrochemical potentials μ_s and μ_d differ just by the bias voltage $V_b = V_s + V_d$ times the elementary charge e . In the following we consider the case $\mu_s > \mu_d$. The electrochemical potential in the quantum dot, μ_\odot , is determined by N_c , the number of electrons in the dot and by the gate voltage, which allows to continuously shift μ_\odot up and down. Neglecting for a moment the possibly discretized energy spectrum of the electron states in the dot, adding an electron changes μ_\odot just by $E_c > 0$:

$$\mu_\odot(N_c + 1) = \mu_\odot(N_c) + E_c.$$

Tunneling into the dot occupied by N_c electrons is not possible if $\mu_\odot(N_c + 1) > \mu_s$. Tunneling out of the dot in the charge state N_c is forbidden if $\mu_\odot(N_c) < \mu_d$. Hence if both conditions are fulfilled, N_c is a stable charge state and no current can flow across the quantum dot. Thus the condition for Coulomb blockade is given by

$$\mu_\odot(N_c + 1) > \mu_s, \quad \mu_d > \mu_\odot(N_c + 1).$$

By varying the gate voltage we can adjust $\mu_\odot(N_c + 1)$ between μ_s and μ_d . Now an electron can tunnel from the source electrode into the dot increasing the number of electrons in the dot to $N_c + 1$. Since $\mu_\odot(N_c + 1) > \mu_d$ the electron can tunnel out of the dot to the drain electrode. The dot recovers its state with N_c electrons and is ready for a new electron to enter. Now the cycle can start again. This chain of tunneling events leads to charge transport, that can be observed experimentally. By

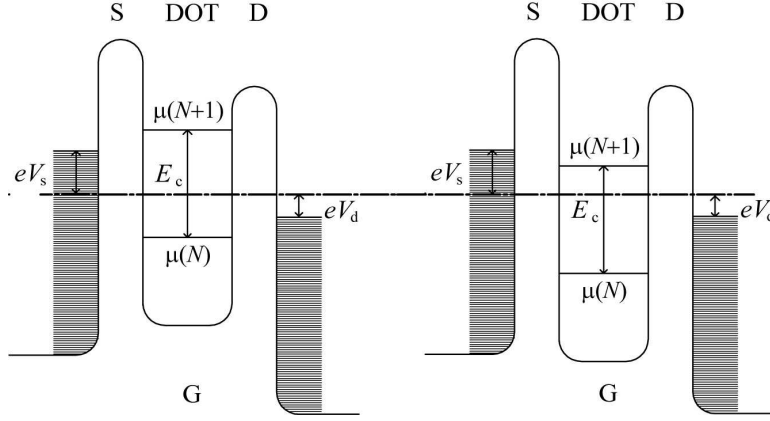


FIGURE 3.1.1. Energy scheme in a quantum dot setup. The states in source and drain are filled up to the actual electrochemical potential. Changing the number of electrons in the dot from N to $N + 1$, raises the electrochemical potential from $\mu_{\odot}(N)$ to $\mu_{\odot}(N + 1)$. The difference of $\mu_{\odot}(N + 1)$ and $\mu_{\odot}(N)$ is the charging energy E_c plus possibly the energy level spacing. In the left setup, tunneling is not possible, since tunneling between the leads and the dot would violate the conservation of energy. In the right quantum dot, there are states in the dot available that are between the electrochemical potentials of the leads, and thus tunneling events from the source to the dot and from the dot to the drain are possible.

fixing the bias voltage to a value below E_c and sweeping the gate voltage, we get alternating intervals of zero conductance (Coulomb blockade) and finite conductance (tunneling off and into the dot is allowed). In Fig. 3.1.2 data from such a so called Coulomb oscillation in a SWNT quantum dot is shown. If eV_b exceeds E_c , there is no stable charge state any more, hence current flows for arbitrary gate voltage. In total Coulomb blockade results in the formation of the so called Coulomb diamonds. These are diamond shaped regions in the V_b - V_g plane, where charge transport is suppressed due to Coulomb blockade (Fig. 3.1.3). The approximation of a constant charging energy E_c for all N_c that we have used here is called constant interaction model. It is based on the assumption that the ground state energy of the dot system depends like $\frac{1}{2}E_c N_c^2$ on the charge state N_c . However, as we already know from our discussion in Chapter 2, in realistic systems generally a more complicated energy dependence on N_c due to shell filling and exchange effects is found.

3.1.1. Energy level quantization. In general the electrons in a quantum dot exhibit discrete energy levels due to the finite system size. We have already seen in the first part of the thesis that the energy levels in finite size metallic SWNTs are indeed

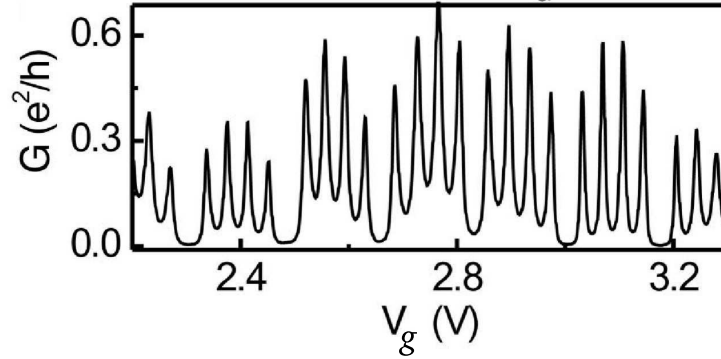


FIGURE 3.1.2. Coulomb oscillations of a SWNT quantum dot [20]: By fixing the bias voltage at low values and varying the gate voltage, the quantum dot Coulomb blockade is alternately switched on and off. Note the fourfold periodicity of the conductance G as a function of the gate voltage V_g . As we will see it results from the Pauli shell filling due to the four electron species in SWNTs characterized by r and σ (see also Fig. 4.4.2).

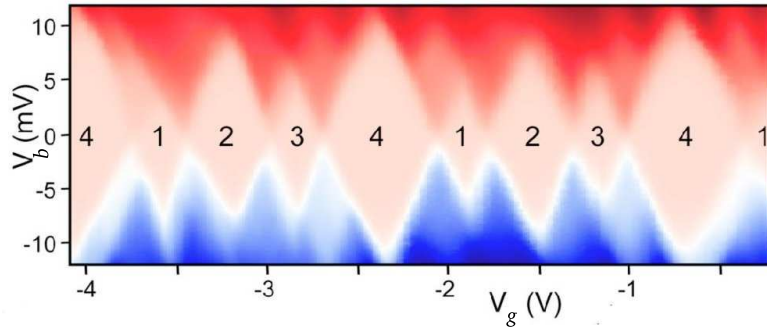


FIGURE 3.1.3. Coulomb diamonds for a SWNT quantum dot [20]. In the diamond shaped regions around $V_b = 0$ no current is flowing due to Coulomb blockade. Note again the fourfold periodicity along the V_g axis.

quantized, although for small diameter tubes a quasi-continuum forms at higher energies due to electron-electron interactions. The magnitude of the typical level splitting ΔE depends strongly on the type of quantum dot and the considered energy regime. Depending on the charging energy E_c and ΔE we can expect to find three different temperature regimes:

- (1) $E_c \ll k_B T$: No effects due to the discrete nature of charge or of the energy spectrum can be observed.

- (2) $E_c \gg k_B T \gg \Delta E$: This is the so called classical Coulomb blockade regime. Coulomb oscillations are present, but thermal fluctuations smear out effects due to a finite energy level splitting.
- (3) $E_c, \Delta E \gg k_B T$: The quantum Coulomb blockade regime. Here transport measurements reveal both charge- and energy level quantization. This is the regime of interest in this thesis.

A similar characterization of different transport regimes also holds with respect to the coupling between electrodes and dot. For highly transparent contacts the energy levels of the dot become life time broadened as a consequence of the uncertainty relation. It holds $\Delta E_{lt} \geq \hbar\Gamma$, where ΔE_{lt} is the broadening and Γ is the tunneling rate. Only for $E_c, \Delta E \gg \hbar\Gamma$ the excitation spectrum can clearly be resolved. With increasing Γ higher order processes like the Kondo effect [54] become effective. In this thesis we concentrate on weak coupling between the SWNT dot and the leads, i.e., on the case $E_c, \Delta E \gg \hbar\Gamma$.

Transport theory for weakly coupled quantum dots

In this section we derive a method to determine the stationary current through a generic quantum dot described by the Hamiltonian (3.2.1), see below, as a function of the electrochemical potentials in the leads and in the dot. The outcomes of this chapter will be used in Chapters 4 and 5 to obtain the I - V_b - V_g characteristics of SWNT quantum dots with unpolarized and polarized leads respectively.

3.2. Model Hamiltonian

Let us now examine the physics of a generic quantum dot in detail. We describe the overall system by the Hamiltonian

$$H = H_\odot + H_s + H_d + H_T + H_{ext}, \quad (3.2.1)$$

where H_\odot can describe an interacting SWNT or any other conductor with known many-body eigenstates. $H_{s/d}$ describe the isolated metallic source and drain contacts as a Fermi gas of noninteracting quasi-particles,

$$H_l = \sum_{\sigma \vec{q}} \varepsilon_{\vec{q}\sigma,l} c_{\vec{q}\sigma l}^\dagger c_{\vec{q}\sigma l}, \quad (3.2.2)$$

where $c_{\vec{q}\sigma l}^\dagger$ creates a quasi-particle with spin σ and energy $\varepsilon_{\vec{q}\sigma,l}$ in lead $l = s, d$. The transfer of electrons between the leads and the central system is taken into account by the tunnelling Hamiltonian

$$H_T = \sum_{l=s,d} \sum_{\sigma} \int d^3r \left(T_l(\vec{r}) \Psi_\sigma^\dagger(\vec{r}) \Phi_{\sigma l}(\vec{r}) + \text{h.c.} \right), \quad (3.2.3)$$

where $\Psi_\sigma^\dagger(\vec{r})$ and $\Phi_{\sigma l}^\dagger(\vec{r}) = \sum_{\vec{q}} \phi_{\vec{q}}^*(\vec{r}) c_{\vec{q}\sigma l}^\dagger$ are electron creation operators in the dot and in lead l , respectively, and $T_l(\vec{r})$ describes the generally position dependent transparency of the tunnelling contact at lead l .

Finally, H_{ext} accounts for the energy dependence of the system on the external voltage sources controlling the electrochemical potentials in the leads and in the dot itself. For completeness we briefly present a derivation of H_{ext} based on modelling

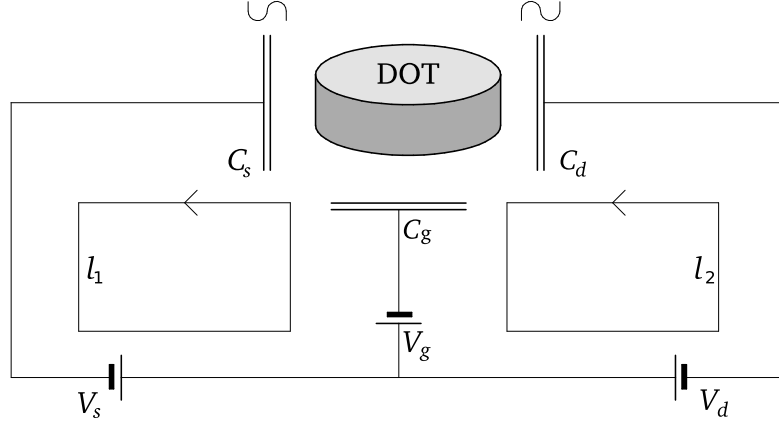


FIGURE 3.2.1. Capacitor model for a quantum dot. The influence of the voltage sources on the electrostatics of the circuit is modelled by the capacitors C_s , C_d and C_g . Waves above the capacitors C_s and C_d indicate that tunneling between the leads and the dot is possible.

the influence of the tunneling junctions and the gate on the electrostatic energy of the setup by assigning capacitors C_j , $j = s, d, g$ to each electrode [55], cf. Fig. 3.2.1. We start by exploiting charge conservation which yields

$$Q_g + Q_s + Q_d + Q_\odot = 0, \quad (3.2.4)$$

where Q_l , $l = s, d, g$ are the charges which have flowed onto the capacitors and $Q_\odot = eN_c$, $N_c \in \mathbb{Z}$ is the number of elementary charges on the dot. By applying Kirchhoff's rule to the two loops l_1 and l_2 indicated in Fig. 3.2.1, we find

$$U_l + V_l - U_g - V_g = 0, \quad l = s, d, \quad (3.2.5)$$

where U_l , $l = s, d, g$ is the voltage drop over capacitor C_l . Note that along the loops l_1 and l_2 the voltage drop over the gate capacitor is opposed to the ones over the lead capacitors. Therefore U_g comes with a minus sign in (3.2.5). Using $U_l = Q_l/C_l$ we find

$$Q_l = C_l \left(V_g + \frac{Q_g}{C_g} - V_l \right). \quad (3.2.6)$$

Combining (3.2.4) and (3.2.6) we obtain the dependence of the capacitor charges on the voltages and the dot charge,

$$Q_l = -\frac{C_l}{C_\Sigma} \left(\sum_{l' \in \{s, d, g\} \setminus l} C_{l'} (V_l - V_{l'}) + Q_\odot \right), \quad (3.2.7)$$

where $C_\Sigma := \sum_{l=s, d, g} C_l$. A tunneling event changes Q_\odot by $\mp e$ if an electron is transferred from one of the leads to the dot and the other way round respectively. This implies also a change of the charges Q_l according to (3.2.7), namely

$$Q_l \rightarrow Q_l + \delta Q_l = Q_l \pm \frac{C_l}{C_\Sigma} e, \quad l = s, d, g.$$

If the tunneling takes place at lead l the charge δQ_l can be decomposed into the charge of the electron that is tunneling and the charge ΔQ_l that flows over the voltage source V_l . It holds

$$\delta Q_l = \pm e + \Delta Q_l \stackrel{!}{=} \pm \frac{C_l}{C_\Sigma} e$$

and hence

$$\Delta Q_l = \pm \left(\frac{C_l}{C_\Sigma} - 1 \right) e.$$

At the other lead \bar{l} and at the gate the charge that passes the voltage source is equal to $\delta Q_{\bar{l}}$ and δQ_g , respectively. In total this yields for the energy provided by the voltage sources when an electron is tunneling into/ out of the dot at lead l ,

$$\Delta E_l = \mp e \left[\left(\frac{C_l}{C_\Sigma} - 1 \right) V_l + \frac{C_{\bar{l}}}{C_\Sigma} V_{\bar{l}} + \frac{C_g}{C_\Sigma} V_g \right]. \quad (3.2.8)$$

Given (3.2.8) it is convenient to replace the Hamiltonian from (3.2.1) by

$$H = H_\odot + H_s + H_d + H_g + H_T, \quad (3.2.9)$$

where upon absorbing terms that are directly related to the tunneling, we now write for the lead Hamiltonians

$$H_l = \sum_{\sigma \bar{q}} (\varepsilon_{\bar{q}\sigma, l} - eV_l) c_{\bar{q}\sigma l}^\dagger c_{\bar{q}\sigma l}, \quad (3.2.10)$$

where the energies have been shifted by the applied voltage, $\varepsilon_{\bar{q}\sigma, l} \rightarrow \varepsilon_{\bar{q}\sigma, l} - eV_l$. Additionally we incorporate the effect of the voltage sources on the electrochemical potential into the dot Hamiltonian by redefining

$$H_\odot \rightarrow H_\odot - \mu_g \mathcal{N}_c. \quad (3.2.11)$$

Here \mathcal{N}_c counts the total electron number in the dot and μ_g is determined by the relation

$$\mu_g = \frac{e}{C_\Sigma} (C_s V_s + C_d V_d + C_g V_g).$$

Commonly it is assumed that $C_s = C_d$ and $V_s = -V_d$ such that

$$\mu_g = \frac{C_g}{C_\Sigma} e V_g.$$

With (3.2.9) we are now ready to determine the dynamics of the quantum dot RDM.

3.3. Dynamics of the reduced density matrix

Our starting point is the Liouville equation for the time evolution of the density matrix $\rho(t)$ of the total system consisting of the leads and the dot. Since we assume a weak coupling between leads and dot, the tunnelling Hamiltonian H_T from equation (3.2.3) is treated as perturbation. We calculate the time dependence of $\rho(t)$ in the interaction picture, i.e., we define

$$\rho^I(t) = U_I(t, t_0) \rho(t_0) U_I^\dagger(t, t_0), \quad (3.3.1)$$

where the time evolution operator $U_I(t, t_0)$ is given by

$$U_I(t, t_0) = e^{\frac{i}{\hbar}(H_\odot + H_s + H_d)(t-t_0)} e^{-\frac{i}{\hbar}(H_\odot + H_s + H_d + H_T)(t-t_0)}, \quad (3.3.2)$$

with t_0 being some reference time. Using (3.3.1) and (3.3.2) the Liouville equation in the interaction picture reads

$$i\hbar \frac{\partial \rho^I(t)}{\partial t} = [H_T^I(t), \rho^I(t)], \quad (3.3.3)$$

with $H_T^I(t) = e^{\frac{i}{\hbar}(H_\odot + H_s + H_d)(t-t_0)} H_T e^{-\frac{i}{\hbar}(H_\odot + H_s + H_d)(t-t_0)}$. Equivalently we can write

$$\rho^I(t) = \rho^I(t_0) - \frac{i}{\hbar} \int_{t_0}^t [H_T^I(t_1), \rho(t_1)] dt_1. \quad (3.3.4)$$

Reinserting (3.3.4) back into (3.3.3) yields

$$\dot{\rho}^I(t) = -\frac{i}{\hbar} [H_T^I, \rho(t_0)] + \left(\frac{i}{\hbar}\right)^2 \int_{t_0}^t dt_1 [H_T^I(t), [H_T^I(t_1), \rho^I(t_1)]] . \quad (3.3.5)$$

Since we are interested in the transport through the central system, it is sufficient to consider the RDM ρ_\odot^I of the dot, which can be obtained from ρ^I by tracing out the lead degrees of freedom, i.e.,

$$\rho_\odot^I = \text{Tr}_{\text{leads}} \rho^I. \quad (3.3.6)$$

In general the leads can be considered as large systems compared to the dot. Besides we only consider the case of weak tunnelling, such that the influence of the central system on the leads is only marginal. Thus from now on we treat the leads as reservoirs which stay in thermal equilibrium and make the following ansatz to factorise the density matrix $\rho^I(t)$ of the total system as

$$\rho^I(t) = \rho_\odot^I(t) \rho_s \rho_d =: \rho_\odot^I(t) \rho_{\text{leads}}, \quad (3.3.7)$$

where ρ_s and ρ_d are time independent and given by the usual thermal equilibrium expression

$$\rho_{s/d} = \frac{e^{-\beta(H_{s/d} - \mu_{s/d} \mathcal{N}_{s/d})}}{Z_{s/d}}, \quad (3.3.8)$$

with $\beta = 1/k_B T$ the inverse temperature. As it can be formally shown [56], the factorization (3.3.7) corresponds, like Fermi's Golden Rule, to a second order treatment in the perturbation H_T . Furthermore, we can significantly simplify equation (3.3.5) by making the so called Markov approximation. The idea is that the dependence of $\dot{\rho}^I(t)$ on $\rho^I(t')$ is only local in time. In more detail, $\rho^I(t')$ is replaced by $\rho^I(t)$ in (3.3.5). The Markov approximation is closely connected to the correlation time τ of the leads. In our case τ is the time after which the correlation functions of the lead electron operators,

$$\langle \Phi_{\sigma l}^\dagger(\vec{r}, \tau) \Phi_{\sigma l}(\vec{r}', 0) \rangle_{\text{th}} := \text{Tr}_{\text{leads}} \left(\Phi_{\sigma l}^\dagger(\vec{r}, \tau) \Phi_{\sigma l}(\vec{r}', 0) \rho_{\text{leads}} \right),$$

are vanishing. Thus τ indicates the time scale on which the system forgets about its past. If the dynamics of the dot is slow enough, i.e., if $\rho^I(t')$ is not considerably changing during τ the Markov approximation is valid. It must be noted that the Markov approximation leads to an averaging of the time evolution of $\rho^I(t)$ on timescales of the order of τ , such that details of the dynamics on short time scales are not accessible. Since we are interested in the dc current through the system, this imposes no restriction on our purpose. Finally we get, by inserting equations (3.3.6), (3.3.7) and (3.3.8) into

(3.3.5), the following expression for the equation of motion for the RDM,

$$\begin{aligned} \dot{\rho}_{\odot}^I(t) = & -\frac{i}{\hbar} Tr_{\text{leads}} [H_T^I, \rho_{\odot}^I(t_0) \rho_{\text{leads}}] \\ & + \left(\frac{i}{\hbar}\right)^2 Tr_{\text{leads}} \int_{t_0}^t dt_1 [H_T^I(t), [H_T^I(t_1), \rho_{\odot}^I(t) \rho_{\text{leads}}]] . \end{aligned} \quad (3.3.9)$$

The first term vanishes because of $\langle \Phi_{\sigma l}(\vec{r}) \rangle_{\text{th}} = 0$. Since we are only interested in the longterm behaviour of the system we send $t_0 \rightarrow -\infty$. Writing out the double commutator in (3.3.9) according to

$$[A, [B, C]] = ABC + CBA - ACB - BCA,$$

and introducing the variable $t' = t - t_1$ one obtains

$$\begin{aligned} \dot{\rho}_{\odot}^I(t) = & -\frac{1}{\hbar^2} Tr_{\text{leads}} \int_0^\infty dt' [(H_T^I(t) H_T^I(t-t') \rho_{\odot}^I(t) \rho_{\text{leads}} + h.c.) \\ & - (H_T^I(t) \rho_{\odot}^I(t) \rho_{\text{leads}} H_T^I(t-t') + h.c.)] . \end{aligned} \quad (3.3.10)$$

Now we insert the explicit form of H_T from equation (3.2.3) into (3.3.10) and perform the trace over the lead degrees of freedom. Thereby we exploit the relations

$$\langle \Phi_{\sigma l} \Phi_{\sigma' l'} \rangle_{\text{th}} = \langle \Phi_{\sigma l}^\dagger \Phi_{\sigma' l'}^\dagger \rangle_{\text{th}} = 0,$$

as well as

$$\langle \Phi_{\sigma l} \Phi_{\sigma' l'}^\dagger \rangle_{\text{th}} = 0 \quad \text{for } \sigma l \neq \sigma' l',$$

such that

$$\begin{aligned} \dot{\rho}_{\odot}^I(t) = & -\frac{1}{\hbar^2} \sum_{l=s,d} \sum_{\sigma} \int d^3x \int d^3y \int_0^\infty dt' \\ & \times \left\{ \left[\mathcal{E}_{\sigma l}(\vec{x}, \vec{y}, t') \Psi_{\sigma}^\dagger(\vec{x}, t) \Psi_{\sigma}(\vec{y}, t-t') \rho_{\odot}^I(t) \right. \right. \\ & + \left. \mathcal{F}_{\sigma l}(\vec{x}, \vec{y}, t') \Psi_{\sigma}(\vec{x}, t) \Psi_{\sigma}^\dagger(\vec{y}, t-t') \rho_{\odot}^I(t) \right] + h.c. \\ & - \left[\mathcal{F}_{\sigma l}^*(\vec{x}, \vec{y}, t') \Psi_{\sigma}^\dagger(\vec{x}, t) \rho_{\odot}^I(t) \Psi_{\sigma}(\vec{y}, t-t') \right. \\ & + \left. \mathcal{E}_{\sigma l}^*(\vec{x}, \vec{y}, t') \Psi_{\sigma}(\vec{x}, t) \rho_{\odot}^I(t) \Psi_{\sigma}^\dagger(\vec{y}, t-t') \right] - h.c. \left. \right\} . \end{aligned} \quad (3.3.11)$$

In (3.3.11) we have introduced

$$\mathcal{E}_{\sigma l}(\vec{x}, \vec{y}, t') := T_l(\vec{x}) T_l^*(\vec{y}) \langle \Phi_{\sigma l}(\vec{x}) \Phi_{\sigma l}^\dagger(\vec{y}, -t') \rangle_{\text{th}} . \quad (3.3.12)$$

Similarly it holds

$$\mathcal{F}_{\sigma l}(\vec{x}, \vec{y}, t') := T_l^*(\vec{x}) T_l(\vec{y}) \langle \Phi_{\sigma l}^\dagger(\vec{x}) \Phi_{\sigma l}(\vec{y}, -t') \rangle_{\text{th}} , \quad (3.3.13)$$

with

$$\langle \Phi_{\sigma l}^\dagger(\vec{x}) \Phi_{\sigma l}(\vec{y}, -t') \rangle_{\text{th}} = \int d\varepsilon \rho_l^\oplus(\varepsilon) \sum_{\vec{q}|\varepsilon} \phi_{\vec{q}}^*(\vec{x}) \phi_{\vec{q}}(\vec{y}) e^{\frac{i}{\hbar}(\varepsilon - eV_l)t'} . \quad (3.3.14)$$

Here $\rho_l^\oplus(\varepsilon) = \rho_l(\varepsilon)f(\varepsilon)$. Via the functions $\mathcal{E}_{\sigma l}(\vec{x}, \vec{y}, t')$ and $\mathcal{F}_{\sigma l}(\vec{x}, \vec{y}, t')$ not only the properties of the leads but also of the tunneling junctions enter the dynamics as we will see later on. In order to proceed, it is convenient to represent the RDM in the eigenstate basis of the dot Hamiltonian H_\odot . Assuming that we can diagonalize the many-body Hamiltonian H_\odot (see Chapter 4 for SWNTs), this allows us to extract the t and t' dependence of the electron operators in (3.3.11): Let $|j\rangle$ and $|k\rangle$ be eigenstates of H_\odot from the N , $N + 1$ particle Hilbert spaces \mathcal{H}_N and \mathcal{H}_{N+1} , respectively. Then it holds

$$\langle k | \Psi_\sigma(\vec{x}, t) | m \rangle =: (\Psi_\sigma(\vec{x}, t))_{km} = (\Psi_\sigma(\vec{x}))_{km} e^{\frac{i}{\hbar}(E_k - E_m)(t - t_0)},$$

where we have used

$$H_\odot |k\rangle = E_k |k\rangle$$

and

$$\Psi_\sigma(\vec{x}, t) = e^{\frac{i}{\hbar}H_\odot(t-t_0)}\Psi_\sigma(\vec{x})e^{-\frac{i}{\hbar}H_\odot(t-t_0)}.$$

To proceed further, we carry out the following two major approximations:

I) We assume that density matrix elements between states representing different charge states vanish (the system is supposed to be always in an eigenstate of the number counting operator \mathcal{N}_c , since the number of electrons in the dot influences the electrostatics of the whole circuit, hence is “measured” permanently). Thus we only have to regard block matrices $\rho^{IN}(t)$ describing the state of the dot containing N electrons. In the eigenbasis of H_\odot equation (3.3.11) then reads

$$\begin{aligned} \dot{\rho}_{nm}^{IN}(t) = & -\frac{1}{\hbar^2} \sum_{l=s,d} \sum_{\sigma} \left[\sum_{j \in \mathcal{H}_N} \left(\sum_{i \in \mathcal{H}_{N-1}} \Gamma_{l,niij}^{(+N-1)} + \sum_{k \in \mathcal{H}_{N+1}} \Gamma_{l,nkkj}^{(+N+1)} \right) \rho_{jm}^{IN}(t) e^{\frac{i}{\hbar}E_{nj}(t-t_0)} \right. \\ & + \sum_{j' \in \mathcal{H}_N} \left(\sum_{i \in \mathcal{H}_{N-1}} \Gamma_{l,j'ii m}^{(-N-1)} + \sum_{k \in \mathcal{H}_{N+1}} \Gamma_{l,j'kk m}^{(-N+1)} \right) \rho_{nj'}^{IN}(t) e^{\frac{i}{\hbar}E_{j'm}(t-t_0)} \\ & - \sum_{i,i' \in \mathcal{H}_{N-1}} \left(\Gamma_{l,i'mni}^{(-N-1)} + \Gamma_{l,i'mni}^{(+N-1)} \right) \rho_{ii'}^{IN-1}(t) e^{\frac{i}{\hbar}(E_{ni} + E_{i'm})(t-t_0)} \\ & \left. - \sum_{k,k' \in \mathcal{H}_{N+1}} \left(\Gamma_{l,k'mnk}^{(-N+1)} + \Gamma_{l,k'mnk}^{(+N+1)} \right) \rho_{kk'}^{IN+1}(t) e^{\frac{i}{\hbar}(E_{nk} + E_{k'm})(t-t_0)} \right], \end{aligned} \quad (3.3.15)$$

where we have introduced the quantities $\Gamma_{l,k'mnk}^{(\alpha)N \pm 1}$ that determine the transition amplitudes between states with N particles to states with $N \pm 1$ particles,

$$\begin{aligned} \Gamma_{l,k'mnk}^{(\alpha)N-1} := & \frac{1}{\hbar^2} \sum_{\sigma} \int d^3x \int d^3y \times \\ & \left(\Psi_{\sigma}^{\dagger}(\vec{x}) \right)_{k'm}^{N-1} \left(\Psi_{\sigma}(\vec{y}, -\alpha t') \right)_{nk}^{N-1} \int_0^{\infty} dt' \mathcal{E}_{\sigma l}(\vec{x}, \vec{y}, \alpha t'), \end{aligned} \quad (3.3.16)$$

and

$$\Gamma_{l,k'mnk}^{(\alpha)N,N+1} := \frac{1}{\hbar^2} \sum_{\sigma} \int d^3x \int d^3y \times \\ (\Psi_{\sigma}(\vec{x}))_{k'm}^{N,N+1} \left(\Psi_{\sigma}^{\dagger}(\vec{y}, -\alpha t') \right)_{nk}^{N+1,N} \int_0^{\infty} dt' \mathcal{F}_{\sigma l}(\vec{x}, \vec{y}, \alpha t'). \quad (3.3.17)$$

Furthermore we have introduced the following notation for the matrix elements of the electron operator,

$$(\Psi_{\sigma}(\vec{x}))_{km}^{N,N+1} := \langle k | \Psi_{\sigma}(\vec{x}) | m \rangle, \quad (3.3.18)$$

with the states $|k\rangle$ and $|m\rangle$ having particle number N , $N+1$ respectively and being eigenstates of H_{\odot} . The energy differences E_{nj} appearing in (3.3.15) are given by

$$E_{nj} = E_n - E_j.$$

II) Secondly the so called *secular approximation* is applied, i.e., we only retain those terms in the equation of motion, which have no oscillatory behavior in t . For the dynamics this means that we can not resolve the evolution of $\rho_{\odot}^I(t)$ on time scales of $\hbar/(E_m - E_n)$, where E_m and E_n are two distinct energy levels of H_{\odot} . From the second and third line of (3.3.15) we find that the secular approximation leads to the conditions

$$E_n = E_j, \quad (3.3.19)$$

$$E_m = E_{j'}, \quad (3.3.20)$$

and from the fourth and fifth line it follows

$$E_n - E_k + E_{k'} - E_m = 0, \quad E_n - E_i + E_{i'} - E_m = 0. \quad (3.3.21)$$

If we choose $E_n = E_m$, $E_n \neq E_m$ in (3.3.19) of (3.3.20) then of course also $E_m = E_j$, $E_m \neq E_j$ and $E_n = E_{j'}$, $E_n \neq E_{j'}$ must hold. Additionally if $E_n = E_m$, $E_n \neq E_m$ in (3.3.21), $E_{k,i} = E_{k',i'}$, $E_{k,i} \neq E_{k',i'}$ must be fulfilled. With this consideration it is now easy to see that the equations of motion (3.3.15) of the RDM elements between degenerate states and those between non-degenerate states become decoupled as a consequence of the secular approximation. Because the current is determined by the dynamics of the occupations (the diagonal elements of the RDM) we can henceforth focus on the time evolution of the degenerate matrix elements. Hence we can decompose the $\rho_{\odot}^I(t)$ further into block matrices $\rho_{\odot}^{IE_N}(t)$ restricted to the Hilbert space \mathcal{H}_{E_N} spanned by the states belonging to a certain energy level E_N and charge state N . A scheme of the resulting structure of the RDM is shown in Fig. 3.3.1. To simplify the notation we give the resulting equations of motion for $\rho_{\odot}^{IE_N}(t)$ in Bloch-Redfield form,

$$\dot{\rho}_{nm}^{I,E_N}(t) = - \sum_{kk'} R_{nm, kk'}^{E_N} \rho_{kk'}^{I,E_N}(t) + \sum_{M=N\pm 1} \sum_{E'} \sum_{kk'} R_{nm, kk'}^{E_N E'_M} \rho_{kk'}^{I,E'_M}(t), \quad (3.3.22)$$

where the indices n, m, k, k' refer to the eigenstates of H_{\odot} . The Redfield tensors are given by ($l = s, d$)

$$R_{nm, kk'}^{E_N} = \sum_l \sum_{M, E', j} \left(\delta_{mk'} \Gamma_{l, njjk}^{(+E_N E'_M)} + \delta_{nk} \Gamma_{l, k'jjm}^{(-E_N E'_M)} \right), \quad (3.3.23)$$

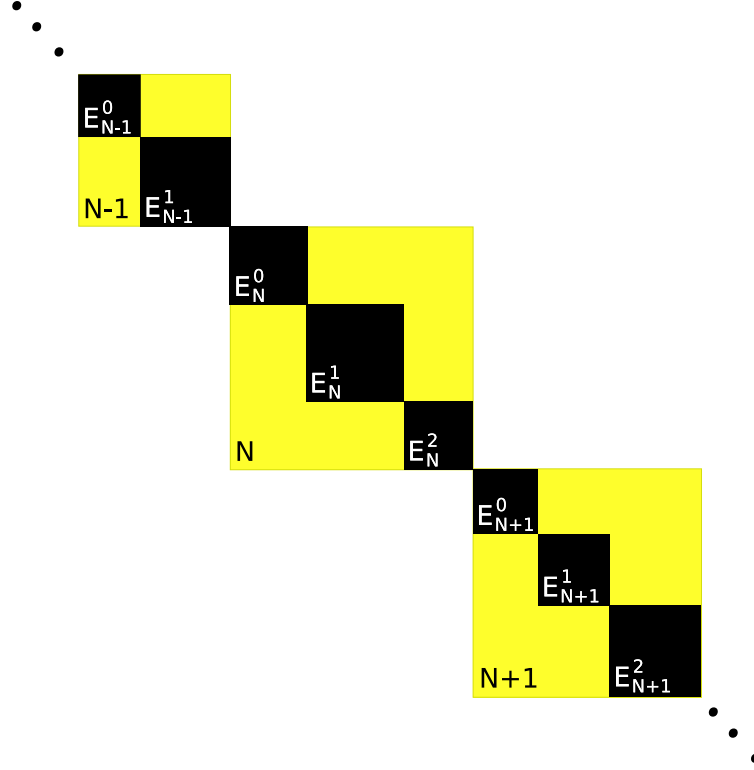


FIGURE 3.3.1. Scheme of the reduced density matrix. Only coherences between states with identical particle number and energy are kept.

and

$$R_{nm\,kk'}^{E_N\,E'_M} = \sum_{l,\alpha=\pm} \Gamma_{l,k'mnk}^{(\alpha)E'_M\,E_N}. \quad (3.3.24)$$

In analogy to $\Gamma_{l,k'mnk}^{(\alpha)N\,N\pm 1}$ we have introduced the transition amplitudes $\Gamma_{l,k'mnk}^{(\alpha)E_N\,E'_{N\pm 1}}$ from states with N particles and energy E_N to states with $N \pm 1$ particles and energy $E'_{N\pm 1}$. In detail we obtain from (3.3.15) for transitions $N \rightarrow N + 1$

$$\begin{aligned} \Gamma_{l,k'mnk}^{(\alpha)E_N\,E'_{N+1}} = & \frac{1}{\hbar^2} \sum_{\sigma} \int d^3x \int d^3y (\Psi_{\sigma}(\vec{x}))_{k'm}^{E_N\,E'_{N+1}} \left(\Psi_{\sigma}^{\dagger}(\vec{y}) \right)_{nk}^{E'_{N+1}\,E_N} \times \\ & \int_0^{\infty} dt' \mathcal{F}_{\sigma l}(\vec{x}, \vec{y}, \alpha t') e^{-\alpha \frac{i}{\hbar} (E'_{N+1} - E_N) t'}. \end{aligned} \quad (3.3.25)$$

For transitions $N \rightarrow N - 1$ is

$$\begin{aligned} \Gamma_{l,k'mnk}^{(\alpha)E_N E_{N-1}} = & \frac{1}{\hbar^2} \sum_{\sigma} \int d^3x \int d^3y \left(\Psi_{\sigma}^{\dagger}(\vec{x}) \right)_{k'm}^{E_N E'_{N-1}} \left(\Psi_{\sigma}(\vec{y}) \right)_{nk}^{E'_{N-1} E_N} \times \\ & \int_0^{\infty} dt' \mathcal{E}_{\sigma l}(\vec{x}, \vec{y}, \alpha t') e^{-\alpha \frac{i}{\hbar} (E'_{N-1} - E_N) t'}, \end{aligned} \quad (3.3.26)$$

where now

$$(\Psi_{\sigma}(\vec{x}))_{km}^{E_N E'_{N+1}} := \langle k | \Psi_{\sigma}(\vec{x}) | m \rangle, \quad (3.3.27)$$

denotes the matrix element of the dot electron operator between the states $|k\rangle$ and $|m\rangle$ having energy E_N , E'_{N+1} and particle number N , $N + 1$, respectively.

Equation (3.3.22) governs the dynamics of the dot electrons. In the following we deduce therefrom the current through the system.

3.4. Current

The current is essentially the net tunnelling rate in a certain direction at one of the leads. Thus the current at lead l will be of the form

$$I_l = le \sum_N \left(\Sigma_l^{N \rightarrow N+1} - \Sigma_l^{N \rightarrow N-1} \right), \quad (3.4.1)$$

where we use the convention $l = s/d = \pm 1$. On the long run the currents at the two leads have to be equal, otherwise charge would accumulate on the dot which is prevented by the charging energy. The rates $\Sigma_l^{N \rightarrow N \pm 1}$ can be obtained from the time evolution of the occupation probabilities $P_N = Tr \left(\rho_{\odot}^{I,N} \right)$. In more detail, the occupation probability of the charge state N is reduced by tunnelling events changing the number of electrons from N to $N \pm 1$ and is increased by processes transferring the charge states $N \pm 1$ to N , hence

$$\dot{P}_N = Tr \left(\dot{\rho}_{\odot}^{I,N} \right) = \sum_l \left(-\Sigma_l^{N \rightarrow N+1} - \Sigma_l^{N \rightarrow N-1} + \Sigma_l^{N+1 \rightarrow N} + \Sigma_l^{N-1 \rightarrow N} \right).$$

Using $Tr \left(\dot{\rho}_{\odot}^{I,N} \right) = \sum_{E_N} Tr \left(\dot{\rho}_{\odot}^{I,E_N} \right)$ together with (3.3.22) we can easily identify the rates appearing in (3.4.1):

$$\Sigma_l^{N \rightarrow N \pm 1} = \sum_{E, E'} \sum_{nkj} \left(\Gamma_{l,njjk}^{(+E_N E'_{N \pm 1}} \rho_{kn}^{I,E_N} + \rho_{nk}^{I,E_N} \Gamma_{l,kjjn}^{(-E_N E'_{N \pm 1}} \right). \quad (3.4.2)$$

Since the relation $\Gamma_{l,njjk}^{(+E_N E'_{N \pm 1}} = \left(\Gamma_{l,kjjn}^{(-E_N E'_{N \pm 1}} \right)^*$ holds, we arrive, by inserting (3.4.2) into (3.4.1), at the following expression,

$$I_l = l2e \text{Re} \sum_{N, E, E'} \sum_{nkj} \left(\Gamma_{l,njjk}^{(+E_N E'_{N+1}} - \Gamma_{l,njjk}^{(+E_N E'_{N-1}} \right) \rho_{kn}^{I,E_N}. \quad (3.4.3)$$

For the actual calculations we are going to replace ρ^{I,E_N} in (3.4.3) by the stationary solution ρ_{st}^{I,E_N} of (3.3.11), because we are only interested in the longterm behavior of

the system.

Note: The expression for the current explicitly contains coherences of the RDM. From a mathematical point of view the inclusion of the coherences is necessary in order to assure the invariance of the transport calculation under any unitary transformation U_{E_N} within the Hilbert spaces \mathcal{H}_{E_N} that contain all dot eigenstates with a certain energy and particle number. In Appendix G we rewrite the master equation (3.3.22) and the expression (3.4.3) for the current in a form that is obviously independent of the chosen basis of \mathcal{H}_{E_N} . On the other hand the RDM is hermitian, thus there is always an appropriate eigenbasis of H_\odot in which all coherences are vanishing. The problem is that for a complex system it is not trivial to find the diagonalizing basis a priori. Moreover this “diagonal” basis depends sensitively on the available energies, especially on the bias and gate voltage. \diamond

Until now our treatment has been quite general, having made no assumptions about the nature of the dot so far. But the actual transport properties depend on the microscopic structure of the system. As seen from equations (3.3.25) and (3.3.26), we have to know the spectrum of H_\odot and the matrix elements $(\Psi_\sigma(\vec{x}))_{kk'}^{E_N E'_N \pm 1}$ in order to get from (3.3.22) the system specific master equation. Moreover the properties of the leads and the geometry of the tunnelling contacts will influence the system via the quantities $\mathcal{F}_{\sigma l}$ and $\mathcal{E}_{\sigma l}$ as discussed in Section 4.2.2 of the subsequent chapter.

CHAPTER 4

Metallic SWNT quantum dots with unpolarized leads

In collaboration with Milena Grifoni. Parts of the results presented in this chapter have been published in the Physical Review B **74**, 121403(R) (2006) and in the European Journal of Physics B **56**, 107 (2007).

With our general transport theory for generic quantum dots from the previous section and the knowledge about the SWNT eigenstates and spectrum from Chapter 2, we are now well prepared to determine the $I - V_b - V_g$ characteristics of a SWNT quantum dot. The scheme of such a device is shown in Fig. 4.0.1. Here we consider the case of leads that are unpolarized with respect to the spin degree of freedom. The extension to the case of spin-dependent transport through SWNT quantum dots with magnetized leads will be presented in Chapter 5. From here on we concentrate on SWNTs with large diameters such that exchange effects resulting from the non-forward scattering processes discussed in Chapter 2 can be safely ignored.

4.1. Electronic properties of metallic large size SWNTs

From the discussion in Chapter 3 we know that the transport properties of quantum dots depend on the microscopic properties of the dot system itself. As announced before we subsequently concentrate on devices with a medium to large size metallic SWNT as dot. Our discussion in Chapter 4 on the electronic properties of SWNTs has shown that the amplitude of the short ranged interaction processes scales inversely with the tube size, such that those non-forward scattering processes can finally be neglected when going to large enough tubes. As large enough we would denote for example the SWNT from Sample C of reference [20] with a diameter of 2.7nm and a length of 800nm. In Section 4.3 we will demonstrate that both the experimental and theoretical findings indicate a negligible effect due to the short-ranged interactions for this device.

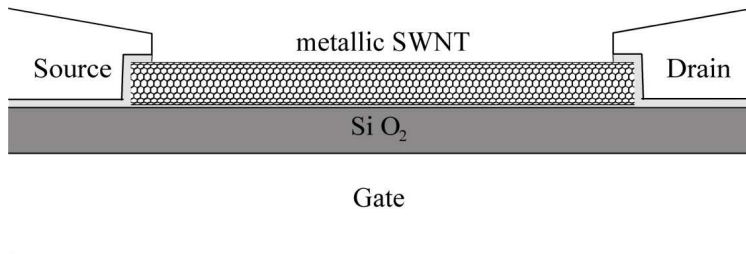


FIGURE 4.0.1. Sketch of a SWNT quantum dot coupled to metal leads.

In principle with our general approach for the calculation of the transport properties also small SWNT quantum dots can be analyzed. Thereby the examination of the low bias regime where no bosonic excitations are present is straightforward. However, the secular approximation used in order to derive equation (3.3.22) can not be fully maintained in the high bias regime of small SWNT quantum dots due the appearance of the quasi-continuum in the spectrum of small sized tubes at higher energies, cf. Fig. 2.6.3. Coherences between quasi-degenerate states with energies E_n and E_m can not be neglected if the ratio $\hbar/|E_n - E_m|$ is larger or of the same order as τ , the typical time scale for the dynamics of the RDM. In turn, τ will depend on the transparency of the tunneling contacts, the applied voltages and the electronic properties of the dot itself. Excluding small sized nanotubes from the discussion we avoid those complications caused by the non-forward scattering processes.

As just explained we can describe large size SWNTs by keeping only the long ranged forward scattering contribution V_{fff} to the SWNT interaction in (2.3.1). Hence, in order to obtain the diagonalized Hamiltonian of large size SWNTs we merely have to set the coupling constants u^+ and $u_{S_F}^\Delta$ of the short ranged interaction processes in equation (2.5.11) to zero. We obtain the following Hamiltonian:

$$H_\odot = H_0 + V_{fff} - \mu_g \mathcal{N}_c = \sum_{j\delta q > 0} \varepsilon_{j\delta q} a_{j\delta q}^\dagger a_{j\delta q} + \frac{1}{2} E_c \mathcal{N}_c^2 + \frac{1}{2} \sum_{r\sigma} (\varepsilon_0 \mathcal{N}_{r\sigma}^2 + r \mathcal{N}_{r\sigma} \varepsilon_\Delta) - \mu_g \mathcal{N}_c, \quad (4.1.1)$$

with the excitation energies of the charged,

$$\varepsilon_{c+q} = \varepsilon_{0q} \sqrt{1 + 8W_q/\varepsilon_0}, \quad (4.1.2)$$

and of the neutral modes,

$$\varepsilon_{s-q} = \varepsilon_{c-q} = \varepsilon_{s+q} = \varepsilon_{0q}. \quad (4.1.3)$$

The eigenstates of H_\odot are of the form (2.5.18),

$$|\vec{N}, \vec{m}\rangle := \prod_{j\delta q > 0} \frac{(a_{j\delta q}^\dagger)^{m_{j\delta q}}}{\sqrt{m_{j\delta q}!}} |\vec{N}, 0\rangle, \quad (4.1.4)$$

where the creation/annihilation operators of the collective excitations, $a_{j\delta q}^\dagger/a_{j\delta q}$, of the interacting system are related to their counterparts of the noninteracting system, $b_{r\sigma q}$ and $b_{r\sigma q}^\dagger$, via equations (2.5.15), (2.5.16) and (2.5.17). The spectrum of H_\odot with its huge degeneracies is shown in Fig. 2.6.3.

4.2. Generalized master equation for unpolarized SWNT quantum dots

Knowing the properties of the dot system we can now take a look back to Chapter 3 and derive from the general expression (3.3.22) the generalized master equation for a SWNT quantum dot. In order to determine the specific form of the Bloch Redfield tensors $R_{nmkk'}^{E_N}$ and $R_{nmkk'}^{E_N E'_{N\pm 1}}$ we have to find the correct values for the transition amplitudes $\Gamma_{l,k'mnk}^{(\alpha)E_N E'_{N\pm 1}}$ given by (3.3.25) and (3.3.26). For this purpose in turn it is

necessary to calculate the matrix elements of the dot electron operators in the eigenbasis of H_\odot and to examine the quantities $\mathcal{E}_{\sigma l}(\vec{x}, \vec{y}, \alpha t')$ and $\mathcal{F}_{\sigma l}(\vec{x}, \vec{y}, \alpha t')$, see (3.3.12) and (3.3.13), which contain the information about the tunneling contacts and the lead electrodes. We start with the matrix elements of the electron operators.

4.2.1. The matrix elements of the electron operators. As we know from equation (1.4.27) the 3D electron operators $\Psi_\sigma(\vec{x})$ can be written in terms of the 1D operators $\psi_{r\sigma F}(x)$,

$$\Psi_\sigma(\vec{r}) = \sqrt{L} \sum_{rF} \text{sgn}(F) \psi_{rF\sigma}(x) \sum_p f_{pr} \varphi_{pF}(\vec{r}). \quad (4.2.1)$$

The calculation of the matrix elements $(\Psi_\sigma(\vec{x}))_{kk'}^{E_N E'_{N\pm 1}}$ is very similar to the determination of the matrix elements of $V_{n\rho\rho}$ in Chapter 2 and can again be performed with the help of the bosonization formalism. Denoting the SWNT eigenstates $|k\rangle$ and $|k'\rangle$ as $|\vec{N}, \vec{m}\rangle$ and $|\vec{N}', \vec{m}'\rangle$ according to equation (4.1.4), we get, as shown in Appendix H,

$$\begin{aligned} \langle \vec{N}, \vec{m} | \psi_{r\sigma F}(x) | \vec{N}', \vec{m}' \rangle &= \delta_{\vec{N} + \vec{e}_{r\sigma}, \vec{N}'} (-1)^{\sum_{j=1}^{r\sigma-1} N_j} \times \\ & K_{rF(\vec{N}')_{r\sigma}}(x) \underbrace{\frac{e^{-\frac{1}{2} \sum_{q>0} e^{-\alpha q} \sum_{j\delta} |\lambda_{r\sigma F}^{j\delta q}(x)|^2}}{\sqrt{1 - e^{-\alpha \frac{\pi}{L}}}}}_{=: W(x)} \prod_{q>0} \prod_{j\delta} F(\lambda_{r\sigma F}^{j\delta q}(x), m_{j\delta q}, m'_{j\delta q}). \end{aligned} \quad (4.2.2)$$

The parameters $\lambda_{r\sigma F}^{j\delta q}(x)$ (cf. Appendix H) for the three neutral modes $j\delta = c-, s+, s-$ are given by

$$\lambda_{r\sigma F}^{j\delta q}(x) = \frac{e^{i \text{sgn}(Fr)qx}}{\sqrt{n_q}} \Lambda_{r\sigma}^{j\delta}, \quad (4.2.3)$$

where $\Lambda_{r\sigma}^{j\delta}$ is given by equation (2.5.8) and for the $c+$ mode we have

$$\lambda_{r\sigma F}^{c+q}(x) = \frac{1}{2\sqrt{n_q}} \left(\sqrt{\frac{\varepsilon_{c+q}}{\varepsilon_{0q}}} \cos(qx) + i \sqrt{\frac{\varepsilon_{0q}}{\varepsilon_{c+q}}} \text{sgn}(Fr) \sin(qx) \right). \quad (4.2.4)$$

The function $F(\lambda, m, m') = \langle m | e^{\lambda a^\dagger} e^{\lambda a} | m' \rangle$ we have already encountered in Chapter 2. For its explicit form see Appendix E. It is interesting to note that the interaction leads to the formation of a non-oscillatory x dependence of the matrix elements $\langle \vec{N}, \vec{m} | \psi_{r\sigma F}(x) | \vec{N}', \vec{m}' \rangle$. For matrix elements between states with *no* bosonic $c+$ excitations this effect is described solely by the function $W(x)$, which in analogy to the function $A_{S_{rF}}(x)$ from Chapter 2 is a result of the normal ordering of the bosonic operators in $\langle \vec{N}, \vec{m} | \psi_{r\sigma F}(x) | \vec{N}', \vec{m}' \rangle$ after expressing $\psi_{r\sigma F}(x)$ in terms of $a_{j\delta q}$ and $a_{j\delta q}^\dagger$ by using the bosonization identity (A.0.15). Explicitly we find

$$W(x) = e^{-\sum_{q>0} \frac{1}{8n_q} \left(\frac{\varepsilon_{c+q}}{\varepsilon_{0q}} \cos^2(qx) + \frac{\varepsilon_{0q}}{\varepsilon_{c+q}} \sin^2(qx) - 1 \right)}, \quad (4.2.5)$$

as demonstrated in Appendix H. From Fig. 2.5.1 we know that the ratio $\varepsilon_{c+q}/\varepsilon_{0q}$ goes to 1 for large q and hence the sum in (4.2.5) converges. In Fig. 4.2.1 we show $W(x)$

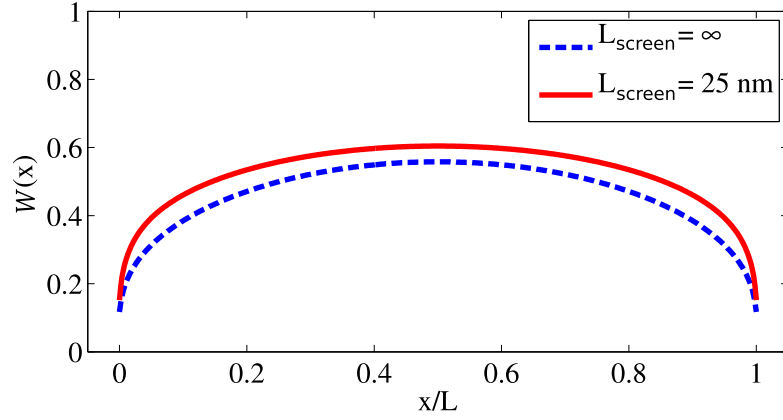


FIGURE 4.2.1. The non-oscillatory position dependence of the matrix elements is described by $W(x)$, if no $c+$ excitations are involved. For a repelling interaction, $W(x)$ is strongly suppressed at the SWNT ends. Here we used the values of $\varepsilon_{c+q}/\varepsilon_{0q}$ of a (20,20) armchair SWNT ($L = 980$ nm) as shown in Fig. 2.5.1.

for a (20,20) armchair SWNT with screened and unscreened Coulomb potential, using the values of $\varepsilon_{c+q}/\varepsilon_{0q}$ as shown in Fig. 2.5.1. It is evident that $W(x)$ (and hence the tunnelling amplitude at low energies) is smallest at the tube ends and increases towards the middle of the nanotube. For an attractive interaction the opposite behavior would be found and for the noninteracting system $W(x) \equiv 1$. Hence $W(x)$ is closely related to the dispersion relation for the excitation energies ε_{c+q} . However, in this thesis the contact geometry is fixed and so the actual form of $W(x)$ doesn't influence the transport properties qualitatively, as we will show below when discussing the role of the tunnelling contacts.

4.2.2. Influence of the lead electrodes. The final step in order to calculate the rates $\Gamma_{l,k'mnk}^{(\alpha)E_N E'_{N\pm 1}}$ from equations (3.3.25) and (3.3.26) is the examination of the functions $\mathcal{E}_{\sigma l}(\vec{x}, \vec{y}, t)$ and $\mathcal{F}_{\sigma l}(\vec{x}, \vec{y}, t)$. Those functions together with the position dependent electron operators lead to a dependence of $\Gamma_{l,k'mnk}^{(\alpha)E_N E'_{N\pm 1}}$ on the geometry of the tunnelling contact. This effect can be accounted for by introducing new parameters $\Phi_{lrr'}(\varepsilon)$, which are closely related to the notion of pseudo spin polarized leads. As we will prove below it holds

$$\Gamma_{l,k'mnk}^{(\alpha)E_N E'_{N+1}} = \frac{1}{\hbar^2} \sum_{rr'\sigma} \int d\varepsilon f_l(\varepsilon) \Phi_{lrr'}(\varepsilon) (\psi_{r\sigma l})_{k'm}^{E_N E'_{N+1}} \left(\psi_{r'\sigma l}^\dagger \right)_{nk}^{E'_{N+1} E_N} \times \int_0^\infty dt' e^{\alpha \frac{i}{\hbar} (\varepsilon - eV_l - (E'_{N+1} - E_N))t'}, \quad (4.2.6)$$

where we use the notation $\psi_{r\sigma l} := \psi_{r\sigma K_0}(x_l)/W(x_l)$, with $x_l = 0, L$ for $l = s, d$ and $f_l(\varepsilon)$ denotes the Fermi function. Assuming that the electrons in the leads form a 3D electron gas with Fermi wave length that are small compared to the SWNT lattice

spacing a_0 , we will find

$$\Phi_{lrr'}(\varepsilon) = \delta_{rr'}\phi_l(\varepsilon), \quad (4.2.7)$$

where the generally energy dependent parameter $\phi_l(\varepsilon)$ determines the coupling strength between the leads and the dot. In the same way the parameterization of the tunneling contact properties can also be performed for (3.3.26), yielding

$$\Gamma_{l,k'mnk}^{(\alpha)E_N E_{N-1}} = \frac{1}{\hbar^2} \sum_{rr'\sigma} \int d\varepsilon (1 - f_l(\varepsilon)) \Phi_{lrr'}^*(\varepsilon) \left(\psi_{r\sigma l}^\dagger \right)_{k'm}^{E_N E_{N-1}} (\psi_{r'\sigma l})_{nk}^{E_{N-1} E_N} \times \int_0^\infty dt' e^{\alpha \frac{i}{\hbar} (-\varepsilon + eV_l - (E_{N-1}' - E_N))t'}. \quad (4.2.8)$$

The integrals over ε and t' in (4.2.6) and (4.2.8) can be carried out by using

$$\int d\varepsilon g(\varepsilon) \int_0^\infty dt' e^{\alpha \frac{i}{\hbar} (\varepsilon - E)t'} = \pi \hbar g(E) + \alpha i \hbar \mathcal{PV} \int \frac{g(\varepsilon)}{\varepsilon - E} d\varepsilon, \quad (4.2.9)$$

where \mathcal{PV} denotes the Cauchy principal value. The first term on the right hand side of (4.2.9) corresponds to processes which conserve the energy. Additionally, we have the imaginary principal value terms which can be attributed to so called virtual transitions since they cancel in the expression for the current but nevertheless can affect the transport properties indirectly via the time evolution of the RDM.

Taking into consideration the relations (4.2.2), (4.2.9) and (4.2.7) we can now easily evaluate the rates $\Gamma_{l,k'mnk}^{(\alpha)E_N E_{N\pm 1}}$ determining the system dynamics via equations (4.2.6) and (4.2.8). The hurried reader can directly advance to Section 4.3. Those who want to see the explicit derivation of (4.2.6) or who want to learn something about pseudo spin polarization may continue here.

PROOF. In the following we prove relation (4.2.6). We start with equations (3.3.12) and (3.3.13) for $\mathcal{E}_{\sigma l}(\vec{x}, \vec{y}, t)$ and $\mathcal{F}_{\sigma l}(\vec{x}, \vec{y}, t)$,

$$\mathcal{E}_{\sigma l}(\vec{x}, \vec{y}, t') = T_l(\vec{x}) T_l^*(\vec{y}) \left\langle \Phi_{\sigma l}(\vec{x}) \Phi_{\sigma l}^\dagger(\vec{y}, -t') \right\rangle_{\text{th}} \quad (4.2.10)$$

and

$$\mathcal{F}_{\sigma l}(\vec{x}, \vec{y}, t') := T_l^*(\vec{x}) T_l(\vec{y}) \left\langle \Phi_{\sigma l}^\dagger(\vec{x}) \Phi_{\sigma l}(\vec{y}, -t') \right\rangle_{\text{th}}. \quad (4.2.11)$$

In order to calculate the correlation functions in the previous two equations we reexpress the lead electron operators with help of $\rho_l(\varepsilon)$, the density of states in the leads,

$$\Phi_{\sigma l}(\vec{r}) = \int d\varepsilon \rho_l(\varepsilon) \sum_{\vec{q}|\varepsilon} \phi_{\vec{q}}(\vec{r}) c_{\vec{q}\sigma l},$$

and exploit that for non-magnetic leads the single particle energies are spin independent such that the Hamiltonian from (3.2.10) simplifies to

$$H_l = \sum_{\sigma \vec{q}} (\varepsilon_{\vec{q}, l} - eV_l) c_{\vec{q}\sigma l}^\dagger c_{\vec{q}\sigma l}. \quad (4.2.12)$$

Using (3.3.8) for the equilibrium density operator for the leads we find

$$\left\langle \Phi_{\sigma l}(\vec{x}) \Phi_{\sigma l}^\dagger(\vec{y}, -t') \right\rangle_{\text{th}} = \int d\varepsilon \rho_l(\varepsilon) (1 - f(\varepsilon)) \sum_{\vec{q}|\varepsilon} \phi_{\vec{q}}(\vec{x}) \phi_{\vec{q}}^*(\vec{y}) e^{-\frac{i}{\hbar}(\varepsilon - eV_l)t'}, \quad (4.2.13)$$

and

$$\left\langle \Phi_{\sigma l}^\dagger(\vec{x}) \Phi_{\sigma l}(\vec{y}, -t') \right\rangle_{\text{th}} = \int d\varepsilon \rho_l(\varepsilon) f(\varepsilon) \sum_{\vec{q}|\varepsilon} \phi_{\vec{q}}^*(\vec{x}) \phi_{\vec{q}}(\vec{y}) e^{\frac{i}{\hbar}(\varepsilon - eV_l)t'}, \quad (4.2.14)$$

where the sum $\sum_{\vec{q}|\varepsilon}$ extends over all \vec{q} values that correspond to the energy ε . Furthermore $\rho_l(\varepsilon)(1 - f(\varepsilon))$ and $\rho_l(\varepsilon)f(\varepsilon)$, where $f(\varepsilon)$ is the Fermi distribution, denote the densities of empty and occupied states in lead l . We have set the chemical potential in the leads to 0, such that it does not appear within the Fermi function.

We now turn to the influence of the tunneling rates on the geometry of the tunneling contacts and start with (3.3.25),

$$\Gamma_{l,k'mnk}^{(\alpha)E_N E'_{N+1}} = \frac{1}{\hbar^2} \sum_{\sigma} \int d^3x \int d^3y (\Psi_{\sigma}(\vec{x}))_{k'm}^{E_N E'_{N+1}} \left(\Psi_{\sigma}^\dagger(\vec{y}) \right)_{nk}^{E'_{N+1} E_N} \times \int_0^\infty dt' \mathcal{F}_{\sigma l}(\vec{x}, \vec{y}, \alpha t') e^{-\alpha \frac{i}{\hbar} (E'_{N+1} - E_N) t'}, \quad (4.2.15)$$

from where we extract the part that depends explicitly on the tunnelling contact l . That means we define energy dependent quantities $\mathcal{T}_{l,nkk'm}(\varepsilon)$, which contain all the properties of the tunneling contacts, by

$$\Gamma_{l,k'mnk}^{(\alpha)E_N E'_{N+1}} =: \frac{1}{\hbar^2} \sum_{\sigma} \int d\varepsilon f(\varepsilon) \mathcal{T}_{l,nkk'm}(\varepsilon) \int_0^\infty dt' e^{\alpha \frac{i}{\hbar} (\varepsilon - eV_l - E'_{N+1} + E_N) t'}.$$

Expanding $\mathcal{F}_{\sigma l}(\vec{x}, \vec{y}, \alpha t')$ and the electron operators according to (3.3.13) and (4.2.1) respectively we get

$$\begin{aligned} \mathcal{T}_{l,nkk'm}(\varepsilon) &= L \rho_l(\varepsilon) \sum_{FF'} \text{sgn}(FF') \int d^3r \int d^3r' T_l^*(\vec{r}) T_l(\vec{r}') \times \\ &\sum_{\vec{q}|\varepsilon} \phi_{l\vec{q}}^*(\vec{r}) \phi_{l\vec{q}}(\vec{r}') \sum_{rr'} \sum_{pp'} f_{pr} f_{p'r'}^* \varphi_{pF}(\vec{r}) \varphi_{p'F'}^*(\vec{r}') \times \\ &\sum_{\sigma} \left(\psi_{rF\sigma}(x) \right)_{nk} \left(\psi_{r'F'\sigma}^\dagger(x') \right)_{k'm}. \end{aligned} \quad (4.2.16)$$

At low enough energies the product $(\psi_{rF\sigma}(x))_{nk} (\psi_{r'F'\sigma}^\dagger(y))_{k'm}$ contains only slow oscillations that can be ignored along the length of the tunnelling interfaces. Keeping

only the non-oscillating position dependence in (4.2.2) we thus can rewrite (4.2.16) as

$$\begin{aligned} \mathcal{T}_{l,nkk'm}(\varepsilon) = & L\rho_l(\varepsilon) \sum_{FF'} \text{sgn}(FF') \nu_{lFF'}(\Delta) \times \\ & \int d^3r \int d^3r' T_l^*(\vec{r}) T_l(\vec{r}') W(x) W(x') \sum_{\vec{q}|\varepsilon} \phi_{l\vec{q}}^*(\vec{r}) \phi_{l\vec{q}}(\vec{r}') \times \\ & \sum_{rr'} \sum_{pp'} f_{pr} f_{p'r'}^* \varphi_{pF}(\vec{r}) \varphi_{p'F'}^*(\vec{r}') \sum_{\sigma} \left(\psi_{r\sigma l} \right)_{nk} \left(\psi_{r'\sigma l}^\dagger \right)_{k'm}. \end{aligned} \quad (4.2.17)$$

Here the factor $\nu_{lFF'}(\Delta) = e^{i\delta_{l,d}\pi \text{sgn}(F-F')\Delta}$ takes into account a possible phase shift due to the band mismatch Δ and we have used the notation $\psi_{r\sigma l} = \psi_{rK_0\sigma}(x_l)/W(x_l)$, where $x_l = 0, L$ for $l = s, d$. By introducing parameters $\Phi_{lrr'}(\varepsilon)$ expression (4.2.17) acquires the simple form,

$$\mathcal{T}_{l,nkk'm}(\varepsilon) = \sum_{rr'} \Phi_{lrr'}(\varepsilon) \sum_{\sigma} \left(\psi_{r\sigma l} \right)_{nk} \left(\psi_{r'\sigma l}^\dagger \right)_{k'm}. \quad (4.2.18)$$

Comparing equations (4.2.17) and (4.2.18) we find for the parameters $\Phi_{lrr'}(\varepsilon)$,

$$\begin{aligned} \Phi_{lrr'}(\varepsilon) = & \rho_l(\varepsilon) \frac{CL}{N_L} \sum_{FF'} \text{sgn}(FF') \nu_{lFF'}(\Delta) \times \\ & \sum_{pp'} f_{pr} f_{p'r'}^* \sum_{\vec{R}, \vec{R}'} T_l^*(\vec{R} + \vec{\tau}_p) T_l(\vec{R}' + \vec{\tau}_{p'}) W(\vec{R}_x) W(\vec{R}'_x) \times \\ & \sum_{\vec{q}|\varepsilon} \phi_{l\vec{q}}^*(\vec{R} + \vec{\tau}_p) \phi_{l\vec{q}}(\vec{R}' + \vec{\tau}_{p'}) e^{iF R_x} e^{-iF R'_x}. \end{aligned} \quad (4.2.19)$$

In (4.2.19) we have exploited that the Bloch waves $\varphi_{pF}(\vec{r})$ are only non-vanishing around the positions of the carbon atoms in the SWNT lattice. On the length scale of the extension of the p_z orbitals all other quantities in $\Phi_{lrr'}$ are slowly varying. Hence we could rewrite the integrals over \vec{x} and \vec{y} as a sum over the positions of the carbon atoms. The constant C results from the integration over the p_z orbitals. In order to get more insight about the properties of $\Phi_{lrr'}(\varepsilon)$ we assume to have a 3D electron gas in the leads. In this case the wave functions $\phi_{l\vec{q}}(\vec{x})$ are simply given by plane waves,

$$\phi_{l\vec{q}}(\vec{x}) = \frac{1}{\sqrt{V_l}} e^{i\vec{q} \cdot \vec{x}}.$$

Therefore, we can easily perform the sum over the wave numbers \vec{q} associated with the energy ε ,

$$\sum_{\vec{q}|\varepsilon} \phi_{l\vec{q}}^*(\vec{x}) \phi_{l\vec{q}}(\vec{y}) \sim \int_0^{2\pi} d\varphi \int_{-1}^1 d\cos\theta e^{iq|\varepsilon|\vec{x}-\vec{y}|\cos\theta} = \frac{4\pi \sin(q|\varepsilon|\vec{x}-\vec{y}|)}{q|\varepsilon|\vec{x}-\vec{y}|}.$$

The previous expression is peaked around $\vec{x} = \vec{y}$. For $q|\varepsilon| > 1/|\vec{x} - \vec{y}|$ the correlations between \vec{x} and \vec{y} drop off fast with increasing distance. In our case this means that if $q|\varepsilon|$ is larger than $1/a_0$, where a_0 is the nearest neighbor distance on the SWNT lattice, correlations between different carbon atom sites are suppressed such that we arrive at

the following approximation:

$$\sum_{\vec{q}|\varepsilon} \phi_{l\vec{q}}^*(\vec{x}_{\vec{R},p}) \phi_{l\vec{q}}(\vec{x}_{\vec{R}',p'}) \sim 4\pi \delta_{\vec{R},\vec{R}'} \delta_{p,p'},$$

which yields

$$\begin{aligned} \Phi_{lrr'}(\varepsilon) &= \rho_l(\varepsilon) \frac{\tilde{C}L}{N_L} \sum_{FF'} \text{sgn}(FF') \nu_{lFF'}(\Delta) \times \\ &\sum_p f_{pr} f_{pr'}^* \times \sum_{\vec{R}} \left| T_l(\vec{x}_{\vec{R},p}) \right|^2 e^{i(F-F')R_x} W^2(\vec{R}_x), \quad \tilde{C} \in \mathbb{R}. \end{aligned} \quad (4.2.20)$$

Since we assume an extended tunnelling region, the fast oscillating terms with $F = -F'$ are supposed to cancel. Furthermore we assume that both sublattices are equally well coupled to the contacts, such that the sum over \vec{R} in (4.2.20) should approximately give the same result for $p = 1$ and $p = 2$. Hence we can separate the sum over p from the rest. Since the Bloch waves $\varphi_{\text{sgn}(F)rF}$ and $\varphi_{\text{sgn}(F)r'F}$ are orthogonal to each other for $r \neq r'$, we find that the relation

$$\sum_p f_{pr} f_{pr'}^* = \delta_{rr'}$$

must hold, as it can be deduced from the explicit expression for the Bloch wave, equation (1.4.17), and we arrive at

$$\Phi_{lrr'}(\varepsilon) = \delta_{rr'} \rho_l(\varepsilon) \frac{\tilde{C}L}{2N_L} \sum_{\vec{R}p} \left| T_l(\vec{x}_{\vec{R},p}) \right|^2 W^2(\vec{R}_x). \quad (4.2.21)$$

We thus expect $\Phi_{lrr'}(\varepsilon)$ to vanish for $r \neq r'$ and to give equal values for $rr' = ++$ and $rr' = --$. As we will demonstrate below this corresponds to unpolarized leads with respect to the pseudo spin. We should mention that the treatment of the contact geometry here relies on several assumptions that might not be fulfilled under all circumstances and so it should be seen as a first estimate. For example we assume that the transmission functions T_l do not depend on the \vec{q} vector of the incoming wave. But such a dependence would increase the correlation between different atom sites. Furthermore $q|\varepsilon$ will not be much larger than $1/a_0$ for all kind of contacts (for gold the Fermi wave number is about $1.5/a_0$), nor can the lead electrons always be described by a 3D electron gas. \square

Interlude: Pseudo spin polarization. We explain in the following the relation between the parameters $\Phi_{lrr'}(\varepsilon)$ and polarization with respect to the pseudo spin degree of freedom. A condition under which pseudo spin polarized leads can occur will be presented. The discussion here will already give the direction of how to treat quantum dots with ferromagnetic contacts.

As it can be easily deduced from (4.2.19) the coefficients $\Phi_{lrr'}(\varepsilon)$ fulfill up to the normalization condition the properties of density matrix elements, i.e.,

$$\Phi_{lrr'} = \Phi_{l'r'r}^*, \quad \Phi_{lrr} \geq 0, \quad |\Phi_{l+-}|^2 \leq \Phi_{l++} \Phi_{l--},$$

where without loss of generality we have omitted the energy dependence of $\Phi_{lrr'}$. Hence it is appealing to regard the contacts as an ensemble of electrons characterized by the spinors $|r = +\rangle = \begin{pmatrix} 1 \\ 0 \end{pmatrix}$ and $|r = -\rangle = \begin{pmatrix} 0 \\ 1 \end{pmatrix}$. Therefore we introduce density matrices $\tilde{\rho}_l$ by

$$\begin{pmatrix} \Phi_{l++} & \Phi_{l+-} \\ \Phi_{l-+} & \Phi_{l--} \end{pmatrix} =: \phi_l^{(+)} \tilde{\rho}_l = \phi_l^{(+)} \begin{pmatrix} \tilde{\rho}_{l++} & \tilde{\rho}_{l+-} \\ \tilde{\rho}_{l-+} & \tilde{\rho}_{l--} \end{pmatrix}, \quad \tilde{\rho}_{l++} + \tilde{\rho}_{l--} = 1, \quad (4.2.22)$$

where the coefficients $\phi_l^{(+)}$ are proportional to the contact transparency, in detail

$$\phi_l^{(+)} = \Phi_{l++} + \Phi_{l--}.$$

The quantities $\tilde{\rho}_l$ should neither be confused with the density matrices ρ_l describing the equilibrated electron gas in the leads nor with the density of states $\rho_l(\varepsilon)$. In analogy to “real” spin 1/2 particles we can now define the polarization of the contacts with respect to the pseudo spin by [56]

$$\mathcal{P}_{l,i} = \text{Tr}(\tilde{\rho}_l \sigma_i) = \frac{1}{\phi_l^{(+)}} \text{Tr}(\Phi_l \sigma_i), \quad i = x, y, z, \quad (4.2.23)$$

with the well known Pauli matrices σ_i . Then the density matrix $\tilde{\rho}_l$ can be alternatively expressed as

$$\tilde{\rho}_l = \frac{1}{2} \begin{pmatrix} 1 + \mathcal{P}_{l,z} & \mathcal{P}_{l,x} - i\mathcal{P}_{l,y} \\ \mathcal{P}_{l,x} + i\mathcal{P}_{l,y} & 1 - \mathcal{P}_{l,z} \end{pmatrix}. \quad (4.2.24)$$

From our discussion above we know that the properties of $\tilde{\rho}_l$ depend on the geometry of the tunneling contact at lead l . In this respect our result (4.2.21) indicates completely unpolarized leads. To mention it, the concept of the pseudo spin polarization is also relevant in the context of the orbital (or pseudo spin) Kondo effect [57]. In the theoretical work [58] it is shown that this Kondo effect is weakened for pseudo spin polarized leads, $\mathcal{P}_l := |\vec{\mathcal{P}}_l| > 0$, and finally vanishes for $\mathcal{P}_l = 1$. It is interesting to examine whether other types of tunneling junction geometries as the one considered above can exhibit pseudo spin polarization and hence allow for the creation of *pseudo spin valves*. In this respect it is interesting to return to (4.2.20) and assume an asymmetric coupling of the leads to the two sublattices $p = \pm$, i.e., consider the case $|T_{l1}|^2 \neq |T_{l2}|^2$, where $|T_{lp}|^2 := \sum_{\vec{R}} |T_l(\vec{x}_{\vec{R},p})|^2$. Then the sum

$$\sum_p f_{pr} f_{pr'}^* |T_{lp}|^2 = |T_{l1}|^2 + rr' |T_{l2}|^2,$$

will not vanish also for $r \neq r'$ and according to (4.2.24) this means that the pseudo spin polarization of lead l will acquire a component in x direction. In more detail the polarization will be given by

$$\mathcal{P}_l = \frac{1}{|T_{l1}|^2 + |T_{l2}|^2} (|T_{l1}|^2 - |T_{l2}|^2, 0, 0).$$

We think that a more detailed analysis of the relation between pseudo spin polarization and contact geometry is worthwhile in the future, especially due to the analogy with

spin dependent transport which we will discuss in the next chapter. For the discussion there our examination of the pseudo spin polarization can serve as a good starting point. Namely it shows the way of how to treat quantum dot devices with leads that are polarized with respect to the real spin. Essentially we will just have to replace the parameters $\Phi_{lrr'}(\varepsilon)$ by their analogues $\Phi_{l\sigma\sigma'}(\varepsilon)$ whose relation to the polarization of the leads can again be determined by equations (4.2.22) and (4.2.24).

4.3. Excitation lines

If certain transitions are possible depends among other things on the available energy and hence on the applied gate and bias voltages. The resonance conditions for tunnelling in/out of lead l are determined by the rates from (4.2.6) and (4.2.8), especially by the first term on the right hand side of the integral (4.2.9) together with the Fermi function. In detail, at temperature $T = 0$, transitions from a state with N electrons and eigenenergy E_N to a state with $M = N \pm 1$ electrons and eigenenergy E_M are possible under the condition

$$\begin{aligned} eV_l &\leq E_N - E_{N+1}, \text{ for } M = N + 1, \\ eV_l &\geq E_{N-1} - E_N, \text{ for } M = N - 1. \end{aligned} \quad (4.3.1)$$

Note that we have incorporated the influence of the gate voltage into the dot Hamiltonian, cf. equation (3.2.11). Therefore alternatively to (4.3.1) we can also write

$$\begin{aligned} eV_l &\leq \tilde{E}_N - \tilde{E}_{N+1} + \mu_g, \text{ for } M = N + 1, \\ eV_l &\geq \tilde{E}_{N-1} - \tilde{E}_N + \mu_g, \text{ for } M = N - 1, \end{aligned} \quad (4.3.2)$$

where the energies \tilde{E}_N denote the eigenenergies of an isolated SWNT without applied gate voltage. We expect that for low temperatures the current can only change considerably at the position of the lines in the $eV - \mu_g$ plane corresponding to the relations from (4.3.2). But we should mention that in principle the virtual transitions, cf. (4.2.9), are sensitive to the values of the bias and gate voltage outside of the excitation lines if coherences of the RDM influence the transport, as it will become especially relevant in the next chapter on spin dependent transport. However, in our case of unpolarized leads we do not find a significant change of the current between two excitation lines. Furthermore not all of the resonance conditions lead to a considerable change of the current at the corresponding lines in the $eV_b - \mu_g$ plane. Relevant transitions are those between states with considerable overlap matrix elements $\langle \vec{N}, \vec{m} | \psi_{r\sigma F}(x) | \vec{N}', \vec{m}' \rangle$ and for which the occupation probability of the initial state is large enough.

The number of electrons in the SWNT dot is controlled by the chemical potential μ_g , as we know from the discussion in Chapter 3. Assume that μ_g is just large enough that there are N electrons in the dot. Then, in order to add another electron to the N particle ground state, the extra energy $\delta\mu_N = E_{N+1}^0 - E_N^0 - (E_N^0 - E_{N-1}^0)$ has to be paid. Here E_M^0 denotes the ground state energies. From the SWNT Hamiltonian H_\odot , equation (4.1.1), we deduce

$$\begin{aligned} \delta\mu_{4m+1} &= \delta\mu_{4m+3} = E_c, \\ \delta\mu_{4m+2} &= E_c + |\varepsilon_\Delta|, \\ \delta\mu_{4m} &= E_c + \varepsilon_0 - |\varepsilon_\Delta|. \end{aligned} \quad (4.3.3)$$

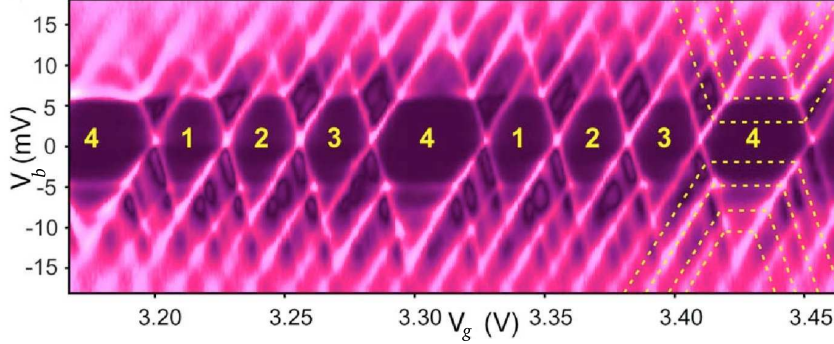


FIGURE 4.3.1. Differential conductance dI/dV_b for Sample C of reference [20]. A very regular pattern of excitation lines in the $V_b - V_g$ plane has been measured. The fourfold periodicity due to the shell filling can be seen very nicely. The excitation lines from the experiment can be reproduced with the choices $E_c = 6.6$ meV, $\varepsilon_0 = 8.7$ meV, $\varepsilon_\Delta = J = 2.9$ meV and equivalently with $E_c = 9.5$ meV, $\varepsilon_0 = 2.9$ meV and $\varepsilon_\Delta = J = 0$. The corresponding excitation lines are indicated by dashed lines. Excitation lines within the Coulomb diamond are due to cotunneling processes not included in our weak coupling theory.

The energy $\delta\mu_N$ is a direct measure of the height and the width of the Coulomb diamonds in the $eV_b - \mu_g$ plane. Thus a repeated pattern of one large Coulomb diamond followed by three smaller ones is expected for $\varepsilon_\Delta = 0$. Otherwise the pattern will consist of a large diamond followed by a small, a medium and again a small one. In the experiments of Sapmaz et al. [20] sample C showed the first pattern repeating very regularly, whereas samples A and B revealed the second pattern.

For sample C not only the Coulomb diamonds but also a bunch of excitation lines could be resolved. In [20] the positions of the Coulomb diamonds and of the lowest lying excitation lines were determined. The mean field theory of [19] containing the exchange splitting J was used for comparison. Apart from the height of the large Coulomb diamonds, all the lines from the experimental $I - V$ characteristics of sample C could be reproduced by an appropriate choice of the mean field parameters E_c , ε_0 , ε_Δ , J . For sample C the choice of Sapmaz et al. was $E_c = 6.6$ meV, $\varepsilon_0 = 8.7$ meV, $\varepsilon_\Delta = J = 2.9$ meV. However, exactly the same Coulomb diamonds and excitation lines are recovered by choosing $E_c = 9.5$ meV, $\varepsilon_0 = 2.9$ meV and $\varepsilon_\Delta = J = 0$, cf. Fig. 4.3.1. We think that in this case the latter choice of parameters is much more realistic than the one made in [20], with an unreasonably high J of 2.9 meV. The SWNT in sample C had a length of 800nm and a diameter of 2.7nm. According to table 1 in Subsection 2.3.3 this corresponds for an assumed dielectric constant $\epsilon = 1.4$ to an exchange splitting of $J \approx 0.05$ meV, a value two orders of magnitude smaller than the value given in [20]. We therefore conclude that our treatment of the interaction, where only forward scattering events are considered and exchange

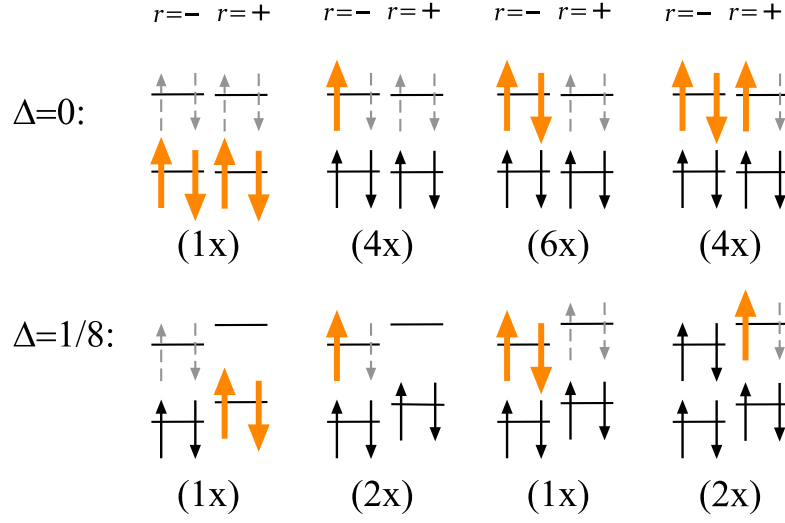


FIGURE 4.4.1. Ground states of the SWNT for different numbers of electrons. For each charge state we show one representative ground state, on top for aligned bands and on the bottom for mismatched bands. In brackets the corresponding degeneracy is given. Full black and orange arrows represent occupied states. The bold (orange) arrows indicate electrons which can contribute to transitions $N \rightarrow N - 1$ in the low bias regime. Incoming electrons for the transitions $N \rightarrow N + 1$ can be accommodated by the states represented by the dashed arrows. So the number of bold and dashed arrows is equal to $C_{N,N-1}$ and $C_{N,N+1}$ respectively.

contributions are not present, is valid here. In Section 4.5, Figure 4.5.1 shows the numerical result for the corresponding current.

4.4. Low Bias Regime

In the following we consider the low bias regime, i.e., the bias voltages and the temperature are low enough that only ground states with N and $N + 1$ particles and energies E_N^0 , E_{N+1}^0 can have a considerable occupation probability. In this case the importance of taking into account the off-diagonal elements of the RDM in (3.3.22) depends crucially on the parameters $\Phi_{lrr'}(\varepsilon)$ in (4.2.6) and (4.2.8). From the expressions (4.2.6) and (4.2.8) for the rates it is evident that for our assumption of unpolarized leads, condition (4.2.7), the time evolution of the RDM elements between states with the same band filling vector \vec{N} is decoupled from elements between states with different \vec{N} . Since the current only depends on the time derivative of the diagonal elements of the RDM, the elements mixing states with different \vec{N} will have no influence on the current and therefore can be ignored. Because all considered ground states do have a different \vec{N} , in the low bias regime we only have to take into account *diagonal* matrix elements in the master equation if unpolarized leads are considered.

We will refer to this kind of master equations where coherences are absent as "commonly used master equations" (CMEs). In the low bias regime the occupation probabilities $\rho_{\vec{N}\vec{N}}^{I, E_M^0}$ of the groundstates containing M particles will all be the same in the stationary solution, since none of the ground states stands out compared with the other ground states in any respect. Therefore, we introduce the probability for finding the system in charge state M by

$$P_M = d_M \rho_{\vec{N}\vec{N}}^{I, E_M^0}(t),$$

where d_M is the degeneracy of the corresponding ground states. Using (3.3.22), the general expression for the master equation, we find the following CME for P_M ,

$$\frac{\dot{P}_M}{d_M} = -R_{\vec{N}\vec{N}\vec{N}\vec{N}}^{E_M^0} \frac{P_M}{d_M} + \sum_{\vec{N}'} R_{\vec{N}\vec{N}\vec{N}'\vec{N}'}^{E_M^0 E_{M'}^0} \frac{P_{M'}}{d_{M'}}. \quad (4.4.1)$$

With equations (3.3.23) and (3.3.24) for the Redfield tensors we obtain

$$\begin{aligned} \dot{P}_M = - \sum_l \left(\Sigma_l^{M \rightarrow M'} - \Sigma_l^{M' \rightarrow M} \right) = \\ - 2 \sum_l \sum_{\vec{N}'} \left(\Gamma_{l \vec{N}\vec{N}'}^{E_M^0 E_{M'}^0} P_M - \frac{d_M}{d_{M'}} \Gamma_{l \vec{N}'\vec{N}}^{E_{M'}^0 E_M^0} P_{M'} \right), \end{aligned} \quad (4.4.2)$$

where we have defined

$$\sum_{\vec{N}'} \Gamma_{l, \vec{N}\vec{N}'}^{E_M^0 E_{M'}^0} := \sum_{\vec{N}'} \Gamma_{l \vec{N}\vec{N}'\vec{N}'\vec{N}}^{(+), E_M^0 E_{M'}^0}. \quad (4.4.3)$$

Using the relation

$$\frac{d_M}{d_{M'}} \sum_{\vec{N}'} \Gamma_{l \vec{N}'\vec{N}}^{E_{M'}^0 E_M^0} = \sum_{\vec{N}'} \Gamma_{l \vec{N}\vec{N}'}^{E_M^0 E_{M'}^0} \quad (4.4.4)$$

the stationary solution of (4.4.2) is easily found,

$$P_M = \frac{\sum_{\vec{N}'} \Gamma_{l \vec{N}\vec{N}'}^{E_M^0 E_{M'}^0}}{\Gamma_{tot}}, \quad (4.4.5)$$

with

$$\Gamma_{tot} = \sum_l \sum_{\vec{N}'} \left(\Gamma_{l \vec{N}\vec{N}'}^{E_N^0 E_{N+1}^0} + \Gamma_{l \vec{N}\vec{N}'}^{E_{N+1}^0 E_N^0} \right). \quad (4.4.6)$$

The current is obtained from (3.4.1). Evaluated at the source for example it yields,

$$I_{N, N+1} = \frac{2e \sum_{\vec{N}'} \left(\Gamma_{s \vec{N}\vec{N}'}^{E_N^0 E_{N+1}^0} \Gamma_{d \vec{N}\vec{N}'}^{E_{N+1}^0 E_N^0} - \Gamma_{s \vec{N}\vec{N}'}^{E_{N+1}^0 E_N^0} \Gamma_{d \vec{N}\vec{N}'}^{E_N^0 E_{N+1}^0} \right)}{\Gamma_{tot}}. \quad (4.4.7)$$

The rates $\Gamma_{l, \vec{N}\vec{N}'}^{E_M^0 E_{M'}^0}$ are obtained by using equations (4.2.6) and (4.2.8),

$$\Gamma_{l \vec{N}\vec{N}'}^{E_N^0 E_{N+1}^0} = \frac{\pi}{\hbar} \phi_l f(\varepsilon_l) \sum_{r\sigma} \left(\psi_{r\sigma l} \right)_{\vec{N}\vec{N}'}^{E_N^0 E_{N+1}^0} \left(\psi_{r\sigma l}^\dagger \right)_{\vec{N}'\vec{N}}^{E_{N+1}^0 E_N^0},$$

and

$$\Gamma_{l \vec{N} \vec{N}'}^{E_{N+1}^0 E_N^0} = \frac{\pi}{\hbar} \phi_l (1 - f(\varepsilon_l)) \sum_{r\sigma} \left(\psi_{r\sigma l}^\dagger \right)_{\vec{N} \vec{N}'}^{E_{N+1}^0 E_N^0} (\psi_{r\sigma l})_{\vec{N}' \vec{N}}^{E_N^0 E_{N+1}^0}.$$

Here we have assumed that Φ_l and ρ_l are constant in the relevant energy range. Furthermore we have defined

$$\varepsilon_{lN} := eV_l - \Delta E_N$$

and

$$\Delta E_N = E_N^0 - E_{N+1}^0.$$

Remember that the electrochemical potential in the dot is already included in E_N^0 , such that $\Delta E_N = \tilde{E}_N^0 - \tilde{E}_{N+1}^0 + \mu_g$. From (4.2.2) we obtain (remember that $\psi_{r\sigma l} := \psi_{r\sigma K_0}(x_l)/W(x_l)$),

$$\sum_{r\sigma} \sum_{\vec{N}'} \left(\psi_{r\sigma l}^\dagger \right)_{\vec{N} \vec{N}'}^{E_M^0 E_{M'}^0} (\psi_{r\sigma l})_{\vec{N}' \vec{N}}^{E_M^0 E_{M'}^0} = \frac{1}{2L} C_{M, M'},$$

where $C_{M, M'}$ is the number of ground states with M' particles that differ from a given band filling vector \vec{N} for one of the ground state with M particles only by a unit vector (see Fig. 4.4.1). Therefore we get

$$2 \sum_{\vec{N}'} \Gamma_{l \vec{N} \vec{N}'}^{E_N^0 E_{N+1}^0} = \gamma_l f(\varepsilon_{lN}) C_{N, N+1} \quad (4.4.8)$$

as well as

$$2 \sum_{\vec{N}'} \Gamma_{l \vec{N} \vec{N}'}^{E_{N+1}^0 E_N^0} = \gamma_l (1 - f(\varepsilon_{lN})) C_{N+1, N}, \quad (4.4.9)$$

with $\gamma_l = \frac{\pi}{L\hbar} \phi_l$. Inserting the rates (4.4.8) and (4.4.9) into expression (4.4.7) for the current results in

$$I_{N, N+1} = e \frac{C_{N, N+1} C_{N+1, N} \gamma_s \gamma_d [f(\varepsilon_{sN}) - f(\varepsilon_{dN})]}{\sum_l \gamma_l [f(\varepsilon_{lN}) C_{N, N+1} + (1 - f(\varepsilon_{lN})) C_{N+1, N}]}. \quad (4.4.10)$$

4.4.1. Linear conductance. In the regime $|eV| \ll kT \ll \varepsilon_0$ we can further simplify (4.4.10) by linearising I_{NN+1} in the bias voltage. We choose $-eV_s = eV_d =: e\frac{V_b}{2}$ and obtain

$$I_{N, N+1} = \frac{e^2 \beta C_{N, N+1} C_{N+1, N} \gamma_s \gamma_d}{\sum_l \gamma_l (f_N C_{N, N+1} + (1 - f_N) C_{N+1, N})} \frac{e^{-\beta \Delta E_N}}{(e^{-\beta \Delta E_N} + 1)^2} V_b, \quad (4.4.11)$$

with $f_N = f(-\Delta E_N)$. Unlike one could expect, the maxima of the conductance $G_{N, N+1} = I_{N, N+1}/V_b$ are not at $\Delta E_N = 0$, but at

$$\Delta E_{\max, N} = \frac{1}{2\beta} \ln \frac{C_{N+1, N}}{C_{N, N+1}}, \quad (4.4.12)$$

which is only zero for $C_{N+1, N} = C_{N, N+1}$. The height of the conductance peaks is

$$G_{N, N+1}^{\max} = \frac{\gamma_s \gamma_d C_{N, N+1} C_{N+1, N}}{(\gamma_s + \gamma_d) (C_{N, N+1} + C_{N+1, N} + 2\sqrt{C_{N, N+1} C_{N+1, N}})} e^2 \beta. \quad (4.4.13)$$

We still have to determine the values of $C_{N,N+1}$ and $C_{N+1,N}$, which depend on the mismatch between the $r = +$ and the $r = -$ band. If both bands are aligned ($\varepsilon_\Delta = 0$) one finds from Fig. 4.4.1, $C_{N,N+1} = 4, 3, 2, 1$ and $C_{N+1,N} = 1, 2, 3, 4$ for $N = 4m, 4m+1, 4m+2, 4m+3$. Then the conductance $G_{N,N+1}$ shows fourfold electron periodicity with two equally high central peaks for $N = 4m+1, 4m+2$ and two smaller ones for $N = 4m, 4m+3$ (cf. Fig. 4.4.2 a)). The relative height between central and outer peaks is $G_{4m+1,4m+2}^{\max}/G_{4m,4m+1}^{\max} = 27/(10 + 4\sqrt{6}) \approx 1.36$. Note that this ratio is *independent* of a possible asymmetry $\gamma_s \neq \gamma_d$ in the lead contacts. In addition, the conductance is symmetric under an exchange of the sign of the bias voltage.

In the case of an energy mismatch between the $r = +$ and the $r = -$ band exceeding well the thermal energy, the degeneracy of the ground states is either 1 or 2 and we get $C_{N,N+1} = 2, 1, 2, 1$ and $C_{N+1,N} = 1, 2, 1, 2$ for $N = 4m, 4m+1, 4m+2, 4m+3$. Therefore, according to (4.4.13), all the conductance peaks have the same height as depicted in Fig. 4.4.3 a).

4.4.2. Low bias regime well outside of the Coulomb diamonds. Now we examine the regime where still only ground states are occupied but where we are well outside the region of Coulomb blockade, $\varepsilon_0 \gg |eV_l \pm \Delta E_N| \gg kT$. Then we have $|f(\varepsilon_s) - f(\varepsilon_d)| = 1$. If e.g. $eV_s - \Delta E_N < 0$ and $eV_d - \Delta E_N > 0$, such that electrons tunnel in from the source and tunnel out at the drain, it holds $f(\varepsilon_s) = 1$ and $f(\varepsilon_d) = 0$ such that (4.4.10) becomes

$$I_{N,N+1} = e \frac{C_{N,N+1} C_{N+1,N} \gamma_s \gamma_d}{\gamma_s C_{N,N+1} + \gamma_d C_{N+1,N}}. \quad (4.4.14)$$

The height of the plateaus in the current of Figures 4.4.2 b) and 4.4.3 b) are described by (4.4.14). If the $r = +$ band is aligned with the $r = -$ band, we still find a fourfold electron periodicity. But only for $\gamma_s = \gamma_d$ the pattern with two central peaks and two smaller outer peaks is preserved. The corresponding ratio of the heights is $3/2$. If $\gamma_s \neq \gamma_d$ this latter symmetry is lost.

For mismatched bands and $\gamma_s = \gamma_d$ we find like for the conductance peaks that all current maxima are of the same size. In the case of asymmetric tunnelling contacts, $\gamma_s \neq \gamma_d$, a pattern of alternating small and large peaks is found.

If we invert the sign of the bias voltage, the current is obtained by flipping its direction and exchanging γ_s with γ_d in (4.4.14). Then, if $\gamma_s \neq \gamma_d$, the current does not only change its sign but also changes its magnitude because of $C_{N,N+1} \neq C_{N+1,N}$.

Note that so far we have assumed that γ_s and γ_d are constant as functions of the applied voltages. However, in experiments it is often observed that the transparency of the tunneling contacts varies with the gate voltage. The dependence of γ_s and γ_d on the gate voltage can be easily determined. First the asymmetry $\alpha = \gamma_s/\gamma_d$ can be obtained from (4.4.14) in the regime $\varepsilon_0 \gg |eV_l \pm \Delta E_N| \gg kT$ by inverting the sign of the bias voltage; it holds

$$\alpha = \frac{|I_{NN+1}|C_{N+1N} - |I_{N+1N}|C_{NN+1}}{|I_{N+1N}|C_{N+1N} - |I_{NN+1}|C_{NN+1}},$$

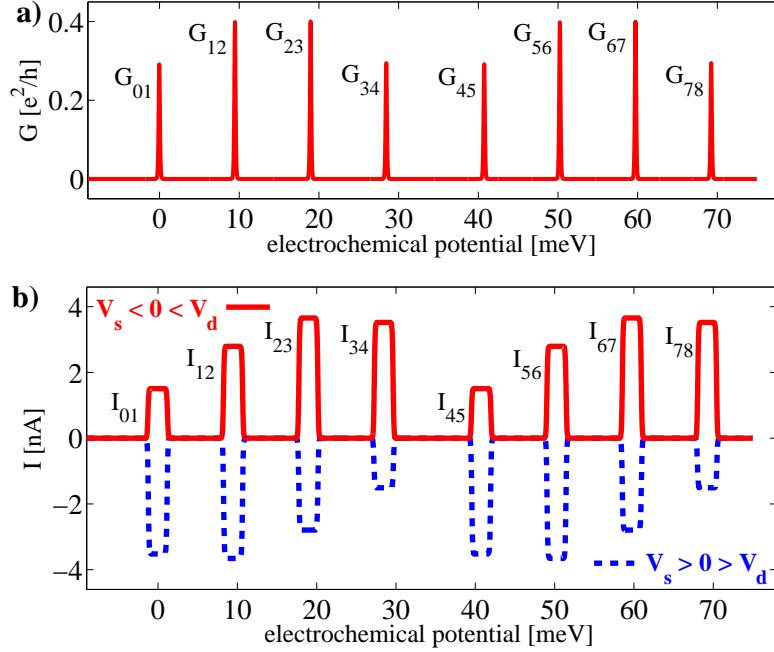


FIGURE 4.4.2. Gate traces for $\varepsilon_\Delta = 0$, i.e., for aligned $r = +$ and $r = -$ bands, at low bias voltage. Parameters are $E_c = 9.5$ meV, $k_B T = 0.10$ meV, $\varepsilon_0 = 2.9$ meV and the chosen asymmetry is $\gamma_s = 5\gamma_d = 4.9 \cdot 10^{10} \text{s}^{-1}$. a) Conductance in the linear regime $eV_b \ll k_B T \ll \varepsilon_0$. Despite asymmetric contacts, we find the repeating pattern of two small outer peaks and two large central peaks. b) Current in the regime $k_B T \ll |eV_l| \ll \varepsilon_0$. Asymmetry effects appear. The fourfold periodicity is retained. The upper and lower pattern correspond to opposite values of the bias voltage.

where I_{N+1N} , I_{NN+1} are measured at the same gate but at opposite bias voltage. Knowing α we can calculate the rates γ_s and γ_d from (4.4.14) and find

$$\gamma_d = \frac{I_{NN+1}}{e} \frac{\alpha C_{NN+1} + C_{N+1N}}{\alpha C_{N+1N} C_{NN+1}}, \quad \gamma_s = \alpha \gamma_d.$$

4.5. High bias regime

In the bias regime $eV > \varepsilon_0$ not only the ground states will contribute to transport but also states with bosonic excitations and band filling configurations \vec{N} different from the ground state configurations. We refer to the latter type of excitations as fermionic excitations. Since the number of relevant states increases rapidly with increasing bias voltage, an analytical treatment is not possible any more and we have to resort to numerical methods in order to calculate the stationary solution of the master equation (3.3.22) and the respective current. From (4.3.2) we know that at low temperatures the current only changes considerably near the excitation lines given therein.

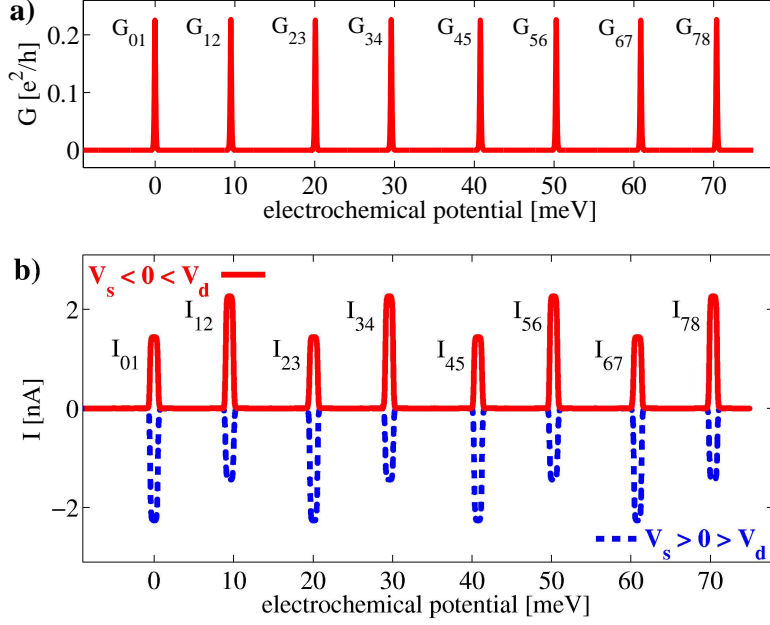


FIGURE 4.4.3. Gate traces for $\Delta = 0.2$, i.e., for mismatched $r = +$ and $r = -$ bands, at low bias voltage. Other parameters are $E_c = 9.5$ meV, $k_B T = 0.10$ meV, $\varepsilon_0 = 2.9$ meV and the chosen asymmetry is $\gamma_s = 5\gamma_d = 4.9 \cdot 10^{10} \text{s}^{-1}$. a) Conductance in the linear regime $eV_b \ll k_B T \ll \varepsilon_0$. The conductance peaks are all of the same height. b) Current in the regime $k_B T \ll |eV_l| \ll \varepsilon_0$. The contact asymmetry leads to alternating large and small current maxima.

Therefore we can reduce drastically the number of (eV, μ_g) points for which we actually perform the numerical calculations, saving computing time. In Figs. 4.5.1 a) and 4.5.2, the current as a function of the applied bias voltage and the electrochemical potential in the dot is depicted. The chosen parameters for E_c , ε_0 and ε_Δ are the ones we have obtained for fitting the data of sample C and sample A of [20], respectively. Hence Figs. 4.5.1 and 4.5.2 show the current for SWNTs with the $r = +$ and $r = -$ band being aligned ($\varepsilon_\Delta = 0$) and mismatched ($\varepsilon_\Delta \approx 0.34\varepsilon_0$). In both cases a symmetric coupling to the leads, $\gamma_s = \gamma_d$, is assumed. In the transport calculations the lowest lying $c+$ excitations are taken into account using $g_{q=\frac{\pi}{L}} = \sqrt{\varepsilon_0 \frac{\pi}{L} / \varepsilon_{c+\frac{\pi}{L}}} = 0.21$ for the Luttinger parameter.

In addition we have also determined the current using the CME, hence ignoring any coherences in the RDM. For the current corresponding to Fig. 4.5.1, the quantitative difference between the calculations with and without coherences is considerable in the region of intermediate bias voltage as we show in Fig. 4.5.1 b). On the other hand the deviation of the CME result from the calculation including coherences is by far less pronounced for the parameter choice of Fig. 4.5.2. The crucial point here is

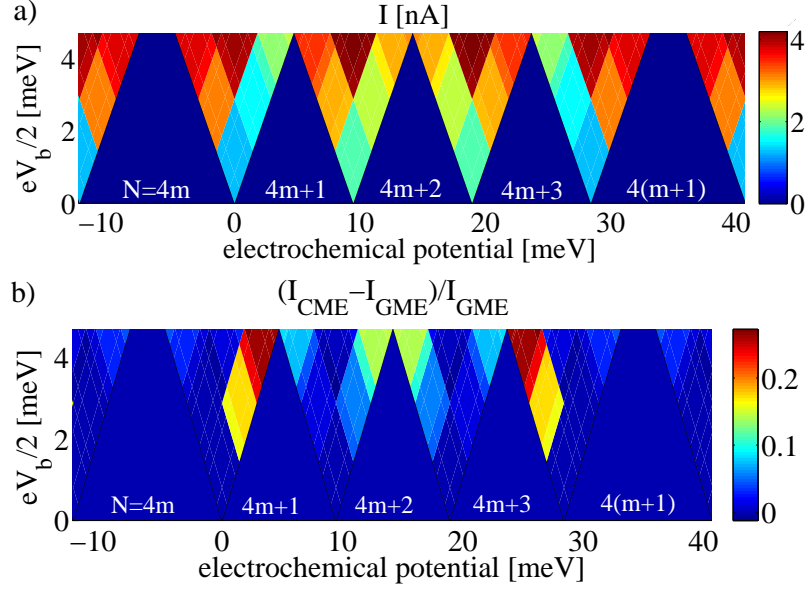


FIGURE 4.5.1. a) Current in a bias voltage - electrochemical potential plane for symmetric contacts case and vanishing band mismatch. b) Difference plot of the current with and without coherences. Here $k_B T = 0.01$ meV and the interaction parameter is $g_q = \frac{\pi}{L} \approx 0.21$. Other parameters are as for Fig. 4.4.2.

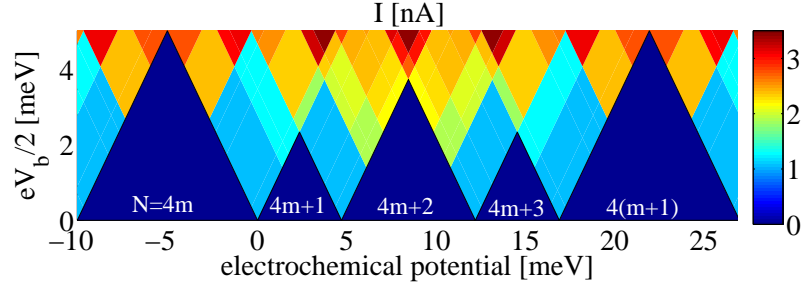


FIGURE 4.5.2. Current as a function of the bias voltage and the electrochemical potential in the SWNT for symmetric contacts but for a finite band mismatch. The parameters here are chosen to fit the positions of the Coulomb diamonds of sample A in [20], i.e. $E_c = 4.7$ meV, $2\Delta\varepsilon_0 = 2.8$ meV, $\varepsilon_0 = 8.2$ meV.

that the charging energy E_c is smaller than ε_0 , the level spacing of the neutral system. Then the subsequent considerations are not strictly valid. Now we explain why coherences can't be generally ignored if considering interacting electrons in a SWNT.

4.5.1. Why and when are coherences needed? As in the low bias regime we assume to have unpolarized leads. Thus we use condition (4.2.7), such that we can ignore coherences between states with different fermionic configurations \vec{N} . Unlike in the low bias regime, we are not only left with diagonal elements of the RDM but there still might be coherences between degenerate states which have the same \vec{N} but different bosonic excitations \vec{m} . For the importance of these kind of coherences it is illuminating to discuss our system without electron-electron interactions, i.e., for the moment let us assume that an eigenbasis of H_\odot is given by the Slater determinants of the single electron states $|\varphi_{r\kappa}\rangle |\sigma\rangle$. Furthermore, we concentrate without loss of generality on the case $\varepsilon_\Delta = 0$, and we assume that the charging energy E_c exceeds ε_0 . Each of the Slater determinants can be denoted by the occupation \vec{n} of the single electron states. In the case of unpolarized leads, it is again easy to show that coherences vanish in the stationary solution of the master equation (3.3.22), if the RDM is expressed in the $|\vec{n}\rangle$ basis. But of course we still could use the states $|\vec{N}, \vec{m}\rangle$ from (4.1.4) as eigenbasis, now with four neutral modes $c+, c-, s+, s-$. In the $|\vec{N}, \vec{m}\rangle$ basis it is crucial to include the off diagonal elements in order to get the right stationary solution as we show in the following example.

We adjust the voltages such that only transitions are possible from the ground state with $4m$ particles and energy E_{4m}^0 to ground and first excited states with $4m+1$ particles and energies E_{4m+1}^0 and $E_{4m+1}^1 = E_{4m+1}^0 + \varepsilon_0$, respectively. From the $4m+1$ ground states only transitions to the $4m$ ground state shall be allowed as depicted in Fig. 4.5.3 a). Note that this situation is only stable, because we have made the choice $E_c > \varepsilon_0$. The master equation expressed in the $|\vec{n}\rangle$ basis reveals that only four of the 16 states with the lowest particle hole excitation are indeed occupied in the stationary limit (cf. side b) of Fig. 4.5.3, because not all of the corresponding energetically allowed transitions from the $N = 4m$ ground state can be mediated by one-electron tunnelling processes.

Whereas in the $|\vec{N}, \vec{m}\rangle$ basis, all 16 states with the energetically lowest bosonic excitations are equally populated. Since the degenerate states of the two bases are connected by a unitary transformation, the same must be true for the corresponding matrix representations of $\rho_\odot^{I, E_{4m+1}^1}$. From the representation of the RDM in the $|\vec{n}\rangle$ basis, we know that the rank of $\rho_\odot^{I, E_{4m+1}^1}$ must be equal to 4. Because a unitary transformation does not change the rank of a matrix, the stationary solution in the $|\vec{N}, \vec{m}\rangle$ basis can maximally have 4 linearly independent columns. Since all diagonal elements are non-vanishing this is only possible if there are also non-vanishing coherences.

Switching on the electron - electron interactions, the $|\vec{n}\rangle$ states are no longer an eigenbasis of the SWNT Hamiltonian and hence we must work in the $|\vec{N}, \vec{m}\rangle$ basis. But then, as we know from the discussion above, the coherences are expected to be of importance. In the next chapter we will see that coherences affect the transport properties of quantum dots with non-collinearly polarized leads even in the low bias regime.

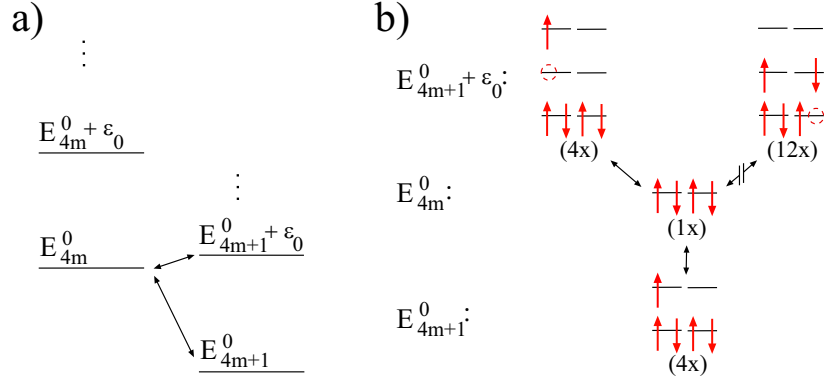


FIGURE 4.5.3. a) Scheme of relevant energy levels, if transitions from the ground state with $N = 4m$ particles to the first excited state with $N = 4m + 1$ particles are energetically allowed, while no transitions from the $N = 4m + 1$ ground states to excited states with $N = 4m$ electrons are possible. b) Possible transitions between the $N = 4m$ and $N = 4m + 1$ electron states of the noninteracting system, which are energetically allowed in situation a). The degeneracy of the eigenstates is given in brackets.

4.5.2. Negative differential conductance. Spin charge separation and therefore non-Fermi liquid behavior could also manifest itself in the occurrence of negative differential conductance (NDC) at certain excitation lines involving transitions to states with fermionic excitations, as was predicted for a spinful Luttinger liquid quantum dot [59] with asymmetric contacts. We also find this effect for the non-equilibrium treatment of the SWNT quantum dot. Since in our case only the energy spectrum of the $c+$ mode depends on the interaction and the other three modes have the same energies as the neutral system, rather large asymmetries are needed in order to observe NDC. In Fig. 4.5.4 we show the current across the first excitation line for transitions from $N = 4m + 1$ to $N = 4m$ in the $\varepsilon_\Delta = 0$ case. The corresponding trace in the $V_b - \mu_g$ plane is indicated in the inset of Fig. 4.5.4 a). Here the origin of the NDC is that some states with fermionic excitations have lower transition rates than non-excited states, since due to the increased energy of the $c+$ modes less channels are available for transport. In Fig. 4.5.4 b) we show some of the excited states with $N = 4m$ electrons which are responsible for the NDC, because their transition amplitudes to states with $N = 4m + 1$ electrons are reduced compared with the one of the $4m$ ground state. Apart from the asymmetries all other parameters are chosen as for Fig. 4.5.1. Only for asymmetries $\alpha = \gamma_d/\gamma_s$ larger than around 45, clear NDC features are seen.

4.5.3. Conclusions. In this section we have analyzed the linear and non-linear current as a function of the gate and bias voltage across metallic SWNT quantum dots with unpolarized leads. Exchange and related effects, which become relevant for small diameter SWNTs and which have been discussed in Chapter 2, have not been taken into account. Yet the applied transport theory is general enough to discuss the

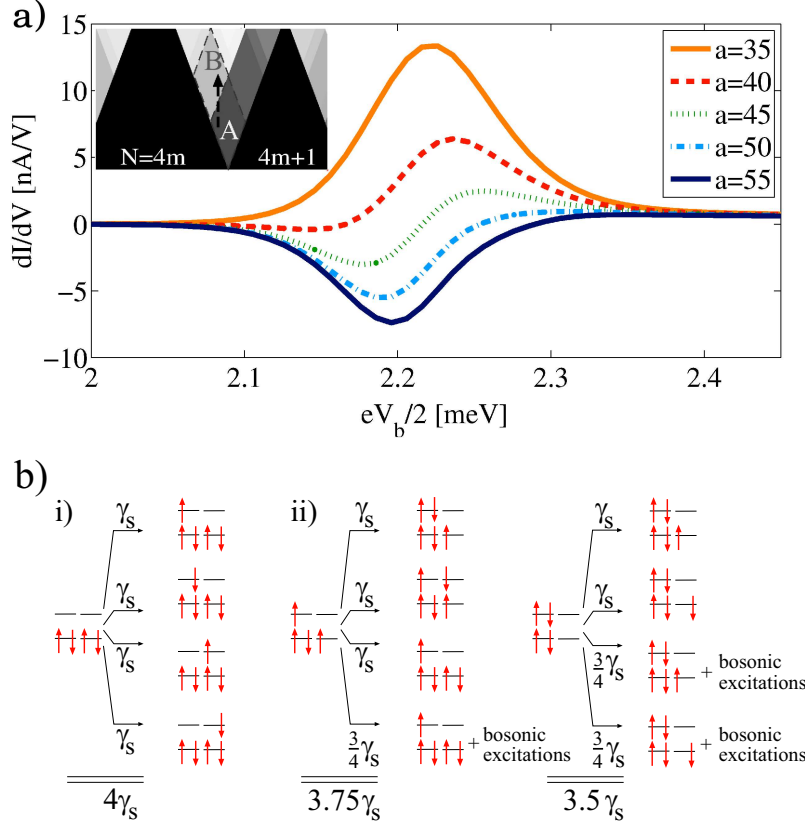


FIGURE 4.5.4. a) Differential conductance as a function of the bias voltage for different asymmetries $a = \gamma_d/\gamma_s$ of the coupling to the leads. The trace in the $V_b - \mu_g$ plane across the boundary between regions A and B is indicated in the inset. Only for asymmetries larger than around 45 negative differential conductance occurs. All parameters here are chosen as for Fig. 4.5.1, except for $k_B T$ a value of 0.026 meV corresponding to $T = 0.22$ K was used. b) The transitions responsible for NDC. i) In region A of the inset from a) only transitions between ground states are possible at low enough temperature. The transition rate from the $N = 4m$ ground state to the $N = 4m + 1$ ground states is given by $4\gamma_s$ (see equation (4.4.8)). ii) In region B additionally excited states become occupied. For some of the states with $N = 4m$ electrons and fermionic excitations the transition rates to states with $N = 4m + 1$ electrons and neutral bosonic excitations is decreased compared to the ground state rate as a consequence of the larger energies of $c+$ excitations, which are not available for transport yet. Notice that we only show the most important types of transitions from $N = 4m$ to $N = 4m + 1$ that take place in region B. Since we are considering a non-equilibrium situation other types of transitions are possible in principle.

influence of exchange effects on the transport properties in the future. The energy spectrum of a large diameter metallic SWNT is highly degenerate as a consequence of both fermionic and bosonic excitations. In the linear bias regime, the degeneracy of the groundstates leads to a characteristic pattern of conductance peaks depending on whether the two branches of the dispersion relation are aligned or not. Leaving the linear regime, asymmetry effects become relevant. Thus measurements of the current at low bias voltages, in the linear and non-linear regime, in principle allow the separate determination of the source and drain tunnelling resistances as a function of the gate voltage. At higher bias voltages also excited states become relevant. The correct calculation of the non-equilibrium dynamics of the system then requires the inclusion of coherences in the reduced density matrix between degenerate states with bosonic excitations. At intermediate bias voltages there is a considerable deviation between the transport calculations with and without coherences. We emphasize that for a non-interacting system with unpolarized leads, coherences do not have to be considered if expressing the reduced density matrix in terms of Slater determinants, formed by the one electron wave functions of the noninteracting system. Another consequence of the electron correlations is the formation of a non-oscillatory spatial dependence of the tunnelling amplitudes along the nanotube axis. For transitions between states with energetically low excitations we find a strong suppression of the tunnelling amplitudes near the SWNT ends. Furthermore we have addressed the influence of the tunnelling contacts on the transport. We have shown that extended contacts described as 3D Fermi gas and equally coupled to the two sublattices do not lead to a polarization of the contacts with respect to the pseudo spin. We think that a further investigation of this point for other types of contacts is worthwhile, especially an asymmetric coupling of the two sublattices to the leads in principle can create arbitrarily polarized leads with respect to the pseudo spin. The discussion of the pseudo spin polarization will also pave the way for the extension of the transport calculations to so called SWNT spin valve devices (SWNT quantum dots with spin polarized leads) presented in the following chapter.

CHAPTER 5

Metallic SWNT quantum dots with polarized leads

In collaboration with Sonja Koller and Milena Grifoni. Parts of the contents of this chapter have been published in the New Journal of Physics **9**, 348 (2007).

The transport properties of SWNT quantum dots with spin polarized leads, so called SWNT spin-valves, have been worked out in detail by Sonja Koller in her diploma thesis [60]. Here we present the necessary steps to extend the approach in Chapter 4 to spin transport and give the main result.

Conventionally it is merely the charge of the electrons and its coupling to the electromagnetic field that is used to control the transport properties of electronic devices. However, more and more also spin dependent transport has become a focus of attention in condensed matter physics and has even made its way to applications, as the award of the Nobel prize 2007 to Grünberg and Fert for the discovery of the giant magneto resistance, exploited in modern hard discs, impressively demonstrates. In the case of quantum dots, spin sensitive devices can be obtained by using magnetized source and drain electrodes. Depending on the relative magnetization of both lead electrodes the resistance of the quantum dot changes. So far only experiments with parallel (P) or antiparallel (AP) magnetization of source and drain could be performed. The quantity characterizing the influence of the magnetization is the so called tunneling magneto resistance TMR which we define as the ratio

$$TMR = \frac{G_P - G_{AP}}{G_P}, \quad (5.0.1)$$

where G_P is the conductance in the parallel and G_{AP} the conductance in the antiparallel configuration. Concerning nanotube spin-valves they are expected to be especially well suited for the study of spin transport, since due to the weak spin-orbit coupling in nanotubes the relaxation of spin is expected to be suppressed. On the other hand spin transport should again be sensitive to the intrinsic properties of the dot system, especially to interactions, and therefore can yield important insights into the considered system itself. Positive TMR values have been detected in various experimental works about SWNTs and MWNTs [61, 62, 63]. But even the occurrence of negative TMR has been reported [64, 65, 66]. In the works [63, 64, 65, 66] the TMR has found to be gate voltage dependent, indicating that the energy spectrum of the nanotubes plays a significant role. On the theoretical side spin dependent transport in interacting mesoscopic systems has been discussed for interacting single level quantum dots [51, 52, 67], metallic islands [68] and Luttinger liquids [70]. It was found that electron-electron interactions in connection with so called virtual transitions [51, 52] (cf. discussion after equation (4.2.9) for the meaning of the virtual transitions) as well

as reflections of the dot electrons at the magnetized leads [67, 68, 70, 71] can lead to a precession of the accumulated spin on the dot and thus influence the transport properties, for example reducing the TMR for non-collinear lead polarizations. The effect of spin precession is only present if the polarizations of the leads are non-collinear. However, going beyond the weak coupling regime the spin-dependent reflections can lead to a Zeeman like energy splitting which can become relevant in transport [65, 67, 69].

Concerning the theoretical treatment of spin-dependent transport through interacting 1D systems the limit of infinitely long tubes has been discussed in reference [70]. Transport properties of finite size SWNTs weakly contacted to ferromagnetic leads have been considered in our article [71] and in the numerical approach [72] focusing on shot noise. The latter calculations were based on the mean field theory of Oreg et al. and only the case of parallel and antiparallel lead magnetizations were discussed.

Generalizing the approach used for the discussion of interacting SWNT quantum dots in Chapter 4, we determine in the following the $I - V_b - V_g$ characteristics of a SWNT spin valve allowing for arbitrary magnetization directions of the leads. Additionally to the virtual transitions that arise automatically from our generalized master equation approach, we take into account the effect of electron reflections at the dot-lead interface. The detailed mechanism is explained e.g. in [68].

5.1. Experimental realization of SWNT spin valves

The leads of spin valve devices consist of ferromagnetic materials as for example Co or Ni-alloys whose magnetizations are adjusted by an external magnetic field. It is obvious that it must be possible to control the relative lead magnetization directions in order to examine a TMR effect. In experiments source and drain contacts of different size and hence with different coercive fields are used. The geometry of the electrodes determines their favoured magnetization direction. Applying a large enough B field parallel to the favoured magnetization axis, both leads will be polarized in the same direction. Lowering the B field and finally inverting its sign the contact with the smaller coercive field will first switch its magnetization direction before also the other contact follows, cf. Fig. 5.1.1. Hence by sweeping the B field up and down an alternating sequence of parallel and antiparallel magnetization is obtained. The controlled adjustment of an arbitrary angle between the magnetizations of source and drain electrodes has not been achieved experimentally so far.

5.2. The model Hamiltonian

Schematically a SWNT quantum dot with polarized leads is depicted in Fig. 5.2.1. We allow for arbitrarily polarized source and drain electrodes. Additionally also the accumulated spin will in general not be collinear with one of the lead magnetizations. As a start we will thus use in each case a different spin quantization axis in source, drain and in the dot. We will use the symbols σ_l , $l = s, d$ and σ in order to denote the z -component of the spins in the reference frame of the leads and of the dot, respectively. In analogy to (3.2.9) we model the SWNT spin valve shown in Fig. 5.2.1 by the Hamiltonian

$$H = H_{\odot} + H_s + H_d + H_T + H_R. \quad (5.2.1)$$

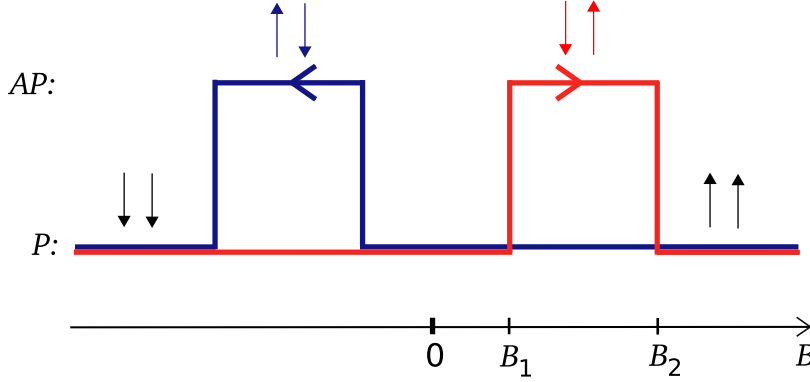


FIGURE 5.1.1. Sweeping the magnetic field in a certain range, parallel and antiparallel configurations of the lead polarizations can be achieved by using ferromagnetic leads with different coercive fields B_1 and B_2 .

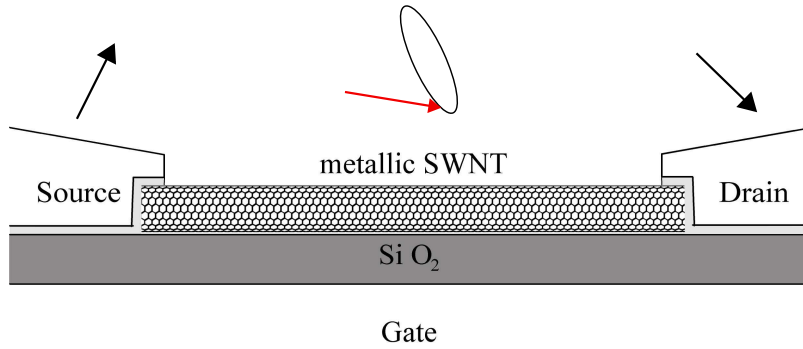


FIGURE 5.2.1. Scheme of a SWNT spin valve setup. We consider leads with arbitrarily polarized leads. Charge transport across the device will lead to a spin accumulation on the SWNT. Virtual transitions and boundary reflections can lead to a spin precession on the dot system.

As for the unpolarized SWNT quantum dot the Hamiltonian H_\odot is given by equation (4.1.1). However, the Hamiltonians H_s and H_d for the ferromagnetic leads now have to be modified compared to the unpolarized case, equation (4.2.12), in order to incorporate the spin polarization. The easiest way to do this is to use the Stoner mechanism. Any other description would serve as well. Hence

$$H_l = \sum_{\vec{q}\sigma_l} (\varepsilon_{\vec{q}} - eV_l - \text{sgn}(\sigma_l)E_S) c_{\vec{q}\sigma_l}^\dagger c_{\vec{q}\sigma_l}, \quad E_S > 0. \quad (5.2.2)$$

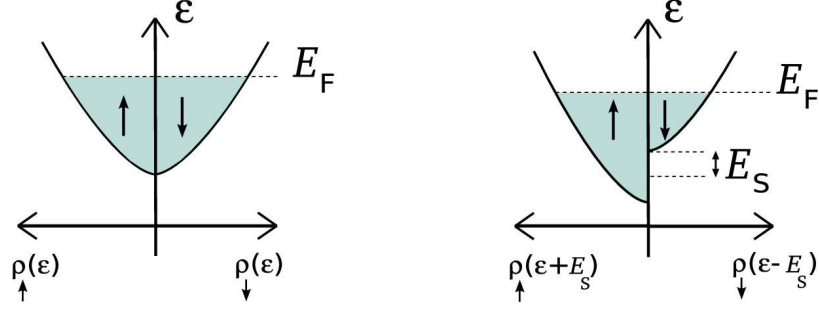


FIGURE 5.2.2. Spin dependent densities of states in a metal without (left side) and with (right side) Stoner exchange.

The effect of the Stoner energy E_S is a relative energy shift of the $\sigma_l = \uparrow_l / \downarrow_l$ electrons down-/upwards, such that the spin up/down electrons constitute the majority/minority species in thermal equilibrium, cf. Fig. 5.2.2. The tunneling Hamiltonian H_T from (3.2.3) does not change, we merely rewrite it in the spin bases of the leads,

$$H_T = \sum_{l=s,d} \sum_{\sigma_l} \int d^3r \left(T_l(\vec{r}) \Psi_{\sigma_l}^\dagger(\vec{r}) \Phi_{\sigma_l}(\vec{r}) + \text{h.c.} \right). \quad (5.2.3)$$

Remember that $\Psi_{\sigma}^\dagger(\vec{r})$ and $\Phi_{\sigma l}(\vec{r})$ denote the dot and lead electron operators. Completely new is the “reflection” contribution H_R to the Hamiltonian. It is well known from multilayers of ferromagnetic and non-magnetic materials that the behaviour of an electron that is backscattered at the interface between two layers crucially depends on the relative orientation of the electron spin and the polarization in the ferromagnet and can lead to ferromagnetic or antiferromagnetic exchange coupling between the ferromagnets depending on the layer thickness. In the works [67, 68] it was realized that also in mesoscopic spin valves the influence of the boundary between polarized leads and the dot must be taken into account. Unlike in the multilayer systems no exchange effects between the ferromagnetic leads are expected, nevertheless the dot electrons that are reflected at the tunneling junctions acquire a phase shift depending on whether their spin is parallel or antiparallel to the lead polarization. Those phase shifts alter the quantization condition for the dot electrons and therefore lead to a spin and position dependent energy splitting $\pm \Delta_{Rl}(\vec{r})$. Rewriting the momentum space expression for H_R from [68] we obtain in the position representation,

$$H_R = - \sum_{l=s,d} \sum_{\sigma_l} \int d^3r \Delta_{Rl}(\vec{r}) \text{sgn}(\sigma_l) \Psi_{\sigma_l}^\dagger(\vec{r}) \Psi_{\sigma_l}(\vec{r}). \quad (5.2.4)$$

Since the phase shift due to electron reflections takes place near the tunneling junctions we will assume later on that $\Delta_{Rl}(\vec{r})$ is nonvanishing only in the vicinity of the contacts.

5.3. Generalized master equation for the SWNT spin valve

In Chapter 3 we have presented a general method to determine how the reduced density matrix (RDM) of a generic quantum dot evolves in time. No assumptions

whether the leads are polarized or not have been made. Therefore our approach is general enough to also yield a transport theory for quantum dots weakly coupled to polarized leads. Remember that in our discussion of SWNT quantum dots with normal-metal leads the possibility of a polarization with respect to the pseudo spin degree of freedom has been automatically incorporated in the transport calculations by starting from the microscopic system Hamiltonian (3.2.9). Though, there is one qualitative difference between (3.2.9) and (5.2.3), namely the reflection term H_R . In order to set up the equations of motion governing the time evolution of the RDM for Hamiltonian (5.2.3), we now treat not only the tunneling Hamiltonian H_T but the sum $H_T + H_R$ as perturbation in the lowest non-vanishing order to the remaining terms in (5.2.3). Thus instead of equation (3.3.3) the Liouville equation for the RDM in the interaction picture now reads,

$$i\hbar \frac{\partial \rho^I(t)}{\partial t} = [H_T^I(t), \rho^I(t)] + [H_R^I(t), \rho^I(t)]. \quad (5.3.1)$$

Since the Liouville equation is linear it is clear from (5.3.1) that the rates $\Gamma_{l k' mnk}^{(\alpha) E_N E'_{N+1}}$ will decompose into two parts, one stemming from the tunneling Hamiltonian H_T and the other from H_R ,

$$\Gamma_{l k' mnk}^{(\alpha) E_N E'_{N+1}} = \Gamma_{T, l k' mnk}^{(\alpha) E_N E'_{N+1}} + \Gamma_{R, l k' mnk}^{(\alpha) E_N E'_{N+1}}. \quad (5.3.2)$$

Let us at first ignore the second term on the right hand side and let us concentrate on the first summand. From the general discussion in Chapter 3 it follows that the amplitudes $\Gamma_{T, l k' mnk}^{(\alpha) E_N E'_{N+1}}$ are given by equations (3.3.25) and (3.3.26). In complete analogy to the unpolarized quantum dots we have to determine the lead correlation functions $\langle \Phi_{\sigma l}(\vec{x}) \Phi_{\sigma l}^\dagger(\vec{y}, -t') \rangle_{\text{th}}$ and $\langle \Phi_{\sigma l}^\dagger(\vec{x}) \Phi_{\sigma l}(\vec{y}, -t') \rangle_{\text{th}}$ which enter the functions $\mathcal{E}_{\sigma l}(\vec{x}, \vec{y}, t')$ and $\mathcal{F}_{\sigma l}(\vec{x}, \vec{y}, t')$, but now in consideration of the Stoner Hamiltonian (5.2.2). Explicitly we obtain

$$\begin{aligned} & \langle \Phi_{\sigma l}(\vec{x}) \Phi_{\sigma l}^\dagger(\vec{y}, -t') \rangle_{\text{th}} = \\ & \int d\varepsilon \rho_l(\varepsilon) [1 - f_l(\varepsilon - \text{sgn}(\sigma_l) E_S)] \sum_{\vec{q}|\varepsilon} \phi_{\vec{q}}(\vec{x}) \phi_{\vec{q}}^*(\vec{y}) e^{-\frac{i}{\hbar}(\varepsilon - eV_l - \text{sgn}(\sigma_l) E_S)t'} \end{aligned} \quad (5.3.3)$$

and

$$\begin{aligned} & \langle \Phi_{\sigma l}^\dagger(\vec{x}) \Phi_{\sigma l}(\vec{y}, -t') \rangle_{\text{th}} = \\ & \int d\varepsilon \rho_l(\varepsilon) f_l(\varepsilon - \text{sgn}(\sigma_l) E_S) \sum_{\vec{q}|\varepsilon} \phi_{\vec{q}}^*(\vec{x}) \phi_{\vec{q}}(\vec{y}) e^{\frac{i}{\hbar}(\varepsilon - eV_l - \text{sgn}(\sigma_l) E_S)t'}, \end{aligned} \quad (5.3.4)$$

where the densities of occupied and empty states are different for the two spin species. With $\rho_l(\varepsilon)$ being the density of energy levels in lead l *without* Stoner exchange, they read $\rho_l(\varepsilon) [1 - f_l(\varepsilon - \text{sgn}(\sigma_l) E_S)]$ and $\rho_l(\varepsilon) f_l(\varepsilon - \text{sgn}(\sigma_l) E_S)$. Again we have set the chemical potential in the leads to 0. For convenience we shift the variable ε in (5.3.3) and (5.3.4), $\varepsilon \rightarrow \varepsilon - \text{sgn}(\sigma_l) E_S$. Inserting the resulting correlation functions

into equations (3.3.12) and (3.3.13) we arrive at

$$\mathcal{E}_{l\sigma_l}(\vec{x}, \vec{y}, t') := T_l(\vec{x})T_l^*(\vec{y}) \int d\varepsilon \rho_{l\sigma_l}(\varepsilon) [1 - f_l(\varepsilon)] \sum_{\vec{q}|\varepsilon + \text{sgn}(\sigma_l)E_S} \phi_{\vec{q}}(\vec{x}) \phi_{\vec{q}}^*(\vec{y}) e^{-\frac{i}{\hbar}(\varepsilon - eV_l)t'} \quad (5.3.5)$$

and

$$\mathcal{F}_{l\sigma_l}(\vec{x}, \vec{y}, t') := T_l^*(\vec{x})T_l(\vec{y}) \int d\varepsilon \rho_{l\sigma_l}(\varepsilon) f_l(\varepsilon) \sum_{\vec{q}|\varepsilon + \text{sgn}(\sigma_l)E_S} \phi_{\vec{q}}^*(\vec{x}) \phi_{\vec{q}}(\vec{y}) e^{\frac{i}{\hbar}(\varepsilon - eV_l)t'}, \quad (5.3.6)$$

where $\rho_{l\sigma_l}(\varepsilon) = \rho_l(\varepsilon + \text{sgn}(\sigma_l)E_S)$ is the density of states for electrons with spin σ_l in the ferromagnet. See also Fig. 5.2.2. As for the unpolarized leads, the rates $\Gamma_{T,l k' mnk}^{(\alpha)E_N E'_{N+1}}$ depend on the geometry of the tunneling junctions. The corresponding examination can be performed in completely the same way as in Chapter 4, where we have shown how to parameterize the effect of the contact geometry by introducing the contact density matrices $\Phi_{lrr'}(\varepsilon)$. Due to the summation over different lead wave functions in (5.3.5) and (5.3.6) for the two spin species, here the parameterization can be achieved by using spin dependent quantities $\Phi_{l\sigma_l\sigma'_l rr'}(\varepsilon)$. Based on the same argumentation that has lead to (4.2.7) in Chapter 4 we will further on make use of the assumption

$$\Phi_{l\sigma_l\sigma'_l rr'}(\varepsilon) = \delta_{rr'} \Phi_{l\sigma_l\sigma'_l}(\varepsilon), \quad (5.3.7)$$

where according to (4.2.21) it holds

$$\Phi_{l\sigma_l\sigma'_l}(\varepsilon) = \delta_{\sigma_l\sigma'_l} \rho_{l\sigma_l}(\varepsilon) \frac{\tilde{C}L}{2N_L} \sum_{\vec{R}p} \left| T_l(\vec{x}_{\vec{R},p}) \right|^2 W^2(\vec{R}_x). \quad (5.3.8)$$

Bearing in mind relations (5.3.5) to (5.3.7) and in analogy to equations (4.2.6) and (4.2.8) the rates $\Gamma_{T,l k' mnk}^{(\alpha)E_N E'_{N\pm 1}}$ can be written as

$$\Gamma_{T,l k' mnk}^{(\alpha)E_N E'_{N+1}} = \frac{1}{\hbar^2} \int d\varepsilon f_l(\varepsilon) \sum_{\sigma_l\sigma'_l} \Phi_{l\sigma_l\sigma'_l}(\varepsilon) \times \sum_r (\psi_{r\sigma_l l})_{k'm}^{E_N E'_{N+1}} (\psi_{r\sigma'_l l}^\dagger)_{nk}^{E'_{N+1} E_N} \int_0^\infty dt' e^{\alpha \frac{i}{\hbar}(\varepsilon - eV_l - (E'_{N+1} - E_N))t'}, \quad (5.3.9)$$

and

$$\Gamma_{T,l k' mnk}^{(\alpha)E_N E'_{N-1}} = \frac{1}{\hbar^2} \int d\varepsilon (1 - f_l(\varepsilon)) \sum_{\sigma_l\sigma'_l} \Phi_{l\sigma_l\sigma'_l}^*(\varepsilon) \times \sum_r (\psi_{r\sigma_l l}^\dagger)_{k'm}^{E_N E'_{N-1}} (\psi_{r\sigma'_l l})_{nk}^{E'_{N-1} E_N} \int_0^\infty dt' e^{\alpha \frac{i}{\hbar}(-\varepsilon + eV_l - (E'_{N-1} - E_N))t'}. \quad (5.3.10)$$

In the considered energy range we assume that $\Phi_{l\sigma_l\sigma'_l}(\varepsilon)$ is energy independent.

From $\Phi_{l\sigma_l\sigma'_l}(\varepsilon)$ we can deduce the spin polarization of lead l in analogy to our discussion of pseudo spin polarization in Chapter 4. Looking back to equation (4.2.23)

we find

$$\mathcal{P}_{li} = \frac{1}{\phi_l^{(+)}} \text{Tr}(\Phi_l \sigma_i), \quad i = x, y, z, \quad \phi_l^{(+)} = \Phi_{l\uparrow_l\uparrow_l} + \Phi_{l\downarrow_l\downarrow_l}.$$

With (5.3.8) the previous equation yields

$$\mathcal{P}_{lx} = \mathcal{P}_{ly} = 0 \text{ and } \mathcal{P}_{lz}(\varepsilon) = \frac{\rho_{l\uparrow_l}(\varepsilon) - \rho_{l\downarrow_l}(\varepsilon)}{\rho_{l\uparrow_l}(\varepsilon) + \rho_{l\downarrow_l}(\varepsilon)}, \quad (5.3.11)$$

such that in the reference frame of lead l the polarization is, not surprisingly, determined by the density of states of the \uparrow_l and \downarrow_l electrons. We want to remark that different lead wave functions belong to the \uparrow_l and \downarrow_l electrons at a given energy. Hence in general a different coupling between the \uparrow_l and \downarrow_l wave functions could lead to a contribution to the polarization beyond the effect of the different densities of states and even to a mixing of the spin and pseudo spin degrees of freedom.

We still have to determine the proper expression of the “reflection” contributions $\Gamma_{R,l}^{(\alpha)E_N E'_N+1}$ to the transition rates. For this purpose we discard for the moment the term describing the tunneling processes in (5.3.1) and concentrate on the time evolution of the system density matrix due to the boundary reflections:

$$i\hbar \frac{\partial \rho^I(t)}{\partial t} = [H_R^I(t), \rho^I(t)].$$

Since we treat H_R as a perturbation we are again allowed to factorize $\rho^I(t)$ into the reduced density matrix of the SWNT $\rho_\odot^I(t)$ and the lead density matrices $\rho_{s,d}$ which we assume to stay in thermal equilibrium, such that

$$i\hbar \frac{\partial \rho_\odot^I(t) \rho_s \rho_d}{\partial t} = [H_R^I(t), \rho_\odot^I(t) \rho_s \rho_d].$$

Tracing out the lead degrees of freedom we get completely rid of any lead density operators because no lead operators appear in H_R and $\text{Tr}_{leads}(\rho_s \rho_d) = 1$. With the explicit form of H_R , equation (5.2.4), we obtain

$$\dot{\rho}_\odot^I(t) = \frac{i}{\hbar} \sum_{l=s,d} \sum_{\sigma_l} \int d^3r \Delta_{Rl}(\vec{r}) \text{sgn}(\sigma_l) \left(\Psi_{\sigma_l}^{I\dagger}(\vec{r}, t) \Psi_{\sigma_l}^I(\vec{r}, t) \rho_\odot^I(t) - h.c. \right).$$

We can simplify the previous equation by expanding the 3D electron operators $\Psi_{\sigma_l}^\dagger(\vec{r})$ in terms of the 1D operators $\psi_{rF\sigma_l}^\dagger(x)$ using equation (4.2.1). Since the spin sensitive reflections at the boundaries are restricted to a small region near the tunneling contacts, $\Delta_{Rl}(\vec{r})$ is only non-vanishing around $x = 0, L$. A calculation similar to the one performed in Section 3.3 yields

$$\dot{\rho}_\odot^I(t) = \frac{i}{\hbar} \sum_{l=s,d} \sum_{\sigma_l} \Delta_{Rl} \text{sgn}(\sigma_l) \left(\psi_{r\sigma_l}^{I\dagger}(t) \psi_{r\sigma_l}^I(t) \rho_\odot^I(t) - h.c. \right), \quad (5.3.12)$$

with the effective reflection parameter Δ_{Rl} , which depends on the detailed structure of the contact geometry. Like in the treatment of the tunneling Hamiltonian we express (5.3.12) in the eigenbasis of H_\odot and apply the secular approximation, i.e., we only keep coherences between degenerate states. Bringing (5.3.12) into Bloch-Redfield

form finally the rates $\Gamma_{R,lk'mnk}^{(\alpha)E_N E'_{N+1}}$ are obtained,

$$\Gamma_{R,lk'mnk}^{(\alpha)E_N E'_M} = -\alpha \delta_{M N-1} \frac{i}{\hbar} \sum_{\sigma_l} \Delta_{Rl} \text{sgn}(\sigma_l) \left(\psi_{r\sigma_l l}^\dagger \right)_{k'm}^{E_N E'_{N-1}} (\psi_{r\sigma_l l})_{nk}^{E'_{N-1} E_N}. \quad (5.3.13)$$

Let us take a short break and summarize.

Starting from the Liouville equation for the spin valve density matrix, equation (5.3.1), we could calculate the transition amplitudes $\Gamma_{lk'mnk}^{(\alpha)E_N E'_M}$ that enter the generalized master equation (3.3.22). With (5.3.9), (5.3.10) and (5.3.13) they read,

$$\Gamma_{lk'mnk}^{(\alpha)E_N E'_{N+1}} = \frac{\pi}{\hbar} \sum_r \sum_{\sigma_l \sigma'_l} (\psi_{r\sigma_l l})_{k'm}^{E_N E'_{N+1}} \left(\psi_{r\sigma'_l l}^\dagger \right)_{nk}^{E'_{N+1} E_N} \times \left(\Phi_{l\sigma_l \sigma'_l}(\varepsilon) f_l(\varepsilon_{lNN+1}) (\varepsilon_{lNN+1}) + \alpha \frac{i}{\pi} \mathcal{P} \mathcal{V} \int \frac{f_l(\varepsilon) \Phi_{l\sigma_l \sigma'_l}(\varepsilon)}{\varepsilon - \varepsilon_{lNN+1}} d\varepsilon \right) \quad (5.3.14)$$

and

$$\Gamma_{lk'mnk}^{(\alpha)E_N E'_{N-1}} = \frac{\pi}{\hbar} \sum_r \sum_{\sigma_l \sigma'_l} \left(\psi_{r\sigma'_l l}^\dagger \right)_{k'm}^{E_N E'_{N-1}} (\psi_{r\sigma_l l})_{nk}^{E'_{N-1} E_N} \times \left[\Phi_{l\sigma_l \sigma'_l}(\varepsilon) (1 - f_l(\varepsilon_{lN-1N})) (\varepsilon_{lN-1N}) - \alpha \frac{i}{\pi} \left(\mathcal{P} \mathcal{V} \int \frac{(1 - f_l(\varepsilon)) \Phi_{l\sigma_l \sigma'_l}(\varepsilon)}{\varepsilon - \varepsilon_{lN-1N}} d\varepsilon + \delta_{\sigma_l \sigma'_l} \text{sgn}(\sigma_l) \pi \Delta_{Rl} \right) \right]. \quad (5.3.15)$$

where we have performed the integrals over ε using relation (4.2.9). Additionally we have introduced the abbreviations

$$\varepsilon_{lNM} := eV_l - E_N + E_M.$$

It is interesting to note that the contribution from the reflection Hamiltonian adds to the virtual transitions in (5.4.6). So far we have used two different spin quantization axes for the description of tunneling processes at the two different leads. Hence we still have to reexpress equations (5.4.5) and (5.4.6) in a common spinor basis before we can perform the actual calculations.

5.4. Coordinate transformations in spinor space

In this section we make convenient choices for the common quantization axis for the spins in (5.4.5) and (5.4.6). It is distinguished between non-collinear and collinear magnetizations of the leads.

5.4.1. Non-collinear lead magnetizations. In this case we follow [52] and introduce new coordinates for the spin polarization with the basis $(\vec{e}_x, \vec{e}_y, \vec{e}_z)$ shown in Fig. 5.4.1, such that the z axis is perpendicular to the plane spanned by the polarization directions of source and drain, \vec{m}_s and \vec{m}_d . This choice will prove to be very convenient for the transport calculations in Section 5.5. The bases $(\vec{e}_{lx}, \vec{e}_{ly}, \vec{e}_{lz})$, $l = s, d$ of the source/ drain reference frames can be aligned with the new common coordinate

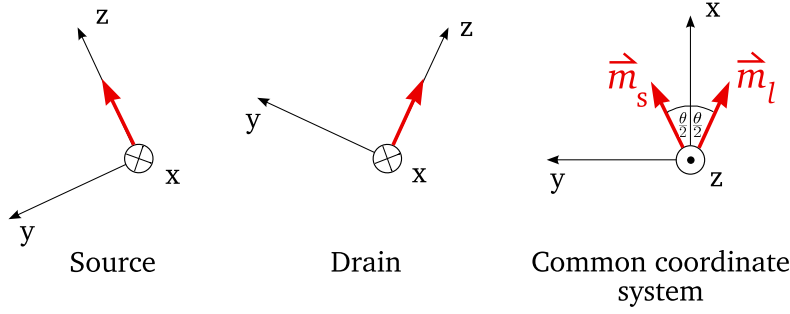


FIGURE 5.4.1. Spin coordinates in source, drain and in the common reference frame we use to evaluate the master equation.

system by rotation of $\theta_l = \mp\theta/2$, $l = s, d$ around the corresponding x axes and subsequent rotation of $\pi/2$ around the y axes. In spinor space this rotation corresponds to the $SU(2)$ transformation

$$U_l = e^{-\frac{i}{2}\sigma_y\frac{\pi}{2}} e^{-\frac{i}{2}\sigma_x\theta_l} = \frac{1}{\sqrt{2}} \begin{pmatrix} e^{i\frac{\theta_l}{2}} & -e^{i\frac{\theta_l}{2}} \\ e^{-i\frac{\theta_l}{2}} & e^{-i\frac{\theta_l}{2}} \end{pmatrix}.$$

Therefore the electron operators $\psi_{r\sigma l}^\dagger$ transform according to

$$\begin{pmatrix} \psi_{r\uparrow l}^\dagger \\ \psi_{r\downarrow l}^\dagger \end{pmatrix} = U_l^{-1} \begin{pmatrix} \psi_{r\uparrow}^\dagger \\ \psi_{r\downarrow}^\dagger \end{pmatrix} = \frac{1}{\sqrt{2}} \begin{pmatrix} e^{-i\frac{\theta_l}{2}} & e^{i\frac{\theta_l}{2}} \\ -e^{-i\frac{\theta_l}{2}} & e^{i\frac{\theta_l}{2}} \end{pmatrix} \begin{pmatrix} \psi_{r\uparrow}^\dagger \\ \psi_{r\downarrow}^\dagger \end{pmatrix} \quad (5.4.1)$$

and likewise

$$\begin{pmatrix} \psi_{r\uparrow l} & \psi_{r\downarrow l} \end{pmatrix} = \begin{pmatrix} \psi_{r\uparrow} & \psi_{r\downarrow} \end{pmatrix} U_l. \quad (5.4.2)$$

Here $\sigma = \uparrow, \downarrow$ denotes the up/ down spins in the common spinor basis.

5.4.2. Collinear lead magnetization. For collinear leads we have to distinguish between the parallel and the antiparallel configuration. In the parallel configuration (P) the coordinate transformations is just the unity matrix,

$$U_l^P = \begin{pmatrix} 1 & 0 \\ 0 & 1 \end{pmatrix}, \quad l = s, d. \quad (5.4.3)$$

For the antiparallel configuration (AP) we use by convention the source magnetization as the quantization axis. Thus

$$U_s^{AP} = \begin{pmatrix} 1 & 0 \\ 0 & 1 \end{pmatrix} \text{ and } U_d^{AP} = \begin{pmatrix} 0 & -i \\ -i & 0 \end{pmatrix}. \quad (5.4.4)$$

With (5.4.1) to (5.4.4) the final expressions for the rates in the non-collinear case read

$$\Gamma_{l k' m n k}^{(\alpha) E_N E'_{N+1}} = \frac{\pi}{\hbar} \sum_r \sum_{\sigma \sigma'} (\psi_{r \sigma l})_{k' m}^{E_N E'_{N+1}} \left(\psi_{r \sigma' l}^\dagger \right)_{n k}^{E'_{N+1} E_N} \times \left(\tilde{\Phi}_{l \sigma \sigma'}(\varepsilon) f_l(\varepsilon_{l N N+1}) + \alpha \frac{i}{\pi} \mathcal{P} \mathcal{V} \int \frac{f_l(\varepsilon) \tilde{\Phi}_{l \sigma \sigma'}(\varepsilon)}{\varepsilon - \varepsilon_{l N N+1}} d\varepsilon \right) \quad (5.4.5)$$

and

$$\Gamma_{l k' m n k}^{(\alpha) E_N E'_{N-1}} = \frac{\pi}{\hbar} \sum_r \sum_{\sigma \sigma'} \left(\psi_{r \sigma' l}^\dagger \right)_{k' m}^{E_N E'_{N-1}} (\psi_{r \sigma l})_{n k}^{E'_{N-1} E_N} \times \left[\tilde{\Phi}_{l \sigma \sigma'}(\varepsilon) (1 - f_l(\varepsilon_{l N-1 N})) - \alpha \frac{i}{\pi} \left(\mathcal{P} \mathcal{V} \int \frac{(1 - f_l(\varepsilon)) \tilde{\Phi}_{l \sigma \sigma'}(\varepsilon)}{\varepsilon - \varepsilon_{l N-1 N}} d\varepsilon + \pi R_{l \sigma \sigma'} \Delta_{Rl} \right) \right], \quad (5.4.6)$$

where

$$\tilde{\Phi}_l(\varepsilon) = U_l \Phi_l(\varepsilon) U_l^{-1}$$

are up to the proper normalization the density matrices describing the lead polarization in the common spin basis, cf. equation (4.2.22). The matrix

$$R_l = U_l \begin{pmatrix} 1 & 0 \\ 0 & -1 \end{pmatrix} U_l^{-1} = \begin{pmatrix} 0 & e^{i\theta} \\ e^{-i\theta} & 0 \end{pmatrix}$$

adds components perpendicular to the lead magnetizations to the polarization of the imaginary parts in (5.4.6), since it has merely off-diagonal elements. The matrix elements of the 1D electron operators in (5.4.5) and (5.4.6) have already been determined in Chapter 4, cf. equation (4.2.2).

5.5. Linear regime

The linear response regime, $eV_l \ll k_B T$, is amenable to an analytical treatment, since in this case the lead electrons do not provide enough energy to tunnel into excited states of the SWNT and we can restrict ourselves to the ground states of the Hamiltonian H_\odot shown in Fig. 4.4.1. In principle, for the virtual processes in the rates $\Gamma_{l k' m n k}^{(\alpha) E_N E'_{N \pm 1}}$ energy conservation does not strictly hold such that they could lead to a coupling of the ground states to excited states in the master equation. However, as detailed in [71] the effects of the virtual transitions on the time evolution of the RDM cancel exactly. Therefore in the linear regime we can indeed ignore any excited states which considerably simplifies the treatment of SWNT spin valves at low energies. Due to the charging energy transport through the spin valve is only possible when the ground states of two neighbouring charge states are almost degenerate. That means we will have to consider like in our discussion of the low bias regime of unpolarized SWNT quantum dots, Section 4.4, the regimes where the ground states E_N^0 and E_{N+1}^0 with N and $N + 1$ electrons are degenerate. Remember that the values of E_N^0 and E_{N+1}^0 can be aligned by the proper choice of the electrochemical potential in the SWNT via the gate voltage. Due to the fourfold periodicity of the shell filling in

SWNTs only the cases $N \bmod 4 = 0, 1, 2, 3$ are relevant. Additionally we only have to consider the cases $N = 4m$ and $N = 4m + 1$ since the corresponding transport properties are mirror symmetric to the ones of $N = 4m + 3$ and $N = 4m + 2$ with respect to the electrochemical potential μ_g in the dot. We also regard only the case of a vanishing band mismatch $\varepsilon_\Delta \ll k_B T$, since at a finite mismatch we can reduce the discussion for all N to the one for $\varepsilon_\Delta = 0$ with a degeneracy between $E_{N=4m}^0$ and $E_{N=4m+1}^0$. The only difference is an additional factor of two for the resulting current due to the pseudo spin degeneracy in the latter case.

5.5.1. Near the degeneracy point of $E_{N=4m}^0$ and $E_{N=4m+1}^0$. As we know from our discussion of the low bias regime of unpolarized SWNT quantum dots, the ground states can be uniquely characterized by their fermionic configuration \vec{N} . The ground state energy $E_{N=4m}^0$ belongs to the onefold degenerate state with $\vec{N} = (n, n, n, n)$ and the $N = 4m + 1$ ground state is fourfold degenerate with the fermionic configurations $\vec{N} = (n + 1, n, n, n) + \text{permutations}$. The RDM $\rho^{I, E_{4m}^0} =: \rho^{I, 4m}$ is only a number namely the probability P_0 of finding an electron in the $N = 4m$ ground state, whereas $\rho^{I, 4m+1}$ is a four by four matrix. However, since we assume that there is no polarization with respect to the pseudo spin, transitions between states with a different number of $r = \pm$ electrons are forbidden. Hence ρ^{I, E_{4m+1}^0} has the block structure

$$\rho^{I, 4m+1} = \begin{pmatrix} \rho_{r=+}^{I, 4m+1} & 0 \\ 0 & \rho_{r=-}^{I, 4m+1} \end{pmatrix},$$

where the two by two matrices $\rho_{r=+}^{I, 4m+1}$ and $\rho_{r=-}^{I, 4m+1}$ must be equal in the stationary solution of the master equation due to the symmetry of $r = +$ and $r = -$. Introducing the spin polarization

$$\vec{S} = \frac{1}{2} \sum_r T_r (\vec{\sigma} \rho_r^{I, 4m+1}),$$

on the dot, the density operators $\rho_r^{I, 4m+1}$ can be written in the following form,

$$\rho_r^{I, 4m+1} = \frac{P_1}{4} \begin{pmatrix} 1 + S_z & S_x - iS_y \\ S_x + iS_y & 1 - S_z \end{pmatrix}, \quad (5.5.1)$$

where P_1 is the probability that $4m + 1$ electrons occupy the SWNT. Inserting (5.5.1) into the generalized master equation (3.3.22) and using (5.4.5) and (5.4.6) for the transition amplitudes, we obtain the subsequent equations of motion for P_1 and \vec{S} :

$$\begin{aligned} \dot{P}_1 &= \frac{\pi}{\hbar} \sum_l \phi_l^{(+)} \times \\ &\left[4f_l(\varepsilon_{lN})P_0 - (1 - f_l(\varepsilon_{lN}))P_1 - 2\mathcal{P}_l(1 - f_l(\varepsilon_{lN}))(\vec{S} \cdot \vec{m}_l) \right], \quad N = 4m \end{aligned} \quad (5.5.2)$$

$$\begin{aligned} \dot{\vec{S}} &= \frac{\pi}{\hbar} \sum_l \phi_l^{(+)} \left[\mathcal{P}_l \left(2f_l(\varepsilon_{lN})P_0 - \frac{1}{2}(1 - f_l(\varepsilon_{lN}))P_1 \right) \vec{m}_l \right. \\ &\quad \left. - (1 - f_l(\varepsilon_{lN}))\vec{S} + \mathcal{P}_l \Pi_l(\varepsilon_{lN}, \varepsilon_{lN+1})(\vec{S} \times \vec{m}_l) \right], \quad N = 4m. \end{aligned} \quad (5.5.3)$$

As in Chapter 4 we abbreviate

$$\varepsilon_{lN} = eV_l - \Delta E_N$$

and

$$\Delta E_N = E_N^0 - E_{N+1}^0.$$

The magnetization of the leads enter via the polarization magnitude $\mathcal{P}_l = \mathcal{P}_{lz}$, cf. equation (5.3.11), and via the magnetization directions \vec{m}_l . We have assumed that $\Phi_l(\varepsilon)$ is independent of ε in the relevant energy range. The function $\Pi_l(\varepsilon_{lN}, \varepsilon_{lN+1})$ includes the imaginary contributions to the rates stemming from the virtual transitions and the reflection Hamiltonian H_R . In detail it is given by

$$\Pi_l(\varepsilon_{lN}, \varepsilon_{lN+1}) = \mathcal{P}\mathcal{V} \int d\varepsilon \frac{1}{\pi} \left(\frac{1 - f_l(\varepsilon)}{\varepsilon - \varepsilon_{lN}} + \frac{f_l(\varepsilon)}{\varepsilon - \varepsilon_{lN+1}} \right) + \frac{\Delta_{Rl}}{\pi \mathcal{P}_l \phi_l^{(+)}}. \quad (5.5.4)$$

For the calculation of the principal part integration we use the approximation that for a Lorentzian $L(\varepsilon) = E_w^2 / (\varepsilon^2 + E_w^2)$ it holds the relation

$$\mathcal{P}\mathcal{V} \int d\varepsilon \frac{L(\varepsilon) f(\pm \varepsilon)}{\varepsilon - E} \approx \ln \frac{E_w}{\max(k_B T, |E|)},$$

which we apply to (5.5.4) in the limit of $E_w \rightarrow \infty$ and obtain

$$\Pi_l(\varepsilon_{lN}, \varepsilon_{lN+1}) = \ln \frac{\max(k_B T, |\varepsilon_{lN+1}|)}{\max(k_B T, |\varepsilon_{lN}|)} + \frac{\Delta_{Rl}}{\pi \mathcal{P}_l \phi_l^{(+)}}.$$

Note that the time evolutions of P_0 and P_1 are not independent. It holds $\dot{P}_0 + \dot{P}_1 = 0$, since in the considered low energy regime no other charge states than $N = 4m, 4m+1$ are allowed. In order to solve for the five unknowns of (5.5.3) we can additionally exploit that $P_0 + P_1 = 1$.

The big advantage of representing the master equation in the form (5.5.3) is that we can assign to each of the appearing terms a concrete physical meaning and therefore can get a deeper insight into the effects in spin dependent transport. Let us start with the first equation in (5.5.3). The first two terms describe the evolution of P_1 for an unpolarized quantum dot as in Section 4.4: The probability of finding $4m+1$ electrons in the SWNT increases when an electron tunnels into the dot containing $4m$ electrons and decreases when an electron leaves the SWNT. But since we deal with polarized leads a correction to the first two summands is necessary, the third term. It accounts for the fact that an electron can tunnel out most easily at a certain lead if the polarization of the dot and of the lead are aligned. The second equation describes the time evolution of the spin on the dot. Due to the polarization of the electrons in the lead, spin in the direction of \vec{m}_l is built up when electrons are tunneling in from lead l (the first term on the rhs). On the other hand electrons with spin in the direction of \vec{m}_l tunnel out of the dot with a higher probability, leading to an accumulation towards $-\vec{m}_l$ (the second term). Once spin has accumulated it relaxes, since an electron leaving the SWNT takes with it some of the spin (the third term). Of special interest is the fourth term which includes all the imaginary contributions to the rates. It leads to a precession of the spin around

$$\vec{B}_{eff}(\varepsilon_{lN}, \varepsilon_{lN+1}) := \sum_l \phi_l^{(+)} \mathcal{P}_l \Pi_l(\varepsilon_{lN}, \varepsilon_{lN+1}) \vec{m}_l.$$

Hence the virtual transitions as well as the spin sensitive boundary reflections act like an effective magnetic field $\sim \vec{B}_{eff}$. Since $\Pi_l(\varepsilon_{lN}, \varepsilon_{lN+1})$ depends on the energy also the strength of the spin precession is energy dependent. To anticipate it, the precession leads to a reduction of the TMR effect: Electrons that tunnel in at the one lead (let us say at the source) with a certain polarization have a lower rate for tunneling out again at the other lead (drain), if the leads have non-parallel magnetizations and hence the current across the dot is reduced. However, if there is a precession of the dot polarization, there will in general be certain points in time when the dot polarization is better aligned with the drain magnetization and electrons can more easily tunnel out again, the TMR effect will decrease. Except for a factor of 2 due to the pseudo spin degeneracy and the inclusion of the boundary reflections the same equations as in (5.5.3) have also been derived for a spin valve with a single spin degenerate energy level in [52].

Solving (5.5.3) in the stationary case $\dot{P}_1 = 0$, $\dot{\vec{S}} = 0$, and inserting the solution into (3.4.3) we are able to give an analytical expression for the current if we assume a symmetric coupling of the SWNT to both leads, i.e.,

$$\phi_s^{(+)} = \phi_d^{(+)} =: \phi^{(+)}, \mathcal{P}_s = \mathcal{P}_d =: \mathcal{P}, \Delta_{Rs} = \Delta_{Rd} =: \Delta_R, \quad (5.5.5)$$

such that source and drain only differ in their magnetization directions by the angle θ . From (5.5.5) follows that $\Pi_s = \Pi_d =: \Pi$. It holds for $N = 4m$,

$$I_{N,N+1}(\theta) = \left(1 - \frac{\mathcal{P}^2 \sin^2(\theta/2)}{1 + B_{eff}^2(-\Delta E_N, -\Delta E_{N+1}) / [2\phi^{(+)} f(\Delta E_N)]^2 \cdot \cos^2(\theta/2)} \right) I_{N,N+1}(0). \quad (5.5.6)$$

The current for unpolarized leads, $I_{N,N+1}(0)$, we have already determined and can be easily deduced from equation (4.4.11),

$$I_{N,N+1}(0) = \frac{2\gamma^{(+)}}{3f(-\Delta E_N) + 1} \frac{e^{-\beta\Delta E_N}}{(e^{-\beta\Delta E_N} + 1)^2} e^2 \beta V_b, \quad N = 4m,$$

where $\gamma^{(+)} = \frac{\pi}{2L\hbar} \phi^{(+)}$. With (5.5.6) we can now examine the TMR effect for arbitrary angles θ . Generalizing (5.0.1), we define

$$TMR(\theta) = \frac{I(0) - I(\theta)}{I(0)}.$$

In Fig. 5.5.1 we show for $N = 4m$ and $N = 4m + 3$ the linear conductance $G_{N,N+1}(\theta) = I_{N,N+1}(\theta)/V_b$ together with the corresponding TMR as a function of ΔE . The comparison between the left and the right figure demonstrates the mirror symmetry of the conductances $G_{4m,4m+1}$ and $G_{4m+3,4(m+1)}$ with respect to the electrochemical potential in the dot. Note that the maxima of the the conductances move towards the degeneracy point $\Delta E_N = 0$ for non-collinear leads. In the case of $\theta = 0, \pi$ the maxima lie at $\Delta E_{\max,N} = \mp \frac{1}{\beta} \ln 2$ for $N = 4m, 4m + 3$ as is easily deduced from equation (4.4.12). This shift of the conductance peaks is closely related to the dependence of the TMR on the gate voltage. Let us regard the case $N = 4m$. From Fig.

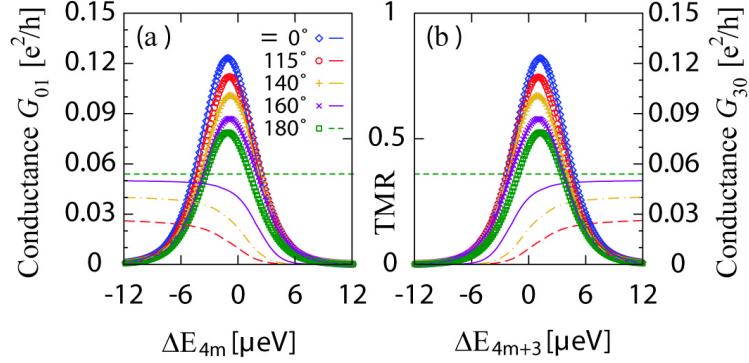


FIGURE 5.5.1. Conductance $G_{4m,4m+1}$ and $G_{4m+3,4(m+1)}$ with the corresponding TMR in the linear regime as a function of the gate voltage and for different polarization angles θ . The values of the current obtained by numerical solution of the master equation are indicated by symbols. No deviations from the analytical expression can be found. The TMR is constant for $\theta = 180^\circ$ but varies monotonously with the gate voltage for non-collinear lead magnetizations. As parameters we have used $\gamma = 6.9 \cdot 10^7 \text{ s}^{-1}$, $k_B T = 1.7 \mu\text{eV}$, $\mathcal{P} = 0.6$, $E_c = 9.5 \text{ meV}$, $\varepsilon_0 = 2.9 \text{ meV}$ and $\Delta_R = 0.1 \Pi_0$, where $\Pi_0 = \ln \frac{\max(k_B T, |\Delta E_{N+1}|)}{\max(k_B T, |\Delta E_N|)}$.

5.5.1 (a) we find that above the resonance the TMR becomes ineffective for $\theta \neq \pi$, while it is a constant for $\theta = \pi$. We can deduce this behaviour easily from (5.5.6). As we increase the electrochemical potential in the dot, the Fermi function in (5.5.6) decays from 1 to 0. Consequently the angle dependent term in (5.5.6) vanishes and for $\theta \neq \pi$ we obtain $I(0) = I(\theta)$ for large enough μ_g . From a physical point of view we can explain the situation with help of the spin precessions. Below the resonance condition the energy of the $N = 4m + 1$ ground state is enhanced compared to the unpolarized one of $N = 4m$. Therefore if occasionally an electron tunnels into the dot it can leave again after a short time. The spin precession due to the imaginary part of the rates can not become active. But if the electrochemical potential is increased and the dot prefers to accommodate $4m + 1$ electrons since the tunneling out events become more seldom, the spin precession becomes more efficient and reduces the TMR as we have already explained above.

The effect of the spin precession depends via the parameter Δ_R on the reflection Hamiltonian H_R . So far we can not provide a proper estimate for the value of Δ_R . For this reason we show in Fig. 5.5.2 the ratio of $I(\theta)/I(0)$ as a function of θ for different values of Δ_R . As we can expect from our previous discussion, the TMR is the more reduced by the spin precession the larger Δ_R is. In the limit $\Delta_R \rightarrow \infty$ a TMR effect is only visible in the AP configuration, i.e., for $\theta = \pi$.

Until now we have discussed the case of leads with equal tunneling transparencies γ_l . If $\gamma_s = \alpha \gamma_d$, $\alpha \neq 1$, we are not able to give simple analytical expressions for the transport properties in the case of arbitrary angles θ . The P and AP current we can still

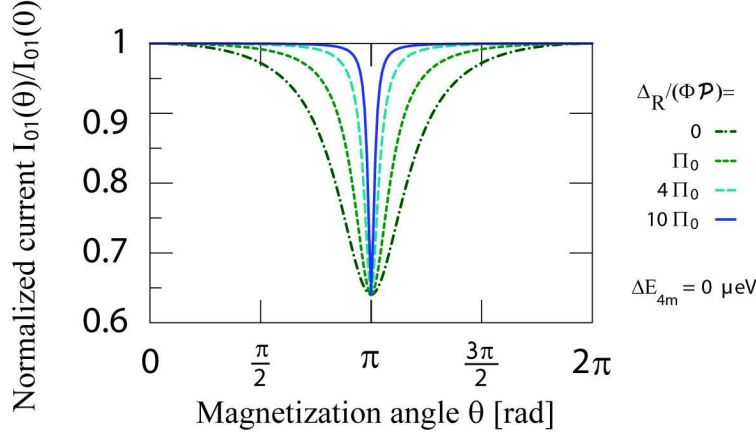


FIGURE 5.5.2. Normalized angle dependent current $I_{4m,4m+1}(\theta)/I_{4m,4m+1}(0)$ for different values of Δ_R at the resonance $\Delta E_{4m} = 0$. All other parameters as in Fig. 5.5.1. With increasing strength of the boundary contribution Δ_R , the TMR effect becomes less effective for $\theta \neq \pi$.

write down,

$$I_{4m,4m+1}(\alpha, \theta = 0) = \frac{2\alpha}{1+\alpha} I_{4m,4m+1}(1, 0) \quad (5.5.7)$$

$$I_{4m,4m+1}(\alpha, \theta = \pi) = \frac{2\alpha(1+\alpha)(1-\mathcal{P}^2)I_{4m,4m+1}(1, 0)}{[(1-\mathcal{P}) + \alpha(1+\mathcal{P})][(1+\mathcal{P}) + \alpha(1-\mathcal{P})]}, \quad (5.5.8)$$

where we have continued to assume $\mathcal{P} = \mathcal{P}_s = \mathcal{P}_d$. In order to calculate the current for $\theta \neq 0, \pi$ we have to solve the master equation numerically. The corresponding results for $I_{4m,4m+1}(0.3, \theta)/I_{4m,4m+1}(0.3, 0)$ at two different values for ΔE and for strongly varying values of Δ_R are shown in Fig. 5.5.3 (a). Unlike in the symmetric case we find that Δ_R has little effect on the TMR, although we have varied Δ_R by a factor of 10^4 . In Fig. 5.5.3 (b) the conductance and the TMR are depicted as functions of ΔE . Striking is that only little variation of the TMR with the gate voltage is found even for non-collinear lead polarizations. Furthermore we can not find any parameter set that exhibits negative TMR, i.e., $I_{4m,4m+1}(\alpha, \theta) > I_{4m,4m+1}(\alpha, 0)$, $\theta \neq 0$.

5.5.2. Near the degeneracy point of $E_{N=4m+1}^0$ and $E_{N=4m+2}^0$. The discussion in this section is also valid for the $N = 4m + 2 \leftrightarrow N = 4m + 3$ resonance, which is mirror symmetric to the case considered here.

Due to the increasing number of degenerate ground states that are involved in transport near the resonance of the $N = 4m + 1$ and $N = 4m + 2$ ground states energies an analytical treatment in this regime is only possible for the P and AP configuration. The ratio $I_{4m+1,4m+2}(\alpha, \pi)/I_{4m+1,4m+2}(\alpha, 0)$ is identical to the result obtained with (5.5.7) and (5.5.8). $I_{4m+1,4m+2}(\alpha, 0)$ can be deduced from (4.4.11). We thus can conclude that in the linear regime the TMR for collinearly magnetized leads does not depend on the gate voltage.

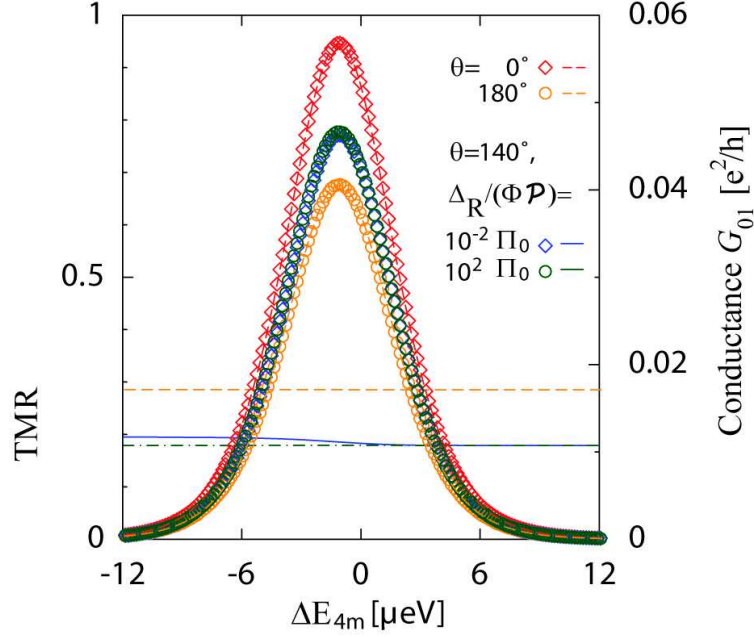


FIGURE 5.5.3. Linear conductance $G_{4m,4m+1}$ with the corresponding TMR for asymmetric lead couplings $\gamma_s = 0.3\gamma$, $\gamma_d = \gamma$. Neither a variation of ΔE_{4m} nor of Δ_R lead to a significant change of the TMR at fixed θ . All parameters apart from Δ_R as in Fig. 5.5.1.

The transport properties for arbitrary angles θ have to be treated numerically. Interestingly we find a non-monotonous dependence of the TMR on ΔE for $\theta \neq 0, \pi$, with a peak in the vicinity of the resonance, cf. Fig. 5.5.4. Additionally, on both sides of the resonance the TMR is not going down to 0. Since in both charge states with $4m + 1$ and $4m + 2$ electrons a finite spin can accumulate which is prone to spin precession, the TMR is reduced at both sides of the resonance. Concerning the positions of the conductance peaks in Fig. 5.5.4 we find as in the case of the $4m \leftrightarrow 4m + 1$ a shift towards the resonance point for non-collinear magnetizations.

5.6. Nonlinear regime

In the nonlinear regime excited states of the SWNT become occupied. An analytical treatment is as in the unpolarized case not possible any more. We even have to restrict our discussion to bias voltages that are at most comparable to the excitation energy of the lowest neutral excitations, ε_0 , since at higher energies we are restricted due to the strongly enhanced consumption of computing time and memory. As in the linear transport regime we present data for the $4m \leftrightarrow 4m + 1$ and $4m + 1 \leftrightarrow 4m + 2$ resonances. For a symmetric setup the other resonances are again mirror symmetric to the cases discussed here.

5.6.1. In the vicinity of the $4m \leftrightarrow 4m + 1$ resonance. In the non-collinear case, here for $\theta = 140^\circ$, we find a very similar behaviour of the TMR as in the linear regime.

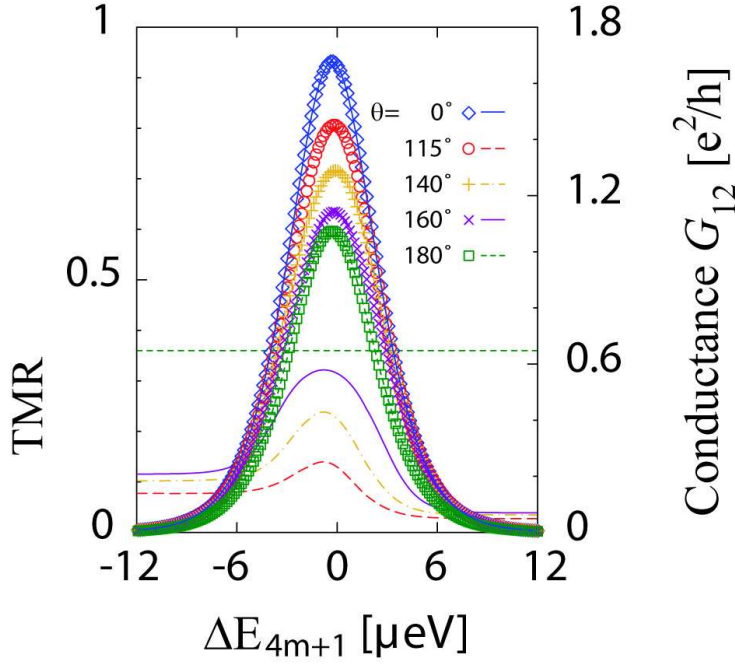


FIGURE 5.5.4. Linear conductance $G_{4m+1,4m+2}$ and the corresponding TMR. For collinear leads the TMR evolves non-monotonically with the electrochemical potential in the dot. All parameters as in Fig. 5.5.1.

The TMR changes from a constant value to 0 when ΔE exceeds a certain value, cf. Fig. 5.6.1. The transition line where the switching occurs, coincides with the boundary of the Coulomb diamond that corresponds to the charge state $N = 4m + 1$. As we have already explained only if $4m + 1$ electrons occupy the SWNT a spin can accumulate on the dot. If the lifetime of the $4m + 1$ state is large enough the dot polarization will start to precess and the TMR is reduced. A qualitative difference compared to the linear regime is found for the AP configuration. We find that the value of the TMR in the region well outside of the Coulomb diamonds differs from its constant value in the linear regime (which is also found inside of the Coulomb diamonds) and thus is not constant as a function of the electrochemical potential and of the bias voltage any more.

In order to explore the higher bias region, we fix the gate voltage such that $\Delta E_N = 0$ and increase the bias voltage from 0 up to a value above $2\varepsilon_0$, such that we can resolve the onset of transitions to the excited states, the step in the current data at 6 meV in Fig. 5.6.2. At around 8 meV a second step appears which is due to tunneling from highly excited states to the ground states with $N = 4m - 1$ and $N = 4m + 2$ electrons, cf. also Chapter 4. Interesting is the appearance of NDC for non-collinear leads appearing below the first excitation step. It results from the energy dependence of the virtual transitions. Increasing the bias voltage the magnitude of the principal part integrals

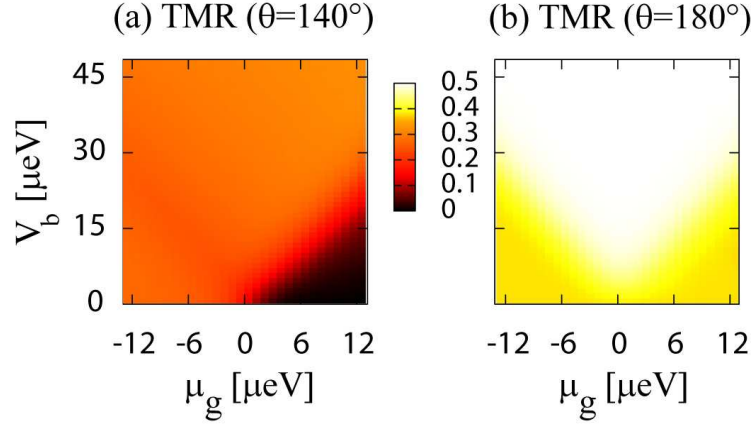


FIGURE 5.6.1. TMR for non-collinear (a) and collinear (b) lead magnetizations around the $4m \leftrightarrow 4m + 1$ resonance in the nonlinear regime. All parameters as in Fig. 5.5.1.

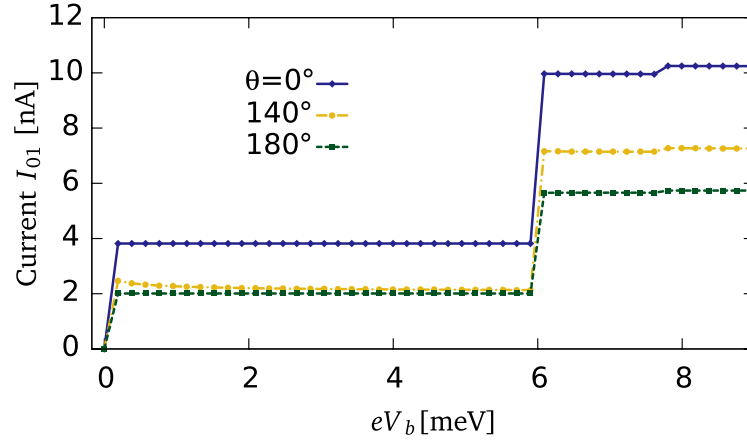


FIGURE 5.6.2. Current $I_{4m,4m+1}$ in the non-linear regime. For the non-collinear magnetization configuration NDC occurs. Here we have used $\gamma = 2.7 \cdot 10^{10} s^{-1}$. All other parameters as in Fig. 5.5.1.

and hence of the virtual transitions is decreased. Therefore the famous reduction of the TMR due to the spin precession becomes less pronounced with increasing V_b . The NDC features are especially pronounced for high polarizations. Then the current for non-collinear leads almost reaches the same value as the current in the P configuration before it decreases with increasing bias voltage.

5.6.2. Near the $4m + 1 \leftrightarrow 4m + 2$ resonance. The TMR near the $4m + 1 \leftrightarrow 4m + 2$ resonance in the nonlinear regime is shown in Fig. 5.6.3. In the non-collinear configuration of the lead polarizations ($\theta = 140^\circ$), there is again no qualitative difference to the behaviour in the linear regime. To the left and to the right of the resonance,

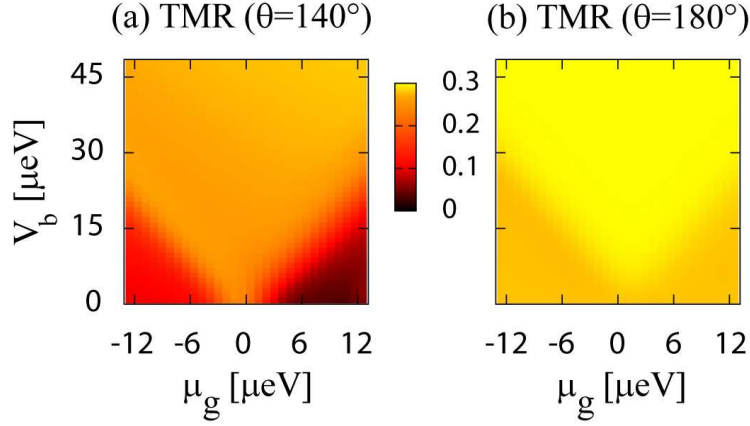


FIGURE 5.6.3. TMR for non-collinear (a) and collinear (b) lead magnetizations in the nonlinear regime around the $4m + 1 \leftrightarrow 4m + 2$ resonance. All parameters as in Fig. 5.5.1.

i.e., in the Coulomb blockade region, the TMR is constant at two different values. Well outside of the Coulomb diamonds the TMR peaks from the linear regime evolve into a plateau of constant TMR. As for the $4m \leftrightarrow 4m + 1$ resonance, in the region that is separated by the Coulomb diamonds by at least $k_B T$ the TMR of collinearly polarized leads is increased compared to its constant value in the linear regime. But unlike in the $4m \leftrightarrow 4m + 1$ case the enhancement amounts only to about 10%. The current outside the blockade regime and below the first excitation step is increased compared to the $4m \leftrightarrow 4m + 1$ case by a factor of $3/2$ as we have already found for the unpolarized SWNT quantum dot, see equation (4.4.14). Again we find the occurrence of NDC due to the virtual transitions.

5.7. Conclusions

In this chapter we have generalized our transport theory for weakly coupled SWNT quantum dots with unpolarized leads to spin-valve transistors with ferromagnetic leads. The main extensions compared to the unpolarized case are the description of the polarized leads by the contact parameters $\tilde{\Phi}_l(\varepsilon)$, that can be derived from the form of the lead Hamiltonians and the geometry of the tunneling contacts, and the consideration of the reflection Hamiltonian H_R .

Linear regime: Analytical expressions for the current as a function of the angle θ between the lead polarizations and of the bias and gate voltage have been obtained in the linear regime for the P and AP configuration. It turned out that the ratio $I(\pi)/I(0)$ is constant as a function of the gate voltage also for asymmetric lead transparencies, equations (5.5.7) and (5.5.8). Furthermore for arbitrary angles near the $4m \leftrightarrow 4m + 1$ resonance the linear conductance was derived, equation (5.5.6). In this situation the SWNT spin-valve has essentially the same properties as a single energy level spin-valve discussed in [51, 52]. For a finite band mismatch $\varepsilon_\Delta \gg k_B T$ this result also holds near all other degeneracy points. Due to the enhanced degeneracy of the ground

states in the regime $4m + 1 \leftrightarrow 4m + 2$, $\varepsilon_\Delta \lesssim k_B T$ the transport properties are not accessible analytically any more and have to be determined by solving the equation of motion for the RDM numerically. Compared to the single-level spin-valve the behaviour of the TMR changes qualitatively. The evolution of the TMR with the gate voltage is non-monotonous. Starting from a constant value, the TMR increases at the resonance and decreases again to a finite value.

Nonlinear regime: Also in this case the transport properties are amenable to numerics only. In the nonlinear but still low bias regime and for non-collinear lead polarization, the behaviour of the TMR is similar to the one in the linear regime. However, for collinear magnetization the TMR ceases to be constant and is enhanced near the resonances. Varying the bias voltage at fixed electrochemical potential, NDC occurs.

Negative TMR as observed in [65] is absent in our calculations. The occurrence of a negative TMR can be explained [69] by assuming a Zeeman like energy splitting of the SWNT states, which can result from a nonperturbative treatment of H_R which becomes necessary if one goes beyond the weak coupling limit. Moreover asymmetric couplings of the leads to the nanotube are needed.

We also want to comment on the relevance of coherences for the spin-valve transition. In the case of non-collinear lead magnetization, the inclusion of coherences in the RDM describing the SWNT becomes mandatory even in the linear regime as the relevance of the spin precession due to the virtual transitions and the boundary reflection demonstrates. In order to confirm the significance of coherences experimentally one has to look for the various signatures of the spin precession on the transport properties of spin-valves with non-collinear leads. The most important signatures are summarized in the following:

1. Non-constant TMR as a function of the gate voltage in the linear regime, especially the monotonous decrease of the TMR with increasing gate voltage near the $4m \leftrightarrow 4m + 1$ resonance and the TMR peak at the $4m + 1 \leftrightarrow 4m + 2$ resonance.
2. Shift of the conductance peaks towards the resonance condition $\Delta E = 0$ for $\theta \neq 0, \pi$.
3. The occurrence of NDC in the nonlinear regime.

But note that we have also found a reduction of all those features for an asymmetric coupling of the leads to the SWNT.

Summary and outlook

With this thesis we have provided a thorough examination of the electronic and transport properties of interacting metallic SWNTs in the low energy regime, corresponding to excitation energies in the range of about 1eV around the charge neutrality point. We have been able to reveal the nature of the eigenstates and of the spectrum of metallic SWNTs away from half-filling. A theory for weakly coupled SWNT quantum dots and spin valves has been derived. Our guideline has been to base our examinations on a solid microscopic fundament, i.e., all of our calculations start from a basic microscopic model or theory. The validity of necessary approximations has been checked carefully for the relevant regimes.

The first part of the thesis has been dedicated to explore the electronic properties of interacting electrons in metallic SWNTs. In order to be well prepared for the discussion of interaction effects, in Chapter 1 a review on the noninteracting p_z electrons in SWNTs has been presented. Special emphasis has been put on the proper treatment of finite size effects by imposing open boundary conditions. The low energy eigenstates of the noninteracting system form the framework for the further discussion in Chapter 2 where the Coulomb interaction between the electrons is included. As detailed in the introduction to Chapter 2, interactions change qualitatively the properties of fermions in 1D compared to the noninteracting case. A successful description of interacting 1D systems is provided by the Luttinger liquid theory based on the bosonization formalism. Experimental works on the ground state properties of metallic SWNTs have found exchange effects which are not in accordance with the Luttinger liquid predictions. Our investigations aimed at identifying the microscopic origin of the deviations from Luttinger liquid theory in SWNTs. For this purpose we have derived the effectively 1D interaction on the basis of the noninteracting p_z electrons from Chapter 1. It has turned out that the total Hamiltonian contains apart from the standard Luttinger contribution additional short ranged interactions due to the substructure of the SWNT honeycomb lattice. Those short ranged terms lead to non-forward scattering processes of the pseudo spin degree of freedom and thus to the mixing of different fermionic configurations. Away from half-filling the eigenstates and the spectrum of metallic SWNTs have been calculated by expressing the total Hamiltonian in a truncated eigenbasis of the Luttinger Hamiltonian and by the subsequent diagonalization of the obtained matrix. Qualitative and quantitative agreement with the experimentally observed exchange effects has been established. Additionally, we have made further predictions concerning the effects of the short ranged interactions not observed in experiments so far. Of special relevance is our finding of a spin 1 triplet groundstate of the $4m + 2$ charge states in the case of a small band mismatch. It proves — for a realistic system — that the Lieb-Mattis theorem, forbidding groundstates with spin

larger than $1/2$ in 1D Hubbard models with next neighbour hopping, cannot be applied to 1D systems with an additional degree of freedom for which non-forward scattering is allowed. Concerning the excitation spectrum, we find a partial lifting of the huge degeneracies and a spoiling of the spin-charge separation. At half-filling our diagonalization procedure has failed to give exact results due to a very strong coupling of the eigenstates of the Luttinger Hamiltonian via short ranged umklapp interaction processes which are only of relevance near half-filling.

In the second part we have examined the transport properties of SWNT quantum dots and spin valves. An introduction to general aspects of quantum dot physics has been presented in Chapter 3. There we have also developed a transport theory for generic weakly coupled quantum dots by generalizing the Pauli master equation to systems with degenerate eigenstates. In order to ensure invariance of the results under unitary transformations in the Hilbert spaces of the degenerate states, our approach keeps explicitly coherences between degenerate states in the reduced density matrix of the dot.

The formalism from Chapter 3 has been applied to the case of weakly coupled SWNT quantum dots with unpolarized leads in Chapter 4. The discussion is restricted to devices with large enough SWNTs (like the SWNT in Sample C of reference [20] with a length of 800nm and a diameter of 2.7nm) where the exchange effects due to the short ranged interactions can be neglected. Both the linear and non-linear transport regime have been considered. We have found that due to the ground state degeneracies the linear conductance reveals a characteristic pattern of peaks recurring in groups of four along the gate voltage axis. Two different patterns can be observed depending on whether the band mismatch is smaller or larger than the thermal energy. At higher bias voltages excited states become populated. The corresponding energies are directly related to the position of lines in the bias - gate voltage plane where the current changes its value. We have shown that the inclusion of coherences between degenerate states is indeed necessary in the high bias regime, where considerable deviations between the conventional Pauli master equation and its generalized version are present. Furthermore we have found that the contact geometry and the electronic properties of the leads are closely related to a polarization with respect to the pseudo spin degree of freedom. In a preliminary examination we have demonstrated that pseudo spin polarized leads could be achieved by an asymmetric coupling to the two honeycomb sublattices.

SWNT spin valve transistors, quantum dots with spin polarized leads are the subject of Chapter 5. The transport properties of those devices have been determined by generalizing the approach for unpolarized current in Chapter 4, thereby incorporating the effect of spin dependent reflections of the electrons at the tube ends. Additionally to the parallel and antiparallel configurations of the lead magnetization we have examined the effect of non-collinear polarizations. We have been able to derive analytical expressions for the linear conductance in the case of the collinear configurations and for arbitrary magnetization directions in the vicinity of the $4m \leftrightarrow 4m + 1$ resonance under the condition of symmetric lead couplings. In all other situations we had to resort to a numerical solution of the generalized master equation. We have studied the tunneling magneto resistance as a function of the applied voltages and the angle

between the polarization directions of the lead electrodes. We have shown that in the case of non-collinear lead magnetizations a spin precession on the dot due to virtual transitions and the boundary reflections has considerable impact on the current across the SWNT spin valve. In general it leads to an energy dependent suppression of the tunneling magneto resistance. As a consequence we find a strong gate voltage dependence of the tunneling magneto resistance, even in the linear regime and negative differential conductance in the non-linear regime. In order to properly account for the spin precession it has again been mandatory to keep coherences between degenerate states.

In the course of this work we have given some answers but still open issues are left. Here are some of them:

- What are the electronic properties of metallic finite size SWNTs near half-filling? Does the Luttinger liquid picture completely break down? What is the nature of the ground states at half-filling, e.g. which spin do they have?
- To our opinion the relation between pseudo spin polarized current and the contact geometry deserves further investigation. How could one build a pseudo spin valve? What would be its properties?
- We have excluded the effect of the exchange interactions in our investigations on the transport properties. What can we expect when discussing the transport properties of small size SWNTs? Christoph Schenke tries to find it out.
- So far our approach is restricted to the weak coupling limit. How can we include higher order processes in our transport calculations? Sonja Koller is working on it.
- The exchange effects observed in metallic SWNTs are closely connected to the structure of the honeycomb lattice. Can we find similar phenomena in other small size graphene based objects like nano-ribbons or semiconducting SWNTs?

Acknowledgements

When I decided to write my diploma thesis on carbon nanotubes in Milena Grifoni's group, I did not know that I would enter a field captivating me for four years now. But I have not only chosen a fascinating subject for my work but also an excellent supervisor.

Milena, I have appreciated very much working with you in the last years. You could always give me a guideline when I was lost, you allowed me great latitude but nevertheless you pushed me when it was necessary. Thank you so much!

It is also a pleasure to acknowledge the collaboration with the "nanotube diploma students" Sonja Koller and Mattis Eroms who have done a great job and had considerable impact on my work.

Furthermore I want to thank Sami Sapmaz and Wouter Wetzels from Delft for many fruitful discussions. Together with Wouter I enjoyed many extended runnings in the surroundings of Regensburg during his stay in our group.

Andrea Donarini's provision of the Arnoldi algorithm was of great help for the numerical calculations in the thesis. Thank you.

The place where I have spend the most time during the last four years is probably my office. For this reason I am very happy that I have had such nice office mates. Francesco Nesi was (and is) a real friend and often our office had great resemblance to a debate club. When Silvia Garelli "substituted" Francesco this did neither affect the good atmosphere in our room nor did it reduce the production of entropy ;-)

Special thanks to Lizy Lazar whose kindness and expertise in administrative issues were always highly appreciated.

It was nice to see the group constantly growing and all of the members have contributed to the good spirit in our corridor. Since time is running and this thesis still has to be printed I cannot thank you individually at this place. Therefore a big common THANKS! to all of you.

I am deeply grateful to my parents, my brother and my sisters who are always there when they are needed.

Much was said about one-dimensional systems in this thesis but according to the Isar Indian "Sound of Thunder" (thanks to Georg Begemann for introducing me to the music of Willy Michl) it is the fifth dimension, namely the feeling, that counts. In this spirit: Babe, I love you!

Support of the research school GRK 638 "Nichtlinearität und Nichtgleichgewicht in kondensierter Materie" is acknowledged.

APPENDIX A

Derivation of the bosonization identity

Here we present how to derive the bosonization identity for the 1D operators $\psi_{rF\sigma}(x)$ given in equation (A.0.15). We start by examining the commutation relation between $\psi_{rF\sigma}(x)$ and $b_{r\sigma q}$. Using equations (1.4.26) and (2.4.4) we get

$$[b_{r\sigma q}, \psi_{rF\sigma}(x)] = \frac{1}{\sqrt{2L|n_q|}} \sum_{\kappa, \kappa'} e^{i\text{sgn}F\kappa'x} \underbrace{\left[c_{r\sigma\kappa}^\dagger c_{r\sigma\kappa+q}, c_{r\sigma\kappa'} \right]}_{=-\delta_{\kappa, \kappa'} c_{r\sigma\kappa+q}} = -\frac{e^{-i\text{sgn}Fqx}}{\sqrt{|n_q|}} \psi_{rF\sigma}(x), \quad (\text{A.0.1})$$

as can be easily concluded from the standard anticommutation relations for $c_{r\sigma\kappa}$ and $c_{r\sigma\kappa}^\dagger$. Similarly we find

$$[b_{\sigma q}^\dagger, \psi_{rF\sigma}(x)] = -\frac{e^{i\text{sgn}Fqx}}{\sqrt{|n_q|}} \psi_{rF\sigma}(x). \quad (\text{A.0.2})$$

For $r\sigma \neq r'\sigma'$ the commutators $[b_{r\sigma q}, \psi_{r'F\sigma'}(x)]$ and $[b_{r\sigma q}^\dagger, \psi_{r'F\sigma'}(x)]$ vanish. Relation (A.0.1) reminds strongly of the commutation relation of a bosonic annihilation operator with the creation operator of the corresponding bosonic coherent state, $[b, e^{i\alpha b^\dagger}] = [b, i\alpha b^\dagger] e^{i\alpha b^\dagger} = i\alpha e^{i\alpha b^\dagger}$. This motivates us to introduce the operators

$$e^{-i\phi_{rF\sigma}(x)} := e^{-\sum_{q>0} \frac{e^{i\text{sgn}(rF)qx}}{\sqrt{n_q}} b_{r\sigma q}}, \quad (\text{A.0.3})$$

as well as

$$e^{-i\phi_{rF\sigma}^\dagger(x)} = e^{\sum_{q>0} \frac{e^{-i\text{sgn}(rF)qx}}{\sqrt{n_q}} b_{r\sigma q}^\dagger}. \quad (\text{A.0.4})$$

Indeed, we find commutation relations, whose structure resembles very much (A.0.1):

$$[b_{r\sigma q}, e^{-i\phi_{r'F\sigma'}(x)} e^{-i\phi_{r'F\sigma'}^\dagger(x)}] = \frac{e^{-i\text{sgn}(rF)qx}}{\sqrt{n_q}} e^{-i\phi_{r'F\sigma'}(x)} e^{-i\phi_{r'F\sigma'}^\dagger(x)}. \quad (\text{A.0.5})$$

In order to derive (A.0.5) we have used $[b_{r\sigma q}, e^{-i\phi_{rF\sigma}(x)}] = 0$ — since $[b_{r\sigma q}, b_{r'\sigma'q'}] = 0$ — and

$$[b_{r\sigma q}, e^{-i\phi_{rF\sigma}^\dagger(x)}] = [b_{r\sigma q}, -i\phi_{rF\sigma}^\dagger(x)] e^{-i\phi_{rF\sigma}^\dagger(x)} = \frac{1}{\sqrt{n_q}} e^{-i\text{sgn}(rF)qx} e^{-i\phi_{rF\sigma}^\dagger(x)},$$

what can easily be shown by expanding $e^{-i\phi_{rF\sigma}^\dagger(x)}$ in its power series. But what is the exact relation between $e^{-i\phi_{rF\sigma}(x)} e^{-i\phi_{rF\sigma}^\dagger(x)}$ and $\psi_{rF\sigma}(x)$? To answer this question we define the operator

$$O_{rF\sigma}(x) := \psi_{rF\sigma}(x) e^{-i\phi_{rF\sigma}(x)} e^{-i\phi_{rF\sigma}^\dagger(x)}, \quad (\text{A.0.6})$$

such that

$$\psi_{rF\sigma}(x) = O_{rF\sigma}(x) e^{i\phi_{rF\sigma}^\dagger(x)} e^{i\phi_{rF\sigma}(x)}. \quad (\text{A.0.7})$$

Let us now determine the properties of $O_{rF\sigma}(x)$. First of all $O_{rF\sigma}(x)$ commutes with all bosonic operators $b_{r'\sigma'q}$ and $b_{r'\sigma'q}^\dagger$. In the case of $r\sigma \neq r'\sigma'$ this is obvious and for $r\sigma = r'\sigma'$ it holds,

$$\begin{aligned} [b_{r\sigma q}, O_{rF\sigma}(x)] &= \\ \psi_{rF\sigma}(x) e^{-i\phi_{rF\sigma}(x)} e^{-i\phi_{rF\sigma}^\dagger(x)} &\left(\frac{e^{-i\text{sgn}(rF)qx}}{\sqrt{|n_q|}} - \frac{e^{-i\text{sgn}(rF)qx}}{\sqrt{|n_q|}} \right) = 0, \end{aligned}$$

$$\text{and similarly } [b_{r\sigma q}^\dagger, O_{rF\sigma}(x)] = 0.$$

Since the bosonic operator $e^{i\phi_{rF\sigma}^\dagger(x)} e^{i\phi_{rF\sigma}(x)}$ doesn't change the number of electrons, cf. (2.4.7), but $\psi_{rF\sigma}(x)$ does decrease $N_{r\sigma}$ by one, $O_{rF\sigma}(x)$ must have the same feature. Moreover since $O_{rF\sigma}(x)$ commutes with all bosonic operators $O_{rF\sigma}(x)$ doesn't create or annihilate any bosonic excitation. Therefore if we apply $O_{rF\sigma}(x)$ on a state $|\vec{N}, \vec{m}\rangle$ it will leave \vec{m} unchanged and only act on \vec{N} . In general we thus can write

$$O_{rF\sigma}(x) |\vec{N}, \vec{m}\rangle = \lambda_{rF\sigma\vec{N}}(x) |\vec{N} - \vec{e}_{r\sigma}, \vec{m}\rangle \quad (\text{A.0.8})$$

As first mentioned in [29] this implies that $O_{rF\sigma}(x)$ can be written explicitly as

$$O_{rF\sigma}(x) = \sum_{\vec{N}} \sum_{\vec{m}} |\vec{N} - \vec{e}_{r\sigma}, \vec{m}\rangle \langle \vec{N}, \vec{m} | \lambda_{rF\sigma\vec{N}}(x).$$

By defining the unitary operator

$$U_{r\sigma} := \sum_{\vec{N}} \sum_{\vec{m}} |\vec{N} - \vec{e}_{r\sigma}, \vec{m}\rangle \langle \vec{N}, \vec{m} |,$$

$O_{rF\sigma}(x)$ becomes

$$O_{rF\sigma}(x) = U_{r\sigma} \lambda_{rF\sigma\vec{N}}(x). \quad (\text{A.0.9})$$

The operator $\lambda_{rF\sigma\vec{N}}(x)$ can be easily determined by evaluating

$$\langle \vec{N}, 0 | U_{r\sigma}^\dagger \psi_{rF\sigma}(x) | \vec{N}, 0 \rangle, \quad (\text{A.0.10})$$

using one time the fermionic (1.4.26) and the other time the bosonic (A.0.7) representation of $\psi_{rF\sigma}(x)$. If we insert the bosonic form of $\psi_{rF\sigma}(x)$ into (A.0.10) and bear in mind equation (A.0.9), we get

$$\begin{aligned} \langle \vec{N}, 0 | U_{r\sigma}^\dagger \psi_{rF\sigma}(x) | \vec{N}, 0 \rangle &= \langle \vec{N}, 0 | \underbrace{U_{r\sigma}^\dagger U_{r\sigma}}_{=1} \lambda_{rF\sigma\vec{N}}(x) e^{i\phi_{rF\sigma}^\dagger(x)} e^{i\phi_{rF\sigma}(x)} | \vec{N}, 0 \rangle = \\ &= \langle \vec{N}, 0 | \lambda_{rF\sigma\vec{N}}(x) | \vec{N}, 0 \rangle = \lambda_{rF\sigma\vec{N}}(x), \end{aligned}$$

Here we have used $e^{i\phi_{rF\sigma}(x)} |\vec{N}, 0\rangle = |\vec{N}, 0\rangle$ and $[\lambda_{rF\sigma\vec{N}}(x), e^{i\phi_{rF\sigma}^\dagger(x)}] = 0$ following from $[b_{r\sigma q}, \vec{N}] = 0$. If $\psi_{rF\sigma}(x)$ is expressed in terms of the fermionic operators

$c_{r\sigma q}$, we realize, since

$$\langle \vec{N}, 0 | U_{r\sigma}^\dagger = \langle \vec{N} - \vec{e}_{r\sigma}, 0 |,$$

that only the one term with $\kappa = \kappa_{N_{r\sigma}}$ in the series (1.4.26) contributes to (A.0.10), if $\kappa_{N_{r\sigma}}$ is the wave number of the highest occupied single electron state of the $r\sigma$ band in $|\vec{N}, 0\rangle$. Comparing the results of the two different ways of calculating the matrix elements $\langle \vec{N}, 0 | U_{r\sigma}^\dagger \psi_{rF\sigma}(x) | \vec{N}, 0 \rangle$ leads to

$$\lambda_{rF\sigma\vec{N}}(x) = \frac{1}{\sqrt{2L}} e^{i \text{sgn}(F) \kappa_{N_{r\sigma}} x} \underbrace{\langle \vec{N}_{r\sigma} - \vec{e}_{r\sigma}, 0 | c_{r\sigma \kappa_{N_{r\sigma}}} | \vec{N}, 0 \rangle}_{=: T_{r\sigma\vec{N}}}.$$

Thus our calculation yields

$$\lambda_{rF\sigma\vec{N}}(x) = \frac{1}{\sqrt{2L}} e^{i \text{sgn}(F) \kappa_{N_{r\sigma}} x} T_{r\sigma\vec{N}}, \quad (\text{A.0.11})$$

where $T_{r\sigma\vec{N}}$ is either 1 or -1 and determines the correct sign if $c_{r\sigma \kappa_{N_{r\sigma}}}$ is applied on $|\vec{N}, 0\rangle$:

$$c_{r\sigma \kappa_{N_{r\sigma}}} |\vec{N}, 0\rangle = T_{r\sigma\vec{N}} |\vec{N} - \vec{e}_{r\sigma}, 0\rangle,$$

Ordering the states $|\varphi_{r\kappa}\rangle |\sigma\rangle$ according to $+\uparrow, +\downarrow, -\uparrow, -\downarrow$ we explicitly get

$$T_{r\sigma\vec{N}} = \prod_{j=1}^{r\sigma-1} (-1)^{N_j}, \quad r\sigma = +\uparrow, +\downarrow, -\uparrow, -\downarrow = 1, 2, 3, 4.$$

The value of $\kappa_{N_{r\sigma}}$ is given by

$$\kappa_{N_{r\sigma}} = \frac{\pi}{L} (r \cdot N_{r\sigma} + \Delta).$$

Combining (A.0.9) and (A.0.11) the operators $O_{rF\sigma}(x)$ reads

$$O_{rF\sigma} = \frac{1}{\sqrt{2L}} U_{r\sigma} T_{r\sigma\vec{N}} e^{i \frac{\pi}{L} \text{sgn} F (r \cdot \mathcal{N}_{r\sigma} + \Delta) x}. \quad (\text{A.0.12})$$

Here we introduce the phase factor

$$K_{rF\sigma}(x) := \frac{1}{\sqrt{2L}} e^{i \frac{\pi}{L} \text{sgn} F (r \cdot \mathcal{N}_{r\sigma} + \Delta) x} \quad (\text{A.0.13})$$

and define the so called Klein factors $\eta_{r\sigma}$ by

$$\eta_{r\sigma} := U_{r\sigma} T_{r\sigma\vec{N}}. \quad (\text{A.0.14})$$

From the definitions of the Klein factors it easy to demonstrate that relations (2.4.12) to (2.4.14) are valid. After we have found the explicit form of $O_{rF\sigma}$, equation (A.0.12), we can, by inserting (A.0.12) into (A.0.7), finally give the bosonization identity for the 1D electron operator:

$$\psi_{rF\sigma}(x) = \eta_{r\sigma} K_{rF\mathcal{N}_{r\sigma}}(x) e^{i \phi_{rF\sigma}^\dagger(x)} e^{i \phi_{rF\sigma}(x)}. \quad (\text{A.0.15})$$

APPENDIX B

Bosonized form of the kinetic part of the Hamiltonian

Here we give the proof of the statement, that

$$H_{0,\text{boson}} = H_0,$$

i.e., the kinetic part of the armchair Hamiltonian can either be written in terms of the fermionic creation and annihilation operators $c_{r\sigma\kappa}^\dagger$ and $c_{r\sigma\kappa}$,

$$H_0 = \varepsilon_0 \sum_{r\sigma} r \sum_{n_\kappa=-\infty}^{\infty} n_\kappa : c_{r\sigma\kappa}^\dagger c_{r\sigma\kappa} : + \varepsilon_0 \Delta \sum_{r\sigma} r : \mathcal{N}_{r\sigma} :, \quad (\text{B.0.16})$$

or equivalently in terms of the bosonic operators $b_{r\sigma q}^\dagger$ and $b_{r\sigma q}$:

$$H_{0,\text{boson}} = \varepsilon_0 \sum_{r\sigma} \left(\sum_{q>0}^{\infty} |n_q| b_{rq\sigma}^\dagger b_{rq\sigma} + \frac{\mathcal{N}_{r\sigma}^2}{2} + \Delta r \mathcal{N}_{r\sigma} \right). \quad (\text{B.0.17})$$

Proof of $H_{0,\text{boson}} = H_0$: In our case the Fock space is a direct sum of Hilbert spaces $\mathcal{H}_{\vec{N}}$ with a fixed fermionic configuration $\vec{N} = (N_{+\uparrow}, N_{+\downarrow}, N_{-\uparrow}, N_{-\downarrow})$,

$$\mathcal{F} = \sum_{\oplus \vec{N}} \mathcal{H}_{\vec{N}}.$$

A basis of each $\mathcal{H}_{\vec{N}}$ is given by the states $|\vec{N}, \{n_{r\sigma\kappa}\}\rangle$ where $n_{r\sigma\kappa}$ denotes the occupation number of the single particle state $|\varphi_{r\sigma\kappa}\rangle$. The set $\{|\vec{N}, \{n_{r\sigma\kappa}\}\rangle\}$ consists of ground state $|\vec{N}, 0\rangle$ of the noninteracting system with fixed \vec{N} , plus all possible states that can be constructed from $|\vec{N}, 0\rangle$ by applying a sequence of particle-hole excitations. It is obvious that the states in this basis are the eigenstates of H_0 . Consequently, in order to prove that $H_{0,\text{boson}}$ is equivalent to H_0 , it suffices to show that $H_{0,\text{boson}}$ and H_0 give the same result if applied to any of the eigenstates of H_0 . Let us start to calculate the action of H_0 on an arbitrary ground state $|\vec{N}, 0\rangle$:

$$\begin{aligned} H_0 |\vec{N}, 0\rangle &= \varepsilon_0 \sum_{r\sigma} \left(\sum_{n_\kappa=-\infty}^{N_{r\sigma}} n_\kappa : c_{r\sigma\kappa}^\dagger c_{r\sigma\kappa} : + \Delta \sum_{r\sigma} r N_{r\sigma} \right) |\vec{N}, 0\rangle \\ &= \left(\varepsilon_0 \sum_{r\sigma} \left(\frac{N_{r\sigma}^2}{2} + \frac{N_{r\sigma}}{2} \right) + \varepsilon_0 \Delta \sum_{r\sigma} r N_{r\sigma} \right) |\vec{N}\rangle_0. \end{aligned} \quad (\text{B.0.18})$$

Comparing (B.0.16) and (B.0.18), it becomes clear that $H_0 \left| \vec{N}, 0 \right\rangle$ is equal to $H_{0,\text{boson}} \left| \vec{N}, 0 \right\rangle$, since

$$b_{r\sigma q} \left| \vec{N}, 0 \right\rangle = 0.$$

Now we turn to the excited eigenstates

$$\left\{ \prod_{r\sigma\kappa\kappa'} \left(c_{r\sigma\kappa}^\dagger c_{r\sigma\kappa'} \right)^{g_{\kappa\kappa'}} \left| \vec{N}, 0 \right\rangle \right\}$$

of $H_{0,\text{TL}}$. We examine in a preliminary step the meaning of the operator $\sum_{r\sigma q > 0} n_q b_{r\sigma q}^\dagger b_{r\sigma q}$. We can write this expression, using (2.4.4) and (2.4.5), in terms of the operators $c_{r\sigma\kappa}$ and $c_{r\sigma\kappa}^\dagger$,

$$\sum_{r\sigma q > 0} n_q b_{r\sigma q}^\dagger b_{r\sigma q} = \sum_{r\sigma} \sum_{q > 0} \sum_{\kappa, \kappa'} c_{r\sigma\kappa+q}^\dagger c_{r\sigma\kappa} c_{r\sigma\kappa'}^\dagger c_{r\sigma\kappa'+q_r}. \quad (\text{B.0.19})$$

It is amazing that most of the terms in (B.0.19) cancel with each other, i.e.,

$$\sum_{q > 0} \sum_{\kappa, \kappa'} c_{r\sigma\kappa+q}^\dagger c_{r\sigma\kappa} c_{r\sigma\kappa'}^\dagger c_{r\sigma\kappa'+q} = \sum_{q > 0} \sum_{\kappa} c_{r\sigma\kappa+q}^\dagger c_{r\sigma\kappa} c_{r\sigma\kappa}^\dagger c_{r\sigma\kappa+q_r}, \quad (\text{B.0.20})$$

as we are going to demonstrate immediately. With (B.0.20) we obtain

$$\sum_{r\sigma q > 0} n_q b_{r\sigma q}^\dagger b_{r\sigma q} = \sum_{r\sigma} \sum_{q > 0} \sum_{\kappa} c_{r\sigma\kappa+q}^\dagger c_{r\sigma\kappa} c_{r\sigma\kappa}^\dagger c_{r\sigma\kappa+q_r}. \quad (\text{B.0.21})$$

In order to verify relation (B.0.20) we focus without loss of generality on the right mover terms and omit the $r\sigma$ -indices. Let us consider the operator

$$C_{\kappa_1 \kappa'_1 q_1} := c_{\kappa_1+q_1}^\dagger c_{\kappa_1} c_{\kappa'_1}^\dagger c_{\kappa'_1+q_1} \text{ for } \kappa_1 > \kappa'_1 \text{ and } q_1 > 0.$$

Then there is exactly one triple $(\kappa_2, \kappa'_2, q_2)$ with $\kappa_2 > \kappa'_2$, $q_2 > 0$ that fulfills

$$C_{\kappa_2 \kappa'_2 q_2} = c_{\kappa_2+q_2}^\dagger c_{\kappa_2} c_{\kappa'_2}^\dagger c_{\kappa'_2+q_2} = c_{\kappa_1+q_1}^\dagger c_{\kappa_1} c_{\kappa'_1+q_1}^\dagger c_{\kappa'_1} = -C_{\kappa_1 \kappa'_1 q_1}.$$

This mapping, that we are going to call M , from $(\kappa_1, \kappa'_1, q_1)$ to $(\kappa_2, \kappa'_2, q_2)$ is given by

$$M : (\kappa_1, \kappa'_1, q_1) \rightarrow (\kappa'_1 + q_1, \kappa_1 - \kappa'_1) = (\kappa_2, \kappa'_2, q_2).$$

As is easily shown,

$$M(M(\kappa_1, \kappa'_1, q_1)) = (\kappa_1, \kappa'_1, q_1)$$

holds. Consequently we can decompose

$$\sum_{q > 0} \sum_{\kappa > \kappa'} c_{\kappa+q}^\dagger c_{\kappa} c_{\kappa'}^\dagger c_{\kappa'+q}$$

into pairs of operators that cancel each other. In an analogous manner it is shown that

$$\sum_{q > 0} \sum_{\kappa < \kappa'} c_{\kappa+q}^\dagger c_{\kappa} c_{\kappa'}^\dagger c_{\kappa'+q} = 0.$$

Thus we have proven the relation

$$\sum_{q > 0} \sum_{\kappa, \kappa'} c_{\kappa+q}^\dagger c_{\kappa} c_{\kappa'}^\dagger c_{\kappa'+q} = \sum_{q > 0} \sum_{\kappa} c_{\kappa+q}^\dagger c_{\kappa} c_{\kappa}^\dagger c_{\kappa+q}$$

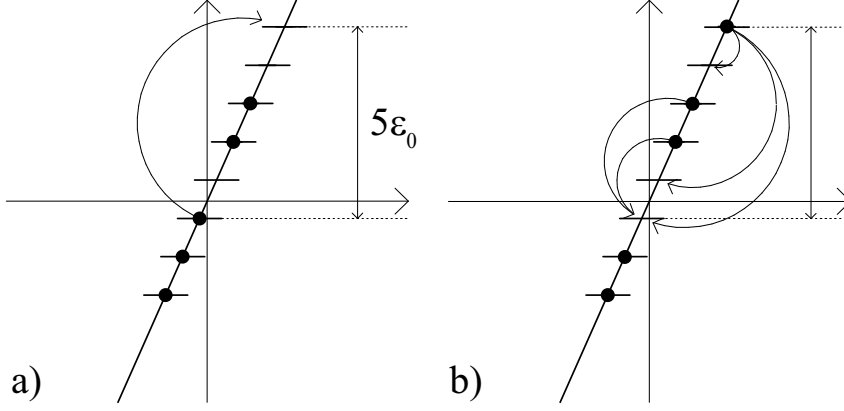


FIGURE B.0.1. Relation between elementary particle-hole excitations and subsequent relaxations. An elementary particle-hole excitation in a), that rises the energy by an integer multiple m of the level spacing (here $m = 5$), increases also the number of additionally possible elementary relaxations by m , as can be seen in b).

and hence (B.0.20).

By means of equation (B.0.21) we can now reveal the meaning of $\sum_{q>0} n_q b_{r\sigma q}^\dagger b_{r\sigma q}$:

We note, all states $|\vec{N}, \{n_{r\sigma\kappa}\}\rangle$ are eigenstates of the operator $c_{r\sigma\kappa+q_r}^\dagger c_{r\sigma\kappa} c_{r\sigma\kappa}^\dagger c_{r\sigma\kappa+q_r}$. The corresponding eigenvalues are given by 1, if an elementary particle-hole relaxation from state $|\varphi_{r\sigma\kappa+q_r}\rangle$ to $|\varphi_{r\sigma\kappa}\rangle$ is possible, i.e., $n_{r\sigma\kappa+q_r} = 1$ and $n_{r\sigma\kappa} = 0$ or by 0 if the relaxation from $|\varphi_{r\sigma\kappa+q_r}\rangle$ to $|\varphi_{r\sigma\kappa}\rangle$ is forbidden due to the Pauli principle, i.e., if $n_{r\sigma\kappa+q_r} = 0$ or $n_{r\sigma\kappa} = 1$. Hence, $\sum_{r\sigma q>0} n_q b_{r\sigma q}^\dagger b_{r\sigma q}$ counts the number of possible elementary relaxations in the eigenstates of $H_{0,TL}$:

$$\sum_{r\sigma q>0} n_q b_{r\sigma q}^\dagger b_{r\sigma q} |\vec{N}, \{n_{r\sigma\kappa}\}\rangle = m_{\{n_{r\sigma\kappa}\}} \cdot |\vec{N}, \{n_{r\sigma\kappa}\}\rangle, \quad (\text{B.0.22})$$

where $m_{\{n_{r\sigma\kappa}\}}$ is the total number of allowed elementary relaxations for the state $|\vec{N}, \{n_{r\sigma\kappa}\}\rangle$.

On the other hand, any elementary particle-hole excitation performed upon an arbitrary state $|\vec{N}, \{n_{r\sigma\kappa}\}\rangle$, that rises the energy by $m \cdot \varepsilon_0$ also rises the number of possible elementary particle-hole relaxations by m (see Fig. B.0.1). Since every state $|\vec{N}, \{n_{r\sigma\kappa}\}\rangle$ can be built up by a chain of particle-hole excitations starting from $|\vec{N}, 0\rangle$, we can conclude that the excitation energy (the difference in the eigenenergies corresponding to $|\vec{N}, \{n_{r\sigma\kappa}\}\rangle$ and $|\vec{N}, 0\rangle$) of $|\vec{N}, \{n_{r\sigma\kappa}\}\rangle$ equals $m_{\{n_{r\sigma\kappa}\}} \cdot \varepsilon_0$.

Thus we can conclude

$$\begin{aligned} H_0 \left| \vec{N}, \{n_{r\sigma\kappa}\} \right\rangle &= \\ &= \varepsilon_0 \left(m_{\{n_{r\sigma\kappa}\}} + \sum_{r\sigma} \left(\frac{N_{r\sigma}^2}{2} + \frac{N_{r\sigma}}{2} \right) + \Delta \sum_{r\sigma} r N_{r\sigma} \right) \left| \vec{N}, \{n_{r\sigma\kappa}\} \right\rangle \quad (\text{B.0.23}) \end{aligned}$$

Comparing (B.0.22) and (B.0.23) yields

$$H_0 = \varepsilon_0 \left(\sum_{r\sigma q > 0}^{\infty} n_q b_{r\sigma q}^\dagger b_{r\sigma q} + \sum_{r\sigma} \left(\frac{\mathcal{N}_{r\sigma}^2}{2} + \frac{\mathcal{N}_{r\sigma}}{2} \right) + \Delta \sum_{r\sigma} r \mathcal{N}_{r\sigma} \right),$$

thus proving that H_0 and $H_{0,\text{boson}}$ are indeed equivalent.

◇

B.1. Completeness of States in Bosonic Representation

Now it is easy to prove the astonishing and important fact that a basis of each Hilbert space $\mathcal{H}_{\vec{N}}$ can be constructed by bosonic excitations instead of fermionic ones, which is, as pointed out in [35], “the deep reason” why the bosonization of 1D fermionic systems is possible. We have shown that the states $|\vec{N}, \{n_{r\sigma\kappa}\}\rangle$ are eigenstates of $H_{0,\text{boson}}$. But since $H_{0,\text{boson}}$ is diagonal in the bosonic operators $b_{r\sigma q}^\dagger$ and $b_{r\sigma q}$ also the states

$$\left\{ \prod_{r\sigma q > 0} \frac{(b_{r\sigma q}^\dagger)^{m_{r\sigma q}}}{\sqrt{m_{r\sigma q}!}} \left| \vec{N}, 0 \right\rangle \right\} = \left\{ \left| \vec{N}, \vec{m} \right\rangle \right\} \quad (\text{B.1.1})$$

form a complete set of eigenstates to $H_{0,\text{boson}}$. Hence, each of the states $|\vec{N}, \{n_{r\sigma\kappa}\}\rangle$ can be written as an appropriate linear combination of the states $|\vec{N}, \vec{m}\rangle$. But then, since the $|\vec{N}, \{n_{r\sigma\kappa}\}\rangle$ form a basis of $\mathcal{H}_{\vec{N}}$, the same must be true for the bosonic excitations $|\vec{N}, \vec{m}\rangle$.

APPENDIX C

Bogoliubov transformation

In this appendix we show how to bosonize a Hamiltonian that is quadratic in operators b_q and b_q^\dagger , fulfilling the canonical bosonic commutation relations, by the method of Bogoliubov [73]. At the end we apply the method to the Hamiltonians $H_{j\delta}$ from (2.5.10), describing the bosonic excitations in $H_0 + V_{\rho\rho}$.

Let us in general consider a Hamiltonian of the form

$$H = \frac{1}{2} \sum_{q>0} X_q (b_q + b_q^\dagger)^2 - \frac{1}{2} \sum_{q>0} (X_q - A_q) (b_q b_q + h.c.) + \text{const.} \quad (\text{C.0.2})$$

The commutation relations between the Hamiltonian and the bosonic operators follow immediately:

$$\begin{aligned} [H, b_q^\dagger] &= [X_q (b_q + b_q^\dagger) - Y_q b_q] = A_q b_q + X_q b_q^\dagger, \\ [H, b_q] &= -[X_q (b_q + b_q^\dagger) - Y_q b_q^\dagger] = -X_q b_q - A_q b_q^\dagger. \end{aligned}$$

To diagonalize (C.0.2), we introduce a transformation from the operators b_q and b_q^\dagger to new bosonic creation and annihilation operators a_q^\dagger and a_q , such that the Hamiltonian becomes diagonal in terms of the new operators,

$$H = \sum_{q>0} \varepsilon_q a_q^\dagger a_q.$$

Constant terms in H are neglected since they merely shift the energy scale. We use the following ansatz for the transformation

$$a_q^\dagger = B_q b_q^\dagger - D_q b_q, \quad (\text{C.0.3})$$

$$a_q = B_q b_q - D_q b_q^\dagger. \quad (\text{C.0.4})$$

In order to determine the real Bogoliubov coefficients B_q and D_q , we require that a_q^\dagger and a_q fulfill the canonical commutation relations,

$$[a_q, a_q^\dagger] = 1 \quad (\text{C.0.5})$$

and diagonalize H ,

$$[H, a_q^\dagger] = \varepsilon_q a_q^\dagger \Leftrightarrow [H, a_q] = -\varepsilon_q a_q. \quad (\text{C.0.6})$$

The elementary bosonic excitation energies ε_q still have to be determined. By inserting the ansatz for the Bogoliubov transformation (C.0.3 and C.0.4) into (C.0.5), the following condition arises,

$$U_q^2 - V_q^2 = 1. \quad (\text{C.0.7})$$

and from C.0.6 we get

$$[H, a_q] = -\varepsilon_{j\delta q} a_{j\delta q} \Leftrightarrow (B_q X_q + D_q A_q) b_q + (B_q A_q + D_q X_q) b_{j\delta q}^\dagger = \varepsilon_q (B_q b_q - D_q b_q^\dagger).$$

This leads to the conditions

$$B_q X_q + D_q A_q = \varepsilon_q B_q \quad (\text{C.0.8})$$

$$B_q A_q + D_q X_q = -\varepsilon_q D_q. \quad (\text{C.0.9})$$

The energies ε_q are determined by requiring that both conditions are fulfilled at the same time. Addition (C.0.8) from (C.0.9) yields

$$(B_q + D_q)(A_q + X_q) = \varepsilon_q (B_q - D_q). \quad (\text{C.0.10})$$

By subtracting (C.0.9) from (C.0.8) we get

$$\begin{aligned} (B_q - D_q)(X_q - A_q) &= \varepsilon_q (B_q + D_q) \\ \Rightarrow (B_q - D_q) &= \varepsilon_q (B_q + D_q)(X_q - A_q)^{-1} \end{aligned} \quad (\text{C.0.11})$$

Inserting (C.0.11) into (C.0.10) gives

$$(B_q + D_q)(A_q + X_q) = \varepsilon_q^2 (B_q + D_q)(X_q - A_q)^{-1}, \quad (\text{C.0.12})$$

yielding

$$\varepsilon_q^2 = X_q^2 - A_q^2 \Rightarrow \varepsilon_q = \sqrt{X_q^2 - A_q^2}. \quad (\text{C.0.13})$$

The additional constraint (C.0.7) finally leads to

$$B_q = \frac{\varepsilon_q + X_q}{\sqrt{(\varepsilon_q + X_q)^2 - A_q^2}}, \quad D_q = -\frac{A_q}{\sqrt{(\varepsilon_q + X_q)^2 - A_q^2}}. \quad (\text{C.0.14})$$

Let us now apply this procedure to the different modes $j\delta = c+, c-, s+, s-$ of the Hamiltonian $H_0 + V_{\rho\rho}$. Using

$$2b_{j\delta q}^\dagger b_{j\delta q} = (b_{j\delta q} + b_{j\delta q}^\dagger)^2 - b_{j\delta q} b_{j\delta q} - b_{j\delta q}^\dagger b_{j\delta q}^\dagger + \text{const.}$$

we can rewrite (2.5.10) as

$$\begin{aligned} H_{j\delta} &= \frac{1}{2} \sum_{q>0} n_q X_{j\delta q} (b_{j\delta q} + b_{j\delta q}^\dagger)^2 \\ &\quad - \frac{1}{2} \sum_{q>0} n_q (X_{j\delta q} - A_{j\delta q}) (b_q b_q + h.c.) + \text{const.}, \end{aligned} \quad (\text{C.0.15})$$

with

$$\begin{aligned} X_{j\delta q} &= n_q (4\delta_{j\delta, c+} W_q - u_b^\Delta + \varepsilon_0) \\ A_{j\delta q} &= n_q (4\delta_{j\delta, c+} W_q - u^+ - \delta u_f^\Delta). \end{aligned}$$

Concerning the dispersion relations of the bosonic operators in the different modes, we obtain from (C.0.13)

$$\varepsilon_{j\delta q} = n_q \sqrt{(4\delta_{j\delta, c+} W_q - u_b^\Delta + \varepsilon_0)^2 - (4\delta_{j\delta, c+} W_q - u^+ - \delta u_f^\Delta)^2}.$$

Exploiting that for metallic SWNTs $\varepsilon_0, W_q \gg u^+, u_{S_f}^\Delta$ holds, we can simplify the dispersion relations further,

$$\varepsilon_{j\delta q} \approx \begin{cases} \varepsilon_0 n_q \sqrt{1 + \frac{8W_q}{\varepsilon_0}}, & j\delta = c+ \\ n_q (\varepsilon_0 - u_b^\Delta), & j\delta = c-, s+, s- . \end{cases}$$

Hence only the energies of the channels $c-$ and $s-$ remain to be degenerate. Rather than of a spin-charge separation one could speak of a separation of total and relative (with respect to the pseudo spin degree of freedom) collective excitations instead.

To a good approximation the Bogoliubov coefficients U_q and V_q do not depend on the coupling constants of the non-forward scattering terms. From (C.0.14) it can easily be deduced that

$$\begin{aligned} B_{j\delta q} &\approx \begin{cases} \frac{1}{2} \left(\sqrt{\frac{\varepsilon_{0q}}{\varepsilon_{cq}}} + \sqrt{\frac{\varepsilon_{cq}}{\varepsilon_{0q}}} \right), & j\delta = c+ \\ 1, & \text{else} \end{cases} \\ D_{j\delta q} &\approx \begin{cases} \frac{1}{2} \left(\sqrt{\frac{\varepsilon_{0q}}{\varepsilon_{cq}}} - \sqrt{\frac{\varepsilon_{cq}}{\varepsilon_{0q}}} \right), & j\delta = c+ \\ 0, & \text{else} \end{cases} . \end{aligned} \quad (\text{C.0.16})$$

For completeness we also give the reversed Bogoliubov transformation, i.e., the dependence of the operators b_q on a_q and a_q^\dagger . As can be easily derived from (C.0.3), (C.0.4) and (C.0.7), it holds

$$b_q = B_q a_q + D_q a_q^\dagger . \quad (\text{C.0.17})$$

APPENDIX D

Modeling the interaction potential

In this Appendix we show how we determine the values of the effective 1D potentials $U_{[F]}^{intra/inter}$ and of the coupling constants $u_{S_r S_F}$. We start with equation (2.2.6) from section 2.2,

$$U_{[F]}^{intra/inter}(x, x') = L^2 \int \int d^2 r_{\perp} d^2 r'_{\perp} \times \varphi_{pF_1}^*(\vec{r}) \varphi_{\pm pF_2}^*(\vec{r}') \varphi_{\pm pF_3}(\vec{r}) \varphi_{pF_4}(\vec{r}') U(\vec{r} - \vec{r}'). \quad (\text{D.0.18})$$

Using equation (1.4.12) in order to reexpress the Bloch waves $\varphi_{pF}(\vec{r})$ in terms of p_z orbitals, we obtain,

$$U_{[F]}^{intra/inter}(x, x') = \frac{L^2}{N_L^2} \int \int d^2 r_{\perp} d^2 r'_{\perp} \times U(\vec{r} - \vec{r}') \sum_{\vec{R}, \vec{R}'} e^{-i(F_1 - F_4)R_x - i(F_2 - F_3)R'_x} \times \left| \chi(\vec{r} - \vec{R} - \vec{\tau}_p) \right|^2 \left| \chi(\vec{r}' - \vec{R}' - \vec{\tau}_{\pm p}) \right|^2. \quad (\text{D.0.19})$$

Instead of a fourfold sum over the lattice sites \vec{R} only the double sum $\sum_{\vec{R}, \vec{R}'}$ remains, since the overlap of different p_z orbitals can be neglected. To proceed we use once more that the spatial extension of the p_z orbitals is small compared to all other appearing length scales and therefore replace $|\chi(\vec{r} - \vec{R} - \vec{\tau}_p)|^2$ by the delta function $\delta(\vec{r} - \vec{R} - \vec{\tau}_p)$. In order to take into account the error induced thereby at small distances $x \approx x'$, we replace the Coulomb potential by the Ohno potential introduced by equation (2.2.2). It interpolates between U_0 , the interaction energy between two p_z electrons in the same orbital, and $\frac{e^2}{4\pi\epsilon_0\epsilon|\vec{r} - \vec{r}'|}$ for $|\vec{r} - \vec{r}'| \gg 0$. Performing the integration in (D.0.19), we obtain,

$$U_{[F]}^{intra/inter}(x, x') = \frac{L^2}{N_L^2} \sum_{\vec{R}, \vec{R}'} \delta(x - R_x) \delta(x' - R'_x) \times e^{-i(F_1 - F_4)R_x - i(F_2 - F_3)R'_x} U(\vec{R} - \vec{R}' + \vec{\tau}_p - \vec{\tau}_{\pm p}). \quad (\text{D.0.20})$$

Now we can easily calculate the values of the coupling constants $u_{S_r S_F}$ for the local interactions, given by (2.3.8),

$$u_{S_r S_F} = 1/(2L^2) \int \int dx dx' U_{[r]_{S_r} [F]_{S_F}}(x, x').$$

Using (D.0.20) together with equation (2.2.5),

$$U_{[r][F]}(x, x') = \frac{1}{4} \left[U_{[F]}^{intra}(x, x')(1 + r_1 r_2 r_3 r_4) + U_{[F]}^{inter}(x, x')(r_2 r_3 + r_1 r_4) \right], \quad (\text{D.0.21})$$

we arrive at

$$u_{fb} =: u^+ = \frac{1}{4N_L^2} \sum_{\vec{R}, \vec{R}'} e^{-i2K_0(R_x - R'_x)} \times \left[U(\vec{R} - \vec{R}') + U(\vec{R} - \vec{R}' + \vec{\tau}_p - \vec{\tau}_{-p}) \right], \quad (\text{D.0.22})$$

$$u_{b/uf} =: u_f^\Delta = \frac{1}{4N_L^2} \sum_{\vec{R}, \vec{R}'} \left[U(\vec{R} - \vec{R}') - U(\vec{R} - \vec{R}' + \vec{\tau}_p - \vec{\tau}_{-p}) \right] \quad (\text{D.0.23})$$

and

$$u_{b/ub} =: u_b^\Delta = \frac{1}{4N_L^2} \sum_{\vec{R}, \vec{R}'} e^{-i2K_0(R_x - R'_x)} \times \left[U(\vec{R} - \vec{R}') - U(\vec{R} - \vec{R}' + \vec{\tau}_p - \vec{\tau}_{-p}) \right]. \quad (\text{D.0.24})$$

Since in the summations in (D.0.22), (D.0.23) and (D.0.24) only terms with $\vec{R} \approx \vec{R}'$ contribute, the number of relevant summands scales like the number of lattice sites N_L . Due to the prefactor $1/N_L^2$, u^+ and $u_{f/b}^\Delta$ in total scale like $1/N_L$. Numerical evaluation of the previous three equations leads to the values given in table 1.

APPENDIX E

Calculation of the matrix elements $M_{[r][F][\sigma]}(\vec{N}, \vec{m}, \vec{N}', \vec{m}', x)$

Using the bosonization identity (A.0.15),

$$\psi_{r\sigma F}(x) = \eta_{r\sigma} K_{rF\sigma}(x) e^{i\phi_{r\sigma F}^\dagger(x)} e^{i\phi_{r\sigma F}(x)},$$

we can separate $M_{[r][F][\sigma]}(\vec{N}, \vec{m}, \vec{N}', \vec{m}', x)$ from equation (2.5.19) into a bosonic and a fermionic part,

$$M_{[r][F][\sigma]}(\vec{N}, \vec{m}, \vec{N}', \vec{m}', x) = M_{[r][F][\sigma]}(\vec{N}, \vec{N}', x) M_{[r][F][\sigma]}(\vec{m}, \vec{m}', x),$$

where

$$M_{[l]}(\vec{N}, \vec{N}', x) = \left\langle \vec{N} \left| K_{l_1}^\dagger(x) \eta_{l_1}^\dagger K_{l_2}^\dagger(x) \eta_{l_2}^\dagger K_{l_3}(x) \eta_{l_3} K_{l_4}(x) \eta_{l_4} \right| \vec{N}' \right\rangle.$$

and

$$M_{[l]}(\vec{m}, \vec{m}', x) = \langle \vec{m} | e^{-i\phi_{l_1}^\dagger(x)} e^{-i\phi_{l_1}(x)} e^{-i\phi_{l_2}^\dagger(x)} e^{-i\phi_{l_2}(x)} e^{i\phi_{l_3}^\dagger(x)} e^{i\phi_{l_3}(x)} e^{i\phi_{l_4}^\dagger(x)} e^{i\phi_{l_4}(x)} | \vec{m}' \rangle. \quad (\text{E.0.25})$$

Improving readability, we have summarized the indices $rF\sigma$ by a single index l .

E.1. The Fermionic part of $M_{[r][F][\sigma]}(\vec{N}, \vec{m}, \vec{N}', \vec{m}', x)$

First we consider the contribution $M_{[l]}(\vec{N}, \vec{N}', x)$ depending on the fermionic configurations \vec{N} and \vec{N}' . Using relation (2.4.11) for the Klein factors $\eta_{r\sigma}$ and the definition of the phase factor $K_{r\sigma F}(x)$, equation (A.0.13), we obtain

$$M_{[r][F][\sigma]}(\vec{N}, \vec{N}', x) = \frac{1}{(2L)^2} \delta_{\vec{N}, \vec{N}' + \vec{E}_{[r][\sigma]}} T_{\vec{N} \vec{N}'[r][\sigma]} Q_{\vec{N} \vec{N}'[r][F]}(x),$$

where $\vec{E}_{[r][\sigma]} := \vec{e}_{r_1\sigma} + \vec{e}_{r_2\sigma'} - \vec{e}_{r_3\sigma'} - \vec{e}_{r_4\sigma}$. Furthermore $T_{\vec{N} \vec{N}'[r][\sigma]}$ is given by

$$T_{\vec{N} \vec{N}'[r][\sigma]} = (-1)^{\sum_{j_4=1}^{(r_4\sigma_4)-1} (\vec{N}')_{j_4} + \sum_{j_3=1}^{(r_3\sigma_3)-1} (\vec{N}' - \vec{e}_{r_4\sigma_4})_{j_3}} \times (-1)^{\sum_{j_2=1}^{(r_2\sigma_2)-1} (\vec{N} - \vec{e}_{r_1\sigma_1})_{j_2} + \sum_{j_1=1}^{(r_1\sigma_1)-1} (\vec{N})_{j_1}}. \quad (\text{E.1.1})$$

Here we use the convention $j = + \uparrow, + \downarrow, - \uparrow, - \downarrow = 1, 2, 3, 4$. It turns out that $T_{\vec{N} \vec{N}'[r][\sigma]}$ only depends on the scattering types S_r and S_σ . Explicitly with $T_{\vec{N}' S_r S_\sigma} := T_{\vec{N} \vec{N}'[r] S_r[\sigma] S_\sigma}$,

$$T_{\vec{N}' u f -} = -(-1)^{3N'_{R\uparrow} + 2N'_{R\downarrow} + N'_{L\uparrow}}, \quad (\text{E.1.2})$$

$$T_{\vec{N}' b f -} = (-1)^{3N'_{R\uparrow} + 2N'_{R\downarrow} + N'_{L\uparrow}} \quad (\text{E.1.3})$$

and $T_{\vec{N}' S_r S_\sigma} = 1$ for all other (S_r, S_σ) . The function $Q_{\vec{N} \vec{N}' [r][F]}(x)$ yields a phase and is given by

$$Q_{\vec{N} \vec{N}' [r][F]}(x) = \exp \left\{ i \frac{\pi}{L} \left[\text{sgn}(r_4 F_4)(\vec{N}')_{l_4} + \text{sgn}(r_3 F_3)(\vec{N}' - \hat{e}_{l_4})_{l_3} - \text{sgn}(r_2 F_2)(\vec{N} - \hat{e}_{l_1})_{l_2} - \text{sgn}(r_1 F_1)(\vec{N})_{l_1} \right] \right\}. \quad (\text{E.1.4})$$

E.2. The bosonic part of $M_{[r][F][\sigma]}(\vec{N}, \vec{m}, \vec{N}', \vec{m}', x)$

The calculation of the bosonic part $M_{[r][F][\sigma]}(\vec{m}, \vec{m}', x)$ is based on expressing the fields $i\phi_{r\sigma F}(x)$ in equation (E.0.25) in terms of the bosonic operators $a_{j\delta q}$, $a_{j\delta q}^\dagger$ and subsequent normal ordering, i.e., commuting all annihilation operators $a_{j\delta q}$ to the right side and all creation operators $a_{j\delta q}^\dagger$ to the left side. In a first step we use the relation

$$e^{i\phi_l(x)} e^{i\phi_l^\dagger(x)} = e^{i\phi_l^\dagger(x)} e^{i\phi_l(x)} e^{[i\phi_l(x), i\phi_l^\dagger(x)]},$$

following from the Baker-Hausdorff formula,

$$e^A e^B = e^{A+B} e^{\frac{1}{2}[A, B]}, \quad [A, B] \in \mathbb{C},$$

to obtain from (E.0.25),

$$M_{[l]}(\vec{m}, \vec{m}', x) = C_{[l]}(x) \left\langle \vec{m} \left| e^{-i\tilde{\sum}_{n=1}^4 \phi_{l_n}^\dagger(x)} e^{-i\tilde{\sum}_{n=1}^4 \phi_{l_n}(x)} \right| \vec{m}' \right\rangle, \quad (\text{E.2.1})$$

where $\tilde{\sum}_{l=1}^4 \phi_{l_n}$ denotes the sum $\phi_{l_1} + \phi_{l_2} - \phi_{l_3} - \phi_{l_4}$ and

$$C_{[l]}(x) = e^{[i\phi_{l_3}(x), i\phi_{l_4}^\dagger(x)]} e^{[-i\phi_{l_2}(x), i\phi_{l_3}^\dagger(x) + i\phi_{l_4}^\dagger(x)]} \times e^{[-i\phi_{l_1}(x), -i\phi_{l_2}^\dagger(x) + i\phi_{l_3}^\dagger(x) + i\phi_{l_4}^\dagger(x)]}.$$

Applying the Baker-Hausdorff formula once more, we obtain

$$e^{-i\tilde{\sum}_{n=1}^4 \phi_{l_n}^\dagger(x)} e^{-i\tilde{\sum}_{n=1}^4 \phi_{l_n}(x)} = e^{-i\tilde{\sum}_{n=1}^4 (\phi_{l_n}(x) + \phi_{l_n}^\dagger(x))} e^{\frac{1}{2} [i\tilde{\sum}_{n=1}^4 \phi_{l_n}^\dagger(x), i\tilde{\sum}_{n'=1}^4 \phi_{l_{n'}}(x)]}. \quad (\text{E.2.2})$$

In order to go on we express the operators $i\phi_{rF\sigma}(x) + i\phi_{rF\sigma}^\dagger(x)$ in terms of the operators $a_{j\delta q}^\dagger$ and $a_{j\delta q}$ that diagonalize the Hamiltonian $H_0 + V_{\rho\rho}$. Using equation (2.4.16) we can write

$$i\phi_{rF\sigma}(x) + i\phi_{rF\sigma}^\dagger(x) = \sum_{q>0} \frac{1}{\sqrt{n_q}} \left(e^{i\text{sgn}(Fr)qx} b_{r\sigma q} - e^{-i\text{sgn}(Fr)qx} b_{r\sigma q}^\dagger \right).$$

The operators $b_{r\sigma q}$ and $b_{r\sigma q}^\dagger$ in turn are related to $a_{j\delta q}^\dagger$ and $a_{j\delta q}$ via equation (2.5.15), such that we obtain

$$i\phi_{rF\sigma}(x) + i\phi_{rF\sigma}^\dagger(x) = \sum_{j\delta} \Lambda_{r\sigma}^{j\delta} \sum_{q>0} \frac{1}{\sqrt{n_q}} \left[e^{i\text{sgn}(Fr)qx} \left(B_{j\delta q} a_{j\delta q} + D_{j\delta q} a_{j\delta q}^\dagger \right) - e^{-i\text{sgn}(Fr)qx} \left(B_{j\delta q} a_{j\delta q}^\dagger + D_{j\delta q} a_{j\delta q} \right) \right]$$

or

$$i\phi_{rF\sigma}(x) + i\phi_{rF\sigma}^\dagger(x) = \sum_{j\delta q>0} \left(\lambda_{rF\sigma}^{j\delta q} a_{j\delta q} - \left(\lambda_{rF\sigma}^{j\delta q} \right)^* a_{j\delta q}^\dagger \right), \quad (\text{E.2.3})$$

with

$$\lambda_{rF\sigma}^{j\delta q} = \frac{\Lambda_{r\sigma}^{j\delta}}{\sqrt{n_q}} \left(e^{i\text{sgn}(Fr)qx} B_{j\delta q} - e^{-i\text{sgn}(Fr)qx} D_{j\delta q} \right). \quad (\text{E.2.4})$$

By defining

$$\tilde{\lambda}_{[l]}^{j\delta q}(x) := -\sum_{n=1}^4 \lambda_{l_n}^{j\delta q}(x) \quad (\text{E.2.5})$$

and again using the Baker-Hausdorff formula, we arrive at the normal ordered expression

$$e^{-i\sum_{n=1}^4 (\phi_{l_n}(x) + \phi_{l_n}^\dagger(x))} = e^{-\sum_{j\delta q>0} \tilde{\lambda}_{[l]}^{*j\delta q}(x) a_{j\delta q}^\dagger e^{\sum_{j\delta q>0} \tilde{\lambda}_{[l]}^{j\delta q}(x) a_{j\delta q}} e^{-\frac{1}{2} \sum_{j\delta q>0} |\tilde{\lambda}_{[l]}^{j\delta q}(x)|^2}}.$$

Inserting the previous equation into (E.2.2) yields

$$\left\langle \vec{m} \left| e^{-i\sum_{n=1}^4 \phi_{l_n}^\dagger(x)} e^{-i\sum_{n=1}^4 \phi_{l_n}(x)} \right| \vec{m}' \right\rangle = A_{[l]}(x) \prod_{j\delta q} F(\tilde{\lambda}_{[l]}^{j\delta q}(x), m_{j\delta q}, m'_{j\delta q}), \quad (\text{E.2.6})$$

where we have introduced

$$A_{[l]}(x) := e^{\frac{1}{2} [i\sum_{n=1}^4 \phi_{l_n}^\dagger(x), i\sum_{n'=1}^4 \phi_{l_{n'}}(x)]} e^{-\frac{1}{2} \sum_{j\delta q>0} |\tilde{\lambda}_{[l]}^{j\delta q}(x)|^2} \quad (\text{E.2.7})$$

and

$$F(\lambda, m, m') := \left\langle m \left| e^{-\lambda^* a^\dagger} e^{\lambda a} \right| m' \right\rangle, \quad (\text{E.2.8})$$

where the states $|m\rangle$ are bosonic excitations created by the operators a^\dagger , i.e., $|m\rangle = (a^\dagger)^m / \sqrt{m!} |0\rangle$. An analytical expression for $F(\lambda, m, m')$ is derived at the end of this appendix.

Combining equations (E.2.1) and (E.2.6) we finally obtain

$$M_{[l]}(\vec{m}, \vec{m}', x) = C_{[l]}(x) A_{[l]}(x) \prod_{j\delta q} F(\tilde{\lambda}_{[l]}^{j\delta q}(x), m_{j\delta q}, m'_{j\delta q}).$$

Explicitly, equation (E.2.7) yields that $A_{[l]}(x)$ only depends on the scattering type for the product rF . For $S_{rF} \neq u$ we find $A_{[l]S_{rF}} =: A_{S_{rF}} \equiv 1$ whereas A_u is strongly enhanced leading to an increased importance of non-density-density interactions at

half-filling. Due to its relevance we show the detailed calculation of A_u in the following.

E.2.1. Evaluation of $A_u(x)$. Exemplarily we present the calculation of the function $A_{[r]_{S_r}[F]_{S_F}[\sigma]_{S_\sigma}}(x)$ for the scattering process $(S_r, S_F, S_\sigma) = (b, f^-, f^+)$, i.e., for

$$[r] = (r, -r, r, -r), [F] = (F, -F, -F, F) \text{ and } [\sigma] = (\sigma, \sigma, \sigma, \sigma).$$

It is easily checked that for this choice $S_{rF} = u$ holds. Before starting with the actual calculation we first determine the coefficients $\tilde{\lambda}_{[r][F][\sigma]}^{j\delta q}(x)$ for the considered case. With equations (E.2.4) and (E.2.5) we find

$$\begin{aligned} \tilde{\lambda}_{[r]_b[F]_{f^-}[\sigma]_{f^+}}^{j\delta q}(x) = \\ - \frac{1}{\sqrt{n_q}} \sum_{n=1}^4 \Lambda_{r_n \sigma_n}^{j\delta} \left(e^{i \operatorname{sgn}(r_n F_n) q x} B_{j\delta q} - e^{-i \operatorname{sgn}(r_n F_n) q x} D_{j\delta q} \right). \end{aligned}$$

The values for $B_{j\delta q}$, $D_{j\delta q}$ are known from the Bogoliubov transformation, cf. equation (C.0.16), and $\Lambda_{r\sigma}^{j\delta}$ is given by (2.5.8). For the different channels $j\delta$ this leads to

$$\begin{aligned} \tilde{\lambda}_{[r]_b[F]_{f^-}[\sigma]_{f^+}}^{c+q}(x) &= -\frac{2i \operatorname{sgn}(rF)}{\sqrt{n_q}} \sqrt{\frac{\varepsilon_{0q}}{\varepsilon_{c+q}}} \sin(qx), \\ \tilde{\lambda}_{[r]_b[F]_{f^-}[\sigma]_{f^+}}^{c-q}(x) &= 0, \\ \tilde{\lambda}_{[r]_b[F]_{f^-}[\sigma]_{f^+}}^{s+q}(x) &= -\frac{2i \operatorname{sgn}(rF\sigma)}{\sqrt{n_q}} \sin(qx), \\ \tilde{\lambda}_{[r]_b[F]_{f^-}[\sigma]_{f^+}}^{s-q}(x) &= 0. \end{aligned}$$

Using (E.2.7) we get in this case,

$$\begin{aligned} A_{[l]}(x) := e^{\frac{1}{2} [i\phi_{l_1}^\dagger(x) - i\phi_{l_3}^\dagger(x), i\phi_{l_1}(x) - i\phi_{l_3}(x)]} \\ e^{\frac{1}{2} [i\phi_{l_2}^\dagger(x) - i\phi_{l_4}^\dagger(x), i\phi_{l_2}(x) - i\phi_{l_4}(x)]} e^{-\frac{1}{2} \sum_{q>0} \left(|\tilde{\lambda}_{[l]}^{c+q}(x)|^2 + |\tilde{\lambda}_{[l]}^{s+q}(x)|^2 \right)}. \end{aligned} \quad (\text{E.2.9})$$

Improving readability we have again replaced the indices $rF\sigma$ by a single index l . With (2.4.16) we obtain

$$\begin{aligned} [i\phi_{rF\sigma}^\dagger(x), i\phi_{r\pm F\sigma}(x)] = \\ - \sum_{q>0} \frac{1}{n_q} e^{-i \operatorname{sgn}(rF) q(x \mp x)} [b_{\sigma r, q}^\dagger, b_{\sigma r, q}] = \sum_{q>0} \frac{1}{n_q} e^{-i \operatorname{sgn}(rF) q(x \mp x)}. \end{aligned}$$

In total this leads to

$$A_{[r]_b[F]_{f^-}[\sigma]_{f^+}}(x) := e^{2 \sum_{q>0} \frac{1}{n_q} (1 - \cos(2qx))} e^{-2 \sum_{q>0} \frac{1}{n_q} \left(\frac{\varepsilon_{0q}}{\varepsilon_{c+q}} + 1 \right) \sin^2(qx)}.$$

Because of $\sin^2(qx) = \frac{1}{2} (1 - \cos(2qx))$ the final result is

$$A_{[r]_b[F]_{f^-}[\sigma]_{f^+}}(x) := e^{2 \sum_{q>0} \frac{1}{n_q} \left(1 - \frac{\varepsilon_{0q}}{\varepsilon_{c+q}} \right) \sin^2(qx)}.$$

The same result is also obtained for all other processes with $S_{rF} = u$.

E.2.2. The function $F(\lambda, m, m')$. Expanding the exponentials $e^{\lambda a}$ in (E.2.8) all summands which are of higher order than m' vanish because of $a|0\rangle = 0$. Analogously, all terms in the expansion of $e^{-\lambda^* a^\dagger}$ of higher order than m do not contribute. Hence we get

$$\left\langle m \left| e^{-\lambda^* a^\dagger} e^{\lambda a} \right| m' \right\rangle = \left\langle m \left| \sum_{i=0}^m \frac{(-\lambda^* a^\dagger)^i}{i!} \sum_{j=0}^{m'} \frac{(\lambda a)^j}{j!} \right| m' \right\rangle. \quad (\text{E.2.10})$$

In (E.2.10) only terms with $m - i = m' - j$ survive. For $m' \geq m$ we conveniently express j in terms of i and find

$$F(\lambda, m, m') = \left\langle m \left| \sum_{i=0}^m \frac{(-\lambda^* a^\dagger)^i}{i!} \frac{(\lambda a)^{m'-m+i}}{(m'-m+i)!} \right| m' \right\rangle.$$

With $a^k |m\rangle = \sqrt{\frac{m!}{(m-k)!}} |m-k\rangle$ and $(a^\dagger)^k |m\rangle = \sqrt{\frac{(m+k)!}{m!}} |m+k\rangle$ this leads to

$$F(\lambda, m, m') = \lambda^{m'-m} \sqrt{\frac{m!}{m'!}} \sum_{i=0}^m \frac{(-|\lambda|^2)^i}{i!(m'-m+i)!} \frac{m'!}{(m-i)!}, \quad m' > m$$

A similar relation holds in the case $m > m'$,

$$F(\lambda, m, m') = (-\lambda)^{m-m'} \sqrt{\frac{m'!}{m!}} \sum_{i=0}^{m'} \frac{(-|\lambda|^2)^i}{i!(m-m'+i)!} \frac{m!}{(m'-i)!}, \quad m > m'$$

and for general m, m' the final result for $F(\lambda, m, m')$ is given by

$$\begin{aligned} F(\lambda, m, m') = & \left(\Theta(m' - m) \lambda^{m'-m} + \Theta(m - m') (-\lambda^*)^{m-m'} \right) \\ & \times \sqrt{\frac{m_{\min}!}{m_{\max}!}} \sum_{i=0}^{m_{\min}} \frac{(-|\lambda|^2)^i}{i!(i + m_{\max} - m_{\min})!} \frac{m_{\max}!}{(m_{\min} - i)!}, \end{aligned} \quad (\text{E.2.11})$$

where $m_{\min}/m_{\max} = \min/\max(m, m')$. Similar expressions for $F(\lambda, m, m')$ were found by Kim et al. [74] when investigating charge plasmons in a spinless Luttinger liquid quantum dot.

APPENDIX F

Regularization of $\langle \vec{N}\vec{m} | V_{f^+ b f^-} | \vec{N}\vec{m} \rangle$

As already mentioned in the main text, expression (2.5.27) for the matrix element $\langle \vec{N}\vec{m} | V_{S_r S_F S_\sigma} | \vec{N}'\vec{m}' \rangle$ diverges if $\sum_{j\delta q} |m_{j\delta q} - m'_{j\delta q}| \leq 1$ and if $V_{S_r S_F S_\sigma}$ is \vec{N} conserving. Here we show in detail how the matrix element can be properly regularized for the case $\vec{m} = \vec{m}'$ and $V_{S_r S_F S_\sigma} = V_{f^+ b f^-}$. We start with equation (2.5.27),

$$\begin{aligned} \langle \vec{N}\vec{m} | V_{f^+ b f^-} | \vec{N}\vec{m} \rangle &= \frac{1}{4L} u^+ \sum_{rF\sigma} \int dx \frac{e^{-2i\text{sgn}(rF)(N_{r\sigma} - N_{r-\sigma})\frac{\pi}{L}x}}{4\sin^2(\frac{\pi}{L}x)} \\ &\quad \times \prod_{j\delta q} F(\tilde{\lambda}_{[r]_{f^+}[F]_b[\sigma]_{f^-}}^{j\delta q}(x), m_{j\delta q}, m_{j\delta q}). \quad (\text{F.0.12}) \end{aligned}$$

In a first step we rewrite the fraction $e^{-2i\text{sgn}(rF)(N_{r\sigma} - N_{r-\sigma})\frac{\pi}{L}x} / (4\sin^2(\frac{\pi}{L}x))$ as

$$\frac{e^{-2i\text{sgn}(rF)(N_{r\sigma} - N_{r-\sigma})\frac{\pi}{L}x}}{4\sin^2(\frac{\pi}{L}x)} = \frac{e^{-2i\text{sgn}(rF)N_{r\sigma}\frac{\pi}{L}x}}{1 - e^{i\frac{2\pi}{L}x}} \frac{e^{2i\text{sgn}(rF)N_{r-\sigma}\frac{\pi}{L}x}}{1 - e^{-i\frac{2\pi}{L}x}}$$

and, by using the identity

$$\sum_{n=-\infty}^N e^{-inx} = \frac{e^{-iNx}}{1 - e^{ix}},$$

we transform it into the product of two infinite sums extending over the whole Fermi sea,

$$\frac{e^{-2i\text{sgn}(rF)(N_{r\sigma} - N_{r-\sigma})\frac{\pi}{L}x}}{4\sin^2(\frac{\pi}{L}x)} = \sum_{n=-\infty}^{N_{r\sigma}} e^{-2i\text{sgn}(rF)n\frac{\pi}{L}x} \sum_{n'=-\infty}^{N_{r-\sigma}} e^{2i\text{sgn}(rF)n'\frac{\pi}{L}x}. \quad (\text{F.0.13})$$

An important observation is, that the multiplication with

$$e^{-in_q x} - e^{in_q x} = e^{-in_q x} (1 - e^{2in_q x})$$

recasts the infinite sum $\sum_{n=-\infty}^N e^{-2inx}$ into a finite sum,

$$e^{-in_q x} (1 - e^{2in_q x}) \sum_{n=-\infty}^N e^{-2inx} = e^{-in_q x} \sum_{n=N-n_q+1}^N e^{-2inx}. \quad (\text{F.0.14})$$

Let us now have a closer look at the coefficients $\tilde{\lambda}_{[r]_{f+}[F]_b[\sigma]_{f-}}^{j\delta q}$, which according to (E.2.5) are given by

$$\tilde{\lambda}_{[r]_{f+}[F]_b[\sigma]_{f-}}^{j\delta q}(x) = \frac{1}{\sqrt{n_q}} \left[\Lambda_{r\sigma}^{j\delta} \left(e^{-i\text{sgn}(rF)qx} - e^{i\text{sgn}(rF)qx} \right) + \Lambda_{r-\sigma}^{j\delta} \left(e^{i\text{sgn}(rF)qx} - e^{-i\text{sgn}(rF)qx} \right) \right].$$

Then because of (F.0.14), the product

$$\prod_{j\delta q} \left(\tilde{\lambda}_{[r]_{f+}[F]_b[\sigma]_{f-}}^{j\delta q}(x) \right)^{t_{j\delta q}} \sum_{n=-\infty}^{N_{r\sigma}} e^{-2i\text{sgn}(rF)n\frac{\pi}{L}x} \sum_{n'=-\infty}^{N_{r-\sigma}} e^{2i\text{sgn}(rF)n'\frac{\pi}{L}x}, \quad t_{j\delta q} \in \mathbb{N}$$

is a finite sum for $\sum_{j\delta q} t_{j\delta q} \geq 2$. But from (E.2.11) we can conclude that

$$\prod_{j\delta q} F(\tilde{\lambda}_{[r]_{f+}[F]_b[\sigma]_{f-}}^{j\delta q}(x), m_{j\delta q}, m_{j\delta q}) = 1 + \mathcal{O}(\lambda^2),$$

where $\mathcal{O}(\lambda^2)$ collects all the terms that contain a factor $\prod_{j\delta q} \left(\tilde{\lambda}_{[r]_{f+}[F]_b[\sigma]_{f-}}^{j\delta q}(x) \right)^{t_{j\delta q}}$ with $\sum_{j\delta q} t_{j\delta q} \geq 2$. Thus

$$\int dx \frac{e^{-2i\text{sgn}(rF)(N_{r\sigma}-N_{r-\sigma})\frac{\pi}{L}x}}{4 \sin^2\left(\frac{\pi}{L}x\right)} \left(\prod_{j\delta q} F(\tilde{\lambda}_{[r]_{f+}[F]_b[\sigma]_{f-}}^{j\delta q}(x), m_{j\delta q}, m_{j\delta q}) - 1 \right) \quad (\text{F.0.15})$$

is a well defined integral over a finite sum and therefore not diverging. On the other hand we find with (F.0.13)

$$\begin{aligned} \int dx \frac{e^{-2i\text{sgn}(rF)(N_{r\sigma}-N_{r-\sigma})\frac{\pi}{L}x}}{4 \sin^2\left(\frac{\pi}{L}x\right)} &= \\ \int dx \sum_{n=-\infty}^{N_{r\sigma}} e^{-2i\text{sgn}(rF)n\frac{\pi}{L}x} \sum_{n'=-\infty}^{N_{r-\sigma}} e^{2i\text{sgn}(rF)n'\frac{\pi}{L}x} &= \\ L \sum_{n=-\infty}^{N_{r\sigma}} \sum_{n'=-\infty}^{N_{r-\sigma}} \delta_{n,n'} &= \sum_{n=-\infty}^{\min(N_{r\sigma}, N_{r-\sigma})} L. \end{aligned}$$

Regularization of the previous expression now is easily achieved by subtracting in the previous equation e.g. the contribution from below half-filling, such that,

$$\int dx \frac{e^{-2i\text{sgn}(rF)(N_{r\sigma}-N_{r-\sigma})\frac{\pi}{L}x}}{4 \sin^2\left(\frac{\pi}{L}x\right)} = L \min(N_{r\sigma}, N_{r-\sigma}). \quad (\text{F.0.16})$$

Combining (F.0.15) and (F.0.16) we obtain the finite expression

$$\begin{aligned}
\langle \vec{N} \vec{m} | V_{f+b f-} | \vec{N} \vec{m} \rangle &= u^+ \sum_r \min(N_{r\uparrow}, N_{r\downarrow}) \\
&+ \frac{1}{4L} u^+ \sum_{r F \sigma} \int dx \frac{e^{-2i \text{sgn}(r F) (N_{r\sigma} - N_{r-\sigma}) \frac{\pi}{L} x}}{4 \sin^2 \left(\frac{\pi}{L} x \right)} \\
&\times \left(\prod_{j \delta q} F(\tilde{\lambda}_{[r]_{f+} [F]_b [\sigma]_{f-}}^{j \delta q}(x), m_{j \delta q}, m_{j \delta q}) - 1 \right)
\end{aligned}$$

which is equivalent to equation (2.5.28) in the main text. The regularization for the case $\sum_{j \delta q} |m_{j \delta q} - m'_{j \delta q}| = 1$ as well as for the matrix elements of the \vec{N} conserving processes $V_{f-b f}$ and $V_{b f-f+}$ which are only relevant near half-filling can be achieved in a similar way.

APPENDIX G

Invariance of the transport calculation under unitary transformations U_{E_N}

In this appendix we rewrite equations (3.3.22) and (3.4.3) in a basis independent way, thus proving their invariance under any unitary transformations U_{E_N} within the Hilbert spaces H_{E_N} of states with equal energy and particle number. We do not consider more general unitary transformations because we assume that any coherence between states of different particle number and energy vanish, cf. Section 3.3. Let us start with equation (3.3.22). Using the definitions (3.3.23) to (3.3.26), we obtain

$$\begin{aligned}
 \dot{\rho}_{\odot}^{I, E_N}(t) = & -\frac{1}{\hbar^2} \sum_{l=s,d} \sum_{\sigma} \int d^3x \int d^3y \int_0^{\infty} dt' \\
 & \left\{ \left[\sum_{E'_{N-1}} \mathcal{E}_{\sigma l}(\vec{x}, \vec{y}, t') e^{-\frac{i}{\hbar}(E'_{N-1}-E_N)t'} (\Psi_{\sigma}^{\dagger}(\vec{x}))^{E_N E'_{N-1}} (\Psi_{\sigma}(\vec{y}))^{E'_{N-1} E_N} \rho_{\odot}^{I, E_N}(t) \right. \right. \\
 & + \mathcal{F}_{\sigma l}(\vec{x}, \vec{y}, t') \sum_{E'_{N+1}} e^{-\frac{i}{\hbar}(E'_{N+1}-E_N)t'} (\Psi_{\sigma}(\vec{x}))^{E_N E'_{N+1}} (\Psi_{\sigma}^{\dagger}(\vec{y}))^{E'_{N+1} E_N} \rho_{\odot}^{I, E_N}(t) \left. \right] + h.c. \\
 & - \left[\mathcal{F}_{\sigma l}^*(\vec{x}, \vec{y}, t') \sum_{E'_{N-1}} e^{-\frac{i}{\hbar}(E'_{N+1}-E_N)t'} (\Psi_{\sigma}^{\dagger}(\vec{x}))^{E_N E'_{N-1}} \rho_{\odot}^{I, E'_{N-1}}(t) (\Psi_{\sigma}(\vec{y}))^{E'_{N-1} E_N} \right. \\
 & \left. \left. + \mathcal{E}_{\sigma l}^*(\vec{x}, \vec{y}, t') \sum_{E'_{N+1}} e^{-\frac{i}{\hbar}(E'_{N+1}-E_N)t'} (\Psi_{\sigma}(\vec{x}))^{E_N E'_{N+1}} \rho_{\odot}^{I, E'_{N+1}}(t) (\Psi_{\sigma}^{\dagger}(\vec{y}))^{E'_{N+1} E_N} \right] - h.c. \right\}, \tag{G.0.17}
 \end{aligned}$$

obviously not depending on a specific choice of an eigenbasis of H_{\odot} . The electron operators $(\Psi_{\sigma}(\vec{x}))^{E_N E'_{N+1}}$ are acting between the Hilbert spaces \mathcal{H}_{E_N} and $\mathcal{H}_{E'_{N+1}}$. Additionally we can reexpress equation (3.4.3) for the current in the invariant form

$$I_l = \sum_{N, E_N} Tr(\rho_{\odot}^{I, E_N} I_l^{E_N})$$

by introducing the current operators I^{E_N} ,

$$\begin{aligned}
 I_l^{E_N} = & \frac{le}{\hbar^2} \sum_{\sigma} \int d^3x \int d^3y \int_0^{\infty} dt' \\
 & \left[\sum_{E'_{N+1}} (\Psi_{\sigma}(\vec{x}))^{E_N E'_{N+1}} (\Psi_{\sigma}^{\dagger}(\vec{y}))^{E'_{N+1} E_N} \mathcal{F}_{\sigma l}(\vec{x}, \vec{y}, t') e^{-\frac{i}{\hbar}(E'_{N+1} - E_N)t'} - \right. \\
 & \left. \sum_{E'_{N-1}} (\Psi_{\sigma}^{\dagger}(\vec{x}))^{E_N E'_{N-1}} (\Psi_{\sigma}(\vec{y}))^{E'_{N-1} E_N} \mathcal{E}_{\sigma l}(\vec{x}, \vec{y}, t') e^{-\frac{i}{\hbar}(E'_{N-1} - E_N)t'} \right] + h.c.
 \end{aligned} \tag{G.0.18}$$

APPENDIX H

The matrix elements of the electron operators

In this appendix we calculate the expressions for the matrix elements

$$\left\langle \vec{N}, \vec{m} \left| \psi_{rF\sigma}(x) \right| \vec{N}', \vec{m}' \right\rangle.$$

The procedure is very similar to the calculation of $\left\langle \vec{N}, \vec{m} \left| V_{n\rho\rho} \right| \vec{N}', \vec{m}' \right\rangle$ in Appendix E. Again we use the bosonization identity (A.0.15) of the electron operators $\psi_{r\sigma F}(x)$, namely

$$\psi_{rF\sigma}(x) = \eta_{r\sigma} K_{rF\sigma} e^{i\phi_{rF\sigma}^\dagger(x) + i\phi_{rF\sigma}(x)} e^{\frac{1}{2}[i\phi_{rF\sigma}^\dagger(x), i\phi_{rF\sigma}(x)]}, \quad (\text{H.0.19})$$

where we have already made use of the Baker-Hausdorff formula. As a reminder, $\eta_{r\sigma}$ is the Klein factor reducing the electron number by one, the operator $K_{rF\sigma}$ is given by

$$K_{rF\sigma}(x) = \frac{1}{\sqrt{2L}} e^{i\frac{\pi}{L}\text{sgn}(F)(rN_{r\sigma} + \Delta)x} \quad (\text{H.0.20})$$

and yields a phase factor depending on the filling of the band ($r\sigma$). The bosonic fields $\phi_{rF\sigma}(x)$ are given in terms of the bosonic annihilation operators $b_{r\sigma q}$,

$$i\phi_{rF\sigma}(x) = \sum_{q>0} \frac{e^{i\text{sgn}(Fr)qx}}{\sqrt{n_q}} b_{r\sigma q}. \quad (\text{H.0.21})$$

Via the Bogoliubov transformation the operators $b_{r\sigma q}$ can be expressed in terms of the operators $a_{j\delta q}$ and $a_{j\delta q}^\dagger$ which diagonalize the SWNT Hamiltonian H_\odot , see equation (2.5.15). From Appendix E we know

$$i\phi_{r\sigma F}(x) + i\phi_{r\sigma F}^\dagger(x) = \sum_{j\delta q>0} \left(\lambda_{rF\sigma}^{j\delta q} a_{j\delta q} - \left(\lambda_{rF\sigma}^{j\delta q} \right)^* a_{j\delta q}^\dagger \right), \quad (\text{H.0.22})$$

with

$$\lambda_{rF\sigma}^{j\delta q} = \frac{\Lambda_{r\sigma}^{j\delta}}{\sqrt{n_q}} \left(e^{i\text{sgn}(Fr)qx} B_{j\delta q} - e^{-i\text{sgn}(Fr)qx} D_{j\delta q} \right), \quad (\text{H.0.23})$$

where the Bogoliubov parameters $B_{j\delta q}$ and $D_{j\delta q}$ are given by (2.5.16) and (2.5.17). Inserting the bosonization identity (H.0.19) together with expression (H.0.22) into the

matrix element $\langle \vec{N}, \vec{m} | \psi_{rF\sigma}(x) | \vec{N}', \vec{m}' \rangle$, yields

$$\begin{aligned} \langle \vec{N}, \vec{m} | \psi_{rF\sigma}(x) | \vec{N}', \vec{m}' \rangle = \\ \delta_{\vec{N}+\vec{e}_{r\sigma}, \vec{N}'} (-1)^{\sum_{j=1}^{r\sigma-1} N_j} e^{\frac{1}{2}[i\phi_{rF\sigma}^\dagger(x), i\phi_{rF\sigma}(x)]} Q_{\vec{N}'rF\sigma}(x) \times \\ \langle \vec{m} | e^{\sum_{j\delta q>0} (\lambda_{rF\sigma}^{j\delta q}(x) a_{j\delta q} - (\lambda_{rF\sigma}^{j\delta q}(x))^* a_{j\delta q}^\dagger)} | \vec{m}' \rangle, \end{aligned}$$

where we have defined

$$Q_{\vec{N}'rF\sigma}(x) := \frac{1}{\sqrt{2L}} e^{i\frac{\pi}{L}\text{sgn}(F)(rN_{r\sigma}+\Delta)x}.$$

Remember that the factor $(-1)^{\sum_{j=1}^{r\sigma-1} N_j}$ stems from the Klein factor. The term

$$\langle \vec{m} | e^{\sum_{j\delta q>0} (\lambda_{rF\sigma}^{j\delta q}(x) a_{j\delta q} - (\lambda_{rF\sigma}^{j\delta q}(x))^* a_{j\delta q}^\dagger)} | \vec{m}' \rangle \quad (\text{H.0.24})$$

does not depend on the fermionic configuration and therefore we have dropped the \vec{N} index in $|\vec{N}, \vec{m}\rangle$. Normal ordering equation (H.0.24) leads to

$$\begin{aligned} \langle \vec{m} | e^{\sum_{j\delta q>0} (\lambda_{rF\sigma}^{j\delta q}(x) a_{j\delta q} - (\lambda_{rF\sigma}^{j\delta q}(x))^* a_{j\delta q}^\dagger)} | \vec{m}' \rangle = e^{-\frac{1}{2} \sum_{j\delta q>0} |\lambda_{rF\sigma}^{j\delta q}(x)|^2} \times \\ \prod_{q>0} \prod_{j\delta} \langle m_{j\delta q} | e^{-\left(\lambda_{rF\sigma}^{j\delta q}(x)\right)^* a_{j\delta q}^\dagger} e^{\lambda_{rF\sigma}^{j\delta q}(x) a_{j\delta q}} | m'_{j\delta q} \rangle, \quad (\text{H.0.25}) \end{aligned}$$

with $|m_{j\delta\kappa}\rangle = (m_{j\delta\kappa}!)^{-1/2} \left(a_{j\delta\kappa}^\dagger\right)^{m_{j\delta\kappa}} |0\rangle$. As derived in Appendix E it holds

$$\langle m | e^{-\lambda^* a^\dagger} e^{\lambda a} | m' \rangle = F(\lambda, m, m'), \quad (\text{H.0.26})$$

where $F(\lambda, m, m')$ is explicitly given by equation (E.2.11). In the end we obtain for the matrix elements $(\psi_{rF\sigma}(x))_{nm}$ the following expression:

$$\begin{aligned} \langle \vec{N}, \vec{m} | \psi_{rF\sigma}(x) | \vec{N}', \vec{m}' \rangle = \delta_{\vec{N}+\vec{e}_{r\sigma}, \vec{N}'} (-1)^{\sum_{j=1}^{r\sigma-1} N_j} Q_{\vec{N}'rF\sigma}(x) W(x) \times \\ \prod_{j\delta q>0} F(\lambda_{rF\sigma}^{j\delta q}(x), m_{j\delta q}, m'_{j\delta q}), \end{aligned}$$

where we have defined

$$W(x) := e^{\frac{1}{2}[i\phi_{rF\sigma}^\dagger(x), i\phi_{rF\sigma}(x)]} e^{-\frac{1}{2} \sum_{j\delta q>0} |\lambda_{rF\sigma}^{j\delta q}(x)|^2}, \quad (\text{H.0.27})$$

a quantity that is independent of $rF\sigma$ as we show in the following.

H.1. The function $W(x)$

With equation (H.0.21) one finds

$$\left[i\phi_{rF\sigma}^\dagger(x), i\phi_{r\pm F\sigma}(x) \right] = - \sum_{q>0} \frac{1}{n_q} [b_{r\sigma q}^\dagger, b_{r\sigma q}] = \sum_{q>0} \frac{1}{n_q}. \quad (\text{H.1.1})$$

From (H.0.23) we obtain for the parameters $\lambda_{rF\sigma}^{j\delta q}(x)$ in the case of the neutral modes $j\delta = c-, s+, s-$,

$$\lambda_{rF\sigma}^{j\delta q}(x) = \frac{e^{i\text{sgn}(Fr)qx}}{\sqrt{n_q}} \Lambda_{r\sigma}^{j\delta} \quad (\text{H.1.2})$$

and for the $c+$ mode we have

$$\lambda_{r\sigma}^{c+q}(x) = \frac{1}{2\sqrt{n_q}} \left(\sqrt{\frac{\varepsilon_{c+q}}{\varepsilon_{0q}}} \cos(qx) + i \sqrt{\frac{\varepsilon_{0q}}{\varepsilon_{c+q}}} \text{sgn}(Fr) \sin(qx) \right). \quad (\text{H.1.3})$$

Hence it holds

$$\left| \lambda_{rF\sigma}^{j\delta q}(x) \right|^2 = \frac{1}{4n_q} \left[1 + \delta_{j\delta, c+} \left(\frac{\varepsilon_{c+q}}{\varepsilon_{0q}} \cos^2(qx) + \frac{\varepsilon_{0q}}{\varepsilon_{c+q}} \sin^2(qx) - 1 \right) \right]. \quad (\text{H.1.4})$$

Inserting (H.1.1) and (H.1.4) into (H.0.27) we finally obtain

$$W(x) = e^{-\frac{1}{8} \sum_{q>0} \frac{1}{n_q} \left(\frac{\varepsilon_{c+q}}{\varepsilon_{0q}} \cos^2(qx) + \frac{\varepsilon_{0q}}{\varepsilon_{c+q}} \sin^2(qx) - 1 \right)}. \quad (\text{H.1.5})$$

Because $\frac{\varepsilon_{c+q}}{\varepsilon_{0q}} \rightarrow 1$ for large q , the sum in (H.1.5) is finite.

Bibliography

- [1] M.S. Dresselhaus, G. Dresselhaus, Ph. Avouris (Eds.), *Carbon Nanotubes—Synthesis, Structure, Properties, and Applications*, Springer-Verlag, Berlin Heidelberg (2001).
- [2] S. Iijima, *Nature* **354**, 56 (1991).
- [3] M. Monthieux and V. L. Kuznetsov, *Carbon* **44**, 1621 (2006).
- [4] L.V. Radushkevich and V.M. Lukyanovich, *Zurn Fisic Chim* **26**, 88 (1952).
- [5] S. Iijima, T. Ichihashi, *Nature* **363**, 603 (1993).
- [6] D. S. Bethune et al., *Nature* **363**, 605 (1993).
- [7] K. S. Novoselov et al., *Science* **306**, 666 (2004).
- [8] K. S. Novoselov et al., *Proc. Natl. Acad. Sci.* **102**, 10451 (2005).
- [9] A. K. Geim and K. S. Novoselov, *Nature materials* **6**, 183 (2007).
- [10] M. Endo et al., *Phil. Trans. R. Soc. Lond. A* **362**, 2223 (2004).
- [11] S. Tomonaga, *Prog. Theor. Phys.* **5**, 544 (1950).
- [12] F. D. M. Haldane, *J. Phys. C* **14**, 2585 (1981).
- [13] R. Egger and A. O. Gogolin, *Phys. Rev. Lett.* **79**, 5082 (1997); *Eur. Phys. J. B* **3**, 281 (1998).
- [14] H. Yoshioka, A. A. Odintsov, *Phys. Rev. Lett.* **82**, 374 (1999).
- [15] M. Bockrath et al., *Nature* **397**, 598 (1999).
- [16] H. W. Ch. Postma et al., *Science* **293**, 76 (2001).
- [17] C. Kane, L. Balents and M. P. A. Fisher, *Phys. Rev. Lett.* **79**, 5086 (1997).
- [18] S. Moriyama, T. Fuse, M. Suzuki, Y. Aoyagi, K. Ishibashi, *Phys. Rev. Lett.* **94**, 186806 (2005).
- [19] Y. Oreg, K. Byczuk and B. I. Halperin, *Phys. Rev. Lett.* **85**, 365 (2000).
- [20] S. Sapmaz et al., *Phys. Rev. B* **71**, 153402 (2005).
- [21] D. H. Cobden, *Phys. Rev. Lett.* **81**, 681 (1997).
- [22] A. Loiseau et al., *Understanding Carbon Nanotubes*, Lecture Notes in Physics, Vol. 677 (Springer, Berlin 2006).
- [23] S. Reich, C. Thomsen, J. Maultzsch, *Carbon Nanotubes*, Wiley-VCH, Weinheim, (2004).
- [24] A. A. Odintsov and H. Yoshioka, *Phys. Rev. B* **59**, R10457 (1999).
- [25] M. Fabrizio, A. O. Gogolin, *Phys. Rev. B* **51**, 17827 (1995).
- [26] A. Rubio, *Phys. Rev. Lett.* **82**, 3520 (1999).
- [27] A. A. Abrikosov, L. P. Gorkov, I. E. Dzyaloshinski, *Methods of quantum field theory in statistical physics*, Dover publications, New York (1975).
- [28] J. M. Luttinger, *J. Math. Phys.* **4**, 1154 (1963).
- [29] K. Schönhammer, cond-mat/9710330 (1998).
- [30] K. Schönhammer, cond-mat/0305035 (2003).
- [31] F. D. M. Haldane, *Phys. Rev. Lett.* **45**, 1358 (1980).
- [32] G. A. Fiete, *Rev. Mod. Phys.* **79**, 801 (2007).
- [33] J. Voit, *Rep. Prog. Phys.* **57**, 977 (1994).
- [34] A. O. Gogolin, A. A. Nersisyan, A. M. Tsvelik, *Bosonization and strongly correlated systems*, Cambridge University Press, Cambridge (2004).
- [35] For an introduction to bosonization, see e.g., J. v. Delft, H. Schoeller, *Annalen Phys.* **7**, 225 (1998).
- [36] O. Auslaender et al., *Science* **308**, 88 (2005).
- [37] J. Lee et al., *Phys. Rev. Lett.* **93**, 166403 (2004).
- [38] W. Liang, M. Bockrath and H. Park, *Phys. Rev. Lett.* **88**, 126801 (2002).
- [39] E. Lieb and D. Mattis, *Phys. Rev.* **125**, 164 (1962).

- [40] W. Barford, *Electronic and Optical Properties of Conjugated Polymers*, Clarendon Press, Oxford (2005).
- [41] P. Fulde, *Electron Correlations in Molecules and Solids*, Springer Verlag, Berlin - New York (1995).
- [42] M. Eto and Y. V. Nazarov, Phys. Rev. Lett. **85**, 1306 (2000); Phys. Rev. B **66**, 153319 (2002).
- [43] S. J. Tans et al., Nature **386**, 474 (1997).
- [44] D. H. Cobden and J. Nygård, Phys. Rev. Lett. **89**, 46803 (2002).
- [45] S.-H. Ke, H. U. Baranger and W. Yang, Phys. Rev. Lett. **91**, 116803 (2003).
- [46] S. Bellucci and P. Onorato, Phys. Rev. B **71**, 75418 (2005).
- [47] L. Mayrhofer and M. Grifoni, Physical Review B **74**, 121403(R) (2006).
- [48] L. Mayrhofer and M. Grifoni, European Journal of Physics B **56**, 107 (2007).
- [49] C. W. J. Beenakker, Phys. Rev. B **44**, 1646 (1991).
- [50] S. Braig, P. W. Brouwer, Phys. Rev. B **71**, 195324 (2005).
- [51] J. König and J. Martinek, Phys. Rev. Lett. **90**, 166602 (2003).
- [52] M. Braun, J. König, and J. Martinek, Phys. Rev. B **70**, 195345 (2004).
- [53] Work in progress, Sonja Koller, Universität Regensburg.
- [54] L. Kouwenhoven and L. Glazman, Physics World **14**, No 1, 33 (2001).
- [55] G. L. Ingold and Yu. V. Nazarov in *Single Charge Tunneling*, edited by H. Grabert and M. H. Devoret, Plenum Press, New York (1992).
- [56] K. Blum, *Density Matrix Theory and Applications*, Plenum Press, New York (2006).
- [57] P. Jarillo-Herrero et al., Nature **434**, 484 (2005).
- [58] M. S. Choi, R. Lopez and R. Aguado, Phys. Rev. Lett. **95**, 067204 (2005).
- [59] F. Cavaliere et al., Phys. Rev. Lett. **93**, 36803 (2004).
- [60] S. Koller, Diploma Thesis “*Spin transport in carbon nanotubes*”, Universität Regensburg (2006).
- [61] K. Tsukagoshi, Nature **401**, 572 (1999).
- [62] J.-R. Kim, Phys. Rev. B **66**, 233401 (2002).
- [63] S. Sahoo et al., Appl. Phys. Lett. **86**, 112109 (2005).
- [64] A. Jensen et al., Phys. Rev. B **72**, 35419 (2005).
- [65] S. Sahoo et al., Nat. Phys. **1**, 99 (2005).
- [66] H. T. Man, I. J. W. Wever and A. F. Morpurgo, Phys. Rev. B **73**, 241401(R) (2006).
- [67] A. Cottet and Mahn-Soo Choi, Phys. Rev. B **74**, 235316 (2006).
- [68] W. Wetzels, G. E. W. Bauer and M. Grifoni, Phys. Rev. B **74**, 224406 (2006).
- [69] A. Cottet et al., Europhys. Lett. **74**, 320 (2006).
- [70] L. Balents and R. Egger, Phys. Rev. Lett. **85**, 3464 - 3467 (2000).
- [71] S. Koller, L. Mayrhofer and M. Grifoni, New. J. Phys. **9**, 348 (2007).
- [72] I. Weymann, J. Barnas and S. Krompiewski, Phys. Rev. B **76**, 155408 (2007).
- [73] J. Avery, *Creation and Annihilation Operators*, McGraw-Hill, New York, (1976).
- [74] J. U. Kim, I. V. Krive, J. M. Kinaret, Phys. Rev. Lett. **90**, 176401 (2003).